NASA TECHNICAL TRANSLATION

NASA TT F-455

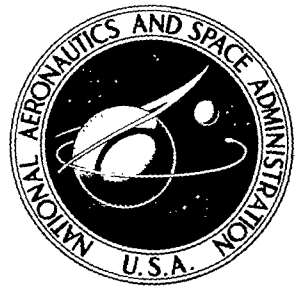

NASA TT F-455
e.1

PROBLEMS OF ASTROPHYSICS

Ye. P. Fedorov, Editor-in-Chief

Izdatel'stvo "Naukova Dumka"
Kiev, 1966

NATIONAL AERONAUTICS AND SPACE ADMINISTRATION • WASHINGTON, D. C. • AUGUST

NASA TT F-455

PROBLEMS OF ASTROPHYSICS

Ye. P. Fedorov, Editor-in-Chief

Translation of "Voprosy astrofiziki."
Izdatel'stvo "Naukova Dumka." Kiev, 1966.

NATIONAL AERONAUTICS AND SPACE ADMINISTRATION

For sale by the Clearinghouse for Federal Scientific and Technical Information
Springfield, Virginia 22151 – CFSTI price $3.00

TABLE OF CONTENTS

CUT ALONG THIS LINE

FOLD LINE

NATIONAL AERONAUTICS AND SPACE ADMINISTRATION
WASHINGTON, D.C. 20546

OFFICIAL BUSINESS

POSTAGE AND FEES PAID
NATIONAL AERONAUTICS & SPACE ADMINISTRATION

NATIONAL AERONAUTICS AND SPACE ADMINISTRATION
CODE USS-T
WASHINGTON, D.C. 20546

NASA TTF No.
455

FOLD LINE

CUT ALONG THIS LINE

NATIONAL AERONAUTICS AND SPACE ADMINISTRATION

TECHNICAL TRANSLATION EVALUATION

Budget Bureau No. 104-R037
Approval Expires: Sept. 30, 1969

TO: THE USERS OF THIS TRANSLATION →

NASA TTF NO. 455

MAINTAINING THE QUALITY OF NASA TRANSLATIONS REQUIRES A CONTINUOUS EVALUATION PROGRAM. PLEASE COMPLETE AND MAIL THIS FORM TO AID IN THE EVALUATION OF THE USEFULNESS AND QUALITY OF THE TRANSLATING SERVICE.

THIS PUBLICATION *(Check one or more)*

- ☐ FURNISHED VALUABLE NEW DATA OR A NEW APPROACH TO RESEARCH.
- ☐ VERIFIED INFORMATION AVAILABLE FROM OTHER SOURCES.
- ☐ FURNISHED INTERESTING BACKGROUND INFORMATION.
- ☐ OTHER *(Explain)*: _____

FOLD LINE FOLD LINE

TRANSLATION TEXT *(Check one)*

- ☐ IS TECHNICALLY ACCURATE.
- ☐ IS SUFFICIENTLY ACCURATE FOR OUR PURPOSE.
- ☐ IS SATISFACTORY, BUT CONTAINS MINOR ERRORS.
- ☐ IS UNSATISFACTORY BECAUSE OF *(Check one or more)*:
  - ☐ POOR TERMINOLOGY.
  - ☐ INCOMPLETE TRANSLATION.
  - ☐ NUMERICAL INACCURACIES.
  - ☐ ILLEGIBLE SYMBOLS, TABULATIONS, OR CURVES.
  - ☐ OTHER *(Explain)*: _____

FOLD LINE FOLD LINE

REMARKS

FROM

DATE

NOTE: REMOVE THIS SHEET FROM THE PUBLICATION, FOLD AS INDICATED, STAPLE OR TAPE, AND MAIL. NO POSTAGE NECESSARY.

NASA Form 1332 AUG 66

GPO 915-777

CUT ALONG THIS LINE

CUT ALONG THIS LINE

RESONANCE SCATTERING OF SOLAR RADIATION IN PROMINENCES

N. A. Yakovkin, M. Yu. Zel'dina

It is shown that the prominences emit in the line H_α on account of the scattering of solar radiation. The proof is based on the solution of an integral equation for the case of fully incoherent scattering. Photospheric radiation in the line H_α enters into the prominence and excites its glow in spite of the great optical thickness of the prominences in this line. The density of diffusion radiation is higher than the average density of the radiation entering into the prominence. The theoretical line profile under great optical thickness ($\tau \geq 10$) has a typical saddle shape. The central intensity and equivalent widths of the calculated line profile agree with the observations.

As of the present, no answer has yet been found for the question of whether prominences are "self-luminous" formations, or whether they may be seen due to scattering of solar radiation. /5* The majority of astrophysicists adhere to the first point of view, and assume that the excitation of atoms takes place either due to the influence of electron collisions, or as the result of electrons recombining with protons (Ref. 2, 7, 19). In a study devoted to the theory of the formation of Balmer lines, V. V. Sobolev (Ref. 12) also postulates the recombination mechanism for the luminescence of prominences. Several authors (Ref. 1, 11, 16) have assumed that the luminescence of prominences is not only caused by eigen emission, but also by scattering of photospheric radiation. The assumption has been advanced (Ref. 5) that the third and fourth levels of a hydrogen atom are excited by solar radiation, and the remaining levels are due to the recombination mechanism. It was shown in (Ref. 15) that the energy radiated by a prominence in each Balmer line equals the energy of the absorbed photospheric radiation in this same line. In this connection, it

---

* Numbers in the margin indicate pagination in the original foreign text.

may be assumed that the luminescence of prominences is the resonance scattering of solar radiation.

In order to solve the problem of the excitation mechanism of hydrogen atoms in prominences, we must examine the diffusion of the radiation and must determine the change in the source function as a function of the optical depth. The problem investigated by Jefferis (Ref. 16) is similar to this problem. Solving the radiation transport equation in the Eddington approximation, Jefferis obtained the emission line profile of H_α, calculating the intensity of the eigen and scattered, photospheric radiation. He did not take into /6 account the incoherence caused by the Doppler effect. In a more recent study (Ref. 17), Jefferis and Orrall also investigated the dependence of the source function on the optical thickness, defining a certain law for this dependence. The source function was also determined by the trial and error method in (Ref. 6).

The study by V. V. Sobolev, which was already mentioned, represents an important step forward in solving this problem. The author determined the source function, investigating not only the radiation diffusion in the line, but also the interrelationship between all the Balmer lines. However, this study is of greater interest for research on flares than it is for research on prominences, since the report formulates a recombination mechanism for the luminescence and a model in the form of a uniform sphere which correspond to a better extent with the nature of flares.

This study investigated diffusion radiation in the H_α line, determined its density, and showed that luminescence of prominences in this line is completely provided by resonance scattering of solar radiation.

Main Equation

The determination of diffusion radiation density may be reduced to solving an integral equation for the source function $B(\tau)$. The derivation of the equation is well known (Ref. 12), but we would like to describe it briefly in connection with the specific calculation of its free term in the case under consideration. Just as in (Ref. 12), in order to solve the problem we shall assume complete incoherence of the radiation during resonance scattering; this incoherence is caused by the Doppler effect. We shall employ a prominence model which is in the form of a thin plate which is perpendicular to the surface of the Sun [see (Ref. 16)]. Let the line of sight intersect the prominence along the normal 30" above the limb. The dilution factor w equals 0.3 in this case, with allowance for the darkening factor u. We shall assume that the geometric thickness of the prominence is small as compared with the height range above the limb, within whose limits the dilution factor barely changes. This condition makes it possible for us to assume layers of equal radiation intensity with parallel boundary planes of the prominence. It is assumed that the layers of equal optical thickness coincide with them. There is no necessity of assuming that the prominences are uniform formations. The population of the second level of the hydrogen atoms may change as a function of the depth according to any law, provided that the given condition that the /7 layers be parallel is fulfilled.

In order to calculate the energy of the direct solar radiation absorbed by a unit volume of prominence, let us introduce the function

$$E_w(\tau) = \frac{1}{4\pi}\int_{\frac{\pi}{2}-\chi_0}^{\frac{\pi}{2}} e^{-\tau\sec\vartheta}\sin\vartheta\int_{-\beta_m}^{+\beta_m}(1-u+u\cos\Theta)\,d\beta d\vartheta, \qquad (1)$$

which represents the intensity of solar radiation, averaged over the angle 4π, at the depth τ, which enters the plane $\tau = 0$ and pertains to the radiation intensity in the center of the disc. As may be seen from Figure 1, angles ϑ and β determine the direction of the radiation which leaves the solar surface at the angle Θ. They are related to the parallactic angle χ_0 by the simple relationships

$$\sin\chi = \sin\chi_0\sin\Theta;$$
$$\cos\chi = \sin\vartheta\cos\beta;$$
$$\cos\chi_0 = \sin\vartheta\cos\beta_m.$$

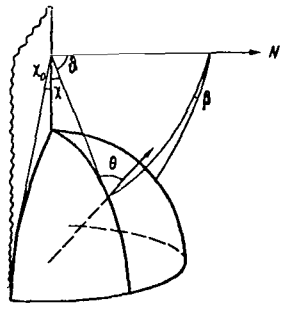

Figure 1

Model of a Prominence in the Form of a Plate Lying in the Plane of a Figure.

In our problem, the function $E_w(\tau)$ plays the role of an integral exponential function, as well as the role of "the physical dilution factor" which takes into account not only the geometric factor, but also the darkening of the disc toward the edge. Actually, in the case of w = 0.5, u = 0, we have

$$4E_{\frac{1}{2}}(x) = E_2(x) = \int_0^{\frac{\pi}{2}} e^{-x\sec\vartheta}\sin\vartheta\,d\vartheta,$$

and in the case of $\tau = 0$ we have

$$2E_w(0) = w = \frac{1}{2\pi}\int_{\frac{\pi}{2}-\chi_0}^{\frac{\pi}{2}}\sin\vartheta\int_{-\beta_m}^{+\beta_m}(1-u+u\cos\Theta)\,d\beta\,d\vartheta. \qquad (2)$$

Employing the continuous spectrum of the center of the disc close to the line H_α as the unit of intensity, and designating the profile of the Fraunhofer line by r_v, we obtain the energy absorbed at the given frequency

$$4\pi k n_2 e^{-v^2} r_v E_w(\tau e^{-v^2}).$$

It is assumed that the absorption coefficient depends only on the Doppler effect. kn_2 is the absorption coefficient computed per cubic centimeter; τ is the optical depth in the center of the line H_α. Integrating over the profile /8

of the Fraunhofer line, we obtain the absorbed energy at the depth τ

$$4\pi k n_2 \int_{-\infty}^{+\infty} r_v e^{-v^2} E_w(\tau e^{-v^2})\, dv. \tag{3}$$

For radiation entering the prominence through the second boundary plane, the absorbed energy may be written in a similar way, only the argument of the function E_w will have the form $(\tau_0 - \tau)e^{-v^2}$.

Besides direct solar radiation, each cubic centimeter absorbs the diffusion radiation

$$4\pi k n_2 \int_{-\infty}^{+\infty} e^{-v^2} \int_0^{\frac{\pi}{2}} I_v(\tau, \vartheta) \sin\vartheta\, d\vartheta.$$

Utilizing the solution of the energy transport equation, after changing the order of integration we obtain the following expression

$$4\pi k n_2 \int_0^{\tau_0} B(\tau) \int_{-\infty}^{+\infty} e^{-2v^2} \int_0^{\frac{\pi}{2}} e^{-(|\tau_0 - x|)\, e^{-v^2} \sec\vartheta} \sec\vartheta \sin\vartheta\, d\vartheta\, dv\, d\tau. \tag{4}$$

The source function $B(\tau)$ contained in this expression represents the ratio of the radiation coefficient j to the absorption coefficient kn_2. The optical thickness of the prominence along the line of sight is designated by τ_0. The energy radiated by a cubic centimeter

$$4\pi \int_{-\infty}^{+\infty} j e^{-v^2} dv,$$

must equal the absorbed energy. Employing this condition, let us formulate the equation of energy balance. Dividing it by /9

$$4\pi \int_{-\infty}^{+\infty} k n_2 e^{-v^2} dv = 4\pi \sqrt{\pi}\, k n_2,$$

we obtain the integral equation

$$B(\tau) = \int_0^{\tau_0} B(t) K(|t-\tau|)\, dt + g(\tau). \tag{5}$$

The kernel of the equation has the following form

$$K(x) = \frac{1}{\sqrt{\pi}} \int_0^{\infty} e^{-2v^2} E_1(\tau e^{-v^2})\, dv, \tag{6}$$

where E_1 is the integral exponential function

$$E_1(x) = \int_0^{\frac{\pi}{2}} e^{-x \sec \vartheta} \sec \vartheta \sin \vartheta d\vartheta.$$

Since the prominence is equally illuminated by the Sun from both sides, the free term of the equation equals the sum of the two components

$$g(\tau) = g^I(\tau) + g^I(\tau_0 - \tau), \tag{7}$$

where

$$g^I(\tau) = \frac{1}{\sqrt{\pi}} \int_{-\infty}^{+\infty} r_v e^{-v^2} E_w(\tau e^{-v^2}) dv. \tag{8}$$

The quantity $4\pi\sqrt{\pi} g^I(\tau) I_\odot d\tau$ represents the energy, which is absorbed by the layer $d\tau$ of direct solar radiation entering the prominence through the boundary plane $\tau = 0$. We may simplify the profile of the Fraunhofer line r_v which is contained in equation (8), by employing a photometric atlas (Ref. 18) and by assuming $\Delta\lambda_D = 0.33$ Å. Figure 2 shows the results derived from calculating $g^I(\tau)$, as well as the free term $g(\tau)$ for $\tau_0 = 10$. The quantities $g(\tau)$ may be expressed in units of intensity for the continuous spectrum of the center of the solar disc. The optical thicknesses are plotted along the abscissa axis. The quantity obtained from equations (2), (7) and (8) is used as the unit of scale of the right ordinate axis, /10

$$B_0 = \frac{w}{\sqrt{\pi}} \int_{-\infty}^{+\infty} r_v e^{-v^2} dv = 0.075, \tag{9}$$

This represents the source function for a prominence of zero optical thickness. This quantity is somewhat higher than the solar radiation intensity, averaged over the angle 4π, in the center of the Fraunhofer line H_α (h = 30")

$$r_c w = 0.21 \cdot 0.3 = 0.063.$$

(According to Tekkereya, the central intensity of the Frauhofer line in the spectrum of the disc center is 0.154. However, as V. A. Krat has indicated (Ref. 8), we must take the value of r_c averaged over the disc for such computations).

The following section presents the solution of the integral equation (5) for prominences having the optical thicknesses $\tau_0 = 0.1$; 1.0; 1.5; 5; 10; 100. The corresponding values of $g(\tau)$ are given in Figure 3. The given optical thicknesses τ_0 are used for each curve as the unit of the abscissa axis, and the value B_0 is used as the unit of the ordinate axis on the right. /11

Solution of the Equation

In recent years, there have been considerable advances regarding a theory for the diffusion of resonance radiation in the case of complete incoherent

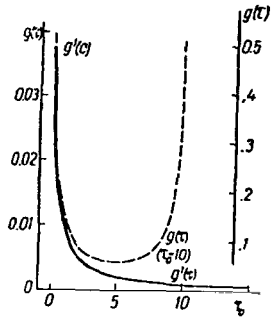

Figure 2

Results Derived from Calculating Direct Solar Radiation Absorbed by a Layer $g\tau$, Located at Different τ (Within an Accuracy of the Factor $4\pi\sqrt{\pi}I_{\odot}d\tau$) When the Prominence is Illuminated from One Side and from Two Sides ($\tau_0 = 10$). The value B_0 is Used as the Scale Unit of the Ordinate Axis to the Right.

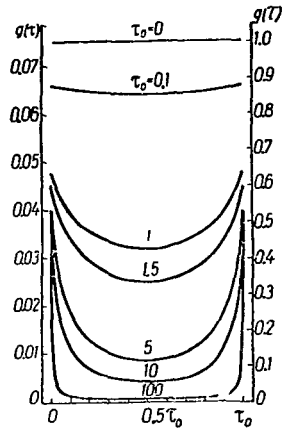

Figure 3

Function $g(\tau)$ for a Prominence Having the Optical Thickness τ_0. The Value B_0 is Used as the Scale Unit of the Ordinate Axis to the Right.

scattering (Ref. 10, 12, 4). We may now compile a resolvent of the integral equation, and may obtain a solution for the problem. However, it is simpler to obtain the solution numerically, if we take the fact into account that in the given case the free term is given graphically, and the resolvent is determined by several complex formulas. For this purpose, we have employed the method advanced by Krylov and Bogolyubov (Ref. 9); this method consists of replacing the integral equation by a system of algebraic equations. For this purpose, the integral is divided into a sum of integrals, in each of which it is assumed that the desired function is constant.

Let B_i be the source function for the middle of the layers, into which the prominence is divided. τ_i, t_{r-1} and t_r are the optical thicknesses in the center of the line H_α, which correspond to the distance from the boundary plane to the middle of the layer i, for which B_i is determined, and to the closest and farthest boundaries of the layer r. We may then write the system which is equivalent to the integral equation (5) as follows

$$\sum_{r=1}^{n} B_r a_{ri} + g_i = 0. \tag{10}$$

The coefficients have the form

$$a_{ri}=\int_{t_{r-1}}^{t_r}K(|\tau_i-t|)\,dt=\Phi(|\tau_i-t_{r-1}|)-\Phi(|\tau_i-t_r|),\quad r\neq i;$$
$$a_{ii}=\int_{t_{i-1}}^{t_i}K(|\tau_i-t|)\,dt-1=-2\Phi\left(\frac{\Delta t_i}{2}\right), \tag{11}$$

where $\Delta t_i = t_i - t_{i-1}$. /12

The condition $r \neq 1$ in equation (11) and the special form of the diagonal coefficients are related to the fact that we must not only take into account direct solar radiation and diffuse radiation of other layers when computing B_i for the middle of the given layer. We must also take into account the radiation of both halves of the layer itself.

When the coefficients are determined, the symmetrical nature of the kernel is employed, and the fact that $\Phi(0) = 0.5$ is taken into account. Utilizing the property of the integral exponential function

$$\int E_1(x,\ \varphi)\,dx=-\varphi^{-1}E_2(x,\ \varphi), \tag{12}$$

we find the expression for the function Φ

$$\Phi(x)=\frac{1}{\sqrt{\pi}}\int_0^{\infty}e^{-v^2}E_2(xe^{\ v^2})\,dv. \tag{13}$$

The values of the functions K(x) and Φ(x) were computed for $0 \leqslant x \leqslant 300$. For $x \leqslant 2$ they were determined according to a formula which was based on expansion in series of the integral exponential function. For large optical thicknesses, they were determined graphically. The results are presented in Figure 4. For purposes of convenience, we have compiled the curves $\tau\Phi(\tau)$ and $\tau^2K(\tau)$ as a function of τ for small optical thicknesses (upper scale) and as a function of $\lg\tau$ for $\tau \leqslant 300$.

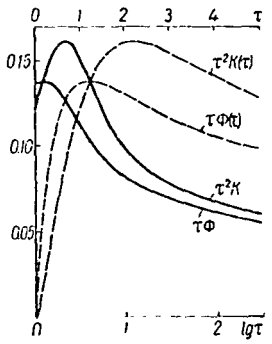

Figure 4

Dependence of the Function $\tau^2K(\tau)$ and $\tau\Phi(\tau)$ on the Optical Thickness (Upper Scale) and on lg (τ).

The system of equations (10) was solved by the method of successive approximations; due to the rapid convergence, we could confine ourselves to 4 — 6 approximations. This is explained by the weak interdependence of the layers which are located far away from each other. Coefficients located in the vicinity of the diagonal elements are of

decisive importance. By way of an example, we shall present a system of ten equations (Table 1) for a prominence which has the optical thickness $\tau_0 = 10$. The coefficients, the free term, and the values of the source function $B(\tau)$ are multiplied by 10^3, for purposes of convenience. The first column gives the optical "distances" of the middle of the layer from the boundary surface, and the last two columns give the free terms obtained by means of Figure 2. The result derived from the solution of this system represents the desired values of the source function. The source function is also symmetrical, due to the symmetrical location of the prominence with respect to the surface of the Sun. This enables us to reduce the number of unknowns by half, compiling a system of /13 equations for only one-half of the prominence.

TABLE 1

τ_i	Coefficients for the Unknowns										g_i	B_i
0.5	−450	134	42	18	9	5	3	2	2	1	16.8	78
1.5	134	−450	134	42	18	9	5	3	2	2	8.3	84
2.5	42	134	−450	134	42	18	9	5	3	2	5.6	87
3.5	18	42	134	−450	134	42	18	9	5	3	4.8	90
4.5	9	18	42	134	−450	134	42	18	9	5	4.4	91
5.5	5	9	18	42	134	−450	134	42	18	9	4.4	91
6.5	3	5	9	18	42	134	−450	134	42	18	4.8	90
7.5	2	3	5	9	18	42	134	−450	134	42	5.6	87
8.5	2	2	3	5	9	18	42	134	−450	134	8.3	84
9.5	1	2	2	3	5	9	18	42	134	−450	16.8	78

The approximate values of the source function B(0) for the boundary surfaces were computed according to the following formula

$$B(0) \cong B_1 - B_1 \int_0^{\frac{\Delta\tau}{2}} K\left(\left|t - \frac{\Delta\tau}{2}\right|\right) dt - g_1 + g(0). \qquad (14)$$

Here, B_1 is the value of the source function for the middle of the first layer. The second term to the right represents the contribution made by the outer half of the first layer to B_1. The last two terms represent the increase in the source function caused by a change in the direct solar radiation when moving from the middle of the layer to its outer surface.

Source Function

Employing the method presented above, we calculated the source function for prominences having optical thicknesses in the line H_α from 0.1 to 100.

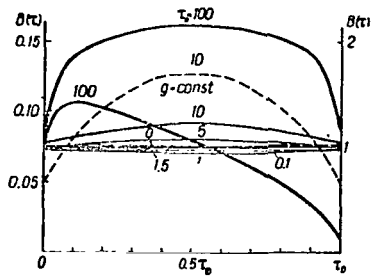

Figure 5

Dependence of the Source Function on the Optical Depth for Different τ_0. The value B_0 is Used as the Scale Unit of the Ordinate Axis to the Right.

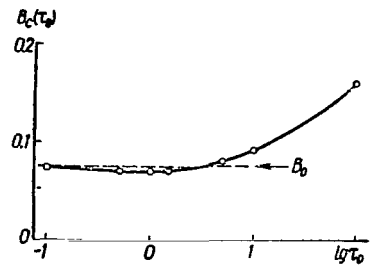

Figure 6

Values of the Source Function in the Center of Prominences Having Different Optical Thicknesses.

The dependence of the source function on the optical depth is shown in Figure 5. The corresponding value of the prominence optical thickness was used as the unit along the abscissa axis, when each curve was drawn. The intensities pertain to the continuous spectrum of the disc center (scale to the left). The value B_0 was used as the scale unit on the right. As may be seen, the numerical values of the source function and its behavior with depth depend to a significant extent on the optical thickness of the prominence. For prominences having a small optical thickness, it may be assumed that the source function is constant over the thickness and equals B_0 -- the source function when there is no prominence. Thus, diffuse radiation, which arises in an optically thin prominence, completely balances the absorption of direct solar radiation along its path to the central regions of the prominence. In the case of $\tau_0 = 3$, the density of the diffuse radiation becomes larger than the density of the incoming radiation -- i.e., it behaves as though there were an "accumulation" of quanta in the substance. For the middle of a prominence having an optical thickness of 100, the effect of "accumulation" leads to a significant increase in the radiation density -- the source function exceeds the value B_0 by a factor of more than 2. /14

The effect of "accumulation" of quanta in the central regions of the prominences is shown in Figure 6 as a function of the logarithm of their optical thickness. The minimum value of the source function corresponds to $\tau_0 = 1$, which could have been expected, since an optical thickness equalling unity corresponds to the mean free path of a quantum. For $\tau_0 < 3$, the source function equals B_0, or is smaller than this value by several percents. With an increase in the optical thickness of the prominence, it rapidly becomes larger. We should point out that the extent to which the quanta are "accumulated" is determined by the ratio $B(\tau)/B_0$. However, in order to determine the role of diffuse radiation in excitation of hydrogen atoms, we may find the ratio /15

$B(\tau)/g(\tau)$ which is 100 times greater than the quantity given above. For example, for a prominence having $\tau_0 = 100$, the number of quanta of diffuse radiation is two and one-half orders of magnitude greater than the number of quanta of direct solar radiation reaching the central region of prominence.

We thus arrive at the following important conclusion. The prominence is filled with diffuse radiation during resonance scattering of solar radiation in the line H_α; the greater is the optical thickness of the prominence, the larger is the density of this diffuse radiation. The phenomenon of "accumulation" of quanta is also observed when a prominence is illuminated from only one side. Figure 5 presents a graph of the source function for $\tau_0 = 100$ when a prominence is illuminated from one side. Just as previously, the computations were performed for the line of sight which intersects the prominence at a height of 30" above the limb. In this case, the phenomenon of quanta "accumulation" reaches its maximum value at a distnace of $\tau \sim 10$ from the plane which is illuminated by the Sun, and not in the central region of the prominence. If the source function is combined with its mirror image, due to the additivity of the radiation fields we obtain a source function which corresponds to illumination of the prominence by the Sun from both sides.

Profile of the Line

The profile of the line H_α, which is emitted by a prominence as a result of resonance scattering of solar radiation, may be computed from the following formula

$$I_v = \int_0^{\tau_0} B(t)\, e^{-(\tau_0 - t)}\, e^{-v^2}\, e^{-v^2}\, dt, \tag{15}$$

i.e., we are investigating radiation which leaves along the normal to the prominence plane. Figure 7 presents profiles of the line H_α in the case when the prominence has an optical thickness of $\tau_0 = 0.1$; 1; 5; 10 and 100. The intensities pertain to the continuous spectrum of the center of the solar disc, and the distances of the line from the center may be expressed in Doppler half-widths. The most characteristic feature of the theoretical profiles in the case of large optical thickness is their saddle-shaped form, which is frequently observed in the spectra of prominences. When the optical thickness decreases, the profiles acquire the form of a Gaussian curve. The areas of the line profiles increase with the optical thickness. This is natural, since the prominence absorbs and, consequently, radiates a great deal of solar energy when τ_0 increases. /16

Let us compare the results obtained with the observations. Table 2 presents the main characteristics of the profiles shown in Figure 7, as well as the observational data taken from (Ref. 14). The "maximum intensity" pertains to the "horns" of the profile. The total halfwidth is measured in the cross section corresponding to half of this intensity. The equivalent widths A_λ are expressed in milliangstroms of the continuous spectrum of the disc center; it

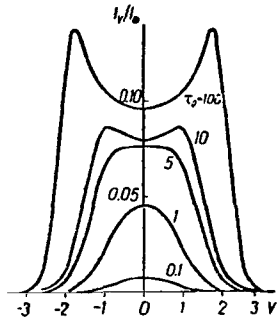

Figure 7

Theoretical Profiles of H_α; Intensities Pertain to the Center of the Solar Disc.

is assumed that $\Delta\lambda_D$ equals 0.33 Å. As may be seen, the theoretical and observational profiles agree very closely. For example, the numbers characterizing the theoretical profile in the case of $\tau_0 = 10$ coincide, within an accuracy of ~10%, with the quantities I_{max}, I_c, $2v_{\frac{1}{2}}$, and $\frac{A_\lambda}{\Delta\lambda_D}$ obtained from observations.

The observed profiles are frequently asymmetrical, and are distorted by absorbing material located in the line of sight between the prominence and the observer. The line profile also assumes an incorrect form, due to the Doppler effect during the random motion of individual prominence sections. However, it is possible to select the parameters /17 $\Delta\lambda_D$ and τ_0, for which the theoretical profiles closely describe the profiles of the observed lines. It is possible to determine these parameters by employing the simple formula

$$I_\nu = \bar{B}(1 - e^{-\tau_\nu}), \tag{16}$$

in which the source function is constant over the entire width of the prominence. The profile described by formula (16) for $\tau_0 = 10$ is shown in Figure 8 by the dotted line. As is known, it has a flat apex. If this profile is drawn through the apexes of the "horns" (see Figure 8), it clearly represents wings of the observed and theoretical profiles obtained from the exact formula (15). This may be explained by the fact that formula (16) is obtained if the mean value of the source function is removed from under the integral in the exact formula. The parameters $\Delta\lambda_D$ and also τ_0 are identical for these

TABLE 2

Date	τ_0	I_{max}	I_c	$2v_{\frac{1}{2}}$	$\frac{A_\lambda}{\Delta\lambda_D}$	$\Delta\lambda_D$, Å	$2\Delta\lambda_{\frac{1}{2}}$, Å	$\mathring{A}_\lambda$, mÅ	h"
Theoretical Data									
	1	0.045	0.045	2.00	92	0.33	0.66	30	30
	5	.076	.076	2.80	218	.33	0.92	72	30
	10	.086	.079	3.20	272	.33	1.06	90	30
	100	.138	.096	4.50	522	.33	1.50	173	30
Observational Data									
5/27 1958	6	.065	.054	2.90	177	.44	1.28	78	15
6/16 1958	8	.084	.073	3.08	249	.45	.42	112	43
7/7 1958	4	.062	.057	2.70	151	.37	.00	56	40
10/9 1959	16	.046	.040	3.80	164	.28	.06	46	20

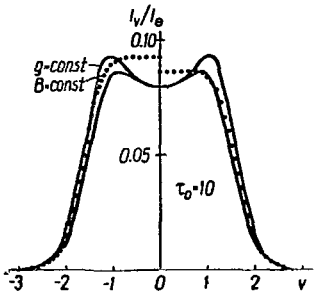

Figure 8

Comparison of Profiles Having Flat Apexes (16) for $\tau_0 = 10$ with Profiles Corresponding to Uniform Distribution of the Sources and Corresponding to the Distribution According to Figure 2.

formulas. Therefore, they may be determined by the previous methods -- for example, by means of "six branch cuts" (Ref. 13). The values of $\Delta\lambda_D$ and τ_0 are given in Table 2, along with the observational data obtained by this method.

Many prominences have an irregular form, and consist of individual filaments, so that the direct solar radiation penetrates to the inner regions of the prominence without absorption. In this connection, it is interesting to obtain a solution of the integral equation for the limiting case -- for uniform distribution of the radiation sources over the prominence thickness. The strength of the sources thus remains undetermined, since -- if the absorption of solar radiation is disregarded -- this leads to an inner contradiction in the formulation of the problem. The source function in the case of uniform distribution of the energy sources ($g(\tau) = \text{const}$) for a prominence having /18 $\tau_0 = 10$ is shown by the dotted line in Figure 5, and the profile of the line is shown in Figure 8. For purposes of comparison, we show the corresponding profile having a flat apex (16) in Figure 8. The maximum of the source function and, consequently, the dip in the center of the line are much more apparent than in the first variation of the calculations. This profile was not compared with the observed profile, because the central intensity and the equivalent width (total energy) were undetermined, since the strength of the sources was assumed to be arbitrary. In this connection, it is our opinion that the comparison of the theoretical profile with the observed profile, which was done in (Ref. 3, 12) is arbitrary to a certain extent. The strength of the sources is not given in these studies; therefore, the central intensities and the equivalent widths were not determined. At an electron temperature of 5000°, which was assumed in these studies, the electron concentration will be too small for recombination radiation in the line H_α. We should also point out that the formula given in (Ref. 12) for computing the profile is not applicable to prominences, since it pertains to the radiation of the entire sphere which is used as the model, whereas observations are customarily made of the spectrum from a small section of the prominence, which is delineated by the spectrograph slit.

* * *

It follows from the statements presented above that the theoretical profiles of the line H_α, computed for different models of a prominence, differ

very little from each other. In actuality, the profiles which we obtained for a prominence having the form of a flat plate are very similar to the profiles computed by Sobolev (Ref. 12) for the model of a spherical prominence. Since we do not know the form and precise structure of each given parameter, there is no point in performing a careful computation of the theoretical line profile, and we may confine ourselves to the results obtained above.

The hypothesis was advanced in the study mentioned above that illumination of the prominence in the line H_α is resonance scattering of solar radiation. This hypothesis enables us, without any additional assumptions, to calculate not only the form of the line, but also the total energy radiated by the prominence in this line. The calculated intensities of the "horns" for saddle-shaped profiles, as well as the central intensities, may be expressed -- without formulating additional hypotheses -- in units of the continuous spectrum of the center of the solar disc.

The central intensities obtained theoretically, the intensities of the /19
"horns", the halfwidths of the profile, and the total energies correspond, within an accuracy of 10-20%, to observations of prominences having the corresponding optical thickness. Thus, the total energy radiated by a prominence in the line H_α is caused by resonance scattering of solar radiation. It is apparent that the electron concentration and the electron temperature must not be too high, since the population of the third level of the hydrogen atom cannot depend on electron collisions and recombinations.

Some of the general conclusions of the study may be employed to interpret the illumination of prominences in other lines in which the optical thickness is small. It was shown that the source function within the prominence having the optical thickness $0 \leqslant \tau_0 \leqslant 3$ differs from $r_c w$ by only a few percents -- the product of the residual intensity of the Fraunhofer line by the dilution coefficient. For large optical thicknesses, the source function is larger than this value -- the phenomenon of quanta "accumulation" within the prominence enters the picture. For a prominence having the optical thickness of 100, the radiation density in the central regions is twice as high as that at the same point in space where there is no prominence due to this phenomenon.

REFERENCES

1. Gurtovenko, E. A., Semenova, N. N. Izvestiya Glavnoy Astronomicheskoy Observatorii (GAO), Akademii Nauk USSR, 4, 31, 1961.
2. Shi-Khuey, Ye. Izvestiya Krymskoy Astrofizicheskoy Observatorii (KrAO), 25, 180, 1961.
3. Zvonareva, M. L. Solnechnyye Dannyye, 7, 64, 1963.
4. Ivanov, V. V. Astronomicheskiy Zhurnal (AZh), 40, 257, 1963.
5. Ivanov-Kholodnyy, G. S. Izvestiya KrAO, 15, 69, 1955.
6. Kostik, R. I., Orlova, T. V. Solnechnyye Dannyye, 9, 54, 1962.
7. Krat, V. A. Doklady Akademii Nauk (DAN), SSSR, 166, 619, 1956.
8. Krat, V. A., Krat, T. V. Izvestiya GAO at Pulkova, 155, 1, 1956.
9. Krylov, N. M. Bogolyubov, N. N. DAN SSSR, 283, 1929.

10. Sobolev, V. V. Perenos Luchistoy energii v atmosferakh zvezd i planet (Radiant Energy Transfer in the Atmospheres of Stars and Planets). Gosudarstvennoye Izdatel'stvo Tekhnicheskoy i Teoreticheskoy Literatury (GITTL), Moscow, 1956.
11. Sobolev, V. M. Izvestiya GAO at Pulkova, 158, 12, 1958.
12. Sobolev, V. V. AZh, 39, 632, 1962.
13. Yakovkin, N. A., Zel'dina, M. Yu. Solnechnyye Dannyye, 12, 67, 1960.
14. Yakovkin, N. A., Zel'dina, M. Yu. AZh, 40, 847, 1963.
15. Yakovkin, N. A., Zel'dina, M. Yu. AZh, 41, 336, 1964.
16. Jefferis, J. T. M. N., 115, 616, 1955.
17. Jefferis, J. T., Orrall, F. Q. Aph. J., 127, 714, 1958.
18. Minnaert, M., Mulders, G. F., Houtgast, J. Fotometria Atlaso de la Sunos-/20 pektro (Photometric Atlas of the Solar Spectrum). Utrecht, 1940.
19. Zirin, H. Aph. J., 131, 714, 1960.

COMPARISON OF FAINT AND BRIGHT PROMINENCES

N. N. Morozhenko

As a result of analyzing hydrogen and metal lines, the values of the electron temperature, electron concentration, concentration of neutral hydrogen and effective thickness in hydrogenous and metallic filaments of bright prominences are obtained. Owing to lack of data, it is possible in faint prominences to determine only the limits of the change of these values in hydrogenous filaments. The distinction in the spectra of faint and bright prominences may be explained by the difference in optical thickness, which is as high as 2-3 orders in the hydrogen and ionized calcium lines.

Observations have shown that during maximum solar activity there is a large amount of extended, comparatively bright prominences, which form long, dense filaments at the edge of the disk. The spectra of particularly dense prominences contain a large amount of lines of metals, helium, and hydrogen up to H_{20} and higher. /21

The faint prominences, as a rule, appear during minimum solar activity. The H and K lines of ionized calcium are observed in their spectra, as well as the faint line D_3 of helium, the hydrogen lines H_α -- of normal brightness -- and the lines of H_β and H_γ which are considerably fainter. The intensity of the line H_δ is insignificant; this line does not develop even at large exposures in spectrograms of the faintest prominences. In order to clarify the difference between the spectra of bright and faint objects, we selected the three brightest prominences (1, 2, 3) which were observed on July 13, 1960, July 24, 1960, September 24, 1961, respectively, and four very faint prominences (I, II, III, IV), which were observed on September 13, 1962, September 18, 1962, June 21, 1963, June 28, 1963.

Hydrogen Filaments of Bright Prominences

Let us investigate the hydrogen spectrum and physical conditions in hydrogen filaments of bright prominences. Table 1 presents the results derived from measuring the hydrogen lines (optical thicknesses τ_0 in the lines from H_α to H_g) and the Doppler halfwidths $\Delta\lambda_D$ of the lines, which pertain to the population of the 3-9th levels of hydrogen atoms, which were found by the method of Conway. This table also presents the relative Doppler halfwidths $\Delta\lambda_D/\lambda$ of the lines H_α - H_{16}. The Doppler halfwidths from H_{10} to H_{16} were determined according to the halfwidths of these lines. /23

In this study we determined the electron temperatures of hydrogen

TABLE 1

Lines	Prominence 1				Prominence 2				Prominence 3			
	τ_0	$\Delta\lambda_D$	$\frac{\Delta\lambda_D}{\lambda}\cdot 10^5$	$\frac{N_i}{N_2}\cdot 10^3$	τ_0	$\Delta\lambda_D$	$\frac{\Delta\lambda_D}{\lambda}\cdot 10^5$	$\frac{N_i}{N_2}\cdot 10^3$	τ_0	$\Delta\lambda_D$	$\frac{\Delta\lambda_D}{\lambda}\cdot 10^5$	$\frac{N_i}{N_2}\cdot 10^3$
H_α	90.00	0.250	3.82	4.97	31.00	0.274	4.18	3.96	—	—	—	—
H_β	12.00	.180	3.71	1.88	—	—	—	—	—	—	—	—
H_γ	4.20	.153	3.52	1.74	1.42	.170	3.90	1.84	—	—	—	—
H_δ	2.00	.145	3.54	1.61	0.67	.158	3.87	1.92	2.60	0.180	4.40	2.04
H_ε	1.10	.135	3.39	1.54	—	—	—	—	0.70	.162	4.08	3.44
H_8	0.75	.133	3.43	2.52	0.20	.150	3.87	2.80	—	—	—	—
H_9	0.50	.130	3.39	3.00	—	.144	3.75	—	0.50	.156	4.06	3.58
H_{10}	0.36	.130	3.42	—	—	.150	3.95	—	0.35	.166	4.36	4.12
H_{11}	0.22	.130	3.45	—	—	.158	4.20	—	0.25	.173	4.59	5.20
H_{12}	0.17	.135	3.60	—	—	.167	4.46	—	—	.178	4.76	—
H_{13}	0.13	.140	3.78	—	—	.171	4.59	—	—	.183	4.93	—
H_{14}	0.10	.150	4.04	—	—	.167	4.50	—	—	.193	5.18	—
H_{15}	0.08	.150	4.05	—	—	—	—	—	—	.198	5.35	—
H_{16}	0.07	.150	4.06	—	—	—	—	—	—	—	—	—

filaments based on the magnitude of the radiation flux in the line L_α at the boundary of the Earth's atmosphere. According to data derived from rockets, this flux comprises 4-6 erg/cm^2·seconds. The temperature of L_α-radiation T_{L_α} at the boundary of the photosphere is thus found to equal 7000-7200°, and at the altitude of the prominence it is about 6800-7000°.

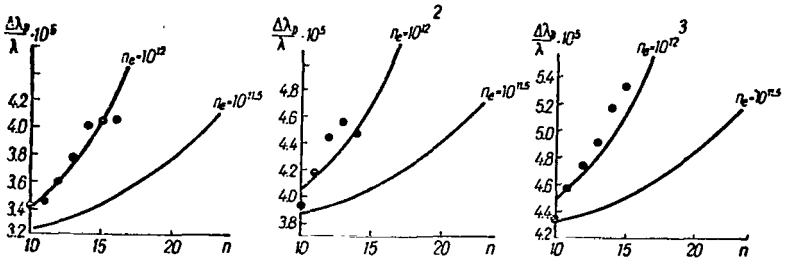

Figure 1

Comparison of Observations (Dots) with Theoretical Curves for the Dependence of $\frac{\Delta\lambda_D}{\lambda}$ on the Number of the Line

Assuming that the flux of L_α-radiation does not change when penetrating the prominence, and under the condition that $T_e = T_{L_\alpha}$ (Ref. 8), we obtained the electron temperatures of hydrogen filaments of the prominences equalling 7000°.

The influence of the Stark effect upon the higher terms of the Balmer series was utilized to determine the electron concentrations in hydrogen filaments of bright prominences. Graphs showing the dependence of $\Delta\lambda_D/\lambda$ on the number of the line for prominences 1, 2, 3 were compared with theoretical curves presented in (Ref. 10). These curves were compiled on the assumption of expansion of the line by the Stark effect. Figure 1 shows that the best agreement with the theoretical curves is obtained in the case of $n_e = 10^{12}$ for prominences 1 and 2, and in the case of $n_e = 10^{12.1}$ for prominence 3.

For $T_e = 7000°$, according to the table given in the article by V. M. Sobolev (Ref. 7), we may select the concentration of neutral hydrogen atoms $n_1 = 1.7\cdot10^{14}$ at which the electron concentrations (obtained from this table and determined according to the Stark effect) are equal. If we know the values/24 of T_{L_α} and N_2, we may employ the Boltzmann formula to determine the amount of hydrogen atoms in the ground state N_1 in a column with a base of 1 cm^2 along the line of sight, and the effective thickness of hydrogen filaments h in bright prominences. This thickness equals $5\cdot10^6$ cm on the average (Table 2).

TABLE 2

Number of Prominence	$N_2 \cdot 10^{-14}$	$N_1 \cdot 10^{-20}$	$n_e \cdot 10^{-12}$	$n_1 \cdot 10^{-13}$	$h \cdot 10^{-7}$
1	1.61	1.61	1 00	2.0	0 8
2	0.57	0.57	1 00	2.0	0.3
3	1.92	1.92	1.12	3.0	0.6

Hydrogen Filaments of Faint Prominences

Table 3 presents the results derived from measuring hydrogen lines of faint prominences. A comparison of the parameters τ_0 of bright and faint prominences shows that bright prominences are considerably more dense -- τ_0 is 50-100 times greater in them than in faint prominences. The ratios of N_i/N_2 differ only within the limits of the errors with which they are determined, which indicates that the mechanism by which hydrogen is excited in prominences of both types is the same.

Faint prominences may be investigated in a similar manner. Since there are no specific data on the change in the intensity of L_α-radiation as a function of the cycle of solar activity, we employed the same values of electron temperatures for faint prominences, which were observed in 1962-1963, as for bright prominences -- $T_e = 7000°$. The number of neutral hydrogen atoms N_1 was found based on the known number of hydrogen atoms in the second quantum state N_2 for faint prominences. This number proved to be almost two orders of magnitude smaller than for hydrogen filaments of bright prominences. With different values of the effective thicknesses given, we may determine certain values of the hydrogen atom concentrations n_1 based on the determined values of N_1. We may find different values of the electron concentrations for the hydrogen atom concentrations, by means of the well known T_e and $T_{L\alpha}$ according to Table 5 given in (Ref. 7). Table 4 presents the results derived from studying the hydrogen lines of faint prominences. The column with the index v_t presents the values of turbulent velocities in the hydrogen filaments of faint prominences, which were determined according to the known $\Delta\lambda_D$ and T_e.

It may be seen from Table 4 that when the effective thickness of hydrogen /25 filaments changes from 10^9 to 10^5, the electron concentrations change from 10^{10} to 10^{12}. There is no possibility of determining the electron concentrations independently for faint prominences, as is done for bright prominences. At an effective thickness of $h = 10^7$ cm, which is obtained for bright prominences, n_e is of the order 10^{11}. If it is assumed that the values of n_e in hydrogen filaments of bright and faint prominences are the same (of the order 10^{12}), we must then assign a value of $h=10^5$ cm for the effective thicknesses of hydrogen

TABLE 3

Line	Prominence I			Prominence II			Prominence III			Prominence IV		
	τ_0	$\Delta\lambda_D$	$\frac{N_i}{N_2}\cdot 10^3$	τ_0	$\Delta\lambda_D$	$\frac{N_i}{N_2}\cdot 10^3$	τ_0	$\Delta\lambda_D$	$\frac{N_i}{N_2}\cdot 10^3$	τ_0	$\Delta\lambda_D$	$\frac{N_i}{N_2}\cdot 10^3$
H_α	1.50	0.300	5.50	1.70	0.295	5.36	3.00	0.347	4.07	1.30	0.295	4.62
H_β	0.20	0.220	2.37	0.20	0.205	3.52	0.42	0.255	2.77	0.30	0.225	1.19
H_γ	—	—	—	0.05	0.183	4.29	0.10	0.228	5.41	0.07	0.200	2.29

filaments of faint prominences. We may select the values of $n_e = 10^{10} - 10^{11}$ and $h = 10^8 - 10^7$ cm, which coincide fairly well with the data provided by other authors.

An investigation of the hydrogen lines of bright and faint prominences has shown that the physical conditions in the hydrogen filaments of these prominences are almost the same. The differences in the nature of the hydrogen spectra of bright and faint prominences may be primarily explained by the great difference between the optical thicknesses of hydrogen filaments. Self-absorption in bright prominences weakens the observed intensity of radiation of the line H_α by almost two orders of magnitude, whereas there is practically no self-absorption in this line in faint prominences. Therefore, if the observed intensities H_α in prominences are almost identical, with an increase in the number of the line the difference between the intensities becomes increasingly larger, as the self-absorption decreases in the bright prominences. As a result of this, we may trace the hydrogen lines in the bright prominences /26 up to H_{20} and above, whereas the line Hδ is barely visible in faint prominences.

TABLE 4

Prominence Number	$N_2\cdot 10^{-12}$	$N_1\cdot 10^{-19}$	$h=10^9$		$h=10^8$		$h=10^7$		$h=10^6$		$h=10^5$		v_t, km/sec
			$n_1\cdot 10^{-10}$	$n_e\cdot 10^{-10}$	$n_1\cdot 10^{-11}$	$n_e\cdot 10^{-10}$	$n_1\cdot 10^{-12}$	$n_e\cdot 10^{-11}$	$n_1\cdot 10^{-13}$	$n_e\cdot 10^{-11}$	$n_1\cdot 10^{-14}$	$n_e\cdot 10^{-12}$	
I	3.2	1.8	1.8	2.0	1.8	6.5	1.8	1.7	1.8	3.6	1.8	1.1	7.5
II	2.9	1.6	1.6	1.8	1.6	5.9	1.8	1.5	1.6	2.5	1.6	0.8	7.0
III	6.8	3.9	3.9	3.6	3.9	11.7	3.9	3.1	3.9	8.2	3.9	2.0	10.9
IV	3.6	2.1	2.1	2.3	2.1	7.6	2.1	1.9	2.1	4.3	2.1	1.0	7.0

Metallic Filaments of Bright Prominences

The lines H and K of ionized calcium and D_1, D_2 of sodium were selected, in order to study the metallic filaments in bright prominences. Tables 5 and 6 present the results derived from analyzing these lines according to the method

of Conway.

Lines of ionized calcium in bright prominences were studied in (Ref. 3). It was established that the opitcal thicknesses of the prominences in this line have values on the order of 10^3.

In our study, we disregarded any assumptions regarding the location of the metallic line luminescence, and also examined the lines D_1 and D_2 of sodium. The equation of the ionization equilibrium was solved for sodium. When this equation was formulated, we took into account photoionization and ionization by electron collision from the levels 3^2P and 3^2S, and recombinations at all the levels indicated in Figure 2. In addition, we determined the number of photoionization events from the levels 4^2S, 4^2P and all the levels lying above, in the form of level 5 with the ionization potential $\chi 5 = 1.24$ eV. The photoionization cross section from this combined level, which was advanced by S. V. Moskvin (Ref. 4), was assumed. The photoionization cross sections from the levels 3^2S, 3^2P, 4^2S, 4^2P were taken from the tables given by Allen (Ref. 1).

Calculations have shown that the number of photoionization events from the level 3^2P is five times greater than from the main level 3^2S, whereas photoionization from the levels 4^2S and 4^2P and above may be disregarded. The number of photoionization events was computed according to the following formula

$$Z_{\Phi}^{(i)} = n_i W \frac{8\pi}{c^2} k_i \nu_i^3 E_i \left(\frac{\chi_i}{kT}\right)$$

TABLE 5 /27

Prominence Number	KCa^+			$Ca_i^+ \cdot 10^{-15}$	D_1Na			D_2Na			$(Na_1)_0 \cdot 10^{-11}$
	τ_0	$\Delta\lambda_D$	$I \cdot 10^{-4}$, erg/cm^2. sec.		τ_0	$\Delta\lambda_D$	$I \cdot 10^{-3}$, erg/cm^2. sec.	τ_0	$\Delta\lambda_D$	$I \cdot 10^{-3}$, erg/cm^2. sec.	
1	1800	0.043	4.05	1.54	0.35	0.072	3.90	0.76	0.072	5.80	4.66
2	1300	0.053	3.95	1.40	0.55	0.073	3.80	0.91	0.073	5.60	6.50
3	2000	0.075	19.50	2.90	0.48	0.100	8.80	0.98	0.100	12.20	8.60

where n_i, k_i, ν_i, χ_i represent, respectively, the population, the photoionization cross section, the limiting frequency of the series, and the ionization potential from the i^{th} level; N and T represent, respectively, the dilution and temperature of ionizing radiation. The temperature of ionizing radiation was computed according to the Planck formula for different levels /28

TABLE 6

/27

Prominence Number	HCa^+			KCa^+			$(Ca_I^+)_0$	$(Ca_I^+)_n$	v_t, km/sec
	τ_0	$\Delta\lambda_D$	I, erg/cm^2·sec.	τ_0	$\Delta\lambda_D$	I, erg/cm^2·sec.			
III	2.10	0.135	$4.8\cdot10^4$	3.90	0.140	$6.5\cdot10^4$	$1.12\cdot10^{13}$	$0.95\cdot10^{13}$	10.2
IV	0.90	0.095	$1.5\cdot10^4$	1.75	0.090	$2.0\cdot10^4$	$3.24\cdot10^{12}$	$5.00\cdot10^{12}$	6.9

$$I_\odot W = \frac{2hc^2}{\lambda^5} e^{-\frac{h\nu}{kT}},$$

where $I_\odot$ is the intensity of the continuous solar radiation beyond the limit of the series of the given level; λ is the limiting wavelength of the series. The value of $I_\odot$ for the series limit of level 3^2S, having the wavelength λ = 2412 Å, was taken from the study by G. M. Nikol'skiy (Ref. 5); its value for the series limits of the remaining levels was taken from (Ref. 1). Different temperatures were obtained for the radiation producing ionization from the levels 3^2S, 3^2P, 4^2S and 4^2P - 4700, 5000, 4000, 3500°, respectively.

The equation of the ionization equilibrium was written in the following form (we have employed the indexes (1) and (2) to designate the levels 3^2S and 3^2P, respectively)

$$Z_{\text{ф}}^{(1)} + Z_{\text{ф}}^{(2)} + Z_{\text{ст}}^{(1)} + Z_{\text{ст}}^{(2)} = \sum_{i=1}^{\infty} R_i,$$

where $\sum_{i=1}^{\infty} R_i$ is the sum of recombinations at every level, taken from (Ref. 4); $Z_p^{(1)}$ and $Z_p^{(2)}$ is the number of photoionization events from the levels 3^2S, 3^2P; $Z_{ct}^{(1)}$ and $Z_{ct}^{(2)}$ -- the number of ionization events by electron collision from the same levels, which are determined according to the following formula

$$Z_{\text{ст}}^{(i)} = n_i n_e q_i \left(\frac{8kT_e}{\pi m}\right)^{\frac{1}{2}} \left(1 + \frac{\chi_i}{kT_e}\right) e^{-\frac{\chi_i}{kT_e}}.$$

The values of the ionization cross sections by electron collision $q_i = \chi_i^{-2}\pi a_0^2$ are: $q_1 = 6.2\cdot10^{-16}$ cm^2; $q_2 = 1.8\cdot10^{-15}$ cm^2. The values of the degree of sodium ionization are given in Table 7 as a function of T_e and n_e.

In order to make a comparison with observations, we computed the number of /29

TABLE 7

T_e \ n_e	10^8	10^9	10^{10}	10^{11}	10^{12}
4000	$2.00 \cdot 10^5$	$2.00 \cdot 10^4$	$2.00 \cdot 10^3$	$2.00 \cdot 10^2$	$2.10 \cdot 10$
6000	$2.69 \cdot 10^5$	$2.70 \cdot 10^4$	$2.70 \cdot 10^3$	$3.50 \cdot 10^2$	$1.08 \cdot 10^2$
8000	$3.26 \cdot 10^5$	$3.34 \cdot 10^4$	$4.20 \cdot 10^3$	$12.8 \cdot 10^2$	$9.90 \cdot 10^2$
10000	$4.17 \cdot 10^5$	$4.60 \cdot 10^4$	$8.94 \cdot 10^3$	$52.3 \cdot 10^2$	$4.86 \cdot 10^2$

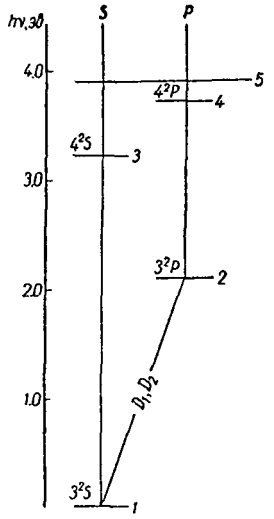

Figure 2

Diagram Showing the Levels of a Neutral Sodium Atom

atoms of neutral sodium and sodium which was ionized once. The total number of neutral sodium atoms Na_1 in metallic and hydrogen filaments was obtained, based on the optical thickness of the prominences in the resonance lines D_1 and D_2, which were analyzed according to the Conway method.

The number of ionized sodium atoms may be determined from the data on the chemical composition of the solar atmosphere. This method was employed in (Ref. 3) to determine the abundance of calcium atoms in the metallic filaments of prominences. This method is based on the fact that such elements as Na, Ca, Ti, Sr, in prominences are primarily found in a state, which has been ionized once, both in hydrogen and metallic filaments. Therefore, the number of ionized atoms of these elements determines their total (in metallic and hydrogen filaments together) abundance in the prominences. The lines Ti^+3761, Ti^+3759 and the resonance lines Sr^+4078, Sr^+4215 may be readily analyzed by the Conway method. Their optical thickness may be used to provide a fairly reliable determination of the number of ionized atoms and, consequently, the total abundance of these elements in the prominences. Employing the data on the relative chemical composition of the solar atmosphere (Ref. 9), based on the abundance of titanium and strontium we may determine both the total abundance of hydrogen, and the total abundance of calcium and sodium, and therefore the total number of ionized calcium and sodium in the prominences being studied. The data thus obtained are given in Table 8. In order to obtain the number of atoms of neutral and ionized sodium in hydrogen and metallic filaments separately, as the first approximation we assumed that hydrogen only emits in hydrogen filaments. The populations N_2, which were determined on the basis of the optical thickness of the hydrogen lines, and the values of N_1, which are given in Table 2 and which were obtained according to the Boltzmann formula, represent the number of hydrogen atoms in the second

TABLE 8

Prominence Number	$Sr_1^+ \cdot 10^{-12}$	$Ti_1^+ \cdot 10^{-14}$	$H_1 \cdot 10^{-21}$	$Ca_1^+ \cdot 10^{-15}$	$Na_1^+ \cdot 10^{-15}$	$Na_1 \cdot 10^{-11}$
1	0.52	0.43	1.10	1.54	2.20	4.66
2	0.29	0.59	1.00	1.40	2.00	6.50
3	0.96	0.83	2.06	2.95	4.12	8.60
Average	0.60	0.61	1.39	1.95	2.77	6.59

and ground states only in hydrogen filaments. The value of $Na^+ = 1.83 \cdot 10^{15}$, which was calculated according to N_1 and according to data on the chemical composition of the solar atmosphere, also represents the number of ionized sodium atoms only in hydrogen filaments. Since the values of the electron temperature and the electron concentration in hydrogen filaments are known, we may employ Table 7 to find the number of neutral sodium atoms $Na_1 = 3.7 \cdot 10^{12}$ in hydrogen filaments. This number is almost one order of magnitude greater than the observed number $(Na_1)_0 = 6 \cdot 10^{11}$ (see Table 5), which represents the total number of neutral sodium atoms both in hydrogen and metallic filaments together. /30

Since the inequality $Na_1 > (Na_1)_0$ has no meaning in physical terms, the conditions in the hydrogen filaments of the prominences to be studied may be characterized by somewhat different values of T_e and n_e, which are different from those which we employed to determine n_1 according to Table 5 given by V. M. Sobolev. It is impossible to change the value of the electron density $n_e = 10^{12}$ significantly, since it is determined according to the Stark effect. However, the electron temperatures of 7000° which we assumed for hydrogen filaments may be incorrect. Based on these considerations, we computed the number of neutral sodium atoms for several values of the electron temperature of hydrogen filaments in the case of $n_e = 10^{12}$. Table 9 presents the results derived from calculating $\frac{n_2}{n_1}$, N_1, Ca_1^+, Na_1^+, Na_1^+/Na_1 in hydrogen filaments of a certain "average" prominence for different values of T_e (and also of $T_{L\alpha}$). Table 10 presents the recalculated values in metallic filaments of an "average" prominence, which were obtained as the difference between the total content of the element in the prominence and its content in hydrogen filaments. The total content of the elements in an "average" prominence was taken from the column titled "average" in Table 8.

It may be seen from Table 9 that the condition $Na_1 \leqslant (Na_1)_0$ is fulfilled in the case of T_e = 7800 - 10,000°. Higher electron temperatures should not be selected, since in the case of T_e > 10,000° electron collision begins to have a considerable influence upon hydrogen excitation. Temperatures of /31

TABLE 9

T_e	$\frac{n_2}{n_1}$	N_1	Ca_1^+	Na_1^+	$\frac{Na_1^+}{Na_1}$	Na_1
7500	6.72·10−7	3.76·10²⁰	5.26·10¹⁴	7.53·10¹⁴	5.61·10²	1.34·10¹²
7800	6.60·10−7	4.12·10²⁰	2.97·10¹⁴	4.25·10¹⁴	7.59·10²	5.60·10¹¹
8000	1.40·10−6	1.40·10²⁰	1.96·10¹⁴	2.80·10¹⁴	8.90·10²	3.15·10¹¹
8500	2.40·10−6	5.83·10¹⁹	8.18·10¹³	1.17·10¹⁴	1.45·10³	8.07·10¹⁰
9000	3. 6·10−6	3.80·10¹⁹	5.32·10¹³	7.60·10¹³	2.42·10³	3.14·10¹⁰
10000	5. 2·10−6	2.66·10¹⁹	3.72·10¹³	5.33·10¹³	4.86·10³	2.11·10¹⁰

7800-8000° seem most probable to us, since they are closest to the temperature of L_α-radiation which we computed previously.

TABLE 10

T_e	$Na_1 \cdot 10^{-21}$	$Ca_1^+ \cdot 10^{-15}$	$Na_1^+ \cdot 10^{-15}$	$Na_1 \cdot 10^{-11}$	$\frac{Na_1^+}{Na_1} \cdot 10^{-3}$
7500	1.01	1.42	2.02	—	—
7800	1.18	1.65	2.35	1.00	23.50
8000	1.25	1.75	2.49	3.44	7.24
8500	1.33	1.87	2.65	5.78	4.57
9000	1.35	1.90	2.69	6.28	4.28
10000	1.36	1.91	2.72	6.48	4.20

Physical conditions in metal filaments were computed as follows. Table 7 was used to determine the electron concentrations in metal filaments for several given values of the electron temperature in metal filaments depending on the degree of sodium ionization; these values were calculated for specific values of the electron temperature of hydrogen filaments. Assuming that $T_e = T_{L_\alpha}$ and that the main electron supplier is hydrogen, we employed Table 5 given in (Ref. 7) to determine the hydrogen concentration in the ground state n_1 which provided the electron concentration which was already determined. The obtained concentrations of electrons and neutral atoms as a function of T_e are presented in Table 11 for different electron temperatures of hydrogen filaments. This same table presents the effective thicknesses of metal filaments, which were obtained by dividing the values of N_1, taken from Table 10, by n_1.

Based on the data presented in Table 11, the conclusion may be reached /33 that the most realistic values for the electron temperature of metal filaments ranges from 4000-5000°. In the case of $T_e < 4000°$, hydrogen concentrations in metal filaments become too large ($n_1 \geqslant 10^{15}$), and for $T_e > 5000°$ they are so small that the effective thickness of metal filaments is larger than the thickness of the entire prominence. Therefore, we may specify the following parameters for the physical conditions in metal filaments of bright prominences: $T_e = 4000\text{-}5000°$; $n_e = 10^9\text{-}10^{10}$; $n_1 = 10^{12}\text{-}10^{14}$; $h = 10^6\text{-}10^9$.

However, these estimates were obtained on the assumption that hydrogen is only emitted in hydrogen filaments. Assuming that only half or 0.1 of the

TABLE 11

T_e	n_e	n_1	h	n_e	n_1	h	n_e	n_1	h
		7800°			8000°			8500°	
4000	$7.8\cdot10^{8}$	$8.5\cdot10^{13}$	$1.4\cdot10^{7}$	$2.8\cdot10^{9}$	$1.0.10^{15}$	$1.2\cdot10^{6}$	$4.4\cdot10^{9}$	$2.5\cdot10^{15}$	$5.3\cdot10^{5}$
4500	$8.9\cdot10^{8}$	$4.8\cdot10^{14}$	$2.5\cdot10^{8}$	$3.1\cdot10^{9}$	$5.0\cdot10^{13}$	$2.5.10^{9}$	$4.8.10^{9}$	$1.2\cdot10^{14}$	$1.1\cdot10^{7}$
5000	$1.0\cdot10^{9}$	$2.2\cdot10^{11}$	$5.4\cdot10^{9}$	$3.3\cdot10^{9}$	$3.1\cdot10^{12}$	$4.0\cdot10^{8}$	$5.2\cdot10^{9}$	$7.3\cdot10^{12}$	$1.8\cdot10^{8}$
6000	$1.2\cdot10^{9}$	$1.0\cdot10^{10}$	$1.2\cdot10^{11}$	$4.1\cdot10^{9}$	$1.1\cdot10^{11}$	$1.2\cdot10^{10}$	$6.3\cdot10^{9}$	$2.3\cdot10^{11}$	$5.8\cdot10^{8}$
		9000°			9500°			10 000°	
4000	$4.5\cdot10^{9}$	$3.0\cdot10^{15}$	$4.5\cdot10^{5}$	$4.6\cdot10^{9}$	$3.1\cdot10^{15}$	$4.4.10^{5}$	$4.7\cdot10^{9}$	$3.1\cdot10^{15}$	$4.4\cdot10^{5}$
4500	$5.0\cdot10^{9}$	$1.4\cdot10^{14}$	$9.7\cdot10^{6}$	$5.3\cdot10^{9}$	$1.4\cdot10^{14}$	$9.4\cdot10^{6}$	$5.6\cdot10^{9}$	$1.5\cdot10^{14}$	$9.1\cdot10^{6}$
5000	$5.5.10^{9}$	$8.5\cdot10^{12}$	$1.6\cdot10^{8}$	$6.1\cdot10^{9}$	$8.6\cdot10^{12}$	$1.6\cdot10^{8}$	$6.8\cdot10^{9}$	$8.6\cdot10^{12}$	$1.6\cdot10^{8}$
6000	$6.8\cdot10^{9}$	$2.5\cdot10^{11}$	$5.4\cdot10^{9}$	$8.4\cdot10^{9}$	$2.6\cdot10^{11}$	$5.3\cdot10^{9}$	$1.0\cdot10^{10}$	$2.6\cdot10^{11}$	$5.2\cdot10^{9}$

observed energy of the hydrogen lines is emitted in hydrogen filaments, we obtain almost the same parameters n_e, n_1 and h, but the lower boundary of the electron temperature of hydrogen filaments is displaced to 7500 or 7000°, respectively. Under the conditions that $T_e = T_{L_\alpha}$ = 4000-5000°; $n_e = 10^9$-10^{10}; $n_1 = 10^{12}$-10^{14}, the degree of hydrogen excitation is too low, and radiation of hydrogen in the metallic filaments is four orders of magnitude lower than the observed radiation. Therefore, this study presents calculations in the form of definite tables, which are compiled on the assumption that hydrogen is mainly emitted in hydrogen filaments. According to the tables given in (Ref. 7), we may select a concentration of neutral hydrogen which provides an electron concentration of $n_e = 10^{12}$ for the electron temperature of hydrogen filaments of 8000°. If we know the concentration and number of hydrogen atoms in the ground state, we may find the effective thickness of hydrogen filaments of the prominences being studied. The quantities N_1, n_e, n_1, and h computed for the temperature T = 8000° are given in Table 2. The values of N_2 which are given in this table were obtained on the basis of the optical thickness of the hydrogen lines.

A comparison of the data presented in Tables 9 and 10 shows that the content of hydrogen, ionized calcium, and ionized sodium in metal filaments of bright prominences is one-two orders of magnitude higher than in hydrogen filaments.

Metal Filaments of Faint Prominences

There are only very limited possibilities for studying the metal filaments of faint prominences. Only the lines H and K of ionized calcium may be observed from the lines of the metals. In prominence I, these lines have a /34
composite profile, consisting of several profiles which are superposed upon each other and each of which is displaced with respect to the other. In prominence II, the lines H and K are overexposed. Since these lines could not be analyzed with the requisite accuracy, we did not investigate them. The profiles of lines H and K in prominences III and IV were analyzed according to the Conway method. The results derived from the analysis are presented in Table 6. It may be seen from the table that the optical thicknesses in the lines H and K in faint prominences are small, and only amount to several units, i.e., they are two-three orders of magnitude smaller than in faint prominences. The turbulent velocities presented in the table agree fairly well with the turbulent velocities of hydrogen filaments of faint prominences (see Table 4). The heading $(Ca^+)_{1\,0}$ in Table 6 designates the total amount of ionized calcium atoms in faint prominences determined according to the optical thickness of the lines H and K. The adjacent column gives the amount of ionized calcium atoms which are only contained in the hydrogen filaments of these prominences. They were determined from the hydrogen content at a temperature of 8000° and from data on the chemical composition. These values almost coincide. If we take the fact into account that the turbulent velocities in hydrogen and metal filaments of faint prominences also coincide fairly well, we may reach

the conclusion that the observed lines H and K of faint prominences are emitted primarily in hydrogen filaments. This means that the calcium content (and consequently the content of the remaining elements) in metal filaments of faint prominences is considerably lower than in hydrogen filaments (in contrast to bright prominences).

REFERENCES

1. Allen, K.U. Astrophysical Quantities. Izdatel'stvo Inostrannoy Literatury (IL), Moscow, 1961.
2. Morozhenko, N.N. Izvestiya Glavnoy Astronomicheskoy Observatorii (GAO), AN USSR, 5, 1, 1963.
3. Morozhenko, N.N. V kn: Spektrofotometricheskiye Issledovaniya aktivnykh obrazovaniy na Solntse (In the Book: Spectrophotometric Research on Active Formations on the Sun). "Naukova Dumka", Kiev, 1964.
4. Moskvin, Yu.V. Optika i Spektroskopiya, 15, 5, 1963.
5. Nikol'skiy, G.M. Geomagnetizm i Aeronomiya, 2, 1, 1962.
6. Sobolev, V.M. Izvestiya GAO, AN SSSR, 21, 163, 1960.
7. Sobolev, V.M. Izvestiya GAO, AN SSSR, 22, 167, 1961.
8. Yakovkin, N.A. Solnechnyye Danyye, 8, 67, 1963.
9. Goldberg, L., Müller, E.A., Aller, L.H. Aph. J., Suppl., 45, 1960.
10. Hirayama, T. Publ. of Astron. Soc. of Japan, 45, No. 2, 1963.

RESULTS DERIVED FROM SPECTROPHOTOMETRY OF SEVERAL PROMINENCES

M. Yu. Zel'dina, A. N. Sergeyeva

Spectra were obtained for four bright prominences with a dispersion of 0.85 Å/mm. The kinetic temperature, Doppler halfwidths and the population of the excited levels of atoms of hydrogen, helium and metals are determined.

This article represents a continuation of spectrophotometric research on /36
prominences which was initiated several years ago at the Kiev Astronomical Observatory. The spectra were photographed on a mirror diffraction spectrograph with a focal length of 6 m and a grid of 82 × 100 mm with a dispersion of 0.85 Å/mm. The image of the Sun on the spectrograph slit was about 73 mm in diameter, and the width of the slit was 0.045 mm. Rot-rapid plates were employed with a dimension of 12 × 24 cm, on which 13 sections of the prominence spectrum were projected. Each of the spectrum sections had a dimension of 100 Å, and the sections of the disc center spectrum had a dimension of 50 Å. Photography was performed in the third series, and only H_α and D_3 -- in the second series. A yellow (YS-16), a green (SGS-18) and an ultraviolet (PS-11) filter were employed. Exposure time was as follows: H_α -- 3 seconds, sodium doublet -- 10 seconds, green magnesium triplet -- 40 seconds, the remaining lines in the visible region -- 15 seconds, and in the ultraviolet up to the line $Ti^+\lambda$ 3685 Å -- 30 seconds. The spectrum of the disc center was photographed through a graduated optical wedge and a neutral filter (NS-9) with the same exposure times as for the prominences. The entire program required about 6 minutes for a prominence, and 7 - 8 minutes for the disc center. The plates were developed in a D-76 developer for 15 minutes at a temperature of 18°C. Since the calibrated-standardized spectra and the spectra of the prominence were on the same plate, they were processed under identical conditions. The /37
total diffuse light of the spectrograph was very small; it comprised about 0.2%.

The photometry of the negatives was performed on a MF-4 recording microphotometer under the following conditions: Transmission -- a factor of 50; amplification -- a factor of 20; slit width -- 0.74 mm; slit height -- 3 mm; recording rate -- 25 mm/min. The intensity curves were compiled from the microphotograms obtained by means of a semi-automatic "Intensigraph" device.

In order to exclude diffuse light, photometric cross sections were taken above the prominence, where there were no emission lines. Since it was necessary to correctly subtract the spectrum of diffuse light from the main spectrum according to wavelengths, two sharp Fraunhofer lines were selected on both sides of the emission line. These Fraunhofer lines were subjected to photometry, together with each of the indicated spectra. By employing this method, we were able to analyze the spectrograms of four bright prominences, in whose spectra all the Balmer lines from H_α to H_{12} - H_{20}, inclusively, were located,

as well as many lines of helium and metals.

TABLE 1

Date	Standard Time	Position Angle	Brightness	Height Above Edge of Sun	Transparency
6/8 1959	9^h50^m	-	-	30"	Very good
7/9 1959	9 40	65 E	3	20	Good
10/28 1959	11 00	115 E	3	30	Satisfactory
6/23 1960	9 25	245 W	3	35 and 50	Good

Table 1 presents the date, the time of observation given in standard time, the positionalangle from the north pole of the Sun, the brightness according to (Ref. 2), the distance of the photometric cross section from the edge of the disk, and the transparency characteristics of the atmosphere at the time of observation.

Figures 1 and 2 present the profiles of all the prominence emission lines observed between June 8 and July 9, 1959. When the spectrograms were analyzed, the instrument profile was not taken into account; its total halfwidth in the second series comprised 0.056 Å, and 0.074 Å in the third series. The intensities are given in units of the continuous spectrum of the center of the solar disk. The wavelengths are given in millimicrons. The central intensities of the lines are also presented. For purposes of convenience, the profiles are /38 presented so that they have the same height and the same scale along the abscissa axis. H_α may be clearly distinguished from all of these lines. It is two times wider than H_β, whereas its central intensity differs by only 10-30%. The profile of H_α has two humps, and H_β has a flat apex. There are two slight humps in the K Ca^+ line.

The majority of the lines in the prominence spectrum have a Gaussian pro- /39 file

$$I_v = I_0 e^{-v^2}.$$

Therefore, their Doppler halfwidth was determined from the following equation

$$\Delta\lambda_D = 1.20\Delta\lambda_{\frac{1}{2}},$$

where $\Delta\lambda_{\frac{1}{2}}$ is half of the line halfwidth.

The brightest lines are distorted by self-absorption, and their profiles /40 may be represented by the following formula

$$I_v = I_0 \frac{1 - e^{-\tau_0 e^{-v^2}}}{1 - e^{-\tau_0}},$$

where τ_0 is the optical thickness of the prominence in the center of the line. Self-absorption was taken into account by the methods described in (Ref. 3).

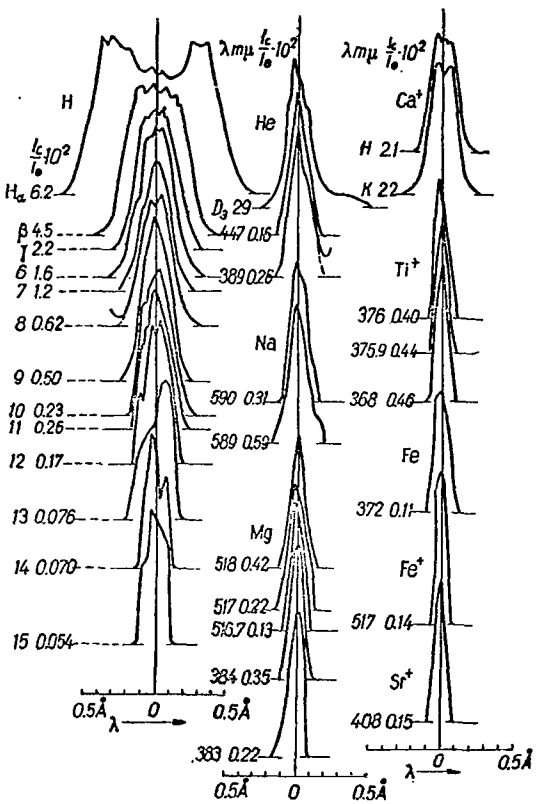

Figure 1

Profiles of the Emission Lines in the Spectrum of a Prominence Observed on June 8, 1959.

The optical thicknesses obtained are given in Table 2. The first column presents the parameters determined by means of the halfwidth curve (determined for all the lines at once); the second column gives the parameters determined according to the profile width in six cross sections of each line separately. It may be seen from the table that the relationship between the optical thicknesses, determined by the second method for the Balmer lines and the H and K Ca^+ lines, does not correspond to the number λf -- the product of the wavelength by the oscillator strength. In addition, this method frequently yields Doppler widths for H_α and H_β which are too high as compared with $\Delta\lambda_D/\lambda$, obtained according to the profiles of the higher terms of the Balmer series. Therefore, observations of the emission lines were analyzed with allowance for τ_0, which were determined according to the halfwidth curve.

When this method is employed, it must be noted that very large optical thicknesses are obtained for the prominence in the H and K Ca^+ lines -- on the

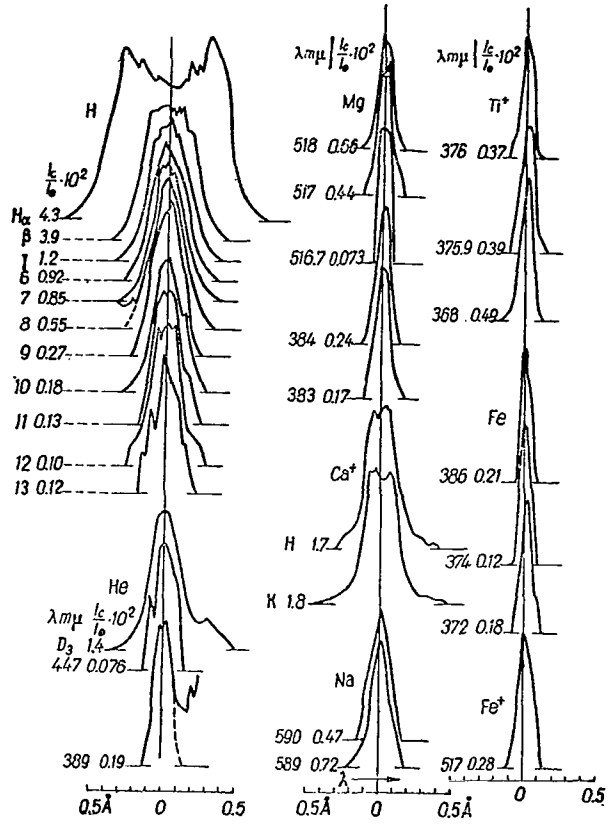

Figure 2

Profiles of the Emission Lines in the Spectrum of a Prominence Observed on July 9, 1959.

order of a thousand. However, they are apparently close to the real values, since the relative content of calcium atoms in this case corresponds to their abundance in space. If we assume that the electron temperature equals the mean kinetic temperature (7000°) and at the same time equals the temperature of L_α-radiation, we obtain $n_2/n_1 = 1.8 \cdot 10^{-7}$ for hydrogen. According to the data presented in (Ref. 5), $n_H/n_{Ca} = 1.4 \cdot 10^6$, and then $n_{Ca} = 3.9\ n_2$ in the case of $n_H = n_1$. In our case, $n_{Ca} = 2.4\ n_2$, if we assume that all of the calcium in the prominences occurs in a state which has been ionized once. /41

N. N. Morozhenko (Ref. 1) also obtained a prominence optical thickness in the H and K Ca^+ lines on the order of one thousand. She determined τ_0, based on the optical thickness of prominences in titanium lines and based on data on

TABLE 2

Prominence	τ_0				$\frac{\Delta\lambda_D}{\lambda}\cdot 10^5$	$N_2\cdot 10^{-13}$	τ_0		$\frac{\Delta\lambda_D}{\lambda}\cdot 10^5$	N_{4S}
	H_α	H_β	H_γ	H_δ			H^+_{Ca}	K^+_{Ca}		
6/8 1959	44	5.8	2.0	0.9	3.4	7.0	91	182	1.3	$1.8\cdot 10^{14}$
	14	5.2	2.5	0.4	3.6	5.8	3.2	5.0	2.1	$0.9\cdot 10^{13}$
7/9 1959	22	3.0	1.0	0.5	3.7	3.9	457	914	1.3	$0.9\cdot 10^{14}$
	14	4.0	0.9	0.6	3.9	3.5	3.5	4.5	2.4	$1.0\cdot 10^{13}$
10/28 1959	17	2.3	0.8	0.4	4.5	3.6	2.3	4.6	4.2	$1.5\cdot 10^{13}$
	7	2.1	1.6	0.8	4.5	5.0	1.6	2.5	4.5	$1.0\cdot 10^{13}$
6/23 1960	16	2.2	0.7	0.3	3.7	2.8	480	960	1.4	$1.0\cdot 10^{14}$
Node 1	–	2.5	1.2	1.0	3.7	3.6	2.5	0.6	2.9	$0.7\cdot 10^{13}$
Node 2	21	2.9	1.0	0.4	3.7	3.7	480	960	1.4	$1.0\cdot 10^{14}$
	—	1.6	0.1	0.0	4.0	3.3	4.0	2.0	4.3	$1.7\cdot 10^{13}$

the chemical composition of the Sun. In addition, she employed the observed lines of the ultraviolet doublet of ionized calcium λλ 3706 and 3737 Å, whose lower level 4^2p is the upper level for H and K.

It follows from Table 2 that self-absorption attenuates the H_α line by a factor of 10 - 20, and the H_β line by a factor of 2 - 4; the H_γ and H_δ lines are also somewhat attenuated. In general, the phenomenon of self-absorption is even observed for the lines H_9 - H_{11}. The H and K Ca^+ lines are attenuated up to 300 times; only for a prominence observed on October 28, 1959, was the attenuation small -- only 2 - 3 times in all.

Employing the expression $\tau_0 = k_0 N$, we determined the population of the lower level of hydrogen atoms and of ionized calcium along the line of sight. The values obtained are given in Table 2. They comprise $4.2\cdot 10^{13}$ and $1.0\cdot 10^{14}$, respectively, on the average for four prominences.

The results derived from analyzing observations of all of the emission lines are presented in Table 3. The central intensities pertaining to the continuous spectrum of the disk center, the total halfwidths, the Doppler halfwidths, the equivalent widths expressed in milliangstroms of the continuous spectrum of the disk center, and the number of excited atoms along the line of sight are given for each prominence. The number of excited atoms was calculated according to the following formula

$$N_m = \frac{4\pi I_\odot}{A_{mn} h\nu} A_\lambda,$$

where A_λ is the equivalent width of the line, corrected for self-absorption when necessary.

The quantities $\Delta\lambda_D/\lambda$ obtained on the basis of each profile separately are given for the Balmer lines. It may be seen from Table 2 that, on the average,

TABLE 3

/42

λ, Å	$\frac{I_c}{I_\odot}\cdot 10^2$	$2\Delta\lambda_{\frac{1}{2}}$, Å	$\frac{\Delta\lambda_D}{\lambda}\cdot 10^5$	A_λ, mÅ	$N_m\cdot 10^{-9}$
		Prominence 6/8 1959			
6563 H	6.2	0.92	4.0	69	340
4861	4.5	0.48	3.6	22	122
4340	2.2	0.33	3.1	7.3	66
4102	1.6	0.26	3.6	4.7	76
3970	1.2	0.22	3.5	2.9	90
3889	0.62	0.25	3.9	1.7	94
3835	0.50	0.24	4.0	1.3	122
3798	0.23	0.24	3.8	0.56	92
3771	0.26	0.24	3.9	0.58	126
3750	0.17	0.21	3.3	0.40	124
3734	0.076	0.24	3.9	0.33	160
3722	0.070	0.17	2.8	0.13	88
3712	0.054	0.19	3.1	0.09	88
5876 He	2.9	0.18	1.8	5.6	1.0
4471	0.16	0.15	2.0	0.26	0.17
3889	0.26	0.17	2.6	0.44	0.51
5896 Na	0.31	0.14	1.4	0.43	0.088
5890	0.59	0.14	1.4	0.97	0.20
5184 Mg	0.42	0.12	1.4	0.54	0.13
5173	0.22	0.14	1.6	0.31	0.12
5167	0.13	0.069	0.80	0.14	0.16
3838	0.35	0.11	1.7	0.40	0.020
3832	0.22	0.12	1.9	0.27	0.015
3968 Ca^+	2.1	0.22	1.3	4.9	15
3934	2.2	0.24	1.3	5.9	32
3761 Ti^+	0.40	0.10	1.5	0.39	—
3759	0.44	0.10	1.5	0.43	0.024
3685	0.46	0.10	1.7	0.47	0.014
3720 Fe	0.11	0.12	2.0	0.13	0.23
5169 Fe^+	0.14	0.079	0.90	0.12	0.012
4078 Sr^+	0.15	0.093	1.4	0.14	0.013
		Prominence 7/9 1959			
6563 H	4.3	0.88	3.8	46	127
4861	3.9	0.51	4.0	21	74
4340	1.2	0.32	3.8	4.0	27
4102	0.92	0.29	4.2	2.7	40
3970	0.85	0.25	3.9	2.5	65
3889	0.55	0.25	3.9	1.5	75
3835	0.27	0.25	4.0	0.69	60
3798	0.18	0.24	3.9	0.46	72
3771	0.13	0.22	3.7	0.30	66
3750	0.10	0.24	3.9	0.27	85
3734	0.12	0.22	3.6	0.25	119
5876 He	1.4	0.27	2.7	4.2	0.75
4471	0.076	0.19	1.5	0.14	0.11
3889	0.19	0.15	2.4	0.32	0.37
5896 Na	0.47	0.18	1.8	0.74	0.15
5890	0.72	0.12	1.3	1.2	0.24

/43

Continuation of TABLE 3

λ, Å	$\frac{I_c}{I_\odot}\cdot 10^2$	$2\Delta\lambda_{\frac{1}{2}}$, Å	$\frac{\Delta\lambda_D}{\lambda}\cdot 10^5$	A_λ, mÅ	$N_m\cdot 10^{-9}$
5184 Mg	0.66	0.12	1.4	0.89	0.22
5173	0.44	0.14	1.6	0.66	0.26
5167	0.073	0.14	1.6	0.10	0.18
3838	0.24	0.11	1.7	0.29	0.014
3832	0.17	0.11	1.7	0.17	0.0096
3968 Ca+	1.7	0.25	1.3	4.7	67
3934	1.8	0.25	1.3	5.7	153
3761 Ti+	0.37	0.087	1.4	0.39	—
3759	0.39	0.095	1.8	0.42	0.023
3685	0.49	0.081	1.3	0.54	0.016
3860 Fe	0.21	0.11	1.7	0.21	0.65
3737	0.12	0.086	1.4	0.11	—
3734	0.048	0.087	1.4	0.043	0.0096
3720	0.18	0.078	1.3	0.17	0.30
5169 Fe+	0.28	0.15	1.9	0.42	0.045
		Prominence 10/28 1959			
6563 He	5.2	1.10	5.5	54	122
4861	3.2	0.50	4.5	16	47
4340	1.6	0.37	3.9	6.2	40
4102	1.0	0.37	4.8	4.3	58
3970	0.71	0.30	4.5	2.1	58
3889	0.38	0.27	4.2	0.98	50
3835	0.24	0.36	4.5	0.74	64
3798	0.16	0.29	4.6	0.48	76
3771	0.10	0.34	5.4	0.32	69
3750	0.12	0.21	3.4	0.27	83
5876 He	3.1	0.32	3.3	11.0	1.9
4471	0.30	0.18	3.0	0.58	0.38
3889	0.30	0.17	2.6	0.55	0.64
5896 Na	0.13	0.28	2.8	0.44	0.090
5890	0.29	0.20	2.1	0.60	0.12
5184 Mg	0.28	0.21	2.5	0.61	0.15
5173	0.12	0.21	2.4	0.26	0.11
3838	0.11	0.14	2.1	0.15	0.0074
3968 Ca+	1.5	0.38	4.2	5.3	0.76
3934	1.6	0.46	4.2	7.6	1.76
3761 Ti+	0.14	0.16	2.6	0.24	—
3759	0.15	0.17	2.7	0.28	0.015
3685	0.15	0.15	2.4	0.26	0.0077
		Prominence 6/23 1960			
		Node 1			
4861 H	2.8	0.40	3.5	12.5	37
4349	1.6	0.29	3.3	5.4	35
4102	1.3	0.27	3.8	3.7	50
3970	1.1	0.25	3.8	3.2	88
3889	0.68	0.22	3.4	1.8	92
3835	0.40	0.25	4.0	1.0	90
3798	0.42	0.23	3.6	1.1	170
3771	0.23	0.27	4.3	0.60	130
3750	0.17	0.24	3.8	0.47	140
3734	0.18	0.26	4.1	0.46	220

/44

Continuation of TABLE 3

λ, Å	$\frac{I_c}{I_\odot} \cdot 10^5$	$2\Delta\lambda_{\frac{1}{2}}$, Å	$\frac{\Delta\lambda_D}{\lambda} \cdot 10^5$	A_λ, mÅ	$N_m \cdot 10^{-9}$
3722	0.16	0.19	3.0	0.37	250
3712	0.10	0.19	3.0	0.23	210
3704	0.049	0.22	3.5	0.11	140
3697	0.045	0.33	5.3	0.15	260
3692	0.034	0.29	4.8	0.11	240
3683	0.029	0.16	2.6	0.054	200
5876 He	1.6	0.26	2.7	4.9	0.88
4471	0.15	0.25	3.0	0.36	0.23
3889	0.27	0.17	2.6	0.46	0.53
5896 Na	0.14	0.18	1.9	0.24	0.050
5890	0.22	0.14	1.5	0.36	0.074
5184 Mg	0.095	0.14	1.6	0.14	0.033
5173	0.080	0.13	1.5	0.10	0.042
3838	0.21	0.17	2.6	0.34	0.017
3832	0.14	0.12	1.9	0.21	0.012
3968 Ca^+	2.5	0.28	1.4	8.4	115
3934	2.4	0.29	1.4	8.5	214
3761 Ti^+	0.37	0.16	2.5	0.59	—
3759	0.42	0.13	2.0	0.64	0.036
3685	0.44	0.16	2.5	0.74	0.022
3860 Fe	0.25	0.14	2.1	0.38	1.1
3737	0.16	0.069	1.1	0.16	—
3720	0.30	0.081	1.3	0.34	0.59
4078 Sr^+	0.18	0.18	2.6	0.34	0.033
		Node 2			
4861 H	1.4	0.47	4.4	7.6	26
4349	1.0	0.30	4.0	3.5	24
4102	0.90	0.31	4.5	2.9	42
3970	0.65	0.31	4.6	2.2	62
3889	0.64	0.26	4.0	1.8	96
3835	0.44	0.25	4.0	1.2	106
3798	0.45	0.27	4.2	1.2	190
3771	0.32	0.21	3.3	0.71	150
3750	0.19	0.24	3.8	0.51	160
3734	0.19	0.23	3.8	0.44	220
3722	0.16	0.21	3.4	0.38	260
3712	0.12	0.22	3.6	0.28	270
3704	0.070	0.20	3.2	0.10	130
3697	0.057	0.31	5.1	0.16	270
3692	0.039	0.30	4.4	0.12	260
3683	0.039	0.20	3.2	0.075	270
5876 He	2.7	0.26	2.7	8.6	1.6
4471	0.18	0.21	2.8	0.38	0.25
3889	0.46	0.17	2.6	0.85	0.99
5896 Na	0.14	0.24	2.4	0.33	0.068
5890	0.19	0.24	2.4	0.49	0.10
5184 Mg	0.12	0.14	1.6	0.18	0.044
5173	0.064	0.15	1.8	0.097	0.039
3838	0.22	0.20	3.0	0.39	0.019
3832	0.12	0.20	3.0	0.26	0.015
3968 Ca^+	1.9	0.29	1.4	6.7	89
3934	1.9	0.30	1.4	7.0	169

/45

Continuation of TABLE 3

λ, Å	$\frac{I_c}{I_\odot}\cdot 10^2$	$2\Delta\lambda_{\frac{1}{2}}$, Å	$\frac{\Delta\lambda_D}{\lambda}\cdot 10^5$	A_λ, mÅ	$N_m\cdot 10^{-9}$
3761 Ti^+	0.41	0.15	2.4	0.70	—
3759	0.47	0.16	2.4	0.78	0.043
3685	0.49	0.18	3.0	0.92	0.027
3860 Fe	0.23	0.14	1.8	0.33	1.0
3737	0.16	0.076	1.2	0.14	—
3720	0.35	0.10	1.7	0.42	0.74
4078 Sr^+	0.12	0.22	3.2	0.23	0.022

for the series, the value of this parameter is fairly close to $\Delta\lambda_D/\lambda$, determined on the basis of the halfwidth curve.

The Doppler widths, obtained by these same methods for the H and K lines of ionized calcium, differ from each other by a factor of 2 — 3. On the average, the Doppler width of the hydrogen line equals $3.8\cdot10^{-5}$, of the helium line -- $2.5\cdot10^{-5}$, and of metal lines -- $1.9\cdot10^{-5}$. The lines of H and K Ca^+ in the spectrum of a prominence observed on October 28, 1959, were excluded in the calculation, since they were 2 — 3 times wider than all of the remaining lines of metals. /46

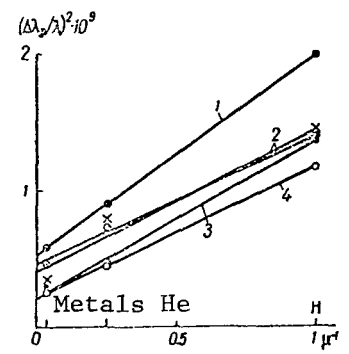

Figure 3

Determination of Temperature and Turbulent Velocity According to All Elements for Prominences:

1 -- 10/28 1959; 2 -- 6/23 1960 (× -- Node 1, ⊙ -- Node 2); 3 -- 7/9 1959; 4 -- 6/8 1959.

The kinetic temperatures and turbulent velocities were determined graphically, for hydrogen, helium, and metals together (Figure 3), and also for the lines He_ζ and H_8, H_ε and H Ca^+ by pairs. The following formula was employed for the computation

$$\frac{\Delta\lambda_D}{\lambda}=\frac{1}{c}\sqrt{\frac{2RT}{\mu}+v_t^2}$$

under the assumption that the turbulent velocity and the kinetic temperature were the same for all the elements. Table 4 presents the results. It may be seen from the table that the kinetic temperature of prominences equals 5000 - 9000°, and the turbulent velocity is 4 — 7 km/sec. The parameters determined according to H_ε and H Ca^+ for a prominence observed on October 28, 1959, differed from these values due to the large width of the H Ca^+ line.

The kinetic temperatures and turbulent velocities which we obtained, as well as other parameters, characterizing the state of matter in the prominences, are close to the corresponding values presented in (Ref. 4). This points to /47

TABLE 4

Prominence	T_{kin}	$v_t \cdot 10^{-5}$	T_{kin}	$v_t \cdot 10^{-5}$	T_{kin}	$v_t \cdot 10^{-5}$
	H_ε and H_{Ca^+}		H_8 and He_ζ		According to All Elements	
6/8 1959	5400°	3.9	3500°	6.8	5200°	4.4
7/9 1959	6500	3.9	5700	5.4	6500	3.9
10/28 1959	1500	12.6	9700	4.6	7700	7.0
6/23 1960						
Node 1	6300	4.2	5000	6.4	5400	6.2
Node 2	6300	4.2	5000	6.4	5100	6.5

the general nature of physical conditions in different prominences.

REFERENCES

1. Morozhenko, N. N. Solnechnyye Dannyye, 4, 50, 1964.
2. Solnechnyye Dannyye, 7, 10, 1959; 10, 30, 1959; 6, 24, 1960.
3. Yakovkin, N. A., Zel'dina, M. Yu. Solnechnyye Dannyye, 12, 67, 1960.
4. Yakovkin, N. A., Zel'dina, M. Yu. Astronomicheskiy Zhurnal, 40, 847, 1963.
5. Goldberg, L., Müller, E. A., Aller, L. H. Aph. J., Suppl., 5, 45, 135, 1960.

MECHANISM OF HYDROGEN EXCITATION IN PROMINENCE SURGES

M. S. Geychenko

The steady state equations are solved for the 3rd, 4th and 6th hydrogen levels of surges. The populations of these levels were obtained in (Ref. 2 — 3). The values of the electronic concentration n_e are calculated. The mechanism of excitation of the 3rd, 4th and 6th hydrogen levels in surges is photospheric radiation and radiative recombination. This is determined by the absolute magnitudes of the terms of these equations.

Up until recently, the mechanism of gas excitation in prominence surges /48
was not understood. The phenomenon of prominence surges was always related to flares (Ref. 6). Since the problem of flares is still far from being solved, an investigation of prominence surges is of great importance. This article proposes a method for determining the mechanism of hydrogen excitation of prominence surges. The method is based on a quantitative analysis of the steady state equations for the third, fourth, and sixth energy levels of hydrogen. The basic data employed are the previously determined (Ref. 1, 11) ratios between the populations of the n_k/n_2 (k = 3, 4, 6) hydrogen levels of 20 prominence surges (10 in absorption and 10 in emission). When the equations were formulated, photorecombinations, absorption of photosphere radiation (transitions from the lower levels to the given level), spontaneous transitions to the lower levels, and photoionization were taken into account. The steady state equations for the 3rd, 4th and 6th levels, divided by n_2, have the following form in the notation which is customarily employed (Ref. 10)

$$\frac{n_e^2}{n_2}R_3+\rho_{23}B_{23}+\sum_{k=4}^{6}\frac{n_k}{n_2}A_{k3}=\frac{n_3}{n_2}\left(A_{31}+A_{32}\right)+\frac{n_3}{n_2}C_{3i}; \tag{1}$$

$$\frac{n_e^2}{n_2}R_4+\sum_{k=2}^{3}\frac{n_k}{n_2}\rho_{k4}B_{k4}+\sum_{k=5}^{6}\frac{n_k}{n_2}A_{k4}=\frac{n_4}{n_2}\sum_{k=1}^{3}A_{4k}+\frac{n_4}{n_2}C_{4i}; \tag{2}$$

$$\frac{n_e^2}{n_2}R_6+\sum_{k=2}^{5}\frac{n_k}{n_2}\rho_{k6}B_{k4}=\frac{n_6}{n_2}\sum_{k=1}^{5}A_{6k}+\frac{n_6}{n_2}C_{6i}. \tag{3}$$

The desired quantities are n_e and T_e. These equations do not include terms /49
which correspond to electron collisions of the first and second kind, ionization by electron collision, Lyman photospheric radiation, "triple" recombinations, and transitions to lower levels under the influence of the radiation field. The fact that the Lyman photospheric radiation in the L_β, L_γ and L_ε lines is disregarded may be explained by the fact that they are very faint, and

measurements of them are extremely unreliable (Ref. 12). A simple investigation shows that transitions to the lower levels under the influence of the radiation field do not play a significant role in the population of the levels under consideration.

In order to determine the magnitude of the electron collision of the first kind when these levels are populated, we shall establish the upper limits for the values of n_e and T_e for prominence surges. For this purpose, we shall compare the spectra of flares and prominence surges. The spectrum of a flare is always an emission spectrum, and the prominence surge spectra on the disk are absorption spectra. At the edge, they are emission spectra both for the customary prominences and for quiet prominences. The population of the hydrogen levels in flares is two — three orders of magnitude greater than for prominence surges and for quiet prominences. A comparison was drawn between the latter in (Ref. 1, 2, 5, 9, 11). As studies have shown (Ref. 7, 8, 13, 15), the values of $n_e = 10^{13}$ and $T_e = 10{,}000°$ are characteristic for flares, but are not encountered in prominences. Lower values of these parameters may be found both in prominences and in flares. Electron collision of the first kind (Ref. 7, 8, 14) plays the predominant role in the hydrogen excitation mechanism in flares. In addition, theoretical calculations have shown that -- if the hydrogen electron temperature T_e equals 10,000° -- electron collision is the decisive factor in excitation of the levels. It is therefore apparent that only electron collision may provide a high population of the hydrogen levels in flares and, consequently, their emission spectrum. This comparison would seem to indicate that electron collision of the first kind does not play a predominant role as a mechanism of hydrogen excitation in prominence surges, as is the case in flares. Calculations have fully substantiated this. Quantitative calculations deliberately employed exaggerated values of the parameters n_e and T_e ($n_e = 10^{13}$ and $T_e = 10{,}000°$) for prominence surges; these values may be regarded as the upper limiting values of these parameters in this case. The relative values of terms in equations (1) — (3), which took into account electron collision of the first kind, were also determined. For purposes of comparison, it is advantageous to take the term in the equation under consideration which corresponds to spontaneous transitions, since it is only calculated on the basis of observational data. When calculating terms in the equations which correspond to transitions under the influence of electron collision of the first kind from the first level to the given level, we must keep the fact in mind that they are very sensitive to a temperature change. Calculations have shown that the ratio between them and the value of the comparison term is close to unity. The remaining ratios, which include terms corresponding to electron collision of the first and second type as well as ionization under the influence of electron collision, are two — three orders of magnitude smaller than unity. These calculations made it possible to disregard quantities corresponding to electron collision in equations (1) - (3). /50

As was shown in (Ref. 4), terms corresponding to "triple" recombinations, which were not considered in equations (1) — (3), greatly exceed the

TABLE 1

T_e, °K	$R_2^{(3)} \cdot 10^{25}$	$R_6 \cdot 10^{14}$	$\frac{R_6}{R_6^{(3)}} \cdot 10^{-11}$
5000	2.30	2.71	1.18
6000	1.85	2.34	1.27
7000	1.53	2.07	1.35
8000	1.29	1.80	1.40
9000	1.11	1.64	1.48
10000	0.98	1.47	1.51

TABLE 2

m	$R_m^{(3)}$
1	$2.44 \cdot 10^{-30}$
2	$2.9 \cdot 10^{-28}$
3	$2.8 \cdot 10^{-27}$
4	$1.5 \cdot 10^{-26}$
5	$5.3 \cdot 10^{-26}$
6	$1.4 \cdot 10^{-25}$

values of terms corresponding to photorecombinations for the case of prominences (of customary quiet prominences), beginning with the 4*th* level. The sixth level is the highest level of those examined in this study. Table 1 presents the coefficients of "triple" recombinations for this level, calculated according to the formula given in (Ref. 4)

$$R_m^{(3)} = \frac{m^4}{1-\left(\frac{m}{m_0}\right)^2} \cdot \frac{e^x}{T^2} \{2.3 \cdot 10^{-20} [e^{-4x} - 2xE_i(4x)] + \\ + 3.8 \cdot 10^{-21} [(0.07 + x^{-1}) e^{-x} - (3.07 + x^{-1}) e^{-4x}]\}, \quad (4)$$

where m is the basic quantum number of the given hydrogen level; m_0 is the basic quantum number of the ionized continuum level;

$$x = \frac{\chi_0}{kT}\left(\frac{1}{m^2} - \frac{1}{m_0^2}\right). \quad (5)$$

The values of m_0, computed by different methods, range from 40 — 65, and /51 depend on n_e. In the case of m = 6, it is apparent that x does not depend on n_e, since $(m/m_0)^2 \ll 1$. Consequently, the second term in the parentheses of (5) may be disregarded. This means that $R_6^{(3)}$ depends slightly on n_e, and this dependence may be disregarded. As follows from Table 1, $R_m^{(3)}$ is inversely proportional to T_e. This table presents the photorecombination coefficients for the same values of the temperature T_e. When the temperature T_e increases by a factor of two, the ratio between the coefficients increases by only a factor of 1.3. Therefore, it may be assumed that $R_6/R_6^{(3)}$ equals the mean value

$$\frac{R_6}{R_6^{(3)}} = 1.3 \cdot 10^{11}. \quad (6)$$

Let us investigate the relationship between the term in equation (3), corresponding to photorecombination, and the term corresponding to "triple" recombinations, which was omitted in this equation

$$\frac{n_e^2 R_6}{n_e^3 R_6^{(3)}} = \frac{R_6}{n_e R_6^{(3)}} = \frac{1.3 \cdot 10^{11}}{n_e}. \quad (7)$$

It may be seen from this relationship that the role of "triple" recombinations increases for m = 6, as compared with photorecombinations when only n_e increases, for m = 4, the role of these recombinations increases for the case $n_e = 10^{13}$; for m = 3 it increases for the case $n_e = 10^{15}$ (Table 2). Since it cannot be assumed that $n_e = 10^{15}$ is tenable for prominence surges, the fact that the term corresponding to"triple" recombinations is disregarded in equation (1) has only a slight influence upon the accuracy with which this equation is solved. Therefore, the value of n_e, obtained from equation (1), may serve as a control for the values of n_e determined according to equations (2) and (3). In equations (2) and (3), there is less basis for disregarding terms corresponding to "triple" recombinations, and this is only possible for $n_e \leqslant 10^{11}$. However, since 10^{11} is typical for prominences, the "triple" recombinations may be disregarded in these equations. The photorecombination coefficients R_m change very little in the temperature range 5000 - 10,000°, which is admissible for prominences (see Table 1). Therefore, we may take the mean values for R_3, R_4 and R_6. As a result, each of the equations (1) — (3) will contain only one unknown -- n_e. The value of n_2^e/n_2 may be obtained on the basis of the three equations (1)— (3) for the case of absorption (Table 3). The value of n_e^2 may /52 be obtained for the case of emission (Table 4). Tables 3 and 4 show the fairly good agreement between these values.

TABLE 3

Plate No.	$\frac{n_e^2}{n_2}\cdot 10^{-19}$, eq. (1)	$\frac{n_e^2}{n_2}\cdot 10^{-19}$, eq. (3)	$\frac{n_e^2}{n_2}\cdot 10^{-19}$, eq. (2)
988	2.39	0.03	0.96
988	3.44	0.09	0.63
988	0.86	0.08	0.49
916	1.49	0.04	0.48
916	1.62	0 11	0.18
916	1.75	0.05	0.55
974	0 72	0.07	0.10
974	0.59	0.06	0.18
737	1 93	0.09	0.76
714	2.48	0.00	0.18
188	1.40	0.00	0.52
222	1.40	0.00	0.41

If we know the population values for the 3rd, 4th, and 6th hydrogen levels n_k for each of the prominence surges under consideration (or the ratio n_k/n_2) and the values of the electron concentration n_e (or n_e/n_2), we may determine the predominant excitation mechanism for the given level of each prominence surge. For this purpose, we must calculate the values of each of the terms in

TABLE 4

Plate No.	$n_e^2 \cdot 10^{-22}$, eq. (1)	$n_e^2 \cdot 10^{-22}$, eq. (3)	$n_2 \cdot 10^{-4}$
770	1.41	1.30	0.3
872	1.03	1.22	0.5
868	0.91	1.13	0.3
862	1.27	6.70	1.4
797	0.93	0.74	0.4
205	4.17	11.10	1.3
210	0.60	5.90	1.4
190	0.46	4.56	1.1
104	1.14	—	0.6
108	—	0.85	1.0

equations (1) — (3). Their absolute values show that photosphere radiation and /53 photorecombinations are the excitation mechanism of the 3rd, 4th, and 6th hydrogen levels in prominence surges. For several prominence surges, the photorecombination mechanism is negligibly small.

Thus, the agreement between the physical parameters and nature of hydrogen excitation for different prominence surges point to the similarity in their physical nature. We must lay particular stress on the similarity between the emission and absorption prominence surges.

REFERENCES

1. Geychenko-Teryayeva, M. S. Solnechnyye Dannyye, 7, 1963.
2. Gurtovenko, E. A., Semenova, N. N. Izvestiya Glavnoy Astronomicheskoy Observatorii (GAO) AN USSR, 4, 1, 1961.
3. Ivanov-Kholodnyy, G. S. Izvestiya Krymskoy Astrofizicheskoy Observatorii (KrAO), 15, 1955.
4. Ivanov-Kholodnyy, G. S., Nikol'skiy, G. M., Gulyayev, R. A. Astronomicheskiy Zhurnal (AZh), 36, 5, 1960.
5. Kazachevskaya, T. V., Severnyy, A. B. Izvestiya KrAO, 19, 1958.
6. Krat, V. A., Krat, T. V. Izvestiya GAO, 167, 1961.
7. Polupan, P. N. AZh, 1032, 38, 1960.
8. Severnyy, A. B. Izvestiya KrAO, 19, 1958.
9. Sobolev, V. M. Izvestiya GAO, 158, 1958.
10. Sobolev, V. M. Izvestiya GAO, 167, 1961.
11. Teryayeva, M. S. Solnechnyye Dannyye, 3, 1964.
12. Hinteregger, H. E. Ultraviolet Solar Radiation and the Interplanetary Medium. IL, Moscow, 47, 1962.
13. Svestka, Z. Bull. of the Astron. Inst. of Czechoslovakia, 14, 6, 1963.
14. Yakovkin, N. A. Solnechnyye Dannyye, 8, 1963.
15. Suemoto, Z., Hiei, E., Hirayama, T. J. Phys. Soc. Japan, Suppl., A-11, 231, 1951.

ON THE MECHANISM OF EMISSION BORDER FORMATION IN FILAMENTS

R. I. Kostik, T. V. Orlova

Additional excitation of the chromosphere by photospheric radiation reflected from a filament is considered as one cause of emission border formation. A formula is obtained for estimating the border brightness. At the same time it explains the principal data (increase of border contrast at the center-limb passage, decrease of border intensity with filament height above the photosphere). The estimated values of the border brightness are in good agreement with the observations.

During the observation of filaments in the H_α line, it was noted that many /54 of them have an emission border. The most comprehensive discussion of this problem was presented in a study by E. A. Gurtovenko, and A. S. Rakhubovskiy (Ref. 3). On the basis of a detailed examination of filaments with a border, which were observed during the IGY on a AFR-2 telescope of the Main Astronomical Observatory of the USSR Academy of Sciences, Gurtovenko and Rakhubovskiy reached the following conclusion (Ref. 3):

(1) The border is observed only from the side of the filament which faces the center of the solar disk;

(2) The border contrast increases from the center to the edge of the solar disk, where it has its maximum brightness;

(3) As a rule, the border is the most intense in lower prominences which come in contact with the chromosphere over almost their entire length;

(4) The border is located in the chromosphere under the filament;

(5) All filaments in which a border is observed have bright prominences where the limb leaves the disk;

(6) A border is a "usual phenomenon, rather than an unusual one, which accompanies a filament".

On the average, the border brightness at the heliocentric distance $\sin \Theta = 0.9$ comprises 1.13 of the brightness of an unperturbed chromosphere (from 1.03 to 1.25) (Ref. 3). Gurtovenko and Rakhubovskiy proposed that one of the possible mechanisms for the border formation is ohmic energy dissipation of the magnetic field of the filament or the prominence. We feel that there may be another possible explanation of the border formation mechanism. Photospheric radiation, reflected by the filament, produces an additional excitation of the chromosphere, and may cause the formation of the emission border. The /55

purpose of this article is to determine the additional excitation and to calculate the border brightness.

According to the following formula

$$I(t_0, x) = \int_0^{t_0} B_1(t)\,\alpha(x)\,e^{-(t_0-t)\,\alpha(x)}\,dt \qquad (1)$$

we may determine the intensity of radiation reflected diffusely by the filament toward the chromosphere (sec Θ = 1). We may determine the source function $B_1(t)$ from the basic integral equation given by the theory of radiation diffusion

$$B_1(t) = \frac{\lambda}{2}\int_0^{t_0} B_1(t')\,K(|t-t'|)\,dt' + g(t), \qquad (2)$$

where λ is the probability that the quantum may survive during an elementary scattering event; t_0 -- optical thickness of the filament; $\alpha(x)$ -- dimensionless absorption coefficient ($\alpha(x) = e^{-x^2}$); $4\pi g(t)$ -- strength of the radiation sources;

$$K(t) = A\int_{-\infty}^{+\infty} \alpha^2(x)\,E_1[\alpha(x)\,t]\,dx;$$

$$E_1(x) = \int_0^{\frac{\pi}{2}} e^{-x\sec\theta}\sin\Theta\sec\Theta\,d\Theta,$$

$$A\int_{-\infty}^{\infty}\alpha(x)\,dx = 1.$$

It may be readily seen that we have the following for our case

$$g(t) = \frac{\lambda w}{2\sqrt{\pi}}\int_{-\infty}^{+\infty} I_0(x)\,E_2[\alpha(x)\,(t_0-t)]\,\alpha(x)\,dx,$$

where w is the dilution factor; $I_0(x)$ -- is the intensity of photospheric radiation in the center of the solar disk in the line H_α ($\Delta\lambda_D$ = 0.460 Å); /56

$$E_2(x) = \int_0^{\frac{\pi}{2}} e^{-x\sec\theta}\sin\Theta\,d\Theta.$$

Equation (2) may be rewritten in the following form

$$B_1(t) = \frac{\lambda}{2}\int_0^{t_0} B_1(t')\,K(|t-t'|)\,dt' + \\ + \frac{\lambda\omega}{2\sqrt{\pi}}\int_{-\infty}^{+\infty} I_0(x)\,E_2[\alpha(x)(t_0-t)]\,\alpha(x)\,dx. \tag{3}$$

This equation was solved by the numerical method for values of t_0 equalling 5, 20, 30, 40, consecutively. The calculations were performed on a M-20 com-

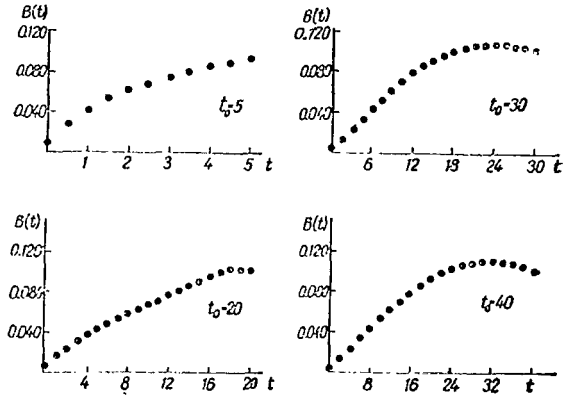

puter. The dependence of the source function upon the optical depth is shown in the figure. It is very interesting to note that the function $B_1(t)$ decreases, beginning with certain values of t for large t_0.

The intensity $I(t_0, x)$, computed according to formula (1), causes additional excitation of the chromosphere under the filament. In its turn, the filament produces additional luminescence of the chromosphere, which may be observed in the form of the emission border. The border intensity may be found from the following expression /57

$$I_2(\tau_0, t_0, \Theta, x) = \int_0^{\tau_0} B_2(\tau)\,\alpha(x)\sec\Theta e^{-(\tau_0-\tau)\alpha(x)\sec\Theta}\,d\tau, \tag{4}$$

wnere $B_2(\tau)$ is the "additional" source function; τ_0 -- optical thickness of the chromosphere in the radial direction.

It may be shown that the following equation is valid for values of τ which are not very large (on the order of several units)

$$B_2(\tau) = a + b\tau. \tag{5}$$

After integration of equation (4), with allowance for equation (5), we finally obtain

$$I_2(t_0, \tau_0, \Theta, x) = \left[a - \frac{b}{\alpha(x)\sec\Theta}\right][1 - e^{-\tau_0 \alpha(x)\sec\Theta}] + b\tau_0. \quad (6)$$

We may determine the function $B_2(\tau)$ similarly to $B_1(t)$ according to the following formula

$$B_2(\tau) = \frac{\lambda}{2}\int_0^{\tau_0} B_2(\tau')\,K(|\tau - \tau'|)\,d\tau' + \\ + \frac{\lambda w}{2\sqrt{\pi}}\int_{-\infty}^{+\infty} I(t_0, x)\,E_2[\alpha(x)(\tau_0 - \tau)]\,\alpha(x)\,dx. \quad (7)$$

Substituting equation (5) in formula (7), and assigning values of τ_0 and 0 to τ, we obtain a system of equations with respect to a and b:

$$\left.\begin{aligned} a &= \frac{\lambda}{2}a\int_0^{\tau_0} K(\tau')\,d\tau' + \frac{\lambda}{2}b\int_0^{\tau_0} K(\tau')\,\tau'd\tau' + g(\tau_0) \\ a + b\tau_0 &= \frac{\lambda}{2}a\int_0^{\tau_0} K(\tau_0 - \tau')\,d\tau' + \frac{\lambda}{2}b\int_0^{\tau_0} K(\tau_0 - \tau')\,\tau'd\tau' + g(0). \end{aligned}\right\} \quad (8)$$

We may determine the function

$$g(\tau) = \frac{\lambda w}{2\sqrt{\pi}}\int_{-\infty}^{+\infty} I(t_0, x)\,\alpha(x)\,E_2[\alpha(x)\tau]\,dx$$

by the numerical method (λ = 1). The values of $K(\tau)$ were taken from the computations of V. V. Ivanov. In order to compare the calculated border brightness with the observed border brightness, we must take into account the profile of the pass band of the IP-filter of the AFR-2 telescope of the Main Astronomical Observatory of the USSR Academy of Sciences (Ref. 1), as well as the darkening of the solar disk toward the edge (Ref. 2). In other words, the following ratio /58

$$\frac{\int_{-\infty}^{+\infty}[mi(\lambda)\,I_0(\lambda) + i(\lambda)\,I_2(t_0, \tau_0, \Theta, \lambda)\,d\lambda}{\int_{-\infty}^{+\infty} mi(\lambda)\,I_0(\lambda)\,d\lambda}, \quad (9)$$

must be compared with the observed ratio; this ratio represents the border brightness with respect to the contiguous unperturbed chromosphere. In expression (9), $i(\lambda)$ is the profile of the Institute of Applied Physics pass band; m -- the coefficient corresponding to the solar disk darkening toward the edge. The table below presents the numerical values of this ratio for different t_0, τ_0 and w in the case of sin Θ = 0.9. As may be seen from this table, the calculated values of the border brightness agree quite well with the

τ_0	t_0 = 5	20	30	40
	$w=0.2$			
2	1.03	1.06	1.07	1.08
5	1.05	1.07	1.08	1.11
	$w=0.3$			
2	1.05	1.09	1.10	1.12
5	1.07	1.11	1.12	1.16
	$w=0.4$			
2	1.07	1.12	1.15	1.17
5	1.08	1.15	1.16	2.21

observed values (we should recall that for different filaments the observations give border brightness values which range between 1.03 — 1.25 units of the contiguous unperturbed chromosphere). In addition, the mechanism which has been advanced makes it possible to explain other peculiarities of this phenomenon which were observed. Thus, it directly follows from formula (6) that:

(1) The border contrast increases from the center of the solar disk to the edge (i.e., with an increase in the angle Θ);

(2) The border is most intense for the lower prominences, since the numerical values of the coefficients a and b are directly proportional to the dilution w [see formula (7)].

It may thus be assumed that photospheric radiation which is reflected by the filament may produce additional illuminescence of the chromosphere, which /59 may be observed in the filaments in the form of an emission border. The numerical values of the emission border brightness, which are given in the table, represent a lower limit, since we assumed that the radiation reflected by the filament is only scattered in the chromosphere. In reality, the photosphere participates in the scattering, i.e., the scattering takes place in a semi-infinite medium. Allowance for this fact does not greatly influence the final results, since the coefficient of continuous absorption plays a significant role in the photosphere. Therefore, the probability of quantum re-emission in the H_α line is very slight.

REFERENCES

1. Gurtovenko, E. A. V Kn: Nablyudeniya Solntsa (In the Book: Observations of the Sun). Izdatel'stvo AN SSSR, 25, 1959.
2. Gurtovenko, E. A., Rakhubovskiy, A. S. Solnechnyye Dannyye, 3, 56, 1962.
3. Gurtovenko, E. A. Rakhubovskiy, A. S. Izvestiya Glavnoy Astronomicheskoy Observatorii (GAO), USSR, 5, 1, 1963.
4. Sobolev, V. V. Perenos Luchistoy energii v atmosferakh zvezd i planet (Transfer of Radiant Energy in the Atmospheres of Stars and Planets). Gostekhizdat, Moscow, 1956.

RESEARCH ON CALCIUM LUMINESCENCE IN A GREAT CHROMOSPHERIC FLARE

K. V. Alikayeva

The paper deals with ionized calcium luminescence in the chromospheric flare of July 12, 1961. The central parts of the H and K line profiles are broadened by non-thermal random velocities, and in the wings by non-Maxwellian velocity distribution. The change in electronic density, temperature and effective length of the calcium filaments with time is determined.

In July, 1961, a large group of spots, No. 198, passed over the solar disk. /60 This group produced a large number of flares of different classes, including three flares of class 3^+. One of these powerful flares was observed on July 12, 1961, at the Main Astronomical Observatory of the USSR Academy of Sciences. It was preceded by several sub-flares of class 1; these sub-flares occurred at the same position where a large chromosphere flare lasting about two hours subsequently flared up. The flare was visible in a chromosphere telescope in the H_α line, in the form of two bright filaments; the distance between these filaments increased as the flare developed (this flare was described in greater detail in [Ref. 1, 3]).

The spectrum was simultaneously recorded on a spectrograph. The spectrograph slit intersected the brightest and most stable portion of the flare, in which the metals emitted most intensely. This node was quite bright, while the flare as a whole was already becoming "extinguished". A drawing was made of this active region, based on the photoheliogram obtained on July 12, 1961, at the the Crimean Astrophysical Observatory, and the position of the spectrograph slit was plotted during the recording time (Figure 1).

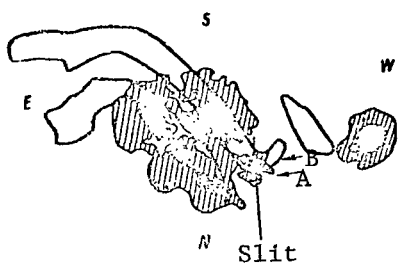

Figure 1

Drawing of the Group of Spots No. 198 and Flare on July 12, 1961, Based on a Photoheliogram and a Filtogram

A series of spectrograms was obtained /61 during the entire development of the flare in several spectral sections. This was the region of the lines D_3, 5183.6 Å, H and K, H_α, H_9. Emission lines of hydrogen, helium, and metals were visible in all the spectrograms on the background of the spectrum for the spot and the penumbra. The intensity of the ionized calcium lines H and K could be distinguished particularly well. At certain times, their intensity exceeded the continuous spectrum intensity of the center of the solar disk by a factor of more than three. A photometric analysis was performed for two nodes of the flare. Node A was located above

the spot penumbra, and node B was located above the spot (their position is indicated by arrows in Figure 1). Node B of the flare was weaker than node A, and it started to develop later, when the flare had subsided at node A.

Spectrograms in the region of the lines H and K were obtained at the following times for two nodes of the flare:

Node A: 10^h	25^m UT	Node B: 10^h	52^m UT
10	37	10	57
10	45	11	15
10	57		
11	02		
11	15		

In addition, the lines Ca II λ 3706 Å and 3737 Å were recorded for node B at the times 10^h57^m and 11^h15^m in the auxilary chamber of the spectrograph. These lines were formed by transition from the level 5S to the levels $4P_{\frac{1}{2}}$ and $4P_{\frac{3}{2}}$, which were the upper levels for the H and K lines.

Emission lines of metals (primarily lines of neutral iron, and the Co λ 3935.9 Å line) were clearly visible close to the brightness maximum of the flare in the wings of the H and K lines. A line of rare-earth element Dy^+ λ 3931.59 Å was recorded in a spectrogram, which was obtained at 10^h25^m, in the blue wing of the K line.

Profiles of the Flare Emission Lines

Line profiles for the flare and the "background" were compiled in units of the continuous spectrum of the solar disk center. Spectrograms of this active region, which were obtained one and one half-two hours before the flare, were employed to compile the line profiles of the spot and the spot penumbra.

The H and K lines have wide wings, and the profile width changes as a function of time as follows: at the node A -- from $\Delta\lambda \approx 5$ Å at 10^h25^m to 1.8 Å at 11^h15^m; at the node B -- from 5 Å at 10^h52^m to 2.6 Å at 11^h15^m. The profiles were somewhat wider above the spot than they were above the penumbra. At the time 10^h25^m, it was not possible to analyze the line Ca II H, since the H_ε line was so wide ($\Delta\lambda > 7$ Å) that its blue wing was superposed on the H line, even distorting the blue wing of the latter. /62

All the profiles of the lines studied were asymmetrical, including λλ 3736.9 and 3706.0. The red wings were somewhat more extended and more intense. The Ca II λ 3736.9Å line blended with the line of iron λ 3737.1Å. In order to remove the influence of this blending, the assumption was advanced that the Fe line was symmetrical. The reflected red wing of the Fe line was then computed from the red wing of the Ca II line. Even when the blending was taken into account in this way, there was considerable asymmetry in the calcium

line. If the occurrence of a more intense red wing in the iron line were assumed, this would only intensify the asymmetry of the λ 3736.9 Å line. All subsequent analyses were performed with allowance for only the blue wing of the H and K and λ 3736.9 Å lines.

TABLE 1

Node A			Node B			
Time	v_H	v_K	Time	v_H	v_K	v_{3737}
$10^h 25^m$	+3.0	+4.5	$10^h 52^m$	+1.9	+2.3	
10 37	+2.0	+2.5	10 57	+1.5	+3.0	−3.0
10 45	0.0	−4.5	11 15	0.0	0.0	−3.0
10 57	+2.3	+4.0				
11 02	+3.0	+7.0				
11 15	+1.5	+2.5				

The cores of the lines being studied were displaced slightly, primarily toward the red side. Table 1 presents the radial velocities (in km/sec) corresponding to these displacements. As may be seen from the table, the radial velocities were smaller above the spot than they were above the penumbra. In addition, the radial velocities, which were determined according to the K line, were systematically larger than the velocities calculated according to the H line. This indicates that the cores of the K and H lines were formed in an optically thick layer at different altitudes. Since the optical thickness for the center of the line H is twice as small as for the line K, the emission for the latter reaches us from a flare layer which is closer to the surface. The flare is examined at a somewhat deeper level for the line H. Therefore, it may be assumed that the velocities decrease with depth.

It is very likely that both of these facts (more intense and more extended red wings and displacement of the lines to the red side) are interrelated and represent the occurrence of one type of motion of matter in the flare -- contraction. /63

The line profiles shown in Figure 2 were obtained at the time 10^h45^m for the node A, and at 10^h57^m for node B. They are typical profiles for this flare, since the nature of the profiles did not change as a function of time. None of the profiles of the observed Ca II lines had an intensity dip in the center. This indicates that the source function changes very slightly with depth in the flare, so that it may be assumed to be constant. In this case, the intensity in the line profile is distributed according to the well known formula

$$I_\lambda = I'_\lambda e^{-\tau_\lambda} + P(1 - e^{-\tau_\lambda}). \quad (1)$$

The profiles of the line λ 3737 Å have a Gaussian form. Therefore, in the case when

$$\tau_\lambda = \tau_0 e^{-\left(\frac{\Delta\lambda}{\Delta\lambda_D}\right)^2}, \quad (2)$$

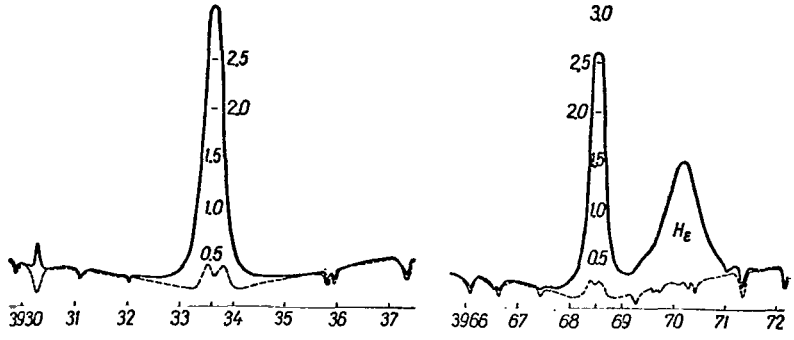

Figure 2

Profiles of the Lines H and K and λ 3737 Å:
a - Node A, time 10^h45^m UT; b - Node B,
time 10^h57^m UT

they were analyzed on the basis of the Conway method.

The Doppler widths of the H and K were determined according to a method advanced by V. A. Krat. This method is as follows. The optical thicknesses /64 are small in the wings of the H and K lines. Therefore, equation (1) for the wings of these lines may be written as follows

$$I_K - I'_K = 2\tau (P_K - I'_K); \tag{3}$$

$$I_H - I'_H = \tau (P_H - I'_H). \tag{3'}$$

Equation (3') may be calculated from equation (3):

$$(I_K - I_H) - (I'_K - I'_H) = \tau [(2P_K - P_H) - (2I'_K - I'_H)]. \tag{4}$$

In the case of the H and K lines, the intensities of the "background" are almost identical. Therefore, we may disregard the second term in the left hand side of equation (4). If the optical thicknesses along the profiles change according to the law (2), then -- taking the logarithm of equation (4) -- we obtain

$$\ln (I_K - I'_H) = \ln \tau_0 - \frac{1}{\Delta\lambda_D^2} \Delta\lambda^2 + C. \tag{5}$$

Only $\Delta\lambda$ is a variable in the right part of equation (5). Graphs showing the dependence of $\ln(I_K - I_H)$ on $\Delta\lambda^2$ were compiled for all the times. If the law (2) were satisfied, then the graphs would represent straight lines, whose inclination would enable us to determine $\Delta\lambda_D$. However, it was found that a rectilinear dependence was only observed in the relatively narrow cores of the lines. Consequently, equation (2) was fulfilled close to the line center, which corresponds to Maxwell velocity distribution of the particles. Figure 3 presents a graph showing the dependence of $\ln(I_K - I_H)$ on $\Delta\lambda^2$ for several

times. The linearity is disturbed due to large optical thicknesses at small distances from the center of the line ($\Delta\lambda < 0.15$ Å).

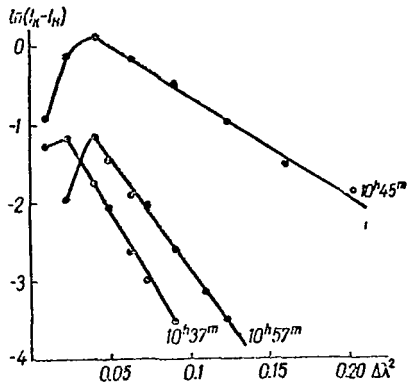

Figure 3

Graph Showing Dependence of $\ln (I_K - I_H)$ on $\Delta\lambda^2$ for Central Regions of the Lines

Above the spot (node B) the Maxwell cores of the lines were so narrow that the Doppler widths were determined with a large amount of error. In this case, $\Delta\lambda_D$ were determined from the following relationship

$$\left(\frac{\Delta\lambda_D}{\lambda}\right)_{H.K} = \left(\frac{\Delta\lambda_D}{\lambda}\right)_{3737}.$$

The optical thicknesses in the center of the lines and the source functions were determined in exactly the same way as in (Ref. 2). The values obtained for τ_0 and P were defined more accurately by adjusting the theoretical profiles to the observed profiles. /65

The parameters τ_0, P, $\Delta\lambda D$ were then employed to calculate the population of the basic level Ca II, and also the ratio N_2/N_1. The computational results for the K line are presented in Table 2 (columns 3-7).

TABLE 2

Node	Time	τ_0	$\Delta\lambda_D$, Å	P	$N_2/N_1 \cdot 10^2$	$N_1 \cdot 10^{-13}$	$\Delta\lambda^*$, Å	$N_1^* \cdot 10^{-13}$
1	2	3	4	5	6	7	8	9
A	10h 37m	4.6	0.150	3.2	2.0	1.34	0.500	1.29
	10 45	3.6	0.250	3.3	2.2	1.75	0.180	0.58
	10 57	2.0	0.180	2.8	1.8	0.70	0.475	0.14
	11 02	3.0	0.140	2.0	1.8	1.10	0.240	1.9
	11 15	3.8	0.152	1.5	1.0	1.12	0.215	0.35
B	10 52						0.260	0.24
	10 57	4.0	0.055	3.2	2.1	0.43	0.220	0.14
	11 15	4.5	0.065	2.8	1.9	0.56	0.150	0.33

Since the relationship between the populations N_2/N_1 and the amount of atoms of Ca II in the basic state are known, we may determine the population of the level $4P_{\frac{3}{2}}$. When there were profiles of the 3737 Å line, N_2 was determined over its optical thickness. The following populations of the level

$4P_{\frac{3}{2}}$ were obtained:

10^h57^m	$N_2^K = 0.905 \cdot 10^{11}$	$N_2^{(3737)} = 1.40 \cdot 10^{11}$
11 15	$1.056 \cdot 10^{11}$	$1.00 \cdot 10^{11}$

The values of N_2^K and $N_2^{(3737)}$ coincide, which substantiates the validity of the optical thicknesses which were found.

In order to determine the wings of the H and K lines, we tested such mechanisms leading to line expansion as radiation damping and the effects of pressure. The calculations showed that it is impossible to explain the observed profiles by damping, while the effects of pressure only play a significant role for hydrogen concentrations of $\approx 10^{17} - 10^{18}$. In this case, the electron concentrations reached $\approx 10^{15} - 10^{16}$, which is several orders of magnitude greater than the electron concentrations in the flares.

It was established that the intensity distribution in the wings best satisfys the relationship /66

$$\ln (I_K - I_H) \sim \Delta\lambda.$$

By way of an example, Figure 4 presents a graphic illustration of the dependence of $\ln(I_K - I_H)$ on $\Delta\lambda^2$ and $\Delta\lambda$ for the time 10^h57^m. This form of the dependence corresponds to a non-Maxwell velocity distribution of the radiating particles. The study (Ref. 8) explained the phenomenon of wings in the flares by the presence of particles with the following velocity distribution:

$$\frac{dN}{N} = av e^{-\frac{v}{v^*}} dv,$$

where v* is a certain characteristic velocity. In our case, the form of the wings for the H and K profiles is poorly represented by this distribution. Therefore, we found a distribution law corresponding to the observed form of the wings.

Let dN be the number of particles having velocities ranging from v to v + dv. The velocity distribution function is given in the general form

$$\frac{dN}{N} = f(v)\, dv. \tag{6}$$

The energy emitted in the frequency interval from ν to $\nu + d\nu$ is

$$E_\nu d_\nu = A_{kl} h\nu_{ik} dN. \tag{7}$$

After small transformations, expression (7) may be written

$$E_\nu = A_{ki} hcNf(v) = af(v). \tag{8}$$

The values of E_ν were determined according to the profile. The analytical expression, corresponding to the observed change in intensity with frequency, was determined for several values of E. It was found that in the wings of /67 the lines H and K the intensity changes for the velocity distribution function

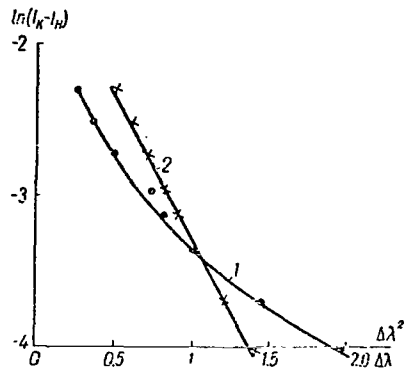

Figure 4

Graph Showing the Dependence: 1 - of $\ell n\ (I_K - I_H)$ on $\Delta\lambda^2$, and 2 - of $\ell n\ (I_K - I_H)$ on $\Delta\lambda$ for the line wings (node A, time 10^h57^m).

of the particles:

$$\frac{dN}{N} = ae^{-\frac{v}{v^*}}dv. \qquad (9)$$

Then the absorption coefficient

$$k_\nu = \frac{\pi e^2}{mc^2} \cdot \frac{a'\lambda^2}{\Delta\lambda^*} e^{-\frac{\Delta\lambda}{\Delta\lambda^*}} \qquad (10)$$

where $a' = \frac{c}{\nu_{1k}} \cdot a$, and $\Delta\lambda^*$ is related to the characteristic velocity $\frac{\Delta\lambda^*}{\lambda} = \frac{v}{c}$, is determined according to the inclination of the line representing the dependence of $\ln(I_K - I_H)$ on $\Delta\lambda$ (see Figure 4).

Since the flare is transparent for its own radiation in the wings of the lines H and K, we may use formula (3) to calculate the optical thicknesses at different distances from the line center. The population of main level 4S may be determined according to formula $N_1 = \tau_\nu/k_\nu$, where k_ν is determined according to formula (10). The populations of the main level determined in this way are given in Table 2 (column 9). The obtained values of N_1 are retained for different $\Delta\lambda$, and differ from N_1, obtained according to the line cores, by no more than one-half order of magnitude. This indicates that the values of N_1, computed according to the central sections of the profiles, are valid.

Physical Conditions

The physical conditions in calcium filaments of the flare were determined by solving the steady state equation for the level $4P_{\frac{3}{2}}$. This level is populated by: (a) the field of the flare eigen radiation; (b) recombinations at this level; (c) transitions from the 4S and 3D levels under the influence electron collision of the first kind; (d) spontaneous transitions from the 5S level. The contribution made by the latter to the population of the $4P_{\frac{3}{2}}$ level is very small, and it may be disregarded. Spontaneous transitions to the 4S and 3D levels, transitions to these same levels under the influence of electron collision of the second kind, and ionization by electron collision lead to destruction of the $4P_{\frac{3}{2}}$ level.

Let us write the steady state equation /68

$$\frac{n_3}{n_1} = \frac{n_e Z_{13} + \rho_{13} B_{13}}{(A_{31} + A_{32}) + n_e (Z_{31} + Z_{32} + Z_{3i})} + \\ + \frac{n_e Z_{23}}{(A_{31} + A_{32}) + n_e (Z_{31} + Z_{32} + Z_{3i})} \cdot \frac{n_2}{n_1} + \\ + \frac{n_e R_{i3}}{(A_{31} + A_{32}) + n_e (Z_{31} + Z_{32} + Z_{3i})} \cdot \frac{n^+}{n_1}, \quad (11)$$

where the index 1 pertains to the 4S level; 2 pertains to the 3D level; 3 pertains to the 4P level; Z_{mn}, Z_{nm} are the excitation and deactivation coefficients, respectively, by electron collision; Z_{3i} -- ionization by electron collision; R_{i3} -- recombination coefficients at the 4P level; n^+ -- number of ions of Ca III in 1 cm^3, A_{31}, A_{32}, B_{13} -- Einstein coefficients; ρ_{13} -- density of the eigen radiation field.

Investigations have shown that the last two terms in equation (11) are several orders of magnitude smaller than the first term. Therefore, equation (11) may be simplified as follows

$$\frac{n_3}{n_1} = \frac{n_e Z_{13} + \rho_{13} B_{13}}{(A_{31} + A_{32}) + n_e (Z_{31} + Z_{32})}. \quad (12)$$

The corresponding coefficients of excitation and deactivation by electron collision were computed in (Ref. 6). Excitation by the eigen radiation field was determined according to the self-absorption factor, just as was done in (Ref. 4)

$$\frac{n_3}{n_1}(1-F) = \frac{\rho_{13} B_{13}}{(A_{31} + A_{32}) + n_e (Z_{31} + Z_{32})}$$

Excitation by electron collision is

$$\frac{n_3}{n_1} F = \frac{n_e Z_{13}}{(A_{31} + A_{32}) + n_e (Z_{31} + Z_{32})}. \quad (13)$$

Equation (13) was solved for several values of electron density: from $n_e = 5 \cdot 10^{12}$ to $n_e = 1 \cdot 10^{14}$ (Table 3). Table 4 presents the relative populations which are produced due to excitation by electron collision, and the electron temperatures for several values of n_e corresponding to $\frac{n_3}{n_1}$. The equation of ionization equilibrium was solved for each time and for different n_e (and, consequently, for different T_e). Allowance was made for ionization from the /69 main level by electron collision and recombination to the main and excited levels (photoionization in the flares did not play a significant role, as compared with ionization by collisions):

$$n_e n(\text{Ca III}) \sum_k R_k = n_e n(\text{Ca II}) Z_{1i},$$

TABLE 3

T_e	$\frac{n_3}{n_1}$			
	$n_e=5\cdot10^{12}$	$n_e=1\cdot10^{13}$	$n_e=5\cdot10^{13}$	$n_e=1\cdot10^{14}$
5000	$0.565\cdot10^{-4}$	$1.05\cdot10^{-4}$	$0.33\cdot10^{-3}$	$0.45\cdot10^{-3}$
6000	$1.83\cdot10^{-4}$	$3.24\cdot10^{-4}$	$1.10\cdot10^{-3}$	$1.86\cdot10^{-3}$
7000	$2.90\cdot10^{-4}$	$5.50\cdot10^{-4}$	$1.92\cdot10^{-3}$	$2.84\cdot10^{-3}$
8000	$5.85\cdot10^{-4}$	$1.12\cdot10^{-3}$	$4.10\cdot10^{-3}$	$6.20\cdot10^{-3}$
9000	$8.82\cdot10^{-4}$	$1.70\cdot10^{-3}$	$6.45\cdot10^{-3}$	$9.90\cdot10^{-3}$
10000	$8.90\cdot10^{-4}$	$1.72\cdot10^{-3}$	$6.75\cdot10^{-3}$	$1.06\cdot10^{-2}$
11000	$1.24\cdot10^{-3}$	$2.40\cdot10^{-3}$	$9.72\cdot10^{-3}$	$1.56\cdot10^{-2}$
12000	$1.60\cdot10^{-3}$	$3.08\cdot10^{-3}$	$1.26\cdot10^{-2}$	$2.03\cdot10^{-2}$
13000	$1.95\cdot10^{-3}$	$3.80\cdot10^{-3}$	$1.56\cdot10^{-2}$	$2.53\cdot10^{-2}$
14000	$2.32\cdot10^{-3}$	$4.48\cdot10^{-3}$	$1.86\cdot10^{-2}$	$3.04\cdot10^{-2}$
15000	$2.68\cdot10^{-3}$	$5.20\cdot10^{-3}$	$2.11\cdot10^{-2}$	$5.42\cdot10^{-2}$
20000	$4.16\cdot10^{-3}$	$8.14\cdot10^{-3}$	$3.35\cdot10^{-2}$	$5.47\cdot10^{-2}$

TABLE 4

Node	Time	F	$\left(\frac{N_3}{N_1}\cdot F\right)\cdot10^2$	T_e					
				$9\cdot10^{12}$	$1\cdot10^{13}$	$2\cdot10^{13}$	$3\cdot10^{13}$	$5\cdot10^{13}$	$1\cdot10^{14}$
A	$10^h\,37^m$	0.168	0.336	12900°	12300°	10180°	8330°	7650°	7180°
	10 45	0.21	0.446	17000	14000	11070	10300	8150	7480
	10 57	0.54	0.971	30000	26000	15000	13000	11000	10000
	11 02	0.22	0.403	14000	13300	10800	8760	8000	7400
	11 15	0.20	0.202	10770	10400	8000	7450	7050	6350
B	10 57	0.185	0.388	13700	13000	10650	8670	7900	7300
	11 15	0.170	0.323	12850	12100	10050	8250	7600	7150

from which we have

$$\frac{n(\text{Ca III})}{n(\text{Ca II})}=\frac{N(\text{Ca III})}{N(\text{Ca II})}=\frac{Z_{1'}}{\sum_k R_k} \tag{14}$$

This enables us to determine the amount of Ca III ions, and consequently the total content of calcium N (Ca) = N (Ca II) + N (Ca III). At temperatures above 10000°, calcium occurs primarily in a state of secondary ionization. Assuming that the total amount of calcium in a flare does not change as a function of time, from Table 4 we selected the values of electron temperature and electron concentration for which the total amount of N (Ca) is one and the same. By means of this method, we found that the total amount of calcium is $5.84\cdot10^{13}$. /70

Assuming that the chemical composition of a flare is the same as in the

photosphere, and employing the data presented by Claas (Ref. 7) on the Ca content in the solar atmosphere, we were able to obtain the number of hydrogen atoms along the line of sight. It equals $1.41 \cdot 10^{20}$.

Using the table given by V. M. Sobolev (Ref. 5) for data on n_e and T_e, we were able to determine the hydrogen atom concentration in the basic state at different times. Since hydrogen supplies the main amount of free electrons, we may assume that n_e equals n_H^+. The total hydrogen concentration is then $n_H = n_e + n_1$. The effective geometric thickness of calcium filaments is determined by the ratio $\frac{N_H}{n_H}$. Table 5 shows the manner in which the physical conditions change at the node A of the flare. The electron temperature decreases as a function of time, beginning at $10^h\ 45^m$.

TABLE 5

Time	n_e	T_e	$n_I \cdot 10^{-13}$	$n_{II} \cdot 10^{-13}$	h, см	v_t, km/sec
$10^h\ 57^m$	$9.0 \cdot 10^{12}$	12900°	0.10	1.00	$1.41 \cdot 10^7$	11.4
10 45	$1.0 \cdot 10^{13}$	13500	0.79	1.79	$0.79 \cdot 10^7$	19.0
10 57	$3.0 \cdot 10^{13}$	13000	5.01	8.01	$1.76 \cdot 10^6$	13.7
11 02	$1.1 \cdot 10^{13}$	12650	0.16	1.26	$1.12 \cdot 10^7$	11.6
11 15	$6.0 \cdot 10^{12}$	12250	0.16	0.76	$1.86 \cdot 10^7$	10.6

Cooling of the calcium filaments is accompanied by changes in the electron concentration and effective thickness of the flare. The effective thickness first decreases by one order of magnitude, and then increases up to the previous value. Consequently, the substance contracts by almost a factor of 10, and then subsequently expands.

The limited number of spectrograms kept us from making a precise determination of the electron concentrations and electron temperatures for the node B. Following are their most probable values: /71

$10^h\ 57^m$ $\quad 0.9 \cdot 10^{13} < n_e < 3 \cdot 10^{13} \quad 13700° > T_e > 8700°$

11 15 $\quad 0.9 \cdot 10^{13} < n_e < 3 \cdot 10^{13} \quad 12850° > T_e > 8250°$

Expansion due to thermal velocities is insignificant in the lines of ionized calcium, as compared with expansion due to non-thermal, "turbulent" motion. Table 5 presents the "turbulent" velocities for the node of a flare located above the penumbra. These velocities are smaller above the spot in the flare, and comprise 4 km/sec at 10^h57^m and 6.5 km/sec at 11^h15^m. This may be explained by the presence of a magnetic field which is stronger above the spot than it is above the penumbra; this magnetic field leads to partial damping of the "turbulent" velocities.

REFERENCES

1. Alikayeva, K.V., Orlova, T.V. Solnechnyye Dannyye, 7, 67, 1961.
2. Alikayeva, K.V. V Kn: Spektrofotometricheskiye issledovaniya aktivnykh obrazovaniy na Solntse (In the Book: Spectrophotometric Research on Active Formations on the Sun). "Naukova Dumka", Kiev, 1964.
3. Vasil'yeva, G.Ya. Solnechnyye Dannyye, 12, 64, 1961.
4. Mamedov, S.G. Solnechnyye Dannyye, 6, 54, 1962.
5. Sobolev, V.M. Izvestiya Glavnoy Astronomicheskoy Observatorii, 167, 52, 1961.
6. Athay, R.G., Zirker, I.B. Aph. J., 136, 242, 1962.
7. Claas, W.J. Rech. Astr. Obs. Utrecht, 12, 1951.
8. Jefferies, J.T., Smith, E.v.P., Smith, H.J. Aph. J. 129, 146, 1959.

SPECTROPHOTOMETRY OF THE SUNSPOT OBSERVED ON JUNE 19, 1959

Ye. N. Zemanek, A. P. Stefanov

The equivalent widths of 107 Fe I lines were measured in the region 6520-4870 Å. A curve of growth was constructed, and the physical parameters for the sunspot were derived: $T_{ex} = 3640 \pm 90°$, $N = (25.2 \pm 6.8)10^{18}$, $v = 3$ km/sec.

A graphic method is proposed for determining excitation temperature from the growth curve.

The dependence of the equivalent widths of the lines on the strength of the magnetic field and the spot's position on the solar disk is shown by comparing them for four spots.

We studied a large spot which passed through the solar disk in June, 1959./72 We studied this spot when it was at different positions with respect to the central meridian. Photographs of the spectra were obtained on June 19, 22 and 27, when the spot was in the eastern hemisphere ($\phi = +11°.0$; $\lambda = -45°$), in the center of the disk ($\phi = +11°.5$; $\lambda = -5°$) and in the western hemisphere ($\phi = +11°.5$; $\lambda = +62°$).

This article investigates the spectrum of the spot, which was obtained on June 19 with good transmission and small image oscillations. The observational method and the processing were described previously (Ref. 3, 4).

For the study, 107 lines of neutral iron in the λλ 6520-4870 Å region were chosen. The equivalent widths W of these lines are given in Table 1. This table also presents the excitation potentials of the lower level E_n (Ref. 5), and the oscillator strengths in the form of lggfλ (Ref.1) and lgW/λ. A determination of the influence of diffuse light upon the equivalent widths showed that the magnitude of the diffuse light was small and could not be taken into consideration.

We employed the equivalent widths of the lines to compile a growth curve. The quantity lg W/λ is plotted along the ordinate axis, and the quantity

$$\lg X_f = \lg gf\lambda - \frac{5040}{T_e} E_n \qquad (1)$$

is plotted along the abscissa axis (T_e - the provisional excitation temperature).

In order to clarify the influence of T_e on the physical parameters which were determined according to the growth curve method, curves were compiled for three values of the provisional temperature (4000; 3800; 3600°).

TABLE 1

№	λ	W	E_n	$\lg gf\lambda$	$\lg W/\lambda$
1	6518.376	0.109	2.82	1.33	—4.776
2	6430.851	.346	2.17	1.58	.269
3	11.658	.275	3.64	3.75	.367
4	08.031	.229	3.67	2.94	.447
5	00.010	.352	3.59	3.73	.259
6	6393.605	.261	2.42	2.19	.389
7	44.154	.156	2.42	0.96	.608
8	36.835	.180	3.67	3.12	.546
9	35.335	.248	2.19	1.35	.407
10	22.693	.140	2.58	1.32	.655
11	11.506	.138	2.82	0.90	.660
12	6297.80	.197	2.21	0.85	.504
13	70.238	.125	2.85	1.33	.700
14	65.140	.205	2.17	0.90	.485
15	52.561	.204	2.39	2.00	.486
16	46.334	.171	3.59	3.49	.563
17	40.266	.094	4.12	2.56	.822
18	29.234	.092	2.83	1.04	.830
19	19.290	.222	2.19	1.09	.447
20	13.438	.189	2.21	0.87	.517
21	00.323	.157	2.60	1.19	.596
22	6191.562	.232	2.42	2.33	.426
23	73.343	.182	2.21	0.76	.530
24	70.492	.174	4.77	3.68	.549
25	37.696	.190	2.58	2.64	.509
26	36.999	.125	2.19	0.88	.691
27	36.620	.193	2.44	2.41	.502
28	02.178	.122	4.81	4.16	.698
29	6078.496	.098	4.77	3.96	.793
30	12.75	.077	4.54	3.20	.893
31	5984.805	.137	4.71	3.99	.640
32	83.704	.104	4.53	3.28	.759
33	5976 799	.105	3.93	2.74	.756
34	34.658	.094	3.91	2.83	.800
35	27.798	.093	4.63	3.77	.805
36	20.520	.039	3.22	1.38	—5.181
37	5809.249	.078	3.87	2.46	—4.872
38	5778.47	.100	2.58	0.51	.762
39	75.090	.117	4.20	2.92	.693
40	53.136	.118	4.24	3.37	.688
41	31.771	.093	4.24	3.00	.790
42	17.845	.128	4.27	3.12	.649
43	01.553	.176	2.55	1.65	.510
44	5679.023	.119	4.63	3.60	.678
45	55.506	.100	4.24	3.19	.753
46	5638.266	0.117	4.20	3.25	—4.683
47	18.646	.089	4.19	2.82	.800
48	15.652	.337	3.32	4.39	.222
49	5586.763	.278	3.35	4.18	.303
50	76.097	.200	3.42	3.36	.445
51	72.849	.289	3.38	4.06	.285
52	67.401	.136	2.60	1.22	.612
53	62.712	.117	4.42	3.20	.677
54	54.895	.131	4.53	4.04	.627
55	43.930	.117	4.20	3.08	.676
56	06.782	.276	0.99	0.90	.300
57	5497.519	.290	1.01	1.09	.278
58	34.527	.343	1.01	1.41	.199

/73

continuation of TABLE 1 /74

№	λ	W	E_n	$\lg gf\lambda$	$\lg W/\lambda$
59	29.699	.591	0.95	1.91	—3.963
60	24.15	.276	4.06	4.89	—4.292
61	05.778	.439	0.99	1.82	.091
62	00.509	.187	4.35	4.91	.460
63	5397.131	.466	0.91	1.69	.063
64	93.174	.253	3.23	3.30	.328
65	83.374	.224	4.29	5.04	.481
66	71.493	.558	0.95	1.91	—3.983
67	67.470	.213	4 40	4 71	—4.402
68	64.874	.185	4.43	4.71	.462
69	39.935	.263	3.25	3.55	.308
70	32.903	.210	1.55	0.85	.404
71	24.185	.350	3.20	4.24	.182
72	02.307	.258	3.27	3.74	.312
73	5281.796	.336	3.03	3.27	.196
74	69.541	.620	0.86	2.40	—3.929
75	66.562	.258	2.99	3.89	—4.310
76	63.314	.258	3.25	3.33	.309
77	53.479	.157	3.27	2.42	.524
78	50.650	.234	2.19	1.83	.350
79	32.946	.342	2.93	3.62	.185
80	17.395	.192	3.20	3.18	.433
81	16.278	.239	1.60	1.53	.338
82	5192.350	.260	2.99	3.81	.300
83	91.460	.218	3.03	3.78	.376
84	51.915	.326	1.01	0.61	.198
85	45.105	.234	2.19	0.62	.341
86	23.723	.222	1.01	0.58	.363
87	5083.342	.232	0.95	0.53	.340
88	74.757	.199	4.20	4.39	.405
89	49.825	.313	2.27	2.54	.207
90	44.221	.250	2.84	2.21	.304
91	5014.950	0.208	3.93	3.82	—4.381
92	02.800	.148	3.38	2.56	.528
93	4950.112	.131	3.40	2.60	.577
94	46.394	.171	3.35	3.09	.461
95	39.690	.224	0.86	0.43	.343
96	38.820	.252	2.86	2.89	.292
97	24.776	.178	2.27	1.96	.441
98	20.509	.490	2.82	4.40	.002
99	18.999	.351	2.85	3.90	.146
100	07.743	.115	3.42	2.24	.629
101	03.317	.244	2.87	3.22	.302
102	4891.496	.368	2.84	4.05	.123
103	90.762	.306	2.86	3 61	.203
104	75.89	.118	3.32	2.09	.616
105	72.144	.304	2.87	3.68	.205
106	71.323	.301	2.85	3.90	.209
107	63.653	.119	3.42	2.36	.611

/75

Table 2 presents the excitation temperatures T_e obtained for each curve, the number of atoms N, and the velocity v. It follows from the table that a change in the provisional temperature has practically no influence upon the final excitation temperatures.

TABLE 2

T_e, °K	T_e, °K	$N \cdot 10^{18}$	v, km/sec
4000	3650± 90	30.4±7.8	3.0
3800	3610±100	25.2±6.8	3.0
3600	3620±100	35.5±9.8	3.0

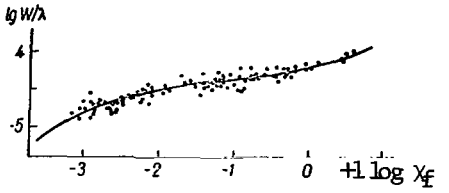

Figure 1

Growth Curve Compiled According to the Fe I Lines for a Spot on June 19, 1959

Figure 1 shows the growth curve for $T_e = 3600°$.

In order to control the computation of the excitation temperature, the growth curve method which we employed entailed a somewhat different procedure. Conditional equations were compiled for the desired corrections $\Delta\Theta$ to the provisional temperature ($\Theta = 5040/T_e$). The problem was solved graphically. In order to do this, the deviation l of points from the growth curve was measured along the abscissa axis. It is understood that the smallest horizontal scattering of points with respect to the curve will occur, if it is displaced by the value /76

$$l_0 = \frac{\Sigma l}{n}, \tag{2}$$

where n is the number of lines (points).

We then obtain the following from equation (1)

$$\Delta\Theta = \frac{l - l_0}{E_n}. \tag{3}$$

Consequently, $\Delta\Theta$ may be determined as the tangent of the angle of inclination for the line expressing the dependence between the excitation potential of the lower level and the deviation of the point from the growth curve.

Figure 2 shows the inclination of the lines for different provisional temperatures. Excitation temperatures of 4000 and 3400° produce an inclination at different sides. If the average of the two values obtained for the temperature is used as the provisional temperature, then the inclination will almost equal zero.

Solving the system of equations (3) according to the method of least squares, we obtain the results shown in Table 3.

Thus, we may conclude on the basis of both methods that the excitation temperature of the spot is the same and comprises 3640°.

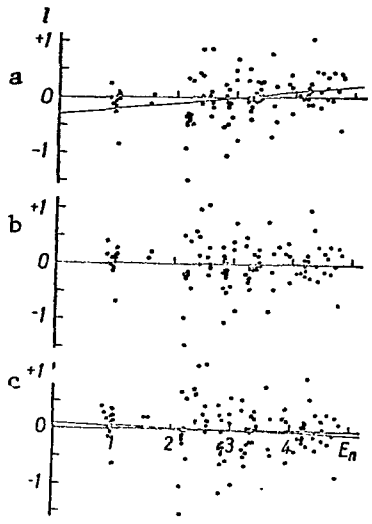

Figure 2

Dependence Between the Excitation Potential of the Lower Level and the Deviation of the Points from the Growth Curve:

a - T_e = 4000°; b - T_e = 3400°;

c - T_e = 3650°.

In order to determine the quantitative index showing the dependence of the equivalent line widths on the magnetic field strength for different positions of the spot on the disk, we formulated the ratio between the sums of the equivalent widths. The same lines appearing for spots on June 19, 22 and 27, 1959, and September 19, 1958 were selected. The sum of the equivalent widths for a spot on June 22, which was located in the center of the disk, was used as the unit. /77

Table 4 gives the coordinates, the areas in fractions of a million for the hemisphere S_p, the magnetic field strength H in Gauss for four spots, the determined excitation temperatures T_e, the number of atoms N, the atom velocity v, and the ratio between the sums of the equivalent widths.

According to the theory advanced by V. Ye. Stepanov (Ref. 2), the increase in the equivalent widths of the lines in the magnetic field is proportional to the splitting displacement and the number of subcomponents. When these sums were compiled, it was advantageous to assign the appropriate weight to the line having magnetic amplification. The line was included in the sum with a weight equalling $n\delta$, where n is the number of splitting subcomponents in the magnetic field, and δ is the splitting displacement for unit strengths and velocities of the atoms.

TABLE 3

T_e, °K	ΣI	I_0	$\Delta\Theta$	$I-I_0$ for $E_n=0$	T_e, °K
4000	−3.97	−0.037	+0.0099	−0.30	3750±100
3400	+0.25	+0.002	−0.026	+0.08	3550±100
3650	+2.39	+0.022	+0.0037	−0.004	3640± 90

A comparison of the magnetic field strengths of the spots and of the ratios between the equivalent width sums shows that there is a definite dependence between them: the sum of the equivalent widths is greater at the point where the magnetic field is stronger. In the case of identical strengths,

TABLE 4

Spot	$\varphi°$	$\lambda°$	S_p	H, Gauss	T_e, °K	$N \cdot 10^{18}$	v, km/sec	$\frac{\Sigma W_i}{\Sigma W_c}$	$\frac{\Sigma W_i^B}{\Sigma W_c^B}$
22.VI 1959	+11.5	— 5	1150	3200	3890±130	7.1±2.1	3.1	1.000	1.000
19.VI 1959	+11.0	—45	1230	3700	3640± 90	25.2±6.8	3.0	1.078	1.029
27.VI 1959	+11.5	+62	1300	2600	3770±140	15.3±5.6	3.0	0.974	0.951
19.IX 1958	+17.5	— 6	720	2600	4070±170	5.2±3.4	3.0	0.937	0.850

a larger ratio corresponds to a position of the spot which is farther from the center of the disk, as must be the case according to the theory of magnetic amplification. Thus, the "magnetic" index $\Sigma W_i/\Sigma W_c$ points to the dependence /78 of the line equivalent widths upon the magnetic field strength and the angle γ between the line of sight and the field direction. It may be assumed that the results derived from the comparison provide statistical confirmation of theory advanced by V. Ye. Stepanov.

REFERENCES

1. Boyarchuk, M.Ye., Boyarchuk, A.A. Izvestiya Krymskoy Astrofizicheskoy Observatorii (KrAO), 22, 234, 1960.
2. Boyarchuk, A.A., Yefimov, Yu.S., Stepanov, V.Ye. Izvestiya KrAO, 24, 52, 1960.
3. Zemanek, Ye.N., Stefanov, A.P. V Kn: Spektrofotometricheskiye issledovaniya aktivnykh obrazovaniy na Solntse (In the Book: Spectrophotometric Research on Active Formations on the Sun). "Naukova Dumka", Kiev, 94, 1964.
4. Zemanek, Ye.N., Stefanov, A.P. Visnik Kiyivs'kogo Universitetu. Seriya Astronomiy 6, 1964.
5. Moore, C. Contr. Princeton Univ. Observatory, 20, 1945.

ON THE H_α LINE EXCITATION MECHANISM IN THE SOLAR CHROMOSPHERE

R. I. Kostik

The profiles of chromospheric H_α are estimated for certain heights above the photosphere. Photospheric radiation is regarded as a source of excitation. It is shown that both external and internal sources are almost equally responsible for the luminescence of the H_α line. The relative role of internal sources of excitation increases with the height above the photospheric level.

V. V. Ivanov (Ref. 1) has calculated the profiles of chromosphere lines, /79
with allowance for incoherent scattering. An exact solution of the problem was obtained, without drawing conclusions as to the physical state of the chromosphere and without making comparisions with observations. A study by M. V. Matveyeva (Ref. 4) was devoted to this same subject. Several assumptions were advanced by this author (one-dimensional medium, excitation by continuous radiation); however, these assumptions made it impossible to perform a detailed comparison with observations.

The present article calculates the profiles of the H_α line, and compares them with observations, in order to determine the luminescence mechanism. Certain formulas presented in (Ref. 1, 4) were employed. The calculation of the profile of a chromosphere line observed on the limb may be reduced to calculating the following integral

$$I(\tau_0,\ t_0,\ x) = \int_0^{t_0} e^{-\alpha(x)t}\,\varepsilon(\tau,\ x)\,dt, \tag{1}$$

where τ_0 is the optical thickness of the chromosphere along the radius of the Sun in the center of the H_α line; τ - optical depth of the chromosphere along the radius of the Sun in the center of the H_α line; t_0 - optical thickness of the chromosphere along the line of sight in the center of the H_α line; $\alpha(x)$ - dimensionless absorption coefficient [$\alpha(x) = e^{-x^2}$]; $\varepsilon(\tau,x)$ - dimensionless radiation coefficient at the frequency x and at the depth τ.

Let us determine the radiation coefficient by means of the following relationship

$$\varepsilon(\tau,\ x) = \alpha(x)\,B(\tau), \tag{2}$$

where $B(\tau)$ is the source function. The determination of $B(\tau)$ may be re- /80
duced to a concurrent solution of the radiation transport equation and the equation of radiative equilibrium (Ref. 5)

$$\cos\Theta\frac{dI(\tau,\ \Theta,\ x)}{d\tau}=-\alpha(x)I(\tau,\ \Theta,\ x)+\alpha(x)B(\tau);$$

$$B(\tau)=\frac{\lambda}{2}A\int_{-\infty}^{+\infty}\alpha(x)\,dx\int_{0}^{\pi}I(\tau,\ \Theta,\ x)\sin\Theta d\Theta \tag{3}$$

for the following boundary conditions

$$I(0,\Theta,x)=0;\qquad I(\tau_0,\Theta,x)=I_0(x), \tag{4}$$

These conditions indicate that the chromosphere is excited by photospheric radiation with the intensity $I_0(x)$ coming from the photosphere. Equations (3) for the boundary conditions (4) may be reduced to one integral equation

$$B(\tau)=\frac{\lambda}{2}\int_{0}^{\tau_0}K(|\tau-\tau'|)B(\tau')\,d\tau'+$$

$$+\frac{\lambda w}{2\sqrt{\pi}}\int_{-\infty}^{+\infty}I_0(x)\,\alpha(x)\,E_2[\alpha(x)(\tau_0-\tau)]\,dx, \tag{5}$$

where λ is the probability of a quantum survival during an elementary scattering event; w - dilution factor

$$K(\tau)=A\int_{-\infty}^{+\infty}\alpha^2(x)\,E_1[\alpha(x)\tau]\,dx;\quad E_1(x)=\int_{0}^{\frac{\pi}{2}}e^{-x\sec\Theta}\sin\Theta\sec\Theta d\Theta;$$

$$E_2(x)=\int_{0}^{\frac{\pi}{2}}e^{-x\sec\Theta}\sin\Theta d\Theta;\quad A\int_{-\infty}^{+\infty}\alpha(x)\,dx=1.$$

Equation (5) was solved for two values: $\tau_0 = 2$; $\tau_0 = 1$. The Doppler halfwidth of the H_α line was assumed to equal 0.460 Å (a change in the Doppler halfwidth within the limits of 20% had hardly any influence upon the final results).

Let us rewrite equation (5) in the following form /81

$$B(\tau)\left[1-\frac{\lambda}{2}\int_{0}^{\tau}K(\tau-\tau')\,d\tau'-\frac{\lambda}{2}\int_{\tau}^{\tau_0}K(\tau'-\tau)\,d\tau'=\right.$$

$$=\frac{\lambda}{2}\int_{0}^{\tau}K(\tau-\tau')[B(\tau')-B(\tau)]\,d\tau'+ \tag{6}$$

$$+\frac{\lambda}{2}\int_{\tau}^{\tau_0}K(\tau'-\tau)[B(\tau')-B(\tau)]\,d\tau'+$$

$$+\frac{\lambda w}{2\sqrt{\pi}}\int_{-\infty}^{+\infty} I_0(x)\,\alpha(x)\,E_2[\alpha(x)(\tau_0-\tau)]\,dx. \tag{6}$$

A numerical method was applied to solve it. The values of K (τ) were taken from the computations of N. A. Yakovkin. The value of 0.5 was taken for the dilution factor. A change in w with height was not taken into account, since it was less than 2% due to the insignificant thickness of the chromosphere. It was found that the function B (τ) is linear in the case of $\tau_0 = 2$. It will apparently be linear for $\tau_0 = 1$. Therefore, we have

$$B(\tau) = a + b\tau. \tag{7}$$

Substituting expression (7) in equation (6) and assuming that $\tau = 0$ and $\tau = \tau_0$, we obtain a system of two linear equations for determining the coefficients a and b

$$\left.\begin{aligned} a\left[1-\frac{\lambda}{2}\int_0^{\tau_0} K(\tau')\,d\tau'\right] &= \frac{\lambda}{2}\,b\int_0^{\tau_0} K(\tau')\,\tau'\,d\tau' + g(\tau_0) \\ a\left[1-\frac{\lambda}{2}\int_0^{\tau_0} K(\tau-\tau')\,d\tau'\right] + b\tau_0\left[1-\frac{\lambda}{2}\int_0^{\tau_0} K(\tau-\tau')\,d\tau'\right] &= \\ = \frac{\lambda}{2}\,b\int_0^{\tau_0} K(\tau_0-\tau')\,(\tau'-\tau_0)\,d\tau' + g(0). & \end{aligned}\right\} \tag{8}$$

In the case of $\tau_0 = 2$ a = 0.0386, b = 0.0383; in the case of $\tau_0 = 1$ a = 0.0488, b = 0.0568.

The values of the function /82

$$g(\tau) = \frac{\lambda w}{2\sqrt{\pi}}\int_{-\infty}^{+\infty} I_0(x)\,\alpha(x)\,E_2[\alpha(x)\,\tau]\,dx$$

were found by numerical integration.

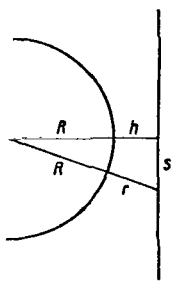

Figure 1

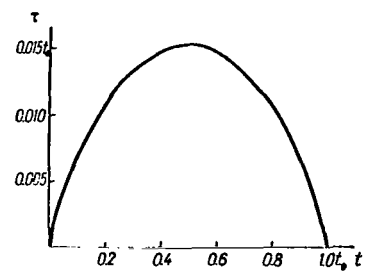

Figure 2

Let us replace $\varepsilon(\tau,x)$ by its value in (2) and (7) in expression (1). The intensity of radiation emanating from the chromosphere along the line of sight is then

$$I(\tau_0, t_0, x) = \int_{t_0}^{0} [1 - e^{-\alpha(x) t}] b\alpha(x) e^{-\alpha(x) t} dt. \tag{9}$$

In order to calculate the second component of the right hand side of equation (9), we must know the dependence of τ on t. The curvature of chromosphere layers is taken into account by this dependence. We shall assume that the number of atoms per unit volume decreases with height above the photosphere level h according to the law $e^{-\beta h}$. The optical depth in the direction of the radius is

$$\tau(r) = \int_{r}^{\infty} \sigma_0 e^{-\beta r} dr, \tag{10}$$

where σ_0 is the absorption coefficient in the center of the line. It may be seen from Figure 1 that

$$r \simeq \frac{s^2}{2R} + h; \tag{11}$$

$$\varepsilon(r) = \frac{1}{\beta} \sigma_0 e^{-\beta h} e^{-\frac{\beta s^2}{2R}}. \tag{12}$$

The optical thickness along the line of sight is /83

$$t(s, h) = \int_{-\infty}^{s} \sigma_0 e^{-\beta r} ds = \frac{1}{2} \sigma_0 e^{-\beta h} \sqrt{\frac{2\pi R}{\beta}} \left[1 - \frac{2}{\sqrt{\pi}} \int_{0}^{\sqrt{\frac{\beta}{2R}}} e^{-x^2} dx\right]. \tag{13}$$

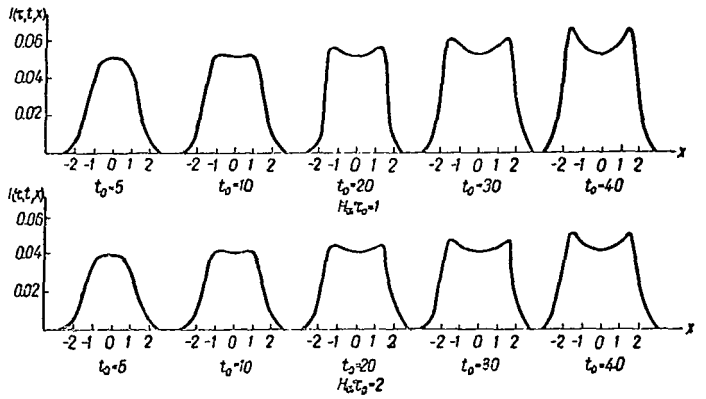

Figure 3

Since

$$\int_{-\infty}^{+\infty} \sigma_0 e^{-\beta r}\, ds = \sigma_0 \sqrt{\frac{2\pi R}{\beta}}\, e^{-\beta h} = t_0, \tag{14}$$

we finally obtain

$$t = \frac{1}{2} t_0 \left[1 - \frac{2}{\sqrt{\pi}} \int_0^{\sqrt{\frac{\beta}{2R}}} e^{-x^2} dx\right]; \tag{15}$$

$$\tau = \frac{1}{\sqrt{2\pi R\beta}} t_0 e^{-\frac{\beta s^2}{2R}}.$$

The dependence of τ on t, computed according to formula (15), is shown in Figure 2 ($\beta = 1.0 \cdot 10^{-8}$ cm). When the profiles of the H_α line were calculated according to the equation (9), the second term of the right hand part was computed by numerical integration. Figure 3 presents the computational results for different values of τ_0 and t_0.

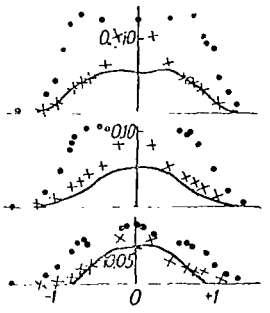

Figure 4

Let us compare the calculated profiles with the observed profiles. A relatively small number of slit spectrograms of the chromosphere lines was obtained. We employed the observations described in (Ref. 2, 3), which were performed when there were no ellipses. Figure 4 shows the observed profiles of the H_α line (h = 1500, 2200, 2900 km above the level of the photosphere) as well as profiles computed according to formula (9) for $\tau_0 = 1$ (Dots - observed values; crosses - reduced profile; solid line - calculated values). /84

The table below presents the total observed and calculated intensities ($\tau_0 = 1$). The last column gives the deviations of the calculated values from the observed values. These deviations may be explained by the influence of inner excitation sources, which we did not take into account. Attention should be called to the increase in the relative portion of inner excitation sources with an increase in the height above the photosphere level.

In summary, it may be stated that luminescence of the H_α line is almost equally caused by outer and inner excitation sources.

h, км	Observational Data			Mean Value	Calculated Value	Deviation, %
1100	—	0.139	—	0.139	0.125	10
1550	0.257	0.147	—	0.202	0.110	46
2200	0.194	0.145	0.200	0.179	0.090	50
2900	0.106	0.121	0.173	0.133	0.070	47
3200	0.081	0.110	0.161	0.117	0.060	49
3600	0.080	0.092	0.146	0.106	0.050	53
3800	0.074	0.083	0.139	0.1 0	0.044	56
4400	0.059	0.059	0.118	0.079	0.031	61
4700	0.048	0.047	0.110	0.065	0.025	62

REFERENCES

1. Ivanov, V.V. Astronomicheskiy Zhurnal, 37, 1021, 1960.
2. Krat, V.A., Krat, T.V. Izvestiya Glavnoy Astronomicheskoy Observatorii (GAO) at Pulkovo, 153, 1955.
3. Krat, V.A., Krat, T.V. Izvestiya GAO at Pulkovo, 155, 1956. /85
4. Matveyeva, M.V. Izvestiya GAO at Pulkovo, 170, 1962.
5. Sobolev, V.V. Perenos Luchistoy energii v atmosferakh zvezd i planet (Transfer of Radiant Energy in the Atmospheres of Stars and Planets). Gostekhizdat, Moscow, 1956.

INFLUENCE OF DISSIPATION ON PLASMA EQUILIBRIUM IN A MAGNETIC FIELD

L. M. Shul'man

Plasma equilibrium conditions are formulated, taking into consideration dissipative processes. The electron thermo- and electroconductivity are specially considered. There are some cases when the investigation of dissipative plasma equilibrium can be reduced to the solution of some plane and one-dimensional problems. One-dimensional equilibrium configurations with a constant magnetic field gradient and constant density of matter are discussed. The effect of volume sources and energy loss is examined in the case when they predominate in the establishment of thermal equilibrium.

This article investigates the influence of finite conductivity and heat transfer upon magnetohydrostatic equilibrium of a thermodynamically ideal plasma. If we may disregard the dissipative processes in the plasma and if there is no field of gravity, the balancing of the magnetic forces and the gas pressure is sufficient for establishing equilibrium. As is known, the only equilibrium condition may thus be reduced to the condition that the sum of the gas pressure gradient and the Maxwell tensor divergence equals zero. It is apparent that equilibrium exists in a non-dissipative plasma in the case of arbitrary distributions of temperature and density of matter. Allowance for dissipative processes significantly constricts this arbitrary condition. In particular, it may be that a strictly determined temperature distribution corresponds to a given magnetic field configuration. /86

Equilibrium Conditions

The motion of a plasma in a magnetic field, with allowance for the finite conductivity and thermoconductivity which are regarded as functions of the thermodynamic parameters, is described (Ref. 1) by the system of equations

$$\frac{d\mathbf{v}}{dt} = -\frac{\nabla p}{\rho} - \frac{1}{4\pi\rho}[\mathbf{H}\,\mathrm{rot}\,\mathbf{H}]; \tag{1}$$

$$\frac{\partial \mathbf{H}}{\partial t} = \mathrm{rot}\,[\mathbf{vH}] - \mathrm{rot}\,(\nu\,\mathrm{rot}\,\mathbf{H}); \tag{2}$$

/87

$$\frac{\partial \rho}{\partial t} + \mathrm{div}\,(\rho\mathbf{v}) = 0; \tag{3}$$

$$\rho T\frac{ds}{dt} = \frac{\nu}{4\pi}(\mathrm{rot}\,\mathbf{H})^2 + \mathrm{div}\,(\varkappa\nabla T); \tag{4}$$

$$s = s_0 + c_v \ln\left(p\rho^{-\gamma}\right): \quad p = \rho RT. \tag{5}$$

In the presence of dissipation, it is apparent that, in addition to the condition of Maxwell equilibrium

$$\nabla p = -\frac{1}{4\pi}[\mathbf{H}\,\mathrm{rot}\,\mathbf{H}] \tag{6}$$

the steady state condition of the magnetic field must be fulfilled

$$\mathrm{rot}(\nu\,\mathrm{rot}\,\mathbf{H}) = 0. \tag{7}$$

The third equilibrium condition -- the steady state condition of the temperature field -- yields one equation

$$\frac{\nu}{4\pi}(\mathrm{rot}\,\mathbf{H})^2 + \nabla(\varkappa\nabla T) = 0. \tag{8}$$

The family of equations (6-8) contains all five unknowns. However, their structure is such that a solution exists, in spite of the overdetermination of the system.

In actuality, integrating equation (7), we obtain

$$\mathrm{rot}\,\mathbf{H} = \frac{1}{\nu}\nabla\varphi, \tag{9}$$

where $\phi(x, y, z)$ is an arbitrary function which is twice differentiable. The remaining equilibrium conditions may now be written in the following form

$$\nabla p = -\frac{1}{4\pi\nu}[\mathbf{H}\nabla\varphi]; \tag{10}$$

$$\frac{1}{4\pi\nu}(\Delta\varphi)^2 + \nabla(\varkappa\nabla T) = 0. \tag{11}$$

It may readily be seen that the system (9-11) has at least two classes of solutions: trivial solutions (ρ = const, T = const), and forceless solutions (rot $\mathbf{H} = \alpha\,\mathbf{H}$). In the latter case, the magnetic field is related to the temp- /88
erature fields by the following relationships

$$\mathbf{H} = \frac{1}{\nu\alpha}\nabla\varphi; \tag{12}$$

$$\nabla(\varkappa\nabla T) = \frac{(\nabla\varphi)^2}{4\pi\nu}. \tag{13}$$

Equilibrium in the Case of Electron Transfer

The transfer coefficients, appearing in the preceding equations, depend on temperature, the vector of the magnetic field strength (anisotropy) and on the plasma density (by means of the Coulomb logarithm). If the transfer is caused primarily by electrons, we may then set

$$\sigma = \sigma_0 T^{3/2}; \quad \varkappa = \varkappa_0 T^{5/2}, \tag{14}$$

where σ_0 and κ_0 are the quantities which depend slightly on density. Without allowance for anisotropy, the equilibrium conditions assume the following form

$$\operatorname{rot} \mathbf{H} = \left(\frac{4\pi\sigma_0}{c^2}\right) T^{3/2} \nabla\varphi; \tag{15}$$

$$\nabla p = -\left(\frac{\sigma_0}{c^2}\right) T^{3/2} [\mathbf{H}\nabla\varphi]; \tag{16}$$

$$\nabla (T^{5/2} \nabla T) + \left(\frac{\sigma_0}{\varkappa_0 c^2}\right) T^{3/2} (\nabla\varphi)^2 = 0. \tag{17}$$

If the conditions at the boundary and the function $\phi(x, y, z)$ are given in the entire region being studied, we may find the temperature distribution according to equation (17). We may then find the magnetic field according to equation (15), and the pressure p(x, y, z) according to equation (16).

Under real physical conditions, the magnetic field depends on all three spatial coordinates. Therefore, strictly speaking, any problem regarding equilibrium of a magnetized plasma is a three-dimensional problem. However, we may point out certain simple cases, when an adequate representation of the equilibrium configuration yields the solution of the plane or even the one-dimensional problem. This simplification makes it possible to reduce the mathematical difficulties connected with an investigation of the system (15-17) in a general form, and makes it possible to obtain the simplest solutions.

Equilibrium in a Plane /89

Symmetry of the configuration may lead to the fact that the equilibrium parameters in a certain plane are independent of their behavior in the vicinity of this plane. They may be determined by solving the corresponding plane problem. This may be verified by setting

$$\varphi = zf(x, y). \tag{18}$$

In the vicinity of the plane z = 0, the gradient of this function has only one non-zero component. This means that the electric current intersects the plane z = 0 at a right angle. If the temperature assumes extreme values in this plane, or if it does not depend on z in general, the magnetic force lines lie in the xy plane. The problem formulated in this way may degenerate into a two-dimensional problem. After simple transformations, a system is obtained from equations (15-17) for determining the fields of the physical quantities in the infinitely small vicinity of the plane xy.

$$\frac{\partial H_y}{\partial x} - \frac{\partial H_x}{\partial y} = \frac{4\pi\sigma_0}{c^2} T^{3/2} f(x, y); \tag{19}$$

$$\frac{\partial p}{\partial x} = -\frac{\sigma_0}{c^2} T^{3/2} H_y f(x, y); \tag{20}$$

$$\frac{\partial p}{\partial y} = \frac{\sigma_0}{c^2} T^{3/2} H_x f(x, y); \tag{21}$$

$$\frac{\partial}{\partial x}\left(T^{5/2}\frac{\partial T}{\partial x}\right) + \frac{\partial}{\partial y}\left(T^{5/2}\frac{\partial T}{\partial y}\right) + \frac{\sigma_0}{\varkappa_0 c^2} T^{3/2} f^2(x, y) = 0. \tag{22}$$

The case f(x, y) = const. occupies a special position. The xy plane loses its priveleged role, since all of the quantities cease to depend on z, not only in the vicinity of the zero plane, but also in the entire space.

The arbitrary function in the system (19-22) makes it possible to obtain different forms of the equilibrium conditions which are suitable for solving a certain specific problem. For example, introducing the new arbitrary function

$$f_1(x, y) = \frac{2\sigma_0}{7\varkappa_0 c^2} T^{3/2} f^2(x, y) > 0,$$

we obtain the Poisson equation for $T^{7/2}$; the general solution of this equation /90 has the following form

$$T^{7/2} = \frac{1}{2\pi}\iint\limits_{(S)} \frac{f_1(x', y')\,dx'\,dy'}{R} + \frac{1}{2\pi}\oint\limits_{(C)} \left\{\frac{1}{R}\cdot\frac{\partial(T^{7/2})}{\partial n} - T^{7/2}\frac{\partial}{\partial n}\left(\frac{1}{R}\right)\right\} dl, \tag{23}$$

where $R = \sqrt{(x - x')^2 + (y - y')^2}$, and $\partial/\partial n$ is the derivative in the direction of the normal; this normal is outside of the Contour C, along which the second integral is taken. It is necessary to know the temperature at the region boundary and the temperature gradient in order to perform the calculation. By determining the temperature according to equation (23), we may calculate the current density

$$j = \frac{\sigma_0}{c^2}\sqrt{\frac{7\varkappa_0}{2\sigma_0}}\, T^{3/4}\sqrt{f_1(x, y)},$$

and we may then calculate the magnetic field by employing the methods of magnetostatics. This computational method is not suitable, if the magnetic field is the given quantity, and not $f_1(x, y)$. In this case, it is advantageous to introduce a certain arbitrary function which is proportional to the current density

$$f_2(x, y) = -\frac{\partial H_y}{\partial x} - \frac{\partial H_x}{\partial y}. \tag{24}$$

The remaining equilibrium conditions acquire the following form

$$\frac{\partial p}{\partial x} = -\frac{H_y}{4\pi} f_2(x, y); \tag{25}$$

$$\frac{\partial p}{\partial y} = \frac{H_x}{4\pi} f_2(x, y); \tag{26}$$

$$\nabla(T^{5/2}\nabla T) + \frac{c^2}{16\pi\varkappa_0\sigma_0} T^{-3/2} f_2(x, y) = 0. \tag{27}$$

The main difficulty which is entailed in calculating the equilibrium configuration for the given portion consists of integrating the non-linear equation (27).

Equilibrium Along a Straight Line

If the magnetic force lines are perpendicular to the xz-plane, then

$H_x = \frac{\partial H_x}{\partial y} = \frac{\partial p}{\partial y} = 0$. In the case of $\frac{\partial T}{\partial y} = 0$, equilibrium along the line Ox does /91
not depend on the temperature distribution, or the density and pressure in the vicinity of this line. It may be calculated by solving the corresponding one-dimensional problem. The equilibrium conditions are now particularly simple:

$$\frac{dH_y}{dx} = \frac{4\pi\sigma_0}{c^2} T^{3/2} f(x); \tag{28}$$

$$\frac{dp}{dx} = -\frac{\sigma_0}{c^2} T^{3/2} H_y f(x); \tag{29}$$

$$\frac{d}{dx}\left(T^{5/2}\frac{dT}{dx}\right) + \frac{\sigma_0}{\varkappa_0 c^2} T^{3/2} f^2(x) = 0. \tag{30}$$

Introducing the new arbitrary functions, we may obtain the explicit form of the solutions investigated above for the case of equilibrium in a plane.

Following are several of the simplest examples. If the plasma is isothermic, then its equilibrium state is trivial -- the plasma must be uniform and uniformly magnetized.

A plasma of constant density may be in equilibrium only in the case of

$$p(x) = \rho_0 RT(x);$$
$$\frac{H^2}{8\pi} = \rho_0 R(T_0 - T),$$

where the temperature distribution is subordinate to the condition

$$\frac{d}{dx}\left(T^{5/2}\frac{dT}{dx}\right) + \frac{\rho_0 R c^2 T^{-3/2}}{8\pi\varkappa_0\sigma_0(T_0 - T)}\left(\frac{dT}{dx}\right)^2 = 0. \tag{31}$$

This equation may be written in dimensionless variables

$$\Theta = \frac{T}{T_0}; \quad \xi = \frac{x}{L},$$

where T_0 is the temperature at the neutral point of the magnetic field, and L is an arbitrary constant with the dimension of length. The condition of thermoequilibrium may now be written as follows

$$\frac{d}{d\xi}\left(\Theta^{5/2}\frac{d\Theta}{d\xi}\right) + K\Theta^{-3/2}(1-\Theta)^{-1}\left(\frac{d\Theta}{d\xi}\right)^2 = 0 \tag{32}$$

and may be integrated by quadratures /92

$$\xi = \pm\int_1^\Theta \Theta^{5/2}(1+\Theta^{-1})^K \exp\left[-K\left(\Theta^{-1} - 2\Theta^{-2} + \frac{1}{3}\Theta^{-3}\right)\right] d\Theta. \tag{33}$$

It is even simpler to calculate the configuration with a constant field gradient. The distribution of the magnetic field and of the gas pressure may thus be described by the following relationships

$$H=(\nabla H_0)\,x;\quad p=p_0-\frac{(\nabla H)_0^2}{8\pi}\,x^2,$$

where p_0 is the pressure at a neutral point. The temperature distribution may be found by integrating the following equation

$$\frac{d^2}{dx^2}(T^{7/2})+\frac{7c^2(\nabla H)_0^2}{32\pi\varkappa_0\sigma_0}T^{-5/2}=0. \tag{34}$$

Its solution has the following form

$$\frac{x}{L}=\int_0^{\arccos T/T_0}\cos^{5/2}\tau\,d\tau, \tag{35}$$

where the following quantity is the unit of spatial scale

$$L=\frac{4(\pi\varkappa_0\sigma_0)^{1/2}T_0^{7/2}}{c(\nabla H)_0}. \tag{36}$$

Role of Volume Sources and Energy Loss

The influence of volume sources and energy loss was ignored in the preceding sections. However, when there are no external sources and losses, the equilibrium configurations investigated above cannot be realized, due to the impossibility of satisfying the correct boundary conditions. If we formally extrapolate the solutions obtained to infinity, we obtain negative values for density, temperature, and pressure. A uniform (in the absence of gravitation) state is the only equilibrium condition of the plasma which satisfies the conditions at infinity.

In order that equilibrium, magnetized non-uniformity may exist in a uniform plasma, surface energy sources are requisite, and in certain cases /93
fields on the boundary of the non-uniform region which specify the correlation between the different solutions of the equilibrium equations. We may compile more complex configurations from the equilibrium configurations investigated above, by introducing external sources on the conjugate surfaces.

The necessity of allowing for volume sources, and not surface sources, arises in astrophysical problems. For example, if a plasma is optically transparent, the possibility of energy loss due to radiation must be taken into account. The inflow of energy may be caused by thermonuclear reactions, by dissipation of waves arriving from the outside, and by other factors. In the case of acoustic plasma heating, we may separate the regular background from the random pulsating motions, and we may regard the latter as a volume source of energy.

The problem formulation in the general case requires the introduciton of appropriate terms in the energy equation (4). However, it may be represented more simply for studying the case when the volume sources are considerably more

effective than the liberation of heat due to dissipation of the regular magnetic field, and when the radiation energy flux is considerably greater than the conductive heat flux. Thermoequilibrium is thus maintained primarily due to balancing of the volume sources and losses.

Let us approximate the specific volumetric inflow of energy by the expression $Q_+ = \alpha_+ p^{m+}T^{n+}$, where α_+ is a certain dimensional coefficient which does not depend on the thermodynamic parameters. We may write a similar quantity for the energy losses in the form $Q_- = \alpha_- p^{m-}T^{n-}$. Thermoequilibrium may be observed in the case of

$$\alpha_+ p^{m+} T^{n+} = \alpha_- p^{m-} T^{n-}. \tag{37}$$

The remaining equilibrium conditions are the same as previously

$$\operatorname{rot} \mathbf{H} = 4\pi N p^{-3\Delta m/2\Delta n} \nabla\varphi; \tag{38}$$

$$\nabla p = -N p^{-3\Delta m/2\Delta n} [\mathbf{H}\nabla\varphi], \tag{39}$$

where

$$\Delta m = m^- - m^+; \quad \Delta n = n^- - n^+; \quad N = \left(\frac{\sigma_0}{c^2}\right)\left(\frac{\alpha_+}{\alpha_-}\right)^{-3/2\Delta n}$$

It may be readily seen that in the case of p = const the field with zero force rot **H** = α **H** may satisfy the equilibrium conditions. The magnetic field is thus

$$\mathbf{H} = \left(\frac{4\pi N}{\alpha}\right) p^{-3\Delta m/2\Delta n} \nabla\varphi. \tag{40}$$

The fact that it is described by a scalar potential once more points to the impracticability of a configuration with zero force in all space [compare with the study (Ref. 2)]. /94

If thermoequilibrium is maintained due to volume sources and energy loss, the necessity arises of introducing and calculating an arbitrary function. The pressure may be calculated directly from equation (6) based on the given magnetic field, and the density and temperature may then be determined from equation (37) and the Clapeyron equation.

Thus, in the case under consideration -- just as in an adibatic plasma -- the selection of the equilibrium configuration is still quite arbitrary. The difference from an adibatic plasma lies only in the fact that a specific distribution of temperature and density corresponds to the given distribution of the magnetic field and the gas pressure.

REFERENCES

1. Landau, L.D., Lifshits, Ye.M. Elektrodinamika sploshnykh sred (Electrodynamics of Continuous Media). GTTI, Moscow, 1957.

2. Shafranov, V.D. V Kn: Voprosy teorii plazmy (Problems of the Theory of a Plasma). Gosatomizdat, Moscow, 2, 92, 1963.

ON THE CHOICE OF THE PRE-FLARE PLASMA STATE MODEL

L. M. Shul'man

The problem of the pre-flare plasma state model is discussed. The pre-flare state has to be an equilibrium state up to very slow processes. It is shown that acoustic heating and radiation rapidly set up thermal equilibrium in the chromospherical plasma. Therefore, the models formerly proposed are incorrect unless they satisfy the thermal equilibrium conditions.

As observations have shown, (Ref. 5), solar flares arise in regions which /95
are characterized by a composite structure of the magnetic field. The flare process itself may be interpreted as a transition of the plasma from the "excited" equilibrium state with excess magnetic energy into another equilibrium state which is accompanied by the transformation of the magnetic field energy into kinetic and thermal plasma energy, as well as into the radiation energy of rapid particles. The more the magnetic fields are rearranged, the more intense is the flare. This fact was established as a result of extensive research carried out at the Crimean Astrophysical Observatory (Ref. 1, 2).

In spite of the fact that certain phenomena related to the flares are more or less clear from a qualitative standpoint, no quantitative theory of flares has yet been formulated. This is due to the fact that the great diversity and complex nature of each individual phenomenon make it difficult to formulate an adequate model of the process, which is sufficiently simple at the same time, and which could sustain a rigorous physical and mathematical analysis. Therefore, it is of interest to formulate a simplified model of a flare in general -- i.e., a rather abstract picture of the transformation of the magnetic field in the plasma, which is accompanied by the change of magnetic energy into other forms. Research on a theory for discharge in the vicinity of a neutral point of a magnetic field belongs to this category (Ref. 3, 6-12, 14-16).

The theory must answer several questions. Certain of these questions are as follows. How may an equilibrium configuration of a plasma with a magnetic field, which does not satisfy the condition of an energy minimum, be produced and exist for a long period of time? How, and for what reason, is the initial /96
equilibrium disturbed? What are the gasodynamic, electrodynamic, and thermodynamic situations in the process after equilibrium has been disturbed? How may we explain the comparatively short duration of a flare?

In order to answer the second question, it is natural to formulate and discuss a hypothesis regarding the instability of the plasma formation, in which the flare arises (Ref. 3, 6, 7, 10, 12). An attempt to study a nonselfconsistent process -- compulsory contraction of the plasma by a magnetic field which is increasing in the vicinity of the neutral point -- in essence represents a special case of this hypothesis. The only difference lies in the

fact that in this case the causes of the instability producing the field amplification are not studied, but rather the causes of the instability which is directly due to this amplification (Ref. 9). This question may be answered by stipulating that motion plays the role of the causative factor in a group of spots. However, it is still not completely clear why a plasma, whose equilibrium is unstable, may be in this state considerably longer than the duration of the transition process into a stable state. What specifies the metastable state of the plasma, and why does the transition into the stable state not occur gradually, in accordance with the deformation of the initial stable configuration? Dungey (Ref. 15) and Sweet (Ref. 17), who studied the unstable configuration of a magnetic field with a neutral point of the X type, which is produced when the magnetic poles converge, avoided this fact.

Not every instability of a plasma configuration may serve as a flare model. Changes in the magnetic field configuration during the development of an instability are insufficient for observing a flare. It is necessary that the instability be accompanied by dissipation of a significant portion of the magnetic energy. Studies performed in the adiabatic approximation are unsatisfactory from this point of view.

The formulation of a theoretical flare model may be initiated with the selection of a certain, comparatively simple configuration of a magnetized plasma, whose stability is then studied. When a pre-flare configuration is selected, it is usually specified that the plasma is in mechanical equilibrium. This makes it possible to select the initial plasma state quite arbitrarily. If attention is called to the dissipative processes, then the arbitrary nature /97 of the selection may be significantly reduced, since electrodynamic and thermo-equilibrium will be observed, in addition to mechanical equilibrium.

The purpose of this article is to clarify the extent to which the model of the pre-flare state, which was studied previously, satisfies these conditions.

The simplest model of the pre-flare state is the one-dimensional equilibrium configuration with a constant magnetic field gradient, which was studied by A. B. Severnyy (Ref. 10). The law governing the density change within the current layer was selected in the following form

$$\rho = \rho_0 \left(\frac{1 - x^2}{L^2} \right), \qquad (1)$$

i.e., it was postulated that the temperature within the layer was constant. If thermal equilibrium in the layer were maintained due to the electron thermoconductivity, then -- as may be seen from the equilibrium condition (30*)* -- the condition of a constant temperature entails the condition $f(x) = 0$. In its turn, this condition requires that the gas pressure be constant, and the magnetic field be uniform. It may be shown that radiation energy losses and acoustic heating in the chromosphere of the Sun play a more significant role in establishing horizontal equilibrium than does Joule dissipation and electron thermoconductivity. However, in this case the isothermality entails uniformity,

* The numbers of formulas from the article (Ref. 13) are designated below by an asterisk.

and is incompatible with the presence of a neutral plane.

Another one-dimensional configuration (Ref. 9) with more complex laws for measuring the density and field strength has also been studied:

$$\rho=\rho_0\left(\frac{1-x^2}{L^2}\right)^{3/2}; \tag{2}$$

$$H=H_0\left[1-\left(\frac{1-x^2}{L^2}\right)^{5/2}\right]^{1/2} \tag{3}$$

The temperature distribution follows from formulas (2) and (3) and the condition of mechanical equilibrium

$$T=T_0\left(\frac{1-x^2}{L^2}\right) \tag{4}$$

Substituting expressions (2) - (4) in formulas (28*) - (30*), we find /98
that the distributions (2), (3) are incompatible with the conditions of thermoequilibrium, which is established due to electron transfer. In actuality, it follows from condition (30*) that

$$\frac{\sigma_0 L^2 f^2(x)}{2\varkappa_0 c^2 T_0^2}=\frac{1-6x^2}{L^2}. \tag{5}$$

The left hand side of this equation is essentially positive, whereas the right hand side becomes negative in the case $x^2 > L^2/6$. It may thus be stated that the electron thermoconductivity is not in a position to provide the temperature distribution (4).

Let us determine whether such a temperature distribution is established due to volumetric energy exchange. The relationship between the local values of pressure and temperature follows from formulas (2) - (4)

$$p=\rho_0 R T_0^{-3/2} T^{5/2}, \tag{6}$$

while it follows from formula (37*) that

$$p=\left(\frac{\alpha_+}{\alpha_-}\right)^{1/\Delta m} T^{-\Delta n/\Delta m}. \tag{7}$$

It is apparent that the plasma will be in thermoequilibrium if the following equations are fulfilled

$$\left(\frac{\alpha_+}{\alpha_-}\right)^{\frac{1}{\Delta m}}=\rho_0 R T_0^{-\frac{3}{2}}; \quad \frac{\Delta n}{\Delta m}=-\frac{5}{2}. \tag{8}$$

Although in principle configuration (2), (3) is compatible with volumetric energy exchange, the sources and losses which occur in actuality do not satisfy conditions (8).

A configuration with a neutral point of the type X has been regarded in (Ref. 3, 10) as the model of a pre-flare state. The dependence of the magnetic field on the coordinates thus has the form

$$H_x=k_2x+k_3y; \quad H_y=-(k_1x+k_2y), \tag{9}$$

where k_1, k_2, k_3 are constants. The pressure distribution is determined from the condition of mechanical equilibrium

$$p=p_{00}-\frac{k_1+k_3}{8\pi}(k_1x^2+2k_2xy+k_3y^2), \tag{10}$$

where p_{00} is the pressure at a neutral point. It may be shown that this distribution of the field and the pressure, in conjunction with the condition of thermoequilibrium, is independent of the mechanism by which thermoequilibrium is established. However, on this basis we cannot assume that the configuration being discussed is suitable for a model of a pre-flare state. In actuality, according to well known determinations, the time required to establish thermal and electrodynamic equilibrium by means of electron transfer is very large, but the radiation-acoustic processes establish thermal equilibrium quite rapidly. It is significant that the thermal relaxation time τ does not depend on the linear configuration dimensions in this case. A specific determination of the relaxation time depends on the assumed chromosphere model. Employing the model of Jager-Kuperus (Ref. 16), we may obtain the expression

/99

$$\tau\simeq 10^{-7.3}T^{1.9}. \tag{11}$$

The substitution of any tenable temperature values at the neutral point yields a time which is less than one minute. If we assume the model advanced by M. A. Livshits and G. M. Nikol'skiy (Ref. 4), the relaxation time decreases by one-two orders of magnitude. In both models of the chromosphere, the density is related to the temperature by the universal relationship

$$p=CT^{3/2}. \tag{12}$$

The coefficient C in the model of Jager-Kuperus is on the order of 10^{-3} ; in the model of G. M. Nikol'skiy it is one order of magnitude less. Thus, equations (8) are not fulfilled. An elementary determination of the maximum field strength by means of the relationship $p = H^2/8\pi$ and expression (13) yields values which are on the order of several Gauss, which sharply diverges from observations.

The reason for this divergence may be indicated. The determination pertains to the strength of a self-consistent field of a magnetized nonuniformity which is entirely located in the chromosphere, or in the intermediate region to the corona. Such weak magnetic fields can actually exist here. The field of the pre-flare configuration belongs primarily to subphotospheric currents, and not to chromospheric currents. This field is almost completely nonvortical in the chromosphere (rot H = 0), and therefore it is a field with zero force. A field with zero force has no influence upon equilibrium, and may have any strength. Thus, the figure eight configuration of the field, which was investigated by Dungey (Ref. 15) is arbitrary to a significant extent. It must be assumed that the configuration postulated by Sweet (Ref. 7) is closer to the real configuration.

REFERENCES

1. Godovnikov, N.V., Ogir', M.B., Shaposhnikova, Ye.F. Izvestiya Krymskoy Astrofizicheskoy Observatorii (KrAO), 31, 216, 1963. /100
2. Gopasyuk, S.I., Ogir', M.B., Severnyy, A.B., Shaposhinkova, Ye.F. Izvestiya KrAO, 29, 15, 1963.
3. Danzhi, Dzh. Kosmicheskaya Elektrodinamika (Space Electrodynamics). Gosatomizdat, Moscow, 1961.
4. Livshits, M.A., Nikol'skiy, G.M. Astronomicheskiy Zhurnal (AZh), 41, 75, 1964.
5. Severnyy, A.B. Izvestiya KrAO, 31, 159, 1964.
6. Severnyy, A.B. Izvestiya KrAO, 20, 22, 1958.
7. Severnyy, A.B. AZh, 35, 335, 1958.
8. Severnyy, A.B., Shabanskiy, V.P. AZh, 37, 609, 1960.
9. Severnyy, A.B. AZh, 38, 402, 1961.
10. Severnyy, A.B. AZh, 39, 990, 1962.
11. The Sun. Edited by J. Kuiper. IL, Moscow, 1957.
12. Syrovatskiy, S.I. AZh, 39, 987, 1962.
13. Shul'man, L.M. Present Collection, p. 72.
14. Shul'man, L.M. Voprosy Kosmogonii, 10, 70, 1964.
15. Dungey, J.W. Electromagnetic Phenomena in Cosmical Physics. Cambridge University Press, 135, 1958.
16. Jager, C.de, Kuperus, M. BAIN, 16, 510, 1961.
17. Sweet, P.A. Electromagnetic Phenomena in Cosmical Physics. Cambridge University Press, 123, 1958.

CONVECTIVE STAR MODEL WITH NON-RIGID ROTATION

V. V. Porfir'yev

The paper deals with the stationary rotation of stars. It is proved that stationary rotation is characterized by a decrease of angular velocity and "equatorial slowing" down on the surface of a star in the presence of sufficiently developed circulation. It is shown that such a law of rotation is not observed in real stars; therefore, it is necessary to consider rotation without circulation.

The equations of star structure in the absence of circulation are derived. In this case the law of rotation is determined by the distribution of temperature and density in the star.

The law of rotation for a star with a convective core and a radiative envelope is given. The angular velocity of rotation increases slowly towards the surface. Distribution of the angular velocity on the surface of such a star is similar to that observed for the Sun.

Selection of the Rotation Law

Up to the present time, when the inner structure of a rotating star has /101
been investigated, it has almost always been assumed that angular velocity does not depend on the coordinates -- i.e., it was assumed that the rotation is rigid. However, as was shown in the study (Ref. 5), this assumption leads to insoluble contradictions. This study determines the stationary law for the rotation of a star. A preliminary investigation was carried out in (Ref. 5), and the results of more comprehensive and precise calculations are presented in this article.

Since we cannot assume that the rotation of a star is rigid, we must determine the law of rotation or the conditions which enable us to find it during the computational process. We shall first investigate the Euler equation for the ϕ-component of velocity. We may immediately set the partial derivative with respect to time equal to zero, since we shall only consider a stationary case.

Let us write the following equation

$$v_r \frac{\partial v_\varphi}{\partial r} + v_\vartheta \frac{\partial v_\varphi}{\partial \vartheta} + \frac{v_r v_\varphi}{r} + \frac{v_\vartheta v_\varphi}{r} \operatorname{cot} \vartheta = 0. \qquad (1)$$

Two assumptions were postulated when this equation was derived: The negligibly small amount of inner frictional force and the retention of the stellar axial symmetry (the latter assumption is obvious).

Substituting $v_\phi = r\omega \sin\vartheta$ in equation (1), after simple transformations we obtain the following equation

$$rv_r \sin\vartheta \frac{\partial\omega}{\partial r} + v_\vartheta \sin\vartheta \frac{\partial\omega}{\partial\vartheta} + 2v_r\omega \sin\vartheta + 2v_\vartheta \omega\cos\vartheta = 0, \tag{2}$$

which represents a determination of the stellar rotation law, if the circulation current system is given. /102

Equation (2) is automatically fulfilled, if the circulation rate equals zero. We shall call this rotation law "the non-circulation law of rotation". We shall show that it is completely determined by the distribution of temperature and density in the star.

When circulation exists in the rotating star, the dependence of the angular velocity on the coordinates is determined by the current distribution -- i.e., by the circulation rate components v_r and v_ϑ. Utilizing the equation of discontinuity and assuming stationarity, we may express the rates v_r and v_ϑ by means of the current function:

$$v_r = \frac{1}{r^2\rho\sin^2\vartheta} \cdot \frac{\partial S}{\partial\vartheta}; \quad v_\vartheta = -\frac{1}{r\rho\sin\vartheta} \cdot \frac{\partial S}{\partial r}. \tag{3}$$

Substituting expression (3) in equation (2), after simple transformations we obtain

$$\frac{1}{r^3\rho\sin^2\vartheta}\left[\left(r^2\sin^2\vartheta\frac{\partial\omega}{\partial r} + 2r\omega\sin^2\vartheta\right)\frac{\partial S}{\partial\vartheta} - \left(r^2\sin^2\vartheta\frac{\partial\omega}{\partial\vartheta} + 2r^2\omega\sin\vartheta\cos\vartheta\right)\frac{\partial S}{\partial r}\right] = 0. \tag{4}$$

It may be readily seen that the angular velocity may be determined by the following relationship for the given current function

$$r^2\omega\sin^2\vartheta = f(S). \tag{5}$$

The function of S has a constant value on the surface of the star, and the dependence of the angular velocity on the latitude may be described by the following formula

$$\omega \sim \frac{1}{\sin^2\vartheta}. \tag{6}$$

In this case, the angular velocity has a singularity close to the stellar poles. Therefore, we must take the inner friction into account in the region which is close to the axis of rotation. This leads to the occurrence of an additional factor of the type $1 - e^{-\alpha\sin^2\vartheta}$ in expression (6).

The problem of the stability of the rotational law is very important. Unfortunately, only general, qualitative statements may be given regarding this problem, since significant difficulties are entailed in a correct mathematical formulation of it. /103

It is apparent that if a law of rotation is established in a rotating star,

which may be determined by formula (5), it will be maintained for an indefinite period of time. However, it is not clear whether this may be determined without the most detailed mathematical studies and whether such a law of rotation can be established in general. In particular, we do not know what transpires with a star which is in a state of rigid rotation at the initial period of time. It is clear that circulation, which may be determined by the theorem of Zeipel, slowly arises in such a star. This circulation changes the law of rotation quite rapidly, which leads to an intensification of the circulation. It is possible that, as a result, a stationary law of rotation is established which corresponds to expression (5). However, it is also possible that the star cannot reach a stationary state, and rotational oscillations are established within it (Ref. 6). Unfortunately, the mathematical problems which arise when such a case is studied are so complex, that it is hardly possible to solve them at the present time.

The stability of a non-circulation rotational law is even more complex. The non-circulation law for regions in radiative equilibrium cannot be barotropic, since in this case Zeipel circulation arises. According to the theorem of Bjerknes-Rosseland, baroclinicity of rotation assumes the formation of circulation. On first glance, it would appear that a non-circulation law of rotation cannot be stable. However, such a conclusion is premature.

We cannot solve the problem of the stability of a non-circulation law of rotation without the appropriate calculations, but we may make a few statements regarding the conditions under which it is stable. First of all, the case is not excluded in which Bjerknes circulation does not arise in general under such a law of rotation. Even if it does arise, it may be so weak that departure from the state of equilibrium requires a period of time which is comparable with the time of evolution for the star.

A change in the law of rotation due to the circulation which is produced cannot lead to a change in the stellar structure. A very intensive preliminary study has shown that circulation arises in the star which proceeds in an opposite direction to the circulation producing the change in the law of rotation. In this case, rotational stability according to Lyapunov is provided. Finally, /104 as Mestel (Ref. 1) has shown, circulation produces asymmetrical distribution of the molecular weight, since a substance rich in helium passes out from the convective core. This must also lead to cessation of circulation in the star. Thus, qualitative considerations point to the conclusion that the non-circula- law of rotation is stable.

Since a mathematical study of the selection of the law of rotation is hardly feasible at the present time, we must turn to observational data and must use them to reach a conclusion regarding the law of rotation in real stars. However, our knowledge is quite limited on this point. The law of rotation for only one star is known -- the Sun, and we only know the dependence of the angular velocity upon latitude on its surface. We may obtain some additional information by studying the effects of rotation in the radial velocity curves for eclipsing binaries. Unfortunately, the accuracy with which radial velocities may be determined is insufficient for a reliable determination of the law of rotation. However, a detailed analysis of observations leads us to

the assumption that a law of rotation which is characterized by equatorial acceleration is most probable. Therefore, we must renounce the law of rotation (5) according to which strong equatorial deceleration must be observed.

Allowance for inner friction cannot change our conclusion in any way, since viscosity can decrease the velocity gradients, but it is absolutely improbable that its effect may change the sign of the gradient.

Thus, we must assume a law of rotation without circulation. This assumption considerably facilitates the problem, since in this case the equation of discontinuity is exactly satisfied, and the derivative with respect to time of the ϕ-component of velocity vanishes in the Euler equation.

Basic Equations of the Theory

Stars of the main sequence may differ considerably in terms of their structure. A model with a convective core and a radiative envelope corresponds to the upper section of the main sequence. A model with radiative equilibrium in the central section and with an envelope which is in a state of convective equilibrium corresponds to stars of the lower section of the main sequence. /105
The present article will investigate a model with a convective core and a radiative envelope; this model was compiled for the star Y Cyg by Rundkjbing (Ref. 7) (this same model was employed in previous studies by the author). The model selection was based on the fact that a study of the effects of rotation in stars of the upper section of the main sequence (where the largest rotational velocities are observed) is of the greatest interest. In addition, an investigation of a model for a rotating star of the main sequence lower section is complicated by the necessity of taking into account the outer convective zone. Clarification is still needed for such phenomena as transfer of the rotational momentum to the convective currents, the role of turbulent friction in the convective zone, etc. These considerations also appeared in the selection of the model.

This study will not investigate the structure of the stellar convective core, since it has been already studied in sufficient detail in (Ref. 2 - 4). Data on the structure of the convective core, which were necessary for computing the envelope, were taken from these studies.

Just as previously, we shall assume that the convective core rotates like a solid body. Vigorous convection in the core apparently provides sufficient internal friction, so that rigid rotation is established for cosmologically short periods of time. The fact that it is impossible to obtain equatorial acceleration on the core surface during rotation of the core according to the law (5) represents an important argument in favor of rigid core rotation.

Let us investigate equations for the structure of the radiative envelope. If there are no circulation currents, then the structure of the star may be described by equations of hydrostatics

$$\frac{1}{\rho}\cdot\frac{\partial P}{\partial r}=\frac{\partial V}{\partial r}+(1-\mu^2)\,\omega^2 r; \tag{7}$$

$$\frac{1}{\rho}\cdot\frac{\partial P}{\partial \mu}=\frac{\partial V}{\partial \mu}-\omega^2 r^2\mu, \tag{8}$$

where P is pressure; ρ -- density; P_c and ρ_c -- values of these quantities in the center of the configuration; V -- gravitational potential.

Let us represent the equation of state in the form of a pseudopolytrope (Ref. 4)

$$P=P_c\rho_c^{-1+1/n}K(r,\ \mu)\rho^{1+1/n} \tag{9}$$

Selecting the constant n and function $K(r, \mu)$ in the appropriate way, we may obtain any equation of state. Substituting equation (9) in equations (7) and (8) /106 and changing to Emden variables

$$\rho=\rho_c\Theta^n;\quad r=\left[\frac{P_c}{4\pi G\rho_c}\right]^{1/2}\xi;\quad \chi=\frac{\omega_0^2}{4\pi G\rho_c}, \tag{10}$$

after obvious transformations we obtain

$$\frac{\partial(K\Theta)}{\partial\xi}=\frac{\rho_c}{P_c}\cdot\frac{\partial V}{\partial\xi}-nK\frac{\partial\Theta}{\partial\xi}+(1-\mu^2)\chi\xi\left(\frac{\omega}{\omega_0}\right)^2; \tag{11}$$

$$\frac{\partial(K\Theta)}{\partial\mu}=\frac{\rho_c}{P_c}\cdot\frac{\partial V}{\partial\mu}-nK\frac{\partial\Theta}{\partial\mu}-\chi\xi^2\mu\left(\frac{\omega}{\omega_0}\right)^2. \tag{12}$$

The latter equations are equivalent to a single vector equation. Taking the divergence of both parts, we obtain

$$\nabla^2(K\Theta)=\frac{\rho_c}{P_c}\nabla^2V-n\left\{\frac{1}{\xi^2}\cdot\frac{\partial}{\partial\xi}\left(\xi^2K\frac{\partial\Theta}{\partial\xi}\right)+\frac{1}{\xi^2}\cdot\frac{\partial}{\partial\mu}\left[(1-\mu^2)K\frac{\partial\Theta}{\partial\mu}\right]+f(\xi,\ \mu)\right. \tag{13}$$

Let us write all the desired functions in the form of a series with respect to the small parameter and with respect to the Legendre polynomial:

$$\left.\begin{aligned}
K(\xi,\ \mu)&=K_0(\xi)+\chi\left[\varkappa_0(\xi)+\sum_{j=2}^{\infty}A_j\varkappa_j(\xi)P_j(\mu)\right];\\
\Theta(\xi,\ \mu)&=\Theta_0(\xi)+\chi\left[\psi_0(\xi)+\sum_{j=2}^{\infty}A_j\psi_j(\xi)P_j(\mu)\right];\\
V(\xi,\ \mu)&=V_0(\xi)+\chi\left[U_0(\xi)+\sum_{j=2}^{\infty}A_jU_j(\xi)P_j(\mu)\right];\\
z(\xi,\ \mu)&=\left(\frac{\omega}{\omega_0}\right)^2=z_0(\xi)+\sum_{j=2}^{\infty}z_j(\xi)P_j(\mu);\\
f&=f_0(\xi)+\sum_{j=2}^{\infty}f_j(\xi)P_j(\mu).
\end{aligned}\right\} \tag{14}$$

The function f may be determined by the following expression /107

$$f=2z+(1-\mu^2)\left(\xi\frac{\partial z}{\partial\xi}-\mu\frac{\partial z}{\partial\mu}\right). \tag{15}$$

From this point on, we shall restrict ourselves to the case of angular velocitites which are so small that we may disregard the terms containing the parameter in the second and higher powers. Then, substituting the expansion (14) in equation (13), we obtain

$$\frac{1}{\xi^2}\cdot\frac{d}{d\xi}\left[\xi^2\frac{d}{d\xi}\left(\frac{\rho_c}{P_c}V_0-K_0\Theta_0\right)\right]=n\frac{1}{\xi^2}\frac{d}{d\xi}\left(\xi^2K_0\frac{d\Theta_0}{d\xi}\right); \tag{16}$$

$$\frac{1}{\xi^2}\cdot\frac{d}{d\xi}\left\{\xi^2\frac{d}{d\xi}\left[\frac{\rho_c}{P_c}U_j-A_j(\varkappa_j\Theta_0+\psi_jK_0)\right]-\frac{j(j+1)}{\xi^2}\left[\frac{\rho_c}{P_c}U_j-A_j(\varkappa_j\Theta_0+\right.\right. \tag{17}$$

$$\left.\left.+K_0\psi_j)\right]\right\}=A_jn\left\{\xi^2\frac{d}{d\xi}\left(\xi^2K_0\frac{d\psi_j}{d\xi}+\varkappa_j\frac{d\Theta_0}{d\xi}\right)-\frac{j(j+1)}{\xi^2}K_0\psi_j\right\}-f_j(\xi).$$

We may readily obtain the expressions for the potentials V_0 and U_j from these equations

$$\left.\begin{aligned}
V_0&=\frac{P_c}{\rho_c}\left[(n+1)K_0\Theta_0-n\int_0^\xi\Theta_0\frac{dK_0}{dx}dx\right];\\
U_j&=\frac{P_0}{\rho_c}\left\{A_j(\varkappa_j\Theta_0+(n+1)K_0\psi_j)-\frac{1}{2j+1}\left\{\xi^j\int_0^\xi[(j+1)\times\right.\right.\\
&\times A_jnQ_j+xf_j(x)]\frac{dx}{x^j}+\xi^{-(j+1)}\int_0^\xi[jA_jnQ_j-xf_j(x)]\times\\
&\left.\left.\times x^{j+1}dx\right\}+B_j\xi^j,\right.
\end{aligned}\right\} \tag{18}$$

where

$$Q_j=\psi_j\frac{dK_0}{d\xi}-\varkappa_j\frac{d\Theta_0}{d\xi}. \tag{19}$$

In addition, let us substitute expansion (14) in the first of the hydrostatic equilibrium equations (11) and let us exclude the potential from the equations obtained by means of expression (18). We shall regard the equations /108 obtained

$$\frac{j}{2j+1}\xi^{j-1}\int_0^\xi[(j+1)A_jnQ_j+xf(x)]\frac{dx}{x^j}-\frac{(j+1)}{2j+1}\cdot\xi^{-(j+2)}\int_0^\xi[jA_jnQ_j- \tag{20}$$

$$-xf(x)]x^{j+1}dx=\sum_{k=-1}^{k=+2}B_{2k,j}z_{j,2k}\xi+jB_j\xi^j$$

as equations determining the dependence of the angular velocity on temperature and density. The functions z_{j-2}, z_j, z_{j+2} with respect to the three unknowns are contained in each of these equations. We may obtain their solution by truncating the series at any term. Further calculations show that the terms of the series rapidly decrease with an increase in j. Therefore, we may confine ourselves to the first two terms of the expansion.

Solving equation (20) first for j = 2 (assuming that all $z_j = 0$ in the case of j > 2), and then for j = 2, we obtain*

$$z_0 = 3B_2 - 3A_2 n \int_0^\xi Q_2 \frac{dx}{x^2} + \frac{110}{9} A_1 n \xi^2 \int_0^\xi Q_4 \frac{dx}{x^4} - \frac{130}{9} A_1 n \int_0^\xi Q_4 \frac{dx}{x^2} + \ldots; \tag{21}$$

$$z_2 = \frac{35}{3} B_4 \xi^2 - \frac{35}{3} A_4 n \xi^2 \int_0^\xi Q_4 \frac{dx}{x^4}. \tag{22}$$

Since the coefficients A_j decrease with an increase in j very rapidly, we may write

$$z_j = \frac{(2j+3)(2j+1)}{j+1} \left[B_j \xi^j - A_{j+2} n \xi^j \int_0^\xi Q_{j+2} \frac{dx}{x^{j+2}} \right]. \tag{23}$$

Substituting (14) - (17) and (21), (22) in (12), we readily find that all B_j, with the exception of B_2, equal zero.

We thus arrive at the conclusion that equilibrium of a rotating star is only possible in the absence of circulation for an angular velocity whose dependence on the coordinates is determined by expressions (21) - (23). In other words, these expressions determine the non-circulation law of rotation. Their physical meaning consists of the fact that equilibrium between the forces of gravitation, pressure, and centrifugal forces is only possible for a specific distribution of temperature, density, and the angular rotational velocities. /109

In addition the model of a rotating star may be described by the equations (16), (17), (21) and (22) or (instead of the last two) (23) and the Pousson equation. In these equations, it must be taken into account that all B_j in the case of j > 2 equal zero. For constant B_2, it is advantageous to assign a value of 1/3, since in this case the parameter ω_0 equals the angular

* In the studies (Ref. 3, 4), incorrect values of the coefficients are given in the expression for z_0 for integrals from Q_4. The error was not discovered, because these terms were not used in subsequent computations.

velocity in the center of the configuration.

Calculation of a Rotating Star Model

It is extremely difficult to employ the equations given above to make a direct formulation of a model, since numerical methods require a great number of computations. However, we may significantly facilitate the computations, if we change to another form of the equations.

It may be readily seen that the function K may be expressed by means of temperature and density

$$K=\beta_c\left[1+\frac{1-\beta_c}{\beta_c}\cdot\frac{\tau^3}{\Theta^3}\right]\frac{\tau}{\Theta} \tag{24}$$

(β_c -- ratio between the gas pressure and the total configuration at the center; τ -- ratio between temperature and its value at the center).

Substituting Θ from formula (14) in formula (24) and expanding τ in double series with respect to the Legendre polynomial and with respect to the small parameter λ

$$\tau=\tau_0+\chi\left[t_0+\sum_{j=2}^{\infty}A_j t_j(\xi)P_j(\mu)\right], \tag{25}$$

we obtain the following expression for the function $\varkappa$

$$\varkappa_j=\frac{\tau_0}{\Theta_0}\left[4(1-\beta_c)\frac{\tau_0^2}{\Theta_0^2}t_j-\beta_c\left(1+4\frac{1-\beta_c}{\beta_c}\right)\frac{\tau_0^3}{\Theta_0^3}\psi_j\right]. \tag{26}$$

From this point on, it will be more convenient for us to use the following re- /110
lationship

$$r=\left[\frac{T_c}{4\pi G\rho_c\beta_c\mu}\right]^{1/2}\eta. \tag{27}$$

instead of expression (10).

Let us now differentiate (24) with respect to η and also the expression obtained, and let us substitute the expression (26) in formula (19). Performing simple transformations, we obtain

$$Q_j=\left(1+4\frac{1-\beta_c}{\beta_c}h^3\right)(g_\Theta t_j-g_\tau h\psi_j), \tag{28}$$

where

$$h=\frac{\tau_0}{\Theta_0};\quad g_\Theta=\frac{d\ln\Theta_0}{d\eta};\quad g_\tau=\frac{d\ln\tau_0}{d\eta}.$$

Let us turn to the equations of equilibrium for a radiative envelope

$$\frac{1}{\rho}\operatorname{grad}P=\operatorname{grad}V+\mathbf{j}; \tag{29}$$

$$\frac{c}{k\rho}\operatorname{grad} P_2=\mathbf{F}; \tag{30}$$

$$\operatorname{div}\mathbf{F}=-\rho\varepsilon; \tag{31}$$

$$\nabla^2 V=-4\pi G\rho, \tag{32}$$

where $\mathbf{j}$ is the vector of the centrifugal acceleration with the components $\{\omega x, \omega y, 0\}$.

Let us take the divergence of both parts of equations (29) and (30). Eliminating the potential by means of equation (32), eliminating F by means of equation (31), and taking the fact into account that $\varepsilon = 0$ in the radiative envelope and that div $\mathbf{J}$ may be represented by expression (15), we obtain a system of the second order with respect to P and ρ. Employing the apparent relationship

$$P=\frac{R}{\mu}\rho T+\frac{a}{3}T^4,$$

we may simplify this system. Employing the expansions (14) and (25) and also the formulas (10) and (28), we obtain the following system of equations**: /111

$$\left.\begin{aligned}\frac{d^2\Theta_0}{d\eta^2}&=-\frac{2}{\eta}\cdot\frac{d\Theta_0}{d\eta}+\Theta_0(g_\Theta-g_\tau)^2-\frac{1}{3}\cdot\frac{\Theta_0^4}{\tau_0}\\ \frac{d^2\tau_0}{d\eta^2}&=-\frac{2}{\eta}\cdot\frac{d\tau_0}{d\eta}+3\frac{d\tau_0}{d\eta}(g_\tau-g_\Theta);\end{aligned}\right\} \tag{33}$$

$$\left.\begin{aligned}\frac{d^2\psi_j}{d\eta^2}&=\left(F_1-\frac{2}{\eta}\right)\frac{d\psi_j}{d\eta}+F_2\frac{dt_j}{d\eta}+\left(F_3+\frac{j(j+1)}{\eta^2}\right)\psi_j+\\ &+F_4\psi_j+G_j\\ \frac{d^2t_j}{d\eta^2}&=\left(F_5-\frac{2}{\eta}\right)\frac{dt_j}{d\eta}+F_6\frac{d\psi_j}{d\eta}+\left(F_7+\frac{j(j+1)}{\eta^2}\right)t_j+\\ &+F_8\psi_j.\end{aligned}\right\} \tag{34}$$

Equations (33) describe an unperturbed star and must be solved by the methods advanced by the theory of internal stellar structure. In particular, we may employ the data obtained when a non-rotating model was calculated. Without dwelling in detail on equations (33), we should note that in several cases they are more convenient than the equations which are written in a form which is customary for the theory of internal structure.

System (34) together with expressions (21) - (23) and (26) describes perturbations of the first order which arise when stellar rotation is taken into account.

The coefficients F_1 - F_8 and G_j have the following values:

** All the intermediate calculations are omitted due to their cumbersome nature.

$$
\left.
\begin{aligned}
&F_1=2(g_\theta-g_\tau);\quad F_2=\frac{2}{h}(g_\tau-g_\theta);\\
&F_3=g_\tau^2-g_\theta^2-\frac{4}{3}\frac{\Theta_0^3}{\tau_0}+\frac{j}{2\eta_1}\left(1+4\frac{1-\beta_c}{\beta_c}h^3\right)g_\tau;\\
&F_4=\frac{2}{h}\left[g_\tau g_\theta-g_\tau^2-\frac{1}{3}\frac{\Theta_0^2}{\tau_0}-\frac{j}{2\eta}\left(1+4\frac{1-\beta_c}{\beta_c}h^3\right)g_\theta\right];\\
&F_5=3g_\theta-6g_\tau;\quad F_6=3hg_\tau;\\
&F_7=3g_\tau^2;\quad F_8=-3g_\tau g_\theta;\\
&G_j=\frac{1}{A_j}\left[a_jz_j+b_j\eta\frac{dz_j}{a\eta}+c_jz_{j+2}+d_j\eta\frac{dz_{j+2}}{d\eta}\right].
\end{aligned}
\right\} \qquad (35)
$$

We may readily obtain the values of the constants a_j, b_j, c_j, d_j by comcomparing expressions (14) and (15).

The boundary conditions for equations (33), (34) are : /112

(1) In the case of $\eta = \eta_0$ (η_0 -- boundary of convective core), the density, temperature, and their first derivatives are continuous;

(2) The angular velocity remains finite in the case of $\eta = \eta_1$ (η_1 -- outer configuration boundary).

According to expression (28), the latter condition may be written in the following form

$$t_j(\eta_1)=h(\eta_1)\,\psi_j(\eta_1). \qquad (36)$$

Let us examine the process for solving the system (34). First of all, let us truncate the expansion at the term with a sufficiently large j. This may be done in expansions for functions t_j, ψ_j, since the coefficients A_j rapidly decrease with an increase in j. However, the assumption that all $z_j = 0$ in the case of $j \neq 2$ leads to a disturbance of the condition (36) -- i.e., we cannot assume that the term G_j equals zero in equation (34). In order to satisfy the condition that the angular velocity be finite, we may approximate the term G_j by an expression of the following type:

$$G_j=-\frac{A_{j+2}}{A_j}\left[1-\left(\frac{\eta}{\eta_0}\right)^{j+2}\right]\eta^j.$$

Assigning the values of ψ_j, t_j and their first derivatives at the boundary of the convective core, we may solve the system (34) for a certain j. Condition (36) makes it possible for us to determine $\frac{A_{j+2}}{A_j}$. The obtained values of $\frac{A_{j+2}}{A_j}$, ψ_j, t_j in their turn make it possible to determine $\frac{A_j}{A_{j-2}}$, etc. -- i.e.,

until the ratio $\frac{A_4}{A_2}$ is determined.

It may be readily seen that condition (36) is not fulfilled in the case of $j = 0$, and we cannot find the coefficient A_2. Therefore, in order to determine the coefficinet A_2, it is necessary to assign one boundary condition. The continuity of the potential and its first derivative at the configuration boundary may serve as this condition. However, specific difficulties are entailed when it is employed.

Let us write this condition in explicit form. Employing the expression for the potential (18) and taking the fact into account that the corresponding expansion harmonic of the outer potential has the form $\frac{C_j}{\xi^{j+1}}$, we obtain /113

$$\left.\begin{aligned} A_j\left[(n+1)K_0(\xi_1)\psi_j(\xi_1) - n(\xi_1^j)\int_0^{\xi_1} Q_j\frac{dx}{x^j}\right] &= -\frac{C_j}{\xi_1^{j+1}} - B_j\xi_1^j; \\ A_j\left[(n+1)K_0(\xi_1)\left(\frac{d\psi_j}{d\xi}\right)_{\xi=\xi_1} - nj\xi_1^{j+1}\int_0^{\xi_1} Q_j\frac{dx}{x^j}\right] &= \\ = -\frac{(j+1)C_j}{\xi_1^{j+2}} - jB_j\xi_1^{j-1}, & \end{aligned}\right\} \qquad (37)$$

where all B_j equal zero in the case of $j \neq 2$. Excluding the constants C_j from equation (37), we obtain

$$A_j\left\{(n+1)K_0(\xi_1)\left[(j+1)\psi_j(\xi_1) + \xi_1\left(\frac{d\psi_j}{d\xi}\right)_{\xi=\xi_1}\right] - (j+1)n\xi_1^j\int_0^{\xi_1} Q_j\frac{dx}{x^j}\right\} = -(2j+1)B_j\xi_1^j. \qquad (38)$$

If $j \neq 2$, then $B_j = 0$, and equation (38) may be satisfied in the case of $A_j = 0$. This must mean that all $z_j = 0$ and that the angular velocity of the pseudopolytropic configuration depends only on the radius. This conclusion directly contradicts observations. However, a direct formulation of the requisite numerical data shows that in the case of $j \neq 2$ the factor vanishes in expression (38) in the case of A_j -- i.e., equation (38) is an identity in the case of $j \neq 2$.

There is no precise proof for the fact that condition (38) is identically fulfilled in the case of $j \neq 2$. Such a proof would be extremely important. If

we could show that condition (38) is never fulfilled identically, this would mean that one relationship between the main parameters of a star has been found. Since -- according to the Voigt-Russell theorem -- the stellar structure is determined by the mass and chemical composition, such an assumption would mean that rotation would provide an additional condition relating these parameters. Nevertheless, observations provide no basis for stating that such a relationship exists, and the automatic fulfillment of condition (38) for all $j \neq 2$ is more probable. /114

For $j = 2$, we obtain the following expression under this condition

$$A_2 = \frac{-\frac{5}{3}\xi_1^2}{(n+1)K_0(\xi_1)\left[3\psi_2(\xi_1)+\xi_1\left(\frac{d\psi_2}{d\xi}\right)_{\xi=\xi_1}\right]-5n\xi_1^2\int_0^{\xi_1}Q_2\frac{dx}{x^2}}. \quad (39)$$

All the fixed problems have been completely determined, and we may formulate a numerical solution, which will provide us with a model of a rotating star.

Calculation of the Rotating Star Model

As was indicated above, the model of a hot star, compiled by Rundkjbing (Ref. 7) as applied to Y Cyg has been employed as the zero approximation. The characteristics of this model are as follows:

$\frac{R}{R_\odot}=5.86$	$\lg\frac{M}{M_\odot}=1.236$	$\lg L=38.43$
$\frac{R_g}{R_*}=0.41$	$\beta_{rp}=0.839$	$x_H=0.38$
$x_{He}=0.54$	$z=0.08$	$x_{CN}=0.0012$
$T_c=3.10\cdot10^7$	$\rho_c=2.40$	$\beta_c=0.761$
$\mu=0.829$		

In order to calculate the rotating star model, it was assumed that the term G_4 may be approximated by the following expression

$$G_4=E_6\eta^4\left[1-\left(\frac{\eta}{\eta_0}\right)^6\right]. \quad (40)$$

As a result of the calculations, the functions z_0 and z_2 determining the stellar law of rotation were calculated. The values of the functions for individual points in the interval between the convective core boundary and the surface of the star are: /115

r/R	z_0	z_2
0.41	1.000	−0.000
0.50	1.001	0.001
0.60	1.009	0.006

r/R	z_0	z_2 (continued)
0.70	1.026	0.009
0.80	1.059	0.012
0.90	1.067	0.015
1.00	1.068	—0.018

The computational results show that the angular velocity depends slightly on the radius. Its maximum change comprises about 10% in all. We may therefore assume that the results obtained for a model with rigid rotation are sufficiently accurate. In this connection, we did not calculate the main characteristics of the model in this study (mass, luminosity, etc.), since they must coincide with those presented in (Ref. 6).

The law of rotation obtained is of the greatest interest for the study. The change in the angular velocity on the surface of the star may be described by the expression

$$\omega(R) = \omega_0[1 - 0.09\ P_2(\cos\vartheta)]. \tag{41}$$

This expression coincides qualitatively with the law of rotation for the Sun

$$\omega_\odot \sim [1 - 0.24 P_2(\cos\vartheta)]. \tag{42}$$

The smaller value of the coefficient in expression (41) for P_2 may be easily explained by the fact that the convective core in a hot star occupies a much larger portion of its volume. Therefore, it is natural that the coefficient must have a smaller value in the model of a hot star. In addition, the integrand in the expression determining z_j must have a larger value for the Sun, since the zone of radiant equilibrium occupies the central regions of the star. Thus, the fact that the dependence of the angular velocity on latitude on the surface of an early-class star is not as pronounced as that for the Sun may be quite simply explained by the theory described.

The presence of an outer convective zone on the Sun complicates the discussion somewhat. The influence of this zone may be only taken into account qualitatively, since it is not clear what type of friction arises due to the development of turbulence in the convective zone. However, certain arguments may be advanced in support of the fact that motion in the outer convective zone is of an orderly nature. In this connection, the turbulent friction plays an insignificant role. Qualitative considerations indicate that in this case the nature of the dependence of ω on latitude is determined by expressions (40) or (41). However, the numerical coefficient for the Legendre polynomial is smaller than would follow from theory. /116

The most unexpected result of the theory is the increase in the angular velocity in the star from the boundary of the convective core to the surface. On first glance, it would appear that this result must lead to the conclusion that the model advanced cannot be stable. However, it was indicated above that the law of rotation must be stable according to Lyapunov. Thus, oscillations arising in the star will be extremely small, and it would be almost impossible to discover them with present day technology. The establishment of

such a law of rotation may be explained quite well on the basis of cosmological considerations.

Thus, on the basis of the above statements we may draw the conclusion that the observed law of rotation for the Sun is a typical law of rotation for stars. It may be expected that the dependence of the angular rotation velocity on the coordinates of early-class stars (O, B) is less pronounced than that for the Sun. On the other hand, it is more pronounced for stars of the K-M spectral class. Disturbances of the law of rotation must lead to strong circulation, and are manifested in the special behavior of the stars (stars of the βCMa type and other objects). In order to explain the solar law of rotation, there is no necessity of resorting to the hypothesis of a strong general magnetic field and other assumptions, since this law is a consequent of the equations of hydrostatics.

REFERENCES

1. Mestel, S. Nuclear Processes in Stars. IL, Moscow, 1960.
2. Porfir'yev, V. V. Tsirkulyar L'vovskoy Astronomicheskoy Observatorii (LAO), 35-36, 1, 12, 1960.
3. Porfir'yev, V. V. Astronomicheskiy Zhurnal (A Zh), 33, 690, 1960.
4. Porfir'yev, V. V. Tsirkulyar LAO, 35-35, 23, 1960.
5. Porfir'yev, V. V. A Zh, 39, 710, 1962.
6. Porfir'yev, V. V. A Zh, 40, 579, 772, 1963.
7. Rundkjbing, M. Ann. d'Aph., 16, 2, 1953.

CATALOG OF PHOTOGRAPHIC MAGNITUDES OF COMPARISON STARS IN GLOBULAR CLUSTER M92

L. I. Paneva, E.S. Kheylo

A catalog of magnitudes of 278 stars in the neighborhood of the globular cluster M92 is contained in this paper. The value of the internal error is $\pm 0^m.02$. A transitional formula of our photometric system into the international one is given.

The present catalog represents the first portion of research on variable /118
stars in globular cluster M 92. Unfortunately, variable stars in this cluster have been studied to a very small extent, in spite of the very favorable position for observers in the northern hemisphere. Photography of this cluster was initiated at the Main Astronomical Observatory of the Ukrainian SSR Academy of Sciences. The plans included several observations lasting many years, a search for variable stars, a determination their precise periods, a clarification of the change in the variability parameters, etc.

Observations were performed on a 70-centimeter AZT-2 reflector. A photographic device of the Cassegrain system was employed (F = 10.5 m). Before May, 1964, non-sensitized Agfa Astro plates of the same series (emulsion No. 1541) were employed with an exposure of 10-30 minutes. More sensitive photographic materials are presently being employed. All of the photographs were taken without a filter.

Four pairs of plates, out of all the photographs between 1961-1963, were selected in order to compile the present catalog. Each pair was obtained in one night. Table 1 presents a list of the negatives employed.

The negatives were subjected to photometric analysis by means of a MF-2 microphotometer with a fixed, circular diaphragm. The measurement method employed has been described in detail in (Ref. 1). Due to the fact that the cluster was located in the center of the plate, the error of the field was not taken into account. The stars were located so close together in the central sections of the cluster that not only was it impossible to measure /119
them, but it was even impossible to separate them. Therefore, the measurement zone was delineated from the inner side by a circle having the radius 1'.2, and from the outer side by a circle having the radius 9'.3. This was due to the fact that at large distances from the center, the density of the stellar cluster almost equalled the density of the field stars.

A photometric standard of H. Arp et al. (Ref. 2) was employed to compile the calibration curve. Stars No. 3, 11, 17, 18 of this standard served as reference stars.

After obtaining several values for each plate, the authors determined the mean catalog values. Since the catalog had to be employed for finding

TABLE 1

Catalog Number	Julian Time of Half Exposure	Exposure Duration, Minutes
K117	2 437 764.4343	20
K118	.4510	20
K164	910.3921	15
K165	.4029	14
K166	12.2893	15
K167	.3025	15
K228	8 177.3422	20
K230	.3741	20

unknown variable stars, it was important that any possible systematic differences between the individual series be reduced to a minimum. Therefore, all the measurements were reduced to one system. Table 2 presents the serial number, the number in the sector (see the identification map), and the stellar magnitude in this system. The stellar magnitude interval ranged from 13.50 to $16^{m}.00$, although a few stars exceeded this limit.

TABLE 2

№	Number in Sector	m	№	Number in Sector	m	№	Number in Sector	m
1	I— 1	14.59	7	7	15.61	13	13	15.06
2	2	15.70	8	8	15.35	14	15	15.66
3	3	15.92	9	9	14.16	15	16	15.07
4	4	15.93	10	10	15.60	16	18	14.83
5	5	14.98	11	11	15.11	17	19	13.71
6	6	14.81	12	12	15.66	18	20	15.26
19	I—22	14.47	61	II—42	14.96	103	IV—8	15.85
20	24	15.98	62	44	16.03	104	9	15.13
21	25	15.34	63	46	15.40	105	10	14.47
22	26	15.54	64	49	15.73	106	14	15.36
23	27	15.50	65	50	15.29	107	15	15.51
24	28	15.32	66	52	16.12	108	16	16.13
25	29	14.79	67	53	15.17	109	18	15.79
26	32	16.01	68	III— 1	15.42	110	19	14.81
27	33	14.87	69	7	15.82	111	20	15.55
28	34	15.54	70	16	15.89	112	21	15.15
29	35	15.02	71	21	14.56	113	22	15.30
30	36	15.33	72	22	14.17	114	23	14.97
31	38	15.94	73	23	14.73	115	24	14.92
32	41	15.95	74	24	15.99	116	28	15.21
33	45	15.76	75	26	14.96	117	30	15.44
34	49	15.33	76	29	14.78	118	39	13.85
35	50	16.01	77	31	13.89	119	41	15.34
36	51	15.39	78	32	15.46	120	42	15.69
37	53	15.34	79	34	15.31	121	44	15.59
38	54	15.16	80	35	15.77	122	45	16.07
39	II— 1	15.77	81	36	15.03	123	51	15.36
40	5	15.06	82	37	14.92	124	52	15.26
41	6	15.60	83	39	15.66	125	53	15.34
42	8	15.76	84	40	15.92	126	54	16.13
43	11	15.84	85	41	11.67	127	56	15.63
44	12	15.81	86	42	15.16	128	57	14.79
45	16	14.75	87	44	15.60	129	58	16.03
46	17	15.45	88	47	14.27	130	59	15.31
47	18	15.84	89	48	15.81	131	60	14.76
48	21	14.21	90	50	14.37	132	61	16.07
49	23 *	15.64	91	51	13.74	133	65	15.31
50	25	15.66	92	52	15.12	134	66	14.92

/120

* Suspected of variability.

Continuation of TABLE 2

№	Number in Sector	m	№	Number in Sector	m	№	Number in Sector	m
51	26	15.58	93	53	15.22	135	68	15.35
52	28	15.86	94	56	15.40	136	69	14.00
53	29	15.11	95	57	15.64	137	70	16.02
54	30	14.37	96	58	15.59	138	V— 4	14.81
55	31	15.40	97	59	15.39	139	5	15.39
56	34	15.79	98	60	15.53	140	6	16.30
57	35	15.44	99	IV— 1	15.31	141	7	15.53
58	37	15.14	100	2	15.32	142	9	15.31
59	38	15.46	101	4	14.47	143	10	15.32
60	41	15.51	102	5	16.02	144	11	15.32
145	V—13	15.34	190	VI—18	15.15	235	VII—38	15.25
146	14	15.09	191	21	13.62	236	39	13.86
147	15	15.42	192	22	15.32	237	40	15.86
148	18	15.20	193	23	15.27	238	42	15.99
149	19	15.25	194	24	14.46	239	43	15.57
150	20	15.88	195	25	15.26	240	44	15.61
151	21	16.05	196	27	15.67	241	45	15.22
152	22	14.99	197	31	15.67	242	47	14.76
153	23	13.77	198	32	14.97	243	VIII— 1	15.03
154	24	14.67	199	37	14.47	244	2	15.34
155	26	13.63	200	38	14.95	245	3	14.76
156	31	15.23	201	40	15.84	246	4	15.56
157	32	14.85	202	41	15.40	247	6	16.04
158	35	15.46	203	44	15.57	248	7	16.05
159	36	16.02	204	46	14.52	249	9	15.61
160	38	14.75	205	48	15.24	250	14	15.61
161	39	15.05	206	49	15.15	251	15	13.64
162	40	15.90	207	52	15.49	252	16	14.60
163	41	14.84	208	53	15.77	253	17	14.81
164	42	15.32	209	54	14.31	254	20	15.94
165	43	14.66	210	55	14.31	255	21	15.64
166	44	15.60	211	VII— 1	15.93	256	22	14.45
167	48	14.74	212	3	15.95	257	25	13.91
168	50	15.95	213	4	15.64	258	27	14.94
169	52	15.54	214	5	15.60	259	28	14.39
170	53	15.24	215	6	15.36	260	29	16.12
171	54	15.91	216	7	15.99	261	31	14.80
172	56	14.98	217	10	15.63	262	32	14.14
173	58	14.98	218	12	15.65	263	33	15.68
174	59	15.26	219	14	14.84	264	34	15.94
175	61	15.89	220	15	16.13	265	35	15.39
176	64	15.50	221	16	15.16	266	36	15.70
177	67	15.42	222	17	15.78	267	37	15.74
178	VI— 1	15.46	223	19	15.85	268	38	15.24
179	2	14.77	224	20	13.61	269	40	14.28
180	3	15.06	225	21	15.18	270	41	15.18
181	6	15.63	226	24	15.01	271	44	15.21
182	7	15.98	227	25	15.38	272	46	16.09
183	8	15.83	228	26	16.08	273	48	15.20
184	9	15.47	229	27	16.16	274	51	14.57
185	10	15.50	230	31	15.21	275	53	15.34
186	11	15.92	231	32	15.93	276	54	14.55
187	12	15.70	232	33	15.20	277	57	15.99
188	13	15.44	233	34	14.93	278	58	14.23
189	14	15.74	234	35	15.26			

/121

A comparison of the stellar magnitudes obtained for different plates shows that only one star -- II - 23 -- could be suspected of variability, since the divergence between the given magnitudes amounted to $0^m.60$ for it. No other variable stars with amplitudes exceeding the measurement error were discovered. The variability of star II - 23 was repeated in all the photographs at our disposal. It should be noted that all of the variable stars, which were discovered previously by other researchers, also changed their brightness considerably on our photographs. /122

In order to determine the accuracy of the catalog, the entire interval of stellar magnitudes was divided into sub-intervals for every $0^m.5$. Within each of these sub-intervals, the mean square errors of one determination ε_i and the mean quadratic errors of the catalog magnitude ε were computed (Table 3).

TABLE 3

Stellar Magnitude Interval	ε_i	ε
$13^m.50-14^m.00$	$0^m.032$	$0^m.020$
14.01--14.50	.030	.020
14.51--15.00	.040	.025
15.01 -15.50	.029	.020
15.51 -16.00	.040	.025
Mean Value	.034	.022

In order to compare our photometric system (m_M) and the international photographic system, several pairs of photographs of the M 92 and M 13 clusters were obtained. The brightness of a large number of stars was measured in cluster M 13 in the international photographic system. With allowance for correction due to differential absorption of light in the atmosphere (difference between zenith distances of both objects at the time of the photograph did not exceed 10°), the stellar magnitudes of several stars were determined in the M 13 cluster according to our system, and the results were compared with results presented in (Ref. 3). It was found that the following relationship exists between the systems

$$m_{ipg} = 1.037 m_M - 0^m.43,$$

and the correction for color is negligibly small.

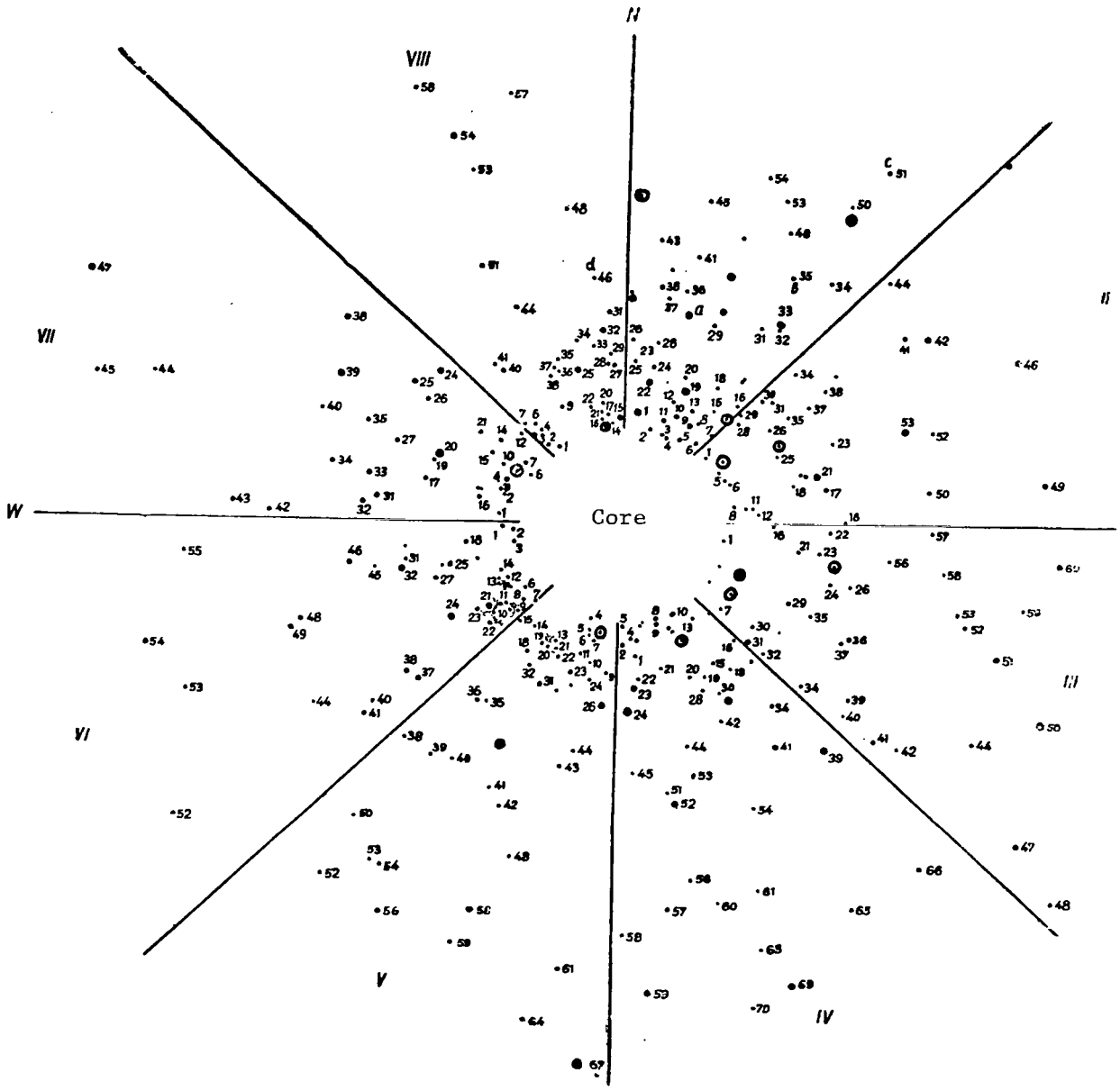

Map of the Region Measured (0 - Variable Stars).

REFERENCES

1. Fedorchenko, G.L. Izvestiya Glavnoy Astronomicheskoy Observatorii, AN USSR, 2, 4, 116, 1962.
2. Arp, H., Baum, W., Sandage, A. A. J., 58, 4, 1953.
3. Arp, H. A. J., 60, 326-327, 1955.

VARIABLE STARS IN GLOBULAR CLUSTER M92

E. S. Kheylo

The observations of six RR-Lyrae stars in M92 and the results of their evaluation are given. The periods are determined, and the variation of the period is found for one star.

Globular cluster M92 (NGC 6341) belongs to the IV class of concentration, /124 in terms of the Shapley classification, and has a comparatively small number of variable stars. The cluster was studied in (Ref. 2, 7). The spatial distribution of the stars was investigated (Ref. 7), and a color-stellar magnitude diagram was obtained (Ref. 2). However, as was pointed out in (Ref. 1), variable stars in the cluster have been studied to a very small extent. Several short series of observations have been performed, and the periods were determined only in one case.

In 1938 Nassau published his 38 observations (Ref. 4). He employed the scale method to estimate the brightness of the variable stars discovered, and the stellar magnitudes were determined within an accuracy of $0^m.1$. The observations encompassed a period of about one year. During the year Hachenberg (Ref. 3) published a detailed investigation of the cluster M92. He discovered several variable stars independently of Nassau, and found periods of brightness change for 13 of them. Later on, Oosterhoff (Ref. 5) again determined the periods of the four stars studied by Hachenberg (Ref. 3). The brightness of certain variable stars was measured incidently when the study was performed (Ref. 2), but they were not published.

Thus, 16 variable stars have been discovered in cluster M92. Out of these 16, 11 belong to the type RR-Lyrae; one belongs to the type W UMa (field star), and the variability was not determined for the remaining types. Nassau and Hachenberg (Ref. 3, 4) performed their observations at almost the same time, but the Hachenberg elements do not correspond to the observations of Nassau in every case. For example, for star No. 2 (number of the variable stars is given according to the Sawyer catalog (Ref. 6) at the time JD 2,428,366.686, Nassau observed an increase in the brightness. According /125 to Hachenberg, the phase $0^p.477$ -- i.e., the region of the minimum -- corresponded to the same time on the brightness curve. This is not the only lack of agreement.

The material which we obtained and the method employed to determine the brightness of the comparison stars are described in (Ref. 1). This article presents a summary of the observations of six stars (No. 1-5, 8) and their analysis. The stellar magnitudes of the variable stars were estimated visually according to the Neyland-Blayzhko method. Two hundred and eighteen photographs obtained between 1961-1963 were studied. Table 1 gives the numbers and brightness of the comparison stars in degrees (for their stellar magnitudes, see [Ref. 1]).

TABLE 1

Comparison Stars	Variable Stars							
	1 & 2	3 & 8		4		5	
	Degree	№	Degree	№	Degree	№	Degree
I—29	0.0	VIII—32	0.0	VIII—32	0.0	III—22	0.0
I—22	7.2	I—22	8.4	I—22	8.4	III—23	10.8
I—18	14.0	I—29	14.8	VIII—3	15.0	III—26	16.2
II—29	19.7	I—35	20.7	VII—24	21.7	III—34	23.1
II—38	24.1	I—51	26.6	VII—25	30.2	III—35	30.7
II—18	31.4	I—45	35.5	VII—17	38.5		

We had to first determine whether the Hachenberg elements (Ref. 3) corresponded to the observations obtained. After reducing our observations to the Hachenberg periods, it was found that the maxima of the brightness curves deviated from the ephemeris computed according to its elements.

In addition, only the elements corresponding to our observations were calculated, without including the observations of Nassau, which were separated by too large a time interval. It was possible that the periods of certain stars had changed since the 20 odd years which had elapsed since these observations. Therefore, we had to know the behavior of these stars during the intermediate years in order to relate the old series of observations with our series.

Information on six of the stars which were studied is presented below.

Variable star 1. Eleven brightness maxima were determined during the observational period. The following formula was found according to these maxima

$$\text{Max JD hel} = 2\,437\,872.415 + 0^d.702\,702\,E, \quad (1)$$

which best satisfies all the observations. However, the behavior of the remainders $O-C_1$ (Figure 1) points to a continuous change in the period. We derived a formula of the following type /126

$$\text{Max JD hel} = 2\,437\,872.373 + 0^d.702\,700\,E + 0^d.00\,000\,019\,E^2. \quad (2)$$

An analysis of the remainders $O-C_2$ shows that formula (2) satisfies all the observational maxima quite well. The unusually large coefficient in the case of E^2 occasions some doubt. It is possible that there was a jump-like change in the period in this case. The time of the "jump" occured at JD 2,437,872. Observations before this time may be described by the formula

$$\text{Max JD hel} = 2\,437\,555.499 + \\ + 0^d.702\,595\,E, \quad (3)$$

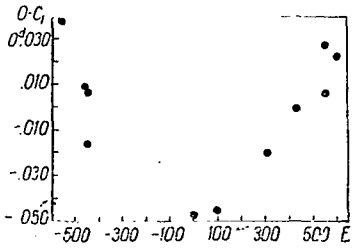

Figure 1

Behavior of Remainders $O-C_1$, for Variable Star 1

and after it

$$\text{Max JD hel} = 2\,437\,872.362 + 0^d.702\,824\,E. \quad (4)$$

The maxima and the remainders $O-C_i$ (for formulas (1) - (4), respectively) are summarized in Table 2.

The mean brightness curves (Table 3, Figures 2 and 3) were obtained according to formulas (3) and (4). The small difference between them may be explained by the small

TABLE 2

Max	E	O—C₁	O—C₂	O—C₃	O—C₄
2 437 411.481	—656	+0.038	—0.007	+0.014	—
548.479	—461	+ .009	+ .011	+ .006	—
53.396	—454	+ .007	+ .011	+ .005	—
5.481	—451	— .016	— .012	— .018	—
872.368	0	— .047	— .004	— .001	+0.006
943.343	+101	— .045	— .004	—	— .004
8 089.530	+309	— .020	+ .006	—	— .005
177.386	+434	— .001	+ .006	—	— .002
260.312	+552	+ .006	— .008	—	— .009
2.441	+555	+ .027	+ .012	—	+ .012
91.247	+596	+ .022	— .002	—	+ .002

accuracy with which the ascending branch of the first curve was compiled, due to a small number of points.

TABLE 3 /127

Before JD hel 2 437 872				After JD hel 2 437 872			
Phase	m	Phase	m	Phase	m	Phase	m
0.003	14.63*	0.454	15.66	0.000	14.59	0.536	15.77
.047	.77	.548	.68	.047	.70	.640	.79
.093	.85	.657	.79	.101	.85	.746	.79
.155	.93	.722	.85	.153	15.02	.839	.80
.257	15.45	.856	.32	.252	.31	.906	.26
.362	.66	.974	14.48	.351	.60	.951	14.70
				.449	.62		

* In all the tables, the stellar magnitudes are given for the mean curves in the international photographic system.

Variable star 2. Very few reliable maxima were obtained for it. Therefore, the period occurred at the time when the brightness of the star reached $14^m.84$ on the ascending branch. The following linear formula coincides with the observations

$$\text{Max JD hel} = 2\,437\,872.335 + 0^d.643\,910\,E.$$

The mean brightness curve, compiled according to this formula, is shown in Figure 4, and the corresponding data are given in Table 4. The rise in the brightness before the minimum is absolutely real.

TABLE 4

Phase	*m*	Phase	*m*	Phase	*m*	Phase	*m*
0.052	14.39	0.254	15.16	0.558	15.83	0.834	15.89
.107	.80	.346	.41	.645	.89	.904	.28
.167	.97	.442	.66	.754	.75	.952	14.98
						.999	.61

Variable star 3. The following elements of the brightness curve were obtained according to seven reliable maxima:

$$\text{Max JD hel} = 2\,437\,872.707 + 0^d.637\,456\,E. \qquad (6)$$

Figure 5 and Table 5 show the mean brightness curve. Since the increase in brightness takes place very rapidly, the individual points, which are indicated by crosses -- and not the average points -- are plotted for the phases 0.91-0P.94.

Variable star 4. The following formula satisfies the observations

$$\text{Max JD hel} = 2\,437\,872.518 + 0^d.628\,909\,E. \qquad (7)$$

/128

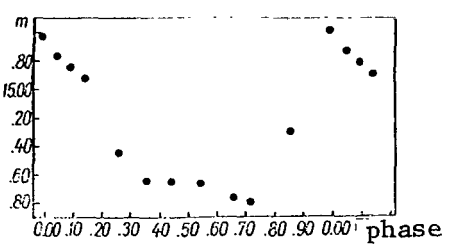

Figure 2

Mean Brightness Curve of Variable Star 1 According to Observations Before JD 2,437,872

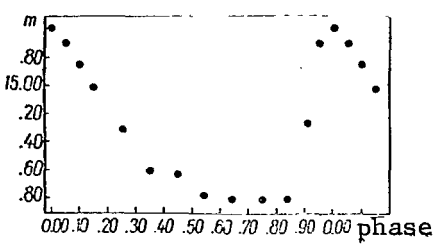

Figure 3

Mean Brightness Curve of Variable Star 1 According to Observations After JD 2,437,872

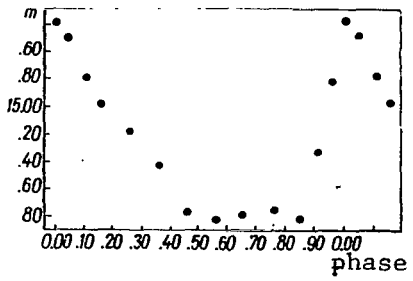

Figure 4

Mean Brightness Curve of Variable Star 2

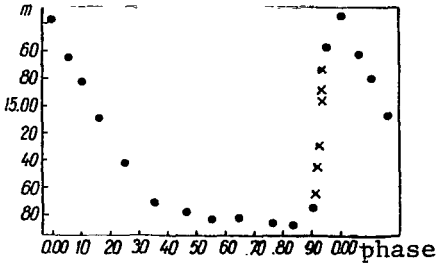

Figure 5

Mean Brightness Curve of Variable Star 3

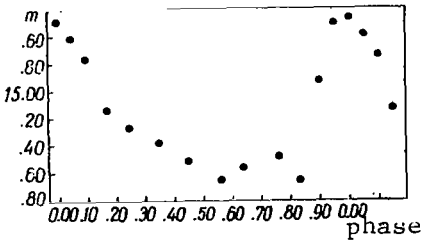

Figure 6

Mean Brightness Curve of Variable Star 4

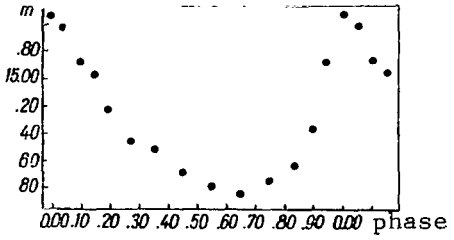

Figure 7

Mean Brightness Curve of Variable Star 5

TABLE 5

/129

Phase	m	Phase	m	Phase	m	Phase	m
0.004	14.36	0.162	15.08	0.464	15.77	0.758	15.85
.056	.63	.251	.41	.547	.82	.834	.86
.101	.81	.348	.70	.640	.81	.902	.75
						.950	14.58

The mean brightness curve is shown in Figure 6, and the corresponding data are presented in Table 6. The brightness increase before the minimum is absolutely real.

Variable star 5. The values of the brightness curve elements

$$\text{Max JD hel} = 2\,437\,872.020 + 0^d.619\,674\,E \qquad (8)$$

TABLE 6

Phase	m	Phase	m	Phase	m	Phase	m
0.006	14.49	0.169	15.14	0.449	15.52	0.758	15.49
.046	.61	.252	.26	.556	.65	.831	.66
.095	.76	.350	.38	.642	.57	.904	14.94
						.952	.52

closely coincide with observations. There is a perceptible scatter of points on the ascending branch. It is possible that the star is influenced by the Blazhko effect, which is expressed in the change of the brightness curve form for a constant amplitude (Table 7, Figure 7).

TABLE 7

Phase	m	Phase	m	Phase	m	Phase	m
0.003	14.55	0.190	15.23	0.549	15.79	0.896	15.37
.040	.63	.267	.46	.647	.85	.942	14.89
.095	.88	.347	.52	.751	.75		
.146	.97	.451	.69	.836	.64		

Variable star 8. Seven observed maxima yield the following formula for the elements

$$\text{Max JD hel} = 2\,437\,872.039 + 0^d.673\,194\,E. \qquad (9)$$

There is a noticeable scatter of points close to the maximum. Future observations will have to determine whether this is due to the Blazhko effect. The mean brightness curve, compiled according to our observations, is shown /130 in Figure 8, and the corresponding data are given in Table 8.

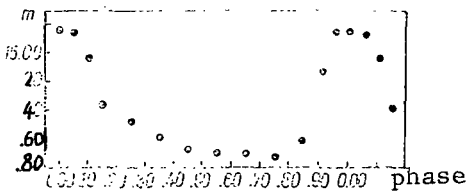

Figure 8

Mean Brightness Curve of Variable Star 8

TABLE 8

Phase	m	Phase	m	Phase	m	Phase	m
0.003	14.85	0.157	15.37	0.452	15.67	0.743	15.72
.050	.86	.251	.48	.552	.68	.842	.61
.098	15.04	.360	.59	.640	.69	.908	.12
						.951	14.84

Table 9 summarizes the observations of variable stars, whose magnitudes are given in the local system.

TABLE 9

JD hel	1	2	3	4	5	8
2 437 373.561	—	—	14.28	—	14.90:	15.20:
.589	14.89	—	.22	—	15.11:	.39:
79.476	15.48	—	15.42	14.34	14.88	14.61
.517	.52	15.49	.56	.60	15.25	.85
535	.63	.47	.50	—	.30	.92
.553	.63	.47	.67	14.88	.42	15.25
81.512	.66	.60:	.74	—	.52:	14.67
.541	.68	.52	.68	15.49	.68	.79
.563	—	—	.64:	—	—	.90:
3.561	15.49	15.02:	.72:	—	15.57	.85:
400.514	.47	.16	.13	15.47	14.90	15.44
.530	.46:	—	.08:	—	.34:	.46:
2 437 404.343	14.59:	14.90	15.01:	15.42	15.48	14.67
5.359	15.47	15.60	.82	—	14.28	15.34
.405	—	.52	14.78:	—	.34	.02:
.424	15.52	—	.65:	—	.37:	.35:
.439	.52	14.90	.24	14.79	.54	.35:
.455	.64	.79	.22	—	.90:	.39
.469	.55	.32	.26	15.12	.90	.34
.484	.46	.34	.55	.09	.67	.49
.499	.58	.19	.55	.33	.90	.49
.514	.49	.34	.75	.09	.90	.49
7.355	.16	15.31	.28	—	.60	.43
.373	.26	.11	.27	15.46	15.30	.39
.404	.25	14.63	.67	.44	.16	.39
.421	.30	.34	.62	.44	.30	.44
.435	.26	.28	.58	.47	.34	.49
.452	.30	.22	.82	.45	.24	.49
.491	.33	.34	.84	.48	.24	.46
.521	.46	.95	.92	.47	.30	.47
.535	—	—	15.06	—	—	.48
411.462	14.81	15.16	.60	14.39	.64	.48
.470	.79	14.96	.67	.39	.59	.45
.478	.67	15.11	.71	.34	.63	.45
.487	.67:	.39:	.53:	—	.31	.33
.496	.90	.25	.67	14.28	.43	.48
.506	.90	.46	.56	.22	.39:	.46
.515	.90	.39	.74	.28	14.85	.34
.525	15.13	.34	.67	.34	.79	.39
.533	14.67:	.44	.67	.36	.54	.46
.541	.79:	.31	.74	.39	.37	.36
2.497	15.30	.39	14.50	15.49	15.20:	.11
.511	.45	14.90	.38	—	.39:	14.84
.519	.20	.78	.70	—	.34	15.02:
.528	.30	.39	.60	—	.39:	.16:
.536	.30	.60	.81	15.16	.30	14.88
.546	.39	.34	.81	.16	.46	15.02
548.479	14.36	—	.96	—	.52	14.67
51.419	.61	—	15.46	—	.68:	15.44
3.386	.32	15.52	14.76	—	.55	.44
.399	.28	.52	.50	15.57	.60	.46
.409	.36	.44	.28	—	.44	.44

/131

Continuation of TABLE 9

JD hel	1	2	3	4	5	8
	m	m	m	m	m	m
.418	.58:	.56	.43	—	.49	.48
.436	.58	.55	.36	15.57	.60	.46
4.503	15.64	.39	15.64	—	.63	14.84
.512	.63	.02	.64	15.13	.60	.88
5.481	14.38	.46	.39	—	14.90	15.47
764.398	15.64	.26	14.81	14.92	15.45	.56
.434	.62	.53	.92	.94	.58	.26
2 473 764.451	15.48	15.66	14.94	15.16	15.62	15.07
.468	.66	.63	15.16	.18	.62	14.40
.484	.64	.73	.18	.18	.60	.24
.500	.66	.64	.24	.24:	.61	.33
.516	.64	.62	.32	.26	.64	.62
5.461	.62	14.64	.68	.39	14.61	15.56
.473	.58:	.65:	.62:	.50:	.70:	.70:
.485	14.98	.71	.62	.65	.55	.60
93.473	15.70:	15.72:	.72:	.18	15.14:	14.68:
.482	.73	.64	.91	.24	.25	.68
.496	.70	.68	.64	.23	.40	.90
871.345	.62	.74	.74	14.89	14.84	15.34:
.362	.66	.74	.64	.92	.46	.45
.376	.70	.70	.50	.90	.40	.64
.396	.72	.66	14.63	15.08	.45	.70
.407	.63	.70	.48	.60	15.32:	.62
.415	.03	.34	.03	.26	14.50	—
.424	.62	.76	.26	.26	.48	15.66
.434	.69	.64	.26	.20	.54	.76
.443	.66	.58	.25	.22	.73	.84
.452	.53	.16	.34	.22	.54	.58
2.356	14.63	14.72	15.60	.30	15.60	.51
.365	.42	.62	.70	.30	.60	.20
.373	.40	.64	.70	.64	.70	.20
.385	.56	.78	.64	.45	.64	.45
.402	.58	.89	.70	.62	.92	.24
.411	.46	.85	.67	.42	.69	.42
.425	.58	.93	.63	.55	.61	.35
.437	.49	.85	.68	.64	.66	.16
.445	.66	.97	.58	.26	.61	.48
.458	.68:	15.20	.62	14.56	.45:	.55
.467	.59	14.98	.42	.72	.45	.34:
.476	.64	.92	.70	.28	.61	.32
3.347	15.55	15.69	14.28	15.24	14.82	.60
.359	.40	.64:	.34	.27	15.12	.64
.371	.54:	.58	.56	.26	14.94	.59
.383	.56	.74:	.40	.07	15.43	.64
.395	.62	.65	.52	.27	.24	.64
.407	.36	.76	.78	.38	.37	.45
.439	.52	.65	.94	.50	.55	.63
910.352	14.63	14.68	—	.20	.70	—
.364	.62	.88	14.73	.10	.50	15.52
.375	.64	.84	.88	.04	.27:	.61
.392	.60	.84	.97	.14	14.65	.59
.403	.61	.96	.94	.18	.58	.63
2.289	15.63	.92	.90	.06	.42	.64
.302	.69	.75	.90	.11	.36	.73
2 437 912.314	15.68:	14.76:	15.02:	15.26:	14.44:	15.62:
.330	.72	.97	14.98	.27	.56	.64
.342	.68	.70	.92	.19	.98	.54
.356	.58	.82	15.17	.23	.72	.64
.371	14.98	15.24	.32	.53	15.16	.66
.383	.63	.11	.20	.28	14.92	.59

/132

/133

Continuation of TABLE 9

JD hel	1	2	3	4	5	8
	m	m	m	m	m	m
.397	.92	.01	.50	.34	15.04	.70
4.329	15.52	14.96	.51	.24	.40	.80
.342	.60	15.22	.59	.55	.25	.68
.354	.64	.16	.62	.62	.56	.64
.370	.70	.15	.57	.63	.57	.59
.381	.73	.05	.56	.61	.44	.62
.393	.66	.55	.62	.58	.56	.68
.409	.73	.24	.54	.59:	.86	.54
43.284	.31	14.99	.67	.51	14.49	.59
.296	14.81	15.17	.62	.30	.52	.68
.307	.61	.29	.74	.64	.48	.48
.319	.60	.16:	.63	.58	.52	.60
.332	.54	.64	.68	.36:	.56	.64
.343	.40	.38:	.70	.35:	.68:	.64
8089.505	.70	.30	14.88	14.48	.51	.62
.517	.58:	.45:	.53:	.40:	.44:	.62:
.528	.58	.08	.92	.66	.35	.28
.545	.60	.64	.94	.64	.49	.54
.556	.43	.69	.91	.66	.50	.70
.568	.73	.72	15.24	.76	.52	.57
.582	.60	.70	.26	15.72:	.79	.24
.593	.61	.83	.20	14.88	.85	.32
.604	.60	.77	.29	15.18	.86	.52
.618	15.00	.86	.43	.23	.79	.42
.630	14.87	.66	.50	.10	.90	.16
109.538	15.66	—	.51:	—	15.13	—
13.431	14.60:	15.67:	.68:	14.63:	.65:	15.30:
.460	.54:	.56:	.64:	—	.89:	.17:
.471	.85:	—	—	—	.77:	.39:
.503	.76:	15.56:	15.68:	14.87:	.77:	.39:
.514	.96:	—	.84:	—	—	.76:
.526	.80	15.56:	.84:	14.83:	15.77:	.68:
61.338	15.11:	.11:	.80:	.80:	.76:	.78:
.353	.27:	.72:	.72:	.94:	.29:	.49:
.369	.38:	14.75:	.84:	15.08:	.16:	.56:
6.389	.43	15.74	.86	.08:	14.56	14.90
.410	.67	.66	.74	.24	.64	.36
6.433	.58	.72	.68	.26	.83	.33
.455	.70	.62	.61	.22:	.88	.34
.478	.70	.76	.72	.22	15.02	.66
71.429	.72:	.74:	.72:	.08:	.22:	15.26:
2 438 176.331	15.70	15.60	15.46	14.53	14.72:	15.58
.346	.60	.22	.60	.62	.74	.52
7.342	14.66	.66	.80	15.29	15.54	.22
.359	.48:	.62:	.32:	.54	.69:	.36:
.374	.68	.70	14.86	.30	.64	.24
.386	.35	.46	—	.18:	.61:	.33:
260.312	.36	.69	14.76	.30	.64	.56
.330	.40	.73	.66	.64	.66	.52
.353	.64	.70	.66	.64	.74:	.53
.378	.57:	—	15.21:	—	.77:	.20:
.409	15.11:	15.30:	.14:	14.91:	.55:	.55:
.426	14.98	.41	.22	15.30	.64	.63
2.309	15.68:	.71:	14.94:	.27	.94	.51
.324	.61	.67	15.18	.44:	.45	.41
.340	.48	.71	.54	.49:	.89	.60
.360	14.94	.76	.51	.78:	.47	.62
.376	.70	.72	.58	14.67:	.14	.65
.391	.36	.71	.52	.95	14.56	.59
.408	.36	.70	.64	.58	.50	.68

/134

Conclusion of TABLE 9

JD hel	1	2	3	4	5	8
	m	m	m	m	m	m
.423	.37	.67	.65	.32	.47	.56
.441	.36	.66	.64	.30	.52	.59
87.311	15.11:	.27:	.38:	—	15.08:	.39:
.354	.00:	.84:	.58:	15.25:	.19:	.65:
.372	.26:	.31:	.64:	—	.62:	.56:
.391	.11:	.48	.66:	15.38:	.52:	.62:
.414	—	—	—	—	—	15.47:
8.241	15.52	15.52	14.82:	14.66	15.68	14.85
9.284	.02	.66	15.66	15.60	.54	15.56
.300	.02	.70	.75	.38:	.54	.58
.317	.03	.66	.68	.60	.62	.28
.348	.28	.70	.74	.38:	.70	.56
.364	.41	.66	.84	.57	.59	.58
.383	.36	.46	.64:	.25:	.83:	.49:
90.254	.62	14.68	14.64	.20	.25:	.20
.269	.60	.93	.62	.20	14.82	14.75
.285	.63	.88	.59	.22	.54	.83
.299	.66	.82	.81	.22	.44	.89
.315	.67	15.01	.95	.28	.46	.68
.331	.69	.02	15.10	.23	.50	.94
.346	.67	.06	14.94	.18	.55	.84
.362	.68	.02	15.20	.27	.65	.95
.381	.72	.04	.12	.55	.86	.92
1.247	14.37	.70	.64	.62	15.52	15.59
.266	.48	.64	.66	.57	.66	.56
.281	.40	.71	.68	.55	.89	.26
.300	.71	.62	.68	.63	.64	.54
.315	.76	.46	.62	.24	.73	.26
2 438 291.330	14.96	15.84	15.82	14.90	15.60	15.33
.352	.92	.72	.60	.34	.77	.60
.367	15.01	.68	.58	.37	.53	.48
.382	.06	.64	.78	.42	.54	.63
3.262	.66	.62	.50	.32	.58	.28
.275	.29	.66	.68	.36	.58	.48
.292	14.67	.84	.88	.65	.57	.51
.311	.66	.58	.72	.50	.77	.60
.344	.64	.24	.82	.74	.86	.69
.361	.66	.00	.72	15.20	.88	.70
.380	.62	14.68	.16	.01:	14.82	.57
4.284	15.28	15.04	.45	.38	15.54	.57
.269	.28	.17	.44	.55	.52	.54
.287	.38	.04	.52	.30	.58	.22
.302	.04	.65	.70	.62	.59	.54
.318	.62	.52	.62	.80:	.62	14.66
.369	.63	.78	.59	.30:	.77	.78

/135

REFERENCES

1. Paneva, L.I., Kheylo, E.S. Present Collection, 98.
2. Arp, H., Baum, W., Sandage, A. A.J., 58, 4, 1953.
3. Hachenberg, O. Zf. Aph., 18, 49, 1939.
4. Nassau, J. Aph. J., 87, 361, 1938.
5. Oosterhoff, P. BAN, 10, 55, 1944.
6. Sawyer, H. DOP, 2, 2, 1955.
7. Tayler, R. A.J., 59, 413, 1959.

CATALOG OF PHOTOVISUAL MAGNITUDES OF STARS IN THE REGION WITH CENTER $\alpha = 19^h$, $\delta = +11°$

V. I. Voroshilov

This paper contains a catalog of photovisual magnitudes of 3440 stars, determined with a mean error of $\pm 0^m.04$. The International System is used in the catalog.

The present catalog represents a supplement to the catalog of 22,000 stars /136
(Ref. 2). This latter catalog was compiled primarily for three colors, and only for area No. 2, containing 3440 stars are photovisual magnitudes lacking. The observational material was obtained on an astrograph having two chambers (Ref. 1) on Agfa Press plates with an exposure of 30 minutes. Photography was performed with a ZhS-12 filter. The magnitudes determined according to these photographs are international magnitudes.

Yellow, photoelectric magnitudes of stars in cluster NGC 6709 were used as the standard (Ref. 3). This cluster is located at the boundary of the region being analyzed; therefore, the region and the standard were obtained on the same photograph. Atmospheric corrections did not exceed $0^m.03$, which falls within the limits of the mean quadratic error of the catalog:

m	ε, m.	m	ε, m
9.0— 9.5	0.04	11.0—11.5	0.03
9.5—10.0	0.03	11.5—12.0	0.04
10.0—10.5	0.03	12.0—12.5	0.05
10.5—11.0	0.03		

The mean quadratic error of the catalog comprises $\pm 0^m.04$. The magnitudes were determined primarily from four photographs.

/137

№	m_{pv}	№	m_{pv}	№	m_{pv}	№	m_{pv}
7008	11.29	7056	11.79	7104	9.76	7152	11.87
7009	11.08	7057	12.15	7105	12.12	7153	10.09
7010	12.24	7058	11.81	7106	11.93	7154	12.18
7011	12.10	7059	12.20	7107	11.49	7155	12.43
7012	12.44	7060	12.30	7108	11.88	7156	12.01
7013	12.28	7061	12.19	7109	10.69	7157	9.32
7014	11.33	7062	11.16	7110	11.88	7158	11.47
7015	12.35	7063	11.87	7111	10.41	7159	11.84
7016	12.38	7064	12.39	7112	11.40	7160	12.22
7017	12.16	7065	11.32	7113	12.06	7161	12.61
7018	12.15	7066	12.41	7114	9.42	7162	11.24
7019	12.40	7067	10.63	7115	10.11	7163	12.02
7020	10.96	7068	11.94	7116	11.54	7164	10.62
7021	11.95	7069	11.63	7117	11.90	7165	11.98
7022	11.49	7070	12.24	7118	11.88	7166	12.38

№	m_{pv}	№	m_{pv}	№	m_{pv}	№	m_{pv}
7023	11.86	7071	9.60	7119	12.25	7167	11 12
7024	11.69	7072	10.29	7120	12.30	7168	11.59
7025	10.92	7073	12.07	7121	10.11	7169	10.57
7026	12.08	7074	9.32	7122	11.48	7170	11.30
7027	10.95	7075	11.63	7123	11.88	7171	12.21
7028	10.71	7076	11.82	7124	12.41	7173	10.81
7029	11.92	7077	12.25	7125	12.45	7174	12.40
7030	12.12	7078	12.30	7126	12.29	7175	10.62
7031	12.32	7079	12.22	7127	11.92	7176	12.00
7032	12.16	7080	12.36	7128	11.89	7177	11.06
7033	11.88	7081	12.02	7129	10.44	7178	12.08
7034	10.33	7082	10.77	7130	12.14	7179	12.27
7035	11.64	7083	12.05	7131	12.22	7180	12.17
7036	11.92	7084	12.45	7132	11.61	7181	11.65
7037	11.88	7085	12.31	7133	11.28	7182	11.83
7038	10.61	7086	11.38	7134	10.26	7183	11.59
7039	11.40	7087	12 24	7135	12.19	7184	11.54
7040	8.94	7088	11.34	7136	11.74	7185	11.45
7041	12.20	7089	12.39	7137	9.97	7186	12.24
7042	11.22	7090	12.47	7138	11.94	7187	11.72
7043	11.99	7091	11.12	7139	12.31	7188	9.84
7044	12.14	7092	11.81	7140	12.00	7189	11.60
7045	12.14	7093	11.79	7141	12.12	7190	12.24
7046	11.00	7094	12.16	7142	11.82	7191	11.00
7047	11.23	7095	11.61	7143	12.16	7192	11.81
7048	11.97	7096	11.74	7144	11.10	7193	12.06
7049	11.58	7097	12.45	7145	11.93	7194	11.85
7050	12.24	7098	10.55	7146	11.79	7195	12.21
7051	11.01	7099	11.97	7147	12.10	7196	12.24
7052	10.55	7100	12.43	7148	12.27	7197	12.09
7053	12.00	7101	12.19	7149	11.98	7198	12.31
7054	9.14	7102	11.87	7150	12.30	7199	11.80
7055	11.82	7103	11.49	7151	11.79	7200	12.38
7201	12.23	7249	11.91	7297	8.81	7345	11.34
7202	12.36	7250	11.93	7298	12.12	7346	12.30
7203	12.23	7251	12.04	7299	11.73	7347	12.16
7204	12.35	7252	11.82	7300	12.20	7348	11.70
7205	9.74	7253	11.89	7301	12.08	7349	12.10
7206	11.73	7254	12.19	7302	12.12	7350	11.47
7207	12.40	7255	12.27	7303	11.91	7351	11.96
7208	12.42	7256	11.06	7304	12.30	7352	11.90
7209	11.88	7257	10.68	7305	12.24	7353	11.74
7210	10.13	7258	11.39	7306	12.46	7354	12.27
7211	11.57	7259	12.02	7307	11.92	7355	11.81
7212	11.67	7260	12.06	7308	12.01	7356	11.96
7213	10.94	7261	11.97	7309	10.63	7357	12.00
7214	11.99	7262	12.32	7310	12.26	7358	11.73
7215	12.20	7263	12.31	7311	12.28	7359	11.24
7216	12.12	7264	11.47	7312	11.07	7360	12.36
7217	10.63	7265	11.38	7313	12.39	7361	12.09
7218	12.29	7266	11.65	7314	11.40	7362	11.80
7219	11.00	7267	11.99	7315	12.12	7363	10.59
7220	11.99	7268	12.32	7316	12.06	7354	11.13
7221	12.29	7269	12.10	7317	12.26	7365	9.48
7222	12.14	7270	10.05	7318	12.32	7366	12.03
7223	12.06	7271	11.90	7319	11.51	7367	11.91
7224	12.29	7272	11.47	7320	11.03	7368	11.95
7225	12.21	7273	11.44	7321	11.67	7369	11.85
7226	12.09	7274	12.03	7322	10.40	7370	11.97
7227	12.42	7275	11.83	7323	10.19	7371	12.20
7228	10.77	7276	11.13	7324	12.44	7372	11.14
7229	10.91	7277	12.19	7325	11.67	7373	12.27

/138

№	m_{pv}	№	m_{pv}	№	m_{pv}	№	m_{pv}
7230	12.14	7278	12.40	7326	12.08	7374	12.24
7231	11.41	7279	11.85	7327	12.40	7375	12.28
7232	11.67	7280	11.49	7328	11.37	7376	9.61
7233	11.15	7281	12.37	7329	12.45	7377	11.66
7234	11.32	7282	12.45	7330	12.32	7378	9.56
7235	11.55	7283	11.31	7331	12.05	7379	12.14
7236	11.55	7284	10.50	7332	12.16	7380	11.99
7237	11.87	7285	11.47	7333	10.12	7381	11.39
7238	11.04	7286	12.13	7334	12.00	7382	11.24
7239	12.02	7287	12.28	7335	11.30	7383	12.05
7240	12.59	7288	10.67	7336	11.93	7384	8.91
7241	12.21	7289	11.21	7337	10.61	7385	10.55
7242	12.20	7290	11.28	7338	11.29	7386	10.30
7243	12.20	7291	12.24	7339	11.95	7387	12.14
7244	11.74	7292	12.02	7340	12.39	7388	11.91
7245	11.17	7293	12.31	7341	12.43	7389	11.05
7246	12.27	7294	11.22	7342	11.66	7390	12.24
7247	11.35	7295	11.84	7343	12.07	7391	11.57
7248	11.99	7296	11.85	7344	8.73	7392	12.00
7393	11.59	7441	9.70	7489	10.11	7537	10.02
7394	12.50	7442	12.03	7490	10.58	7538	11.87
7395	10.50	7443	9.71	7491	10.79	7539	11.41
7396	12.08	7444	12.26	7492	12.03	7540	12.22
7397	11.85	7445	10.58	7493	11.64	7541	12.37
7398	10.06	7446	11.84	7494	10.28	7542	12.41
7399	11.38	7447	12.17	7495	10.45	7543	9.72
7400	12.18	7448	10.81	7496	11.94	7544	12.10
7401	12.21	7449	12.17	7497	12.22	7545	11.45
7402	12.06	7450	12.19	7498	11.02	7546	11.68
7403	10.82	7451	12.27	7499	12.38	7547	11.45
7404	11.60	7452	12.20	7500	12.06	7548	12.25
7405	12.13	7453	10.76	7501	10.93	7549	12.02
7406	11.80	7454	11.59	7502	11.40	7550	11.84
7407	11.73	7455	10.26	7503	11.37	7551	11.30
7408	12.04	7456	11.81	7504	11.90	7552	11.44
7409	11.18	7457	12.22	7505	12.27	7553	12.13
7410	11.06	7458	12.09	7506	10.79	7554	12.07
7411	10.03	7459	11.30	7507	12.10	7555	12.10
7412	12.01	7460	11.31	7508	11.64	7556	12.17
7413	11.08	7461	11.17	7509	10.85	7557	11.96
7414	12.31	7462	11.29	7510	12.07	7558	12.20
7415	12.11	7463	10.11	7511	12.28	7559	11.75
7416	12.36	7464	12.52	7512	12.20	7560	11.90
7417	10.70	7465	10.38	7513	11.30	7561	9.84
7418	11.75	7466	11.62	7514	11.90	7562	11.90
7419	11.05	7467	11.84	7515	10.29	7563	11.07
7420	12.33	7468	11.31	7516	11.08	7564	12.16
7421	11.97	7469	11.49	7517	12.36	7565	12.32
7422	11.74	7470	12.04	7518	12.02	7566	11.88
7423	12.30	7471	11.51	7519	11.19	7567	10.58
7424	11.94	7472	12.08	7520	12.53	7568	11.76
7425	11.96	7473	11.24	7521	11.30	7569	12.01
7426	11.17	7474	12.22	7522	11.62	7570	12.36
7427	11.81	7475	11.14	7523	12.20	7571	12.02
7428	11.54	7476	9.56	7524	11.21	7572	12.24
7429	12.40	7477	9.98	7525	12.14	7573	11.89
7430	11.91	7478	10.41	7526	11.97	7574	11.04
7431	11.20	7479	10.94	7527	11.96	7575	12.09
7432	11.93	7480	12.20	7528	12.40	7576	11.78
7433	12.30	7481	11.54	7529	11.25	7577	11.56
7434	9.44	7482	12.06	7530	11.70	7578	11.31
7435	10.74	7483	11.74	7531	12.08	7579	12.14

/139

№	m_{pv}	№	m_{pv}	№	m_{pv}	№	m_{pv}
7436	10.42	7484	11.47	7532	11.73	7580	11.90
7437	12.27	7485	11.07	7533	12.46	7581	11.19
7438	10.44	7486	12.09	7534	11.44	7582	12.36
7439	11.88	7487	11.48	7535	12.08	7583	11.74
7440	11.94	7488	11.09	7536	10.49	7584	11.99
7585	11.44	7633	12.27	7681	11.10	7729	12.03
7586	10.94	7634	11.71	7682	11.52	7730	12.09
7587	11.42	7635	10.93	7683	12.17	7731	12.11
7588	12.02	7636	12.24	7684	11.49	7732	11.90
7589	11.02	7637	11.56	7685	11.20	7733	9.85
7590	12.31	7638	12.07	7686	12.47	7734	11.87
7591	11.43	7639	11.57	7687	11.48	7735	12.03
7592	11.08	7640	11.88	7688	12.16	7736	10.78
7593	12.07	7641	9.54	7689	11.67	7737	12.24
7594	12.12	7642	12.06	7690	12.45	7738	11.81
7595	12.25	7643	12.18	7691	12.23	7739	11.57
7596	12.03	7644	11.32	7692	11.97	7740	12.19
7597	11.36	7645	12.20	7693	11.33	7741	12.10
7598	9.69	7646	12.18	7694	11.67	7742	11.97
7599	11.99	7647	11.07	7695	12.11	7743	12.12
7600	12.14	7648	12.31	7696	12.36	7744	12.20
7601	11.67	7649	10.75	7697	11.48	7745	11.27
7602	12.20	7650	12.42	7698	12.22	7746	11.80
7603	10.70	7651	11.97	7699	11.04	7747	10.44
7604	12.16	7652	11.93	7700	11.36	7748	11.04
7605	11.67	7653	12.00	7701	11.46	7749	12.06
7606	11.76	7654	12.27	7702	11.83	7750	11.08
7607	12.10	7655	12.17	7703	11.72	7751	11.85
7608	12.09	7656	11.53	7704	12.26	7752	12.16
7609	11.83	7657	11.67	7705	11.17	7753	10.62
7610	11.70	7658	12.41	7706	10.82	7754	11.76
7611	11.91	7659	12.44	7707	12.02	7755	11.94
7612	12.42	7660	12.28	7708	12.46	7756	11.77
7613	12.11	7661	11.15	7709	11.90	7757	11.07
7614	11.91	7662	11.40	7710	12.33	7758	11.36
7615	11.99	7663	10.26	7711	11.82	7759	11.90
7616	11.72	7664	12.25	7712	12.42	7760	12.06
7617	12.39	7665	11.61	7713	12.29	7761	11.87
7618	12.27	7666	9.76	7714	12.52	7762	12.17
7619	12.39	7667	12.05	7715	12.18	7763	8.66
7620	12.01	7668	11.95	7716	10.62	7764	11.93
7621	12.15	7669	9.65	7717	12.14	7765	11.64
7622	11.14	7670	12.25	7718	11.94	7766	12.10
7623	9.79	7671	11.95	7719	12.19	7767	11.96
7624	11.67	7672	12.06	7720	11.81	7768	11.80
7625	11.87	7673	12.50	7721	12.26	7769	12.22
7626	12.35	7674	12.11	7722	11.48	7770	10.54
7627	12.12	7675	12.02	7723	10.19	7771	11.68
7628	12.29	7676	11.66	7724	9.20	7772	12.04
7629	11.82	7677	11.88	7725	11.94	7773	12.14
7630	12.27	7678	12.16	7726	12.36	7774	12.44
7631	10.88	7679	12.38	7727	12.12	7775	12.08
7632	12.32	7680	12.12	7728	12.24	7776	9.65
7777	10.55	7825	11.66	7873	10.02	7921	12.25
7778	11.24	7826	9.84	7874	11.41	7922	12.10
7779	12.16	7827	12.26	7875	12.18	7923	11.26
7780	12.24	7828	10.07	7876	12.40	7924	11.67
7781	11.96	7829	10.13	7877	9.19	7925	10.77
7782	9.28	7830	12.06	7878	12.26	7926	12.14
7783	11.27	7831	12.32	7879	9.18	7927	11.63
7784	12.22	7832	12.30	7880	10.35	7928	12.17

/140

/141

№	m_{pv}	№	m_{pv}	№	m_{pv}	№	m_{pv}
7785	11.71	7833	12.03	7881	12.38	7929	12.24
7786	12.15	7834	12.17	7882	11.88	7930	12.06
7787	12.12	7835	11.80	7883	11.76	7931	11.52
7788	11.85	7836	11.97	7884	11.31	7932	11.08
7789	11.95	7837	11.59	7885	12.32	7933	11.80
7790	10.40	7838	11.41	7886	12.21	7934	12.08
7791	11.93	7839	11.60	7887	11.74	7935	12.19
7792	9.45	7840	12.19	7888	12.10	7936	11.68
7793	11.17	7841	11.74	7889	10.99	7937	12.21
7794	11.90	7842	12.24	7890	11.96	7938	12.18
7795	11.65	7843	11.29	7891	11.81	7939	10.88
7796	11.07	7844	10.63	7892	9.18	7940	11.87
7797	12.13	7845	11.62	7893	11.94	7941	11.51
7798	11.45	7846	12.05	7894	11.85	7942	9.51
7799	10.06	7847	10.64	7895	10.09	7943	11.28
7800	11.20	7848	11.44	7896	9.99	7944	11.98
7801	11.80	7849	10.92	7897	10.85	7945	12.25
7802	12.14	7850	11.29	7898	12.30	7946	12.18
7803	11.79	7851	11.90	7899	11.34	7947	12.30
7804	12.20	7852	12.38	7900	11.87	7948	12.32
7805	12.32	7853	11.34	7901	11.82	7949	10.84
7806	12.30	7854	12.41	7902	9.03	7950	12.34
7807	10.72	7855	12.05	7903	12.34	7951	11.82
7808	12.09	7856	12.34	7904	12.18	7952	12.32
7809	10.26	7857	12.42	7905	11.84	7953	11.80
7810	11.47	7858	11.17	7906	12.30	7954	11.30
7811	8.94	7859	11.94	7907	10.92	7955	11.31
7812	11.44	7860	12.27	7908	11.38	7956	12.09
7813	11.82	7861	12.29	7909	11.20	7957	10.10
7814	12.12	7862	12.00	7910	11.15	7958	12.34
7815	12.29	7863	12.57	7911	12.33	7959	12.05
7816	10.47	7864	12.50	7912	11.90	7960	12.10
7817	12.29	7865	11.19	7913	10.00	7961	12.06
7818	11.04	7866	11.83	7914	11.90	7963	12.30
7819	11.66	7867	11.19	7915	11.44	7964	12.62
7820	10.28	7868	11.39	7916	11.91	7965	11.55
7821	11.32	7869	11.54	7917	12.35	7966	12.02
7822	12.17	7870	10.07	7918	12.19	7967	12.06
7823	9.83	7871	11.36	7919	12.05	7968	11.87
7824	12.20	7872	11.90	7920	11.82	7969	12.35
7970	12.10	8018	11.77	8066	12.34	8114	11.15
7971	11.11	8019	11.62	8067	11.70	8115	8.46
7972	12.26	8020	11.83	8068	12.29	8116	12.16
7973	11.66	8021	10.88	8069	11.74	8117	11.56
7974	12.16	8022	11.47	8070	11.65	8118	12.30
7975	12.21	8023	11.01	8071	12.51	8119	11.15
7976	12.07	8024	11.31	8072	12.10	8120	12.34
7977	10.92	8025	9.84	8073	11.08	8121	11.06
7978	12.12	8026	11.94	8074	12.26	8122	11.56
7979	12.09	8027	12.14	8075	11.80	8123	12.37
7980	12.15	8028	11.71	8076	12.00	8124	12.22
7981	9.10	8029	12.41	8077	12.19	8125	12.32
7982	12.06	8030	11.74	8078	11.48	8126	12.30
7983	10.32	8031	11.08	8079	11.97	8127	9.91
7984	11.43	8032	11.97	8080	10.33	8128	12.14
7985	12.14	8033	11.82	8081	9.44	8129	12.06
7986	12.14	8034	12.08	8082	12.03	8130	11.49
7987	12.36	8035	12.28	8083	10.74	8131	11.47
7988	12.42	8036	11.52	8084	12.43	8132	11.81
7989	11.20	8037	12.08	8085	12.09	8133	11.97
7990	11.59	8038	12.06	8086	11.79	8134	11.47
7991	12.31	8039	12.14	8087	11.98	8135	10.99

/142

№	m_{pv}	№	m_{pv}	№	m_{pv}	№	m_{pv}
7992	10.79	8040	11.56	8088	11.90	8136	9.56
7993	12.12	8041	11.82	8089	12.02	8137	12.23
7994	11.90	8042	11.99	8090	12.37	8138	12.32
7995	11.67	8043	11.93	8091	12.09	8139	11.91
7996	11.77	8044	11.30	8092	12.16	8140	10.23
7997	11.75	8045	11.24	8093	11.04	8141	12.06
7998	12.33	8046	12.14	8094	12.25	8142	11.93
7999	11.32	8047	11.00	8095	11.76	8143	12.18
8000	10.56	8048	12.16	8096	12.12	8144	11.36
8001	12.33	8049	12.24	8097	11.03	8145	11.59
8002	11.06	8050	11.09	8098	11.02	8146	11.04
8003	12.04	8051	12.18	8099	12.14	8147	12.26
8004	12.03	8052	12.33	8100	12.32	8148	11.44
8005	11.89	8053	11.47	8101	10.99	8149	12.24
8006	11.37	8054	12.44	8102	11.45	8150	9.88
8007	12.31	8055	10.81	8103	12.27	8151	12.25
8008	12.03	8056	11.77	8104	12.24	8152	11.59
8009	12.40	8057	10.30	8105	12.10	8153	10.07
8010	11.52	8058	10.47	8106	11.96	8154	12.32
8011	11.87	8059	11.97	8107	11.67	8155	11.00
8012	11.75	8060	12.24	8108	12.09	8156	12.32
8013	9.50	8061	12.22	8109	9.31	8157	11.24
8014	12.34	8062	12.15	8110	12.24	8158	11.98
8015	10.49	8063	12.05	8111	11.63	8159	11.81
8016	12.26	8064	11.90	8112	12.30	8160	11.94
8017	12.38	8065	12.14	8113	10.68	8161	12.37
8162	11.11	8210	10.28	8259	11.50	8307	9.06
8163	11.64	8211	11.51	8260	11.31	8308	11.04
8164	10.74	8212	12.22	8261	12.14	8309	10.35
8165	9.00	8213	10.99	8262	11.25	8310	11.92
8166	11.90	8214	11.84	8263	10.47	8311	12.29
8167	12.01	8215	11.82	8264	11.90	8312	12.05
8168	12.31	8217	10.06	8265	12.01	8313	11.68
8169	12.00	8218	12.17	8266	11.02	8314	12.06
8170	12.06	8219	10.49	8267	11.35	8315	11.52
8171	8.83	8220	9.69	8268	10.20	8316	11.34
8172	11.21	8221	11.18	8269	11.81	8317	12.14
8173	11.82	8222	11.85	8270	11.15	8318	10.49
8174	11.11	8223	11.90	8271	12.16	8319	11.20
8175	11.55	8224	11.46	8272	11.92	8320	9.95
8176	11.93	8225	12.20	8273	12.17	8321	12.16
8177	11.94	8226	11.42	8274	10.90	8322	11.12
8178	9.52	8227	12.02	8275	11.96	8323	11.09
8179	12.19	8228	12.24	8276	12.27	8324	11.81
8180	12.11	8229	12.25	8277	11.64	8325	11.14
8181	11.81	8230	11.89	8278	11.77	8326	9.85
8182	11.43	8231	11.94	8279	11.85	8327	11.02
8183	12.28	8232	12.36	8280	11.77	8328	11.69
8184	11.67	8233	11.82	8281	11.79	8329	12.27
8185	9.53	8234	12.17	8232	11.72	8330	11.61
8186	11.41	8235	11.87	8283	11.67	8331	12.20
8187	10.63	8236	11.63	8284	12.23	8332	11.99
8188	11.56	8237	11.74	8285	9.98	8333	12.23
8189	11.93	8238	12.17	8236	11.65	8334	11.94
8190	11.93	8239	11.59	8287	11.58	8335	12.24
8191	12.11	8240	12.01	8288	8.86	8336	9.00
8192	12.18	8241	11.58	8289	11.91	8337	9.88
8193	12.28	8242	12.25	8290	12.17	8338	12.09
8194	11.76	8243	11.79	8291	10.31	8339	10.13
8195	11.08	8244	11.97	8292	12.09	8340	12.25
8196	12.36	8245	12.19	8293	12.22	8341	12.00
8197	12.12	8246	12.31	8294	11.30	8342	12.25
8198	10.97	8247	11.04	8295	10.71	8343	11.86

/143

№	m_{pv}	№	m_{pv}	№	m_{pv}	№	m_{pv}
8199	11.41	8248	10.30	8296	11.51	8344	11.10
8200	12.30	8249	11.70	8297	12.20	8345	11.49
8201	12.17	8250	11.93	8298	11.81	8346	11.68
8202	11.58	8251	12.34	82 9	11.89	8347	10.66
8203	12.21	8252	12.22	8300	11.73	8348	12.19
8204	12.32	8253	12.30	8301	11.72	8349	11.72
8205	11.55	8254	11.93	8302	12.00	8350	10.55
8206	12.16	8255	10.35	8303	11.24	8351	11.62
8207	12.22	8256	12.14	8304	11.54	8352	12.16
8208	11.04	8257	11.87	8305	11.80	8353	9.57
8209	12.23	8258	12.11	8306	12.38	8354	11.48
8355	12.30	8403	12.29	8451	11.51	8499	12.37
8356	12.39	8404	10.65	8452	11.56	8500	12.14
8357	11.18	8405	12.27	8453	12.19	8501	12.22
8358	10.83	8406	12.35	8454	11.59	8502	10.36
8359	11.96	8407	12.14	8455	12.30	8503	11.86
8360	9.72	8408	12.28	8456	12.16	8504	11.35
8361	12.26	8409	12.04	8457	11.96	8505	9.19
8362	12.18	8410	11.99	8458	11.99	8506	11.95
8363	10.15	8411	10.57	8459	12.35	8507	12.18
8364	11.91	8412	9.07	8460	12.30	8508	12.33
8365	10.78	8413	12.14	8461	12.33	8509	12.30
8366	11.37	8414	12.26	8462	12.13	8510	12.39
8367	9.61	8415	12.10	8463	12.18	8511	12.06
8368	12.33	8416	11.97	8464	12.45	8512	11.52
8369	11.74	8417	11.93	8465	11.47	8513	11.97
8370	8.92	8418	10.10	8466	12.13	8514	12.23
8371	8.86	8419	12.23	8467	12.08	8515	12.03
8372	11.81	8420	10.99	8468	12.29	8516	12.29
8373	11.34	8421	12.06	8469	11.76	8517	12.19
8374	12.14	8422	11.50	8470	11.36	8518	12.14
8375	12.19	8423	11.51	8471	11.00	8519	12.25
8376	9.82	8424	11.49	8472	12.33	8520	11.29
8377	9.03	8425	11.50	8473	12.41	8521	9.89
8378	12.30	8426	12.22	8474	11.04	8522	12.27
8379	12.17	8427	12.12	8475	12.05	8523	11.97
8380	11.76	8428	12.41	8476	12.20	8524	11.97
8381	11.64	8429	12.02	8477	10.22	8525	11.55
8382	11.93	8430	11.97	8478	9.71	8526	11.24
8383	12.14	8431	11.66	8479	12.16	8527	11.85
8384	12.17	8432	12.46	8480	12.36	8528	11.84
8385	11.80	8433	11.86	8481	11.70	8529	11.94
8386	11.50	8434	12.05	8482	11.52	8530	9.50
8387	11.21	8435	11.99	8483	9.93	8531	9.87
8388	11.74	8436	12.16	8484	12.19	8532	12.27
8389	9.34	8437	12.10	8485	11.87	8533	11.74
8390	11.67	8438	11.12	8486	12.01	8534	9.26
8391	12.30	8439	12.25	8487	9.03	8535	12.26
8392	12.28	8440	12.06	8488	11.93	8536	12.09
8393	11.24	8441	11.74	8489	11.62	8537	12.19
8394	12.01	8442	12.24	8490	12.34	8538	12.10
8395	10.27	8443	11.62	8491	11.33	8539	12.41
8396	12.35	8444	12.33	8492	9.83	8540	12.34
8397	12.20	8445	10.81	8493	11.78	8541	10.51
8398	9.71	8446	11.68	8494	12.10	8542	12.00
8399	11.58	8447	12.20	8495	11.77	8543	11.73
8400	12.11	8448	11.59	8496	11.85	8544	12.32
8401	11.77	8449	11.62	8497	11.61	8545	12.10
8402	11.04	8450	12.24	8498	10.97	8546	12.46

/144

№	m_{pv}	№	m_{pv}	№	m_{pv}	№	m_{pv}
8547	11.87	8595	9.13	8643	12.34	8691	12.32
8548	11.66	8596	11.71	8644	11.39	8692	11.11
8549	10.26	8597	11.87	8645	12.05	8693	12.50
8550	11.64	8598	11.75	8646	11.37	8694	12.17
8551	11.90	8599	11.00	8647	10.65	8695	12.22
8552	12.03	8600	12.12	8648	12.25	8696	9.88
8553	12.15	8601	12.08	8649	12.24	8697	11.91
8554	11.39	8602	12.19	8650	12.21	8698	12.18
8555	12.19	8603	12.33	8651	10.49	8699	11.94
8556	11.24	8604	11.88	8652	11.88	8700	12.06
8557	10.73	8605	11.80	8653	11.65	8701	12.19
8558	11.50	8606	11.36	8654	9.36	8702	11.81
8559	10.78	8607	11.40	8655	11.85	8703	11.74
8560	11.45	8608	11.55	8656	11.08	8704	12.02
8561	12.17	8609	11.71	8657	12.34	8705	12.10
8562	12.24	8610	12.20	8658	9.62	8706	12.25
8563	11.49	8611	9.45	8659	12.10	8707	11.74
8564	11.79	8612	9.97	8660	12.30	8708	11.90
8565	11.41	8613	11.97	8661	11.28	8709	12.32
8566	11.89	8614	11.54	8662	10.96	8710	11.52
8567	12.27	8615	10.20	8663	11.30	8711	12.17
8568	12.16	8616	10.73	8664	12.30	8712	9.48
8569	10.74	8617	12.19	8665	11.14	8713	9.93
8570	12.39	8618	12.05	8666	11.05	8714	11.91
8571	11.28	8619	11.89	8667	11.70	8715	12.27
8572	8.93	8620	12.30	8668	11.14	8716	12.00
8573	11.83	8621	12.17	8669	12.10	8717	11.62
8574	11.37	8622	10.53	8670	11.64	8718	12.37
8575	12.27	8623	9.20	8671	11.98	8719	12.19
8576	11.91	8624	12.30	8672	10.87	8720	12.15
8577	11.91	8625	12.34	8673	11.28	8721	12.34
8578	11.95	8626	10.56	8674	11.47	8722	12.26
8579	11.52	8627	11.99	8675	12.27	8723	11.79
8580	11.73	8628	9.59	8676	10.76	8725	10.95
8581	11.60	8629	10.68	8677	12.30	8726	12.36
8582	12.05	8630	10.92	8678	12.27	8727	12.46
8583	10.76	8631	12.09	8679	10.27	8728	11.77
8584	11.07	8632	10.97	8680	12.24	8729	12.46
8585	12.04	8633	9.74	8681	11.94	8730	12.33
8586	10.90	8634	11.66	8682	12.15	8731	12.30
8587	12.31	8635	11.35	8683	11.22	8732	10.90
8588	12.14	8636	11.24	8684	11.31	8733	10.70
8589	10.88	8637	12.16	8685	12.06	8734	9.02
8590	12.30	8638	10.40	8686	10.97	8735	12.42
8591	12.20	8639	12.12	8687	10.73	8736	12.33
8592	12.26	8640	11.93	8688	10.86	8737	11.63
8593	10.70	8641	11.09	8689	11.99	8738	12.14
8594	12.13	8642	11.18	8690	11.28	8739	12.35
8740	12.09	8788	12.14	8837	12.11	8885	12.33
8741	11.92	8789	11.82	8838	9.85	8886	10.85
8742	12.15	8790	11.11	8839	12.09	8887	10.02
8743	11.38	8791	10.50	8840	12.15	8888	10.92
8744	12.47	8792	10.94	8841	12.49	8889	11.81
8745	11.41	8793	12.36	8842	12.27	8890	11.35
8746	12.36	8794	11.85	8843	10.45	8891	10.68
8747	12.02	8795	9.95	8844	12.15	8892	11.59
8748	12.11	8796	11.43	8845	8.80	8893	12.27
8749	12.27	8797	11.43	8846	10.87	8894	12.23
8750	12.34	8798	12.15	8847	11.93	8895	10.92
8751	12.07	8799	12.15	8848	12.19	8896	12.13
8752	11.88	8800	12.37	8849	12.25	8897	10.86

/145

/146

№	m_{pv}	№	m_{pv}	№	m_{pv}	№	m_{pv}
8753	11.94	8801	11.93	8850	12.39	8898	9.79
8754	10.03	8802	8.94	8851	12.08	8899	12.38
8755	11.78	8803	11.73	8852	12.19	8900	11.82
8756	12.13	8804	11.64	8853	11.95	8901	11.70
8757	12.06	8805	11.42	8854	11.80	8902	11.68
8758	12.28	8806	11.74	8855	11.22	8903	11.63
8759	11.87	8807	12.28	8856	12.21	8905	12.19
8760	11.27	8808	11.99	8857	12.33	8906	12.34
8761	11.50	8809	12.21	8858	12.00	8907	12.15
8762	12.32	8810	12.40	8859	12.21	8908	11.27
8763	11.32	8811	9.57	8860	12.40	8909	10.69
8764	11.94	8812	12.25	8861	11.93	8910	12.35
8765	12.36	8813	11.24	8862	12.25	8911	12.33
8766	12.46	8814	11.25	8863	11.72	8912	12.23
8767	11.58	8815	12.22	8864	12.30	8913	10.68
8768	12.20	8816	11.52	8865	11.96	8914	12.17
8769	11.54	8817	12.29	8866	10.44	8915	12.50
8770	12.33	8818	11.96	8867	11.52	8916	11.74
8771	12.00	8819	12.32	8868	11.53	8917	12.09
8772	12.52	8820	11.79	8869	12.08	8918	12.20
8773	12.24	8821	12.12	8870	11.59	8919	10.61
8774	12.43	8822	12.29	8871	12.31	8920	9.99
8775	12.19	8823	12.00	8872	10.95	8921	11.43
8776	11.90	8824	10.37	8873	9.01	8922	12.11
8777	11.12	8825	11.00	8874	11.52	8923	12.26
8778	12.37	8826	11.89	8875	12.05	8924	11.52
8779	12.29	8827	12.27	8876	12.23	8925	12.05
8780	12.38	8828	12.15	8877	12.19	8926	10.28
8781	12.30	8829	12.27	8878	10.88	8927	11.97
8782	12.49	8830	12.05	8879	12.09	8928	10.36
8783	9.24	8831	12.53	8880	11.41	8929	12.42
8784	10.20	8832	12.27	8881	10.41	8930	12.09
8785	12.14	8833	11.51	8882	12.07	8931	12.11
8786	11.13	8834	11.67	8883	12.00	8932	12.39
8787	12.12	8835	11.87	8884	11.71	8933	12.28
8934	11.62	8982	11.38	9030	12.20	9079	11.51
8935	11.89	8983	11.52	9032	11.76	9080	12.46
8936	9.71	8984	12.17	9033	11.98	9081	12.10
8937	12.40	8985	12.10	9034	12.33	9082	10.22
8938	11.90	8986	11.32	9035	11.10	9083	10.38
8939	12.12	8987	12.27	9036	12.11	9084	9.67
8940	12.31	8988	12.21	9037	12.33	9085	12.27
8941	10.18	8989	12.13	9038	11.97	9086	10.31
8942	12.18	8990	12.21	9039	12.38	9087	9.48
8943	12.41	8991	12.35	9040	10.88	9088	12.13
8944	10.96	8992	12.22	9041	12.41	9089	11.42
8945	10.43	8993	11.76	9042	11.93	9090	12.47
8946	11.45	8994	11.67	9043	12.16	9091	12.20
8947	11.71	8995	11.56	9044	10.50	9092	12.42
8948	12.05	8996	12.35	9045	12.07	9093	10.69
8949	10.18	8997	11.01	9046	12.07	9094	11.61
8950	12.18	8998	12.21	9047	11.95	9095	11.47
8951	12.17	8999	11.04	9048	11.30	9096	12.34
8952	11.37	9000	11.31	9049	11.98	9097	12.08
8953	12.19	9001	12.38	9050	11.37	9098	12.35
8954	11.28	9002	12.15	9051	11.52	9099	12.42
8955	11.77	9003	12.25	9052	11.57	9100	10.06
8956	12.11	9004	11.49	9053	10.65	9101	12.19
8957	9.11	9005	11.29	9054	9.90	9102	12.25
8958	11.94	9006	12.06	9055	11.47	9103	12.30
8959	10.95	9007	12.31	9056	10.68	9104	12.01
8960	11.54	9008	10.77	9057	11.77	9105	12.16

/147

№	m_{pv}	№	m_{pv}	№	m_{pv}	№	m_{pv}
8961	11.91	9009	12.10	9058	11.74	9106	12.36
8962	12.46	9010	12.18	9059	10.82	9107	12.06
8963	11.48	9011	11.56	9060	12.41	9108	12.31
8964	12.11	9012	10.53	9061	12.11	9109	11.56
8965	12.42	9013	12.16	9062	12.31	9110	12.13
8966	11.63	9014	11.85	9063	10.86	9111	12.54
8967	12.34	9015	12.55	9064	12.08	9112	12.43
8968	12.13	9016	11.94	9065	12.21	9113	11.71
8969	12.42	9017	11.46	9066	11.79	9114	11.87
8970	10.13	9018	12.38	9067	12.61	9115	12.06
8971	11.97	9019	12.34	9068	11.79	9116	11.03
8972	11.95	9020	10.61	9069	11.76	9117	11.30
8973	12.36	9021	12.25	9070	9.10	9118	12.17
8974	11.13	9022	11.59	9071	12.39	9119	11.09
8975	11.81	9023	11.74	9072	10.94	9120	12.46
8976	12.10	9024	12.19	9073	9.65	9121	12.13
8977	11.36	9025	12.52	9074	11.86	9122	12.15
8978	11.43	9026	11.80	9075	12.21	9123	12.37
8979	11.91	9027	12.13	9076	11.28	9124	12.20
8980	11.56	9028	11.98	9077	11.32	9125	12.17
8981	12.27	9029	12.19	9078	11.94	9126	11.21
9127	11.66	9175	11.96	9223	11.30	9271	10.91
9128	12.11	9176	12.13	9224	11.95	9272	12.62
9129	10.35	9177	10.15	9225	10.94	9273	11.87
9130	11.14	9178	11.53	9226	12.10	9274	11.81
9131	10.35	9179	10.95	9227	10.25	9275	11.26
9132	12.14	9180	11.24	9228	12.00	9276	11.20
9133	12.11	9181	10.79	9229	12.06	9277	10.24
9134	12.19	9182	12.32	9230	11.82	9278	11.85
9135	12.29	9183	11.05	9231	11.65	9279	12.44
9136	12.27	9184	12.14	9232	11.37	9280	9.71
9137	11.59	9185	12.12	9233	11.72	9281	12.29
9138	11.97	9186	12.15	9234	11.37	9282	11.82
9139	10.62	9187	12.33	9235	11.37	9283	10.59
9140	12.24	9188	11.70	9236	11.81	9284	12.21
9141	11.81	9189	12.31	9237	12.06	9285	12.22
9142	10.89	9190	11.63	9238	12.06	9286	9.87
9143	9.86	9191	12.53	9239	11.32	9287	12.02
9144	10.73	9192	12.04	9240	11.50	9288	12.27
9145	11.52	9193	11.11	9241	11.13	9289	12.34
9146	12.31	9194	12.14	9242	10.48	9290	10.92
9147	11.74	9195	11.82	9243	9.68	9291	12.32
9148	11.05	9196	12.38	9244	12.02	9292	12.01
9149	11.79	9197	12.12	9245	12.14	9293	11.52
9150	12.23	9198	12.20	9246	11.82	9294	12.31
9151	10.35	9199	12.05	9247	11.72	9295	11.97
9152	12.31	9200	12.16	9248	10.35	9296	11.60
9153	12.22	9201	12.03	9249	10.74	9297	11.66
9154	12.10	9202	12.10	9250	12.22	9298	10.99
9155	12.21	9203	12.28	9251	11.62	9299	12.01
9156	12.17	9204	12.18	9252	11.53	9300	11.45
9157	12.24	9205	12.20	9253	9.98	9301	11.44
9158	12.02	9206	11.55	9254	11.58	9302	11.81
9159	12.26	9207	11,86	9255	12.35	9303	11.83
9160	11.49	9208	11.38	9256	10.40	9304	12.16
9161	12.24	9209	10.36	9257	12.03	9305	12.14
9162	12.32	9210	12.04	9258	11.34	9306	11.84
9163	12.24	9211	11.88	9259	12.06	9307	12.36
9164	12.12	9212	12.46	9260	12.44	9308	11.86
9165	11.80	9213	11.24	9261	12.43	9309	12.31
9166	11.30	9214	11.30	9262	12.14	9310	11.64
9167	12.52	9215	12.22	9263	10.47	9311	11.15

/148

№	m_{pv}	№	m_{pv}	№	m_{pv}	№	m_{pv}
9168	12.03	9216	10.38	9264	12.51	9312	11.81
9169	12.22	9217	11.95	9265	11.81	9313	12.30
9170	11.78	9218	11.56	9266	11.14	9314	11.62
9171	12.26	9219	12.14	9267	11.42	9315	11.38
9172	11.24	9220	10.78	9268	12.17	9316	12.08
9173	10.91	9221	11.79	9269	11.24	9317	12.29
9174	12.14	9222	10.61	9270	12.21	9318	12.08
9319	11.57	9368	12.12	9416	12.12	9464	11.85
9320	11.64	9369	9.93	9417	12.29	9465	12.24
9321	10.59	9370	11.96	9418	12.34	9466	11.87
9322	11.41	9371	11.23	9419	12.38	9467	12.14
9323	11.20	9372	12.12	9420	12.32	9468	12.03
9324	12.53	9373	11.25	9421	11.56	9469	12.14
9325	11.59	9374	12.06	9422	12.46	9470	10.49
9326	10.07	9375	12.20	9423	12.10	9471	10.71
9327	11.68	9376	11.13	9424	11.52	9472	9.74
9328	12.25	9377	12.36	9425	12.10	9473	12.29
9329	10.82	9378	12.30	9426	12.08	9474	12.46
9330	12.12	9379	10.94	9427	11.86	9475	12.24
9331	12.08	9380	11.76	9428	11.86	9476	10.38
9332	11.14	9381	11.05	9429	11.14	9477	12.32
9333	12.18	9382	11.43	9430	12.16	9478	11.84
9334	12.26	9383	12.29	9431	11.40	9479	10.99
9335	11.64	9384	12.30	9432	11.99	9480	12.38
9336	11.67	9385	12.34	9433	10.99	9481	11.71
9337	12.06	9386	12.24	9434	12.09	9482	12.32
9338	11.69	9387	12.44	9435	11.68	9483	11.02
9339	12.06	9388	11.63	9436	11.39	9484	12.04
9340	12.05	9389	12.40	9437	12.13	9485	12.03
9341	12.30	9390	11.07	9438	11.67	9486	12.29
9342	12.09	9391	12.03	9439	12.14	9487	9.72
9343	10.03	9392	11.69	9440	12.17	9488	10.91
9345	12.02	9393	11.78	9441	11.87	9489	12.20
9346	11.87	9394	12.02	9442	12.04	9490	10.61
9347	12.16	9395	12.32	9443	11.91	9491	8.76
9348	12.23	9396	10.30	9444	12.22	9492	11.85
9349	12.35	9397	11.57	9445	11.16	9493	11.99
9350	11.99	9398	12.14	9446	9.41	9494	12.02
9351	11.98	9399	12.14	9447	11.57	9495	12.04
9352	12.35	9400	11.26	9448	12.05	9496	11.62
9353	11.47	9401	10.38	9449	8.91	9497	12.32
9354	11.77	9402	12.27	9450	12.32	9498	12.27
9355	11.90	9403	11.31	9451	12.38	9499	11.07
9356	11.93	9404	12.48	9452	11.37	9500	12.23
9357	11.05	9405	12.27	9453	12.32	9501	12.12
9358	11.84	9406	12.18	9454	12.13	9502	11.62
9359	11.41	9407	11.93	9455	10.84	9503	12.15
9360	12.30	9408	12.34	9456	12.15	9504	12.39
9361	9.74	9409	10.26	9457	12.27	9505	12.28
9362	12.20	9410	12.02	9458	12.12	9506	12.04
9363	12.15	9411	12.34	9459	12.48	9507	11.79
9364	11.05	9412	11.24	9460	12.06	9508	9.83
9365	11.20	9413	12.36	9461	11.48	9509	11.92
9366	11.39	9414	12.22	9462	10.92	9510	11.67
9367	12.08	9415	11.93	9463	11.00	9511	10.59
9512	10.13	9560	12.26	9608	12.17	9656	11.39
9513	8.95	9561	12.10	9609	12.22	9657	11.59
9514	12.27	9562	11.96	9610	12.32	9658	11.67
9515	11.78	9563	11.36	9611	10.96	9659	12.44
9516	11.82	9564	12.26	9612	10.87	9660	11.71
9517	11.52	9565	10.56	9613	11.67	9661	12.38

/149

/150

№	m_{pv}	№	m_{pv}	№	m_{pv}	№	m_{pv}
9518	12.21	9566	11.88	9614	11.50	9662	11.87
9519	11.97	9567	11.29	9615	12.06	9663	9.94
9520	11.83	9568	11.49	9616	11.14	9664	10.72
9521	12.22	9569	10.88	9617	11.08	9665	12.21
9522	9.32	9570	11.16	9618	11.24	9666	9.41
9523	11.76	9571	10.29	9619	10.93	9667	11.97
9524	11.78	9572	12.10	9620	11.84	9668	12.12
9525	10.93	9573	12.32	9621	10.08	9669	12.09
9526	11.91	9574	12.14	9622	10.75	9670	12.23
9527	10.25	9575	12.13	9623	11.84	9671	12.16
9528	11.52	9576	12.30	9624	11.85	9672	12.07
9529	11.09	9577	10.14	9625	12.00	9673	11.88
9530	12.30	9578	9.87	9626	11.64	9674	12.27
9531	12.37	9579	11.99	9627	11.97	9675	12.34
9532	12.25	9580	12.38	9628	12.49	9676	9.98
9533	8.90	9581	11.80	9629	12.00	9677	12.34
9534	11.88	9582	11.68	9630	11.98	9678	12.13
9535	11.40	9583	12.45	9631	11.88	9679	12.22
9536	10.64	9584	11.87	9632	11.91	9680	11.91
9537	9.48	9585	12.12	9633	11.89	9681	12.36
9538	11.82	9586	12.03	9634	11.37	9682	12.49
9539	12.02	9587	12.18	9635	11.67	9683	12.38
9540	11.74	9588	11.05	9636	12.12	9684	12.34
9541	11.95	9589	12.25	9637	12.45	9685	10.97
9542	11.85	9590	11.59	9638	12.40	9686	12.46
9543	11.10	9591	9.50	9639	11.10	9687	11.74
9544	12.18	9592	11.49	9640	12.24	9688	11.44
9545	11.59	9593	11.56	9641	8.79	9689	12.37
9546	12.10	9594	12.27	9642	12.00	9690	12.49
9547	11.77	9595	11.69	9643	12.35	9691	12.33
9548	11.02	9596	11.28	9644	10.33	9692	12.37
9549	12.10	9597	12.38	9645	12.34	9693	11.30
9550	12.32	9598	11.23	9646	11.74	9694	12.41
9551	12.06	9599	12.19	9647	11.87	9695	11.88
9552	12.25	9600	12.09	9648	12.13	9696	11.40
9553	12.01	9601	12.37	9649	12.40	9697	12.00
9554	12.19	9602	12.12	9650	12.09	9698	12.51
9555	12.33	9603	12.32	9651	12.28	9699	11.32
9556	12.30	9604	10.28	9652	12.12	9700	10.70
9557	11.97	9605	12.18	9653	12.35	9701	12.36
9558	11.69	9606	12.34	9654	12.08	9702	9.98
9559	12.34	9607	11.90	9655	12.45	9703	10.95
9704	11.52	9752	11.26	9800	12.33	9848	11.52
9705	12.50	9753	12.27	9801	11.67	9849	12.31
9706	11.74	9754	11.64	9802	11.31	9850	10.68
9707	12.06	9755	8.72	9803	10.95	9851	11.62
9708	11.72	9756	11.96	9804	12.25	9852	12.05
9709	12.20	9757	12.41	9805	12.37	9853	12.24
9710	11.82	9758	11.47	9806	11.41	9854	12.32
9711	12.31	9759	10.30	9807	11.00	9855	11.82
9712	12.30	9760	12.22	9808	11.24	9856	11.85
9713	11.40	9761	11.24	9809	10.24	9857	12.10
9714	12.45	9762	10.84	9810	10.42	9858	11.80
9715	12.23	9763	10.98	9811	12.10	9859	11.02
9716	11.49	9764	12.22	9812	12.17	9860	11.81
9717	10.57	9765	12.20	9813	11.90	9862	12.19
9718	12.31	9766	12.14	9814	10.97	9863	12.03
9719	10.09	9767	12.34	9815	12.12	9864	12.06
9720	11.75	9768	10.58	9816	11.34	9865	12.26
9721	11.64	9769	12.10	9817	9.36	9866	11.91
9722	11.21	9770	12.40	9818	12.31	9867	10.52
9723	11.80	9771	11.25	9819	12.07	9868	11.93

/151

№	m_{pv}	№	m_{pv}	№	m_{pv}	№	m_{pv}
9724	12.46	9772	11.02	9820	10.58	9869	12.22
9725	12.25	9773	12.15	9821	11.87	9870	12.14
9726	9.93	9774	11.19	9822	10.78	9871	12.11
9727	11.74	9775	9.14	9823	11.81	9872	9.64
9728	12.11	9776	12.30	9824	12.59	9873	9.18
9729	9.58	9777	11.58	9825	12.22	9874	9.05
9730	11.92	9778	11.93	9826	11.24	9875	12.30
9731	12.32	9779	8.84	9827	12.04	9876	10.60
9732	11.15	9780	11.28	9828	12.35	9877	12.17
9733	9.30	9781	11.55	9829	12.36	9878	9.89
9734	10.21	9782	12.32	9830	10.23	9879	11.73
9735	11.96	9783	12.14	9831	12.14	9880	11.01
9736	12.27	9784	12.30	9832	11.79	9881	12.08
9737	11.99	9785	11.14	9833	12.21	9882	9.56
9738	9.58	9786	9.12	9834	11.92	9883	11.11
9739	12.00	9787	9.08	9835	12.19	9884	11.23
9740	12.46	9788	11.95	9836	12.12	9885	10.76
9741	12.06	9789	11.55	9837	12.02	9886	11.10
9742	12.36	9790	10.55	9838	12.37	9887	12.09
9743	10.46	9791	12.02	9839	12.08	9888	12.14
9744	11.85	9792	12.16	9840	11.40	9889	12.20
9745	12.15	9793	12.19	9841	11.29	9890	10.52
9746	12.03	9794	11.47	9842	12.25	9891	10.65
9747	11.27	9795	11.45	9843	12.27	9892	10.29
9748	12.32	9796	10.00	9844	9.51	9893	11.40
9749	11.61	9797	11.81	9845	10.46	9894	12.32
9750	12.36	9798	10.22	9846	11.16	9895	12.41
9751	12.32	9799	11.89	9847	12.30	9896	9.50
9897	12.14	9945	11.07	9993	11.44	10041	11.42
9898	10.35	9946	12.27	9994	11.64	10042	12.13
9899	12.37	9947	12.24	9995	11.17	10043	12.19
9900	12.22	9948	11.59	9996	12.19	10044	12.03
9901	12.20	9949	11.24	9997	12.27	10045	12.28
9902	12.30	9950	12.24	9998	11.52	10046	11.09
9903	10.85	9951	12.27	9999	11.94	10047	11.18
9904	12.44	9952	12.08	10000	10.21	10048	11.98
9905	11.56	9953	11.71	10001	11.94	10049	12.19
9906	10.79	9954	10.20	10002	12.26	10050	10.81
9907	12.08	9955	12.06	10003	11.89	10051	10.80
9908	11.24	9956	11.99	10004	11.98	10052	12.25
9909	11.26	9957	11.48	10005	12.08	10053	11.57
9910	11.94	9958	12.05	10006	11.86	10054	12.17
9911	11.89	9959	12.14	10007	12.10	10055	11.99
9912	11.54	9960	11.07	10008	12.37	10056	12.36
9913	10.53	9961	12.23	10009	12.25	10057	12.10
9914	10.93	9962	11.04	10010	12.27	10058	11.77
9915	11.41	9963	12.32	10011	12.46	10059	12.00
9916	11.59	9964	11.54	10012	12.21	10060	9.83
9917	11.57	9965	12.29	10013	11.88	10061	12.16
9918	11.89	9966	11.52	10014	12.12	10062	11.10
9919	12.10	9967	11.88	10015	10.10	10063	11.85
9920	11.25	9968	10.34	10016	10.90	10064	11.37
9921	12.02	9969	11.87	10017	11.79	10065	10.99
9922	11.05	9970	11.84	10018	12.17	10066	11.43
9923	10.88	9971	11.35	10019	10.51	10067	12.06
9924	10.96	9972	11.05	10020	11.25	10068	11.70
9925	12.00	9973	12.17	10021	11.79	10069	11.67
9926	12.00	9974	12.29	10022	12.12	10070	12.22
9927	11.64	9975	12.20	10023	9.71	10071	11.60
9928	12.21	9976	12.16	10024	9.53	10072	11.57
9929	12.62	9977	11.96	10025	11.69	10073	12.19
9930	11.81	9978	11.44	10026	12.33	10074	9.52

/152

№	m_{pv}	№	m_{pv}	№	m_{pv}	№	m_{pv}
9931	12.29	9979	12.24	10027	11.63	10075	12.40
9932	12.20	9980	12.24	10028	12.29	10076	11.83
9933	10.23	9981	12.24	10029	12.17	10077	12.13
9934	11.20	9982	11.46	10030	10.93	10078	12.26
9935	12.29	9983	11.64	10031	12.16	10079	10.50
9936	10.85	9984	11.09	10032	11.92	10080	11.49
9937	11.27	9985	12.08	10033	11.89	10081	11.96
9938	12.29	9986	12.22	10034	10.73	10082	9.86
9939	11.98	9987	12.12	10035	10.34	10083	9.86
9940	12.28	9988	11.06	10036	11.97	10084	11.35
9941	11.10	9989	11.55	10037	12.36	10085	11.59
9942	11.30	9990	12.07	10038	12.00	10086	10.55
9943	12.06	9991	12.08	10039	9.72	10087	12.32
9944	11.62	9992	11.56	10040	12.24	10088	11.20
10089	12.16	10137	12.12	10185	12.21	10233	10.08
10090	10.34	10138	11.95	10186	12.44	10234	11.35
10091	11.68	10139	11.84	10187	12.32	10235	12.16
10092	10.28	10140	9.99	10188	11.11	10236	12.26
10093	8.84	10141	12.32	10189	9.15	10237	12.00
10094	11.93	10142	10.83	10190	12.19	10238	12.37
10095	12.13	10143	11.87	10191	12.18	10239	12.23
10096	11.04	10144	12.17	10192	10.38	10240	10.45
10097	11.99	10145	12.25	10193	10.05	10241	11.96
10098	10.76	10146	11.81	10194	12.12	10242	12.38
10099	12.45	10147	12.37	10195	11.51	10243	12.06
10100	12.20	10148	11.55	10196	12.26	10244	12.00
10101	11.88	10149	10.17	10197	10.94	10245	11.23
10102	12.30	10150	9.88	10198	9.48	10246	10.46
10103	12.16	10151	11.62	10199	12.12	10247	12.10
10104	12.03	10152	11.20	10200	10.85	10248	10.66
10105	11.96	10153	12.12	10201	12.14	10249	11.93
10106	12.16	10154	12.14	10202	12.24	10250	11.13
10107	11.15	10155	12.24	10203	11.58	10251	11.89
10108	12.03	10156	12.16	10204	12.25	10252	11.26
10109	11.44	10157	12.34	10205	11.01	10253	12.34
10110	12.29	10158	12.09	10206	11.55	10254	11.47
10111	11.46	10159	11.62	10207	11.71	10255	11.81
10112	10.14	10160	11.37	10208	12.13	10256	11.49
10113	12.00	10161	12.41	10209	10.50	10257	11.04
10114	9.61	10162	11.87	10210	12.27	10258	10.67
10115	11.90	10163	11.41	10211	10.94	10259	10.73
10116	12.40	10164	12.12	10212	12.10	10260	11.77
10117	12.38	10165	12.10	10213	11.61	10261	12.51
10118	11.24	10166	11.30	10214	11.35	10262	12.26
10119	12.07	10167	12.34	10215	11.66	10263	10.54
10120	10.26	10168	11.62	10216	12.17	10264	9.73
10121	11.81	10169	12.40	10217	12.31	10265	11.50
10122	11.89	10170	11.82	10218	11.56	10266	11.11
10123	10.24	10171	12.19	10219	12.14	10267	11.23
10124	12.20	10172	12.19	10220	11.96	10268	12.04
10125	12.21	10173	12.04	10221	11.44	10269	12.05
10126	11.63	10174	12.26	10222	10.73	10270	12.09
10127	11.43	10175	11.50	10223	10.25	10271	12.30
10128	12.07	10176	11.69	10224	12.09	10272	12.29
10129	9.98	10177	12.12	10225	11.77	10273	11.65
10130	11.74	10178	12.26	10226	11.38	10274	12.36
10131	11.73	10179	12.18	10227	10.98	10275	9.71
10132	11.85	10180	12.52	10228	11.88	10276	10.70
10133	11.43	10181	12.18	10229	12.27	10277	12.07
10134	12.12	10182	12.05	10230	12.04	10278	11.45
10135	11.52	10183	11.74	10231	10.77	10279	12.34
10136	11.59	10184	11.89	10232	11.59	10280	11.74

/153

№	m_{pv}	№	m_{pv}	№	m_{pv}	№	m_{pv}
10281	11.56	10323	11.53	10365	11.98	10407	10.30
10282	9.30	10324	11.43	10366	12.14	10408	11.28
10283	11.56	10325	9.70	10367	12.44	10409	10.80
10284	11.59	10326	12.22	10368	11.86	10410	8.97
10285	11.10	10327	11.34	10369	12.24	10411	12.13
10286	11.93	10328	11.25	10370	12.26	10412	12.33
10287	9.06	10329	12.16	10371	11.85	10413	12.03
10288	12.37	10330	11.81	10372	11.02	10414	12.14
10289	10.10	10331	11.52	10373	11.78	10415	10.64
10290	12.15	10332	12.08	10374	12.08	10416	12.22
10291	12.04	10333	11.93	10375	11.15	10417	10.14
10292	12.29	10334	10.71	10376	11.67	10418	12.28
10293	12.05	10335	11.85	10377	11.87	10419	12.09
10294	12.03	10336	11.99	10378	12.24	10420	9.27
10295	12.33	10337	12.20	10379	12.08	10421	11.69
10296	11.43	10338	10.86	10380	10.99	10422	11.55
10297	11.92	10339	12.14	10381	10.51	10423	10.12
10298	11.46	10340	12.30	10382	11.47	10424	9.54
10299	12.14	10341	11.96	10383	12.10	10425	12.03
10300	11.74	10342	12.27	10384	11.71	10426	11.87
10301	11.55	10343	8.95	10385	11.00	10427	11.88
10302	11.16	10344	11.45	10386	9.47	10428	11.12
10303	9.88	10345	11.60	10387	12.22	10429	12.09
10304	9.97	10346	10.79	10388	12.48	10430	11.02
10305	12.36	10347	11.56	10389	11.47	10431	12.00
10306	10.63	10348	12.09	10390	12.16	10432	9.74
10307	12.15	10349	12.47	10391	11.91	10433	9.90
10308	11.83	10350	12.17	10392	10.49	10434	11.77
10309	11.64	10351	12.23	10393	12.09	10435	11.92
10310	12.41	10352	9.10	10394	12.18	10436	10.44
10311	12.13	10353	9.46	10395	11.53	10437	12.05
10312	10.95	10354	11.41	10396	11.81	10438	12.10
10313	11.41	10355	11.41	10397	10.86	10439	10.96
10314	12.34	10356	12.09	10398	11.66	10440	11.77
10315	11.40	10357	12.33	10399	12.08	10441	11.75
10316	11.23	10358	12.32	10400	12.30	10442	12.06
10317	12.03	10359	12.32	10401	11.61	10443	12.26
10318	10.64	10360	12.36	10402	12.42	10444	11.04
10319	11.24	10361	12.34	10403	11.90	10445	12.33
10320	11.09	10362	12.25	10404	9.74	10446	12.07
10321	12.19	10363	11.24	10405	12.15	10447	11.73
10322	11.94	10364	12.22	10406	11.64	10448	10.83

/154

REFERENCES

1. Gordeladze, Sh.G. Izvestiya Glavnoy Astronomicheskoy Observatorii (GAO), AN USSR, 1, 2, 1956. /155
2. Voroshilov, V.I., et. al. Katalog Fotograficheskikh, fotovizual'nykh i fotokrasnykh velichin 22,000 zvezd (Catalogue of Photographic, Photovisual and Photored magnitudes of 22,000 Stars). Izdatel'stvo AN USSR, Kiev, 1962.
3. Publ. of the US Naval Obs. Washington, 7, 17, 1961.

SPATIAL DISTRIBUTION OF STARS IN THE REGION WITH CENTER ($\alpha = 18^h50^m$, $\delta = +5°$)

V. I. Voroshilov

The paper deals with the structure of the Milky Way in the direction of the Sagittarius spiral arm and with the relation between the distribution of stars of different spectral types and the distribution of dust and neutral hydrogen. All the O-B2 type stars detected are located in a region with a very low density of absorbing matter and neutral hydrogen. The B8-A5 and gF8-K5 type stars tend to group in the region of dust clouds. For F and G dwarfs, this tendency is slight.

The study of star distribution in a direction perpendicular to the galactic plane shows that the density maxima of O, B and A stars and late giants do not coincide with this plane.

The paper gives a partial picture of the structure of the Sagittarius spiral arm in Aquila. In order to obtain a more complete picture, observations of stars to 16^m in the region of the galactic equator and southern latitudes are necessary.

The present work is a continuation of (Ref. 1 - 3) and deals with the /156
study of the structure of the Milky Way in the constellation of Aquila. About 1700 stars from the Catalog (Ref. 1) up to $12^m.5$ with known spectral classes have been used to study the interstellar absorption in this region. This made it possible to determine true distance of these stars, and to study their distribution in space. The region selected encompasses about 30 square degrees. Table 1 presents data on the distribution of stars according to their spectral classes, and the distance limits within which stars of a given spectral class can be calculated to a sufficient degree. Giants of late spectral classes were divided essentially on the basis of their large color excesses. Such a division [see, for instance (Ref. 5)] is considered sufficiently reliable.

Distance moduli of 89 bright stars, for which photographic magnitudes /157
were lacking, have been determined from photovisual magnitudes available -- after taking absorption into account -- and also from photographic magnitudes taken from AGK2. The results, obtained by both methods, coincide within the limits of error. The spectra of some bright stars were also taken from AGK2.

Structural Characteristics of the Region

The apparent distribution of stars over the region being studied is determined by both real variations in star density and the distribution of the

TABLE 1

Sp	r_{limit}							n
	I	II	III	IV	V	VI	average	
O—B2	2300	2200	2500	1700	2100	2300	2200	58
B5	1300	1700	1400	1100	1300	1200	1300	45
B8—AO	800	1100	950	690	830	880	850	294
A2—A5	700	800	660	670	730	640	700	163
FO—F5	360	400	400	370	380	420	380	180
dF8—G2	280	300	280	260	250	280	270	476
dG5	200	200	200	200	200	200	200	125
gF8—K5	800	1100	970	700	890	800	850	179

absorbing matter. In Table 2, we present schematically the apparent distribution of stars (the number of stars from a given spectral interval per square degree). It may be seen that the density of early-type stars increases somewhat toward the periphery of the region. This appears to be a consequence of the distribution of the absorbing clouds and the characteristics of the stellar distribution of stars as a function of the distance from the galactic plane.

In (Ref. 3) it was ascertained that the densest and closest clouds are concentrated in the region of the galactic equator within $\pm 2°.5$ of the galactic latitude. Here, the absorbing matter begins at a distance of 110-120 parsecs, and extends to 1000 parsecs, filling almost all the space between the spiral arms of Sagittarius and Carina-Cygnus. At higher latitudes, the absorbing matter begins at a distance of 160-170 parsecs, and extends to a distance greater than 2000 parsecs. Below the galactic plane, for $b < -2°.5$, the absorbing clouds extend to 1000 parsecs, and beyond that point a practically completely transparent region begins. At a still higher negative galactic latitude, in a section close to the region under investigation ($l = 12°$, $h = -7°$), McCuskey (Ref. 13, 14) discovered an increase in absorption at a distance of up to 2500 parsecs from the Sun. This means that the absorbing matter in the region of the Sagittarius spiral arm is located at a distance of about 300 parsecs from its axis in the direction of the southern galactic pole. The lack of absorption in the region of the axis of the Sagittarius spiral arm, in the direction toward the region being investigated at distances of 1500-3000 parsecs from the Sun, has been confirmed by the investigations of I. I. Pronik (Ref. 6) and T. A. Uranova (Ref. 8). The selection of the observational material (Ref. 4, 12) cannot change this conclusion. All of the statements pertain to the region being investigated, and do not extend to the entire Sagittarius arm.

After analyzing data on the structure of the Carina-Cygnus spiral arm, /159
I. I. Pronik (Ref. 7) advanced a hypothesis which stipulated that the arm is encircled on the inside by a system of dust clouds. Its stellar component is highly developed, and predominates significantly in terms of "thickness" over the edge, which is composed of dust on its interior side. She came to the following conclusion (Ref. 6): The interstellar matter forms a connecting link between the neighboring arms of Sagittarius and Carina-Cygnus, in which early-type stars are completely absent. The results of research on the

TABLE 2

	O—B2	B5	B8—A0	A2—A5	F0—F5	dF8—G2	dG5	dG8—K	gF8—K5
+3°—+4°									
18^h40^m—44^m	—	—	4	3	8	12	7	5	3
44 —48	1	—	3	2	3	14	5	5	4
48 —52	4	1	4	5	6	11	6	6	3
52 —56	3	1	3	6	3	16	6	6	6
56 —00	—	2	10	1	2	16	3	3	2
19^h00^m—04^m	6	2	11	6	5	9	3	6	4
+4°—+5°									
18^h40^m—44^m	—	2	12	11	13	21	8	3	4
44 —48	1	2	10	2	3	12	4	8	5
48 —52	4	—	3	4	7	18	3	12	2
52 —56	1	1	6	5	8	19	5	7	4
56 —00	1	—	6	8	8	30	5	9	4
19^h00^m —04^m	2	—	8	3	5	11	4	5	3
+5°—+6°									
18^h40^m—44^m	—	2	15	11	9	19	7	8	5
44 —48	2	2	12	3	4	12	3	9	8
48 —52	2	—	5	5	5	18	3	8	4
52 —56	2	1	8	3	6	16	3	5	4
56 —00	2	1	12	6	7	20	4	8	4
19^h00^m—04^m	2	1	7	4	4	13	3	5	4
+6°—+7°									
18^h40^m—44^m	1	2	13	10	7	17	7	8	10
44 —48	3	1	14	9	6	17	3	12	13
48 —52	2	2	12	7	6	19	2	6	8
52 —56	2	2	14	3	4	15	1	4	5
56 —00	2	1	15	3	6	11	3	6	5
19^h00^m—04^m	2	3	8	4	6	13	5	5	9
+7°—+8°									
18^h40^m—44^m	2	1	8	11	8	16	8	4	14
44 —48	3	1	14	14	6	22	4	13	14
48 —52	4	4	17	7	9	20	2	8	10
52 —56	1	3	18	4	5	17	2	5	7
56 —00	—	1	11	2	5	11	4	5	6
19^h00^m—04^m	3	4	11	3	6	11	2	4	5

absorbing matter distribution in that region confirm this hypothesis. However, in order to determine the interior framing of the Sagittarius spiral arm by the absorbing matter, observations of fainter stars are needed.

On the photographs of the region being studied, the apparent density of stars varies from 75 in the region of the galactic equator to 400 stars per square degree at latitudes greater than $\pm 2°.5$. This is mainly due to stars weaker than $12^m.5$. With brighter stars, there is considerably less variation

in density.

The Distribution of Stars According to Their Distances From the Sun

Early-type stars. One feature of the distribution of the O-B2 stars in the region being studied is their complete absence between 0 and 1200 parsecs, i.e., in the region with a high density of absorbing matter. Almost all the stars of these classes may be found at distances ranging from 1200 to 3000 parsecs, where the line of sight intersects the spiral arm in Sagittarius at an angle of 45°. The density of absorbing matter is very low in this region (Ref. 3, 6, 8). A relatively low concentration of neutral hydrogen, in the range from 0.05 to 0.6 atm/cm^2, is also characteristic of the region (Ref. 15).

At present, many observational data have been accumulated indicating that the spiral arms, formed by early-type stars, do not coincide with the gaseous arm determined by radio observations. This fact is, apparently, of great cosmogonic importance, whose significance is not yet clear.

Reddish (Ref. 17), after comparing the variation of the spatial density of early-type stars ($M < -4^m.5$; spectral classes O7 - O9) with the variation in the density of neutral hydrogen in M31 -- based on the data cited in (Ref. 10) -- discovered that the star density maxima decreased in the intervals between the neighboring gas density maxima. He concluded from this that in a region /160 with an increased star density, the process of star formation had essentially ended, and little gas remained. In regions with a higher gas concentration, the critical density has not yet been reached, and there are relatively few bright stars.

In the article (Ref. 19) an investigation was made of the distribution of about 1160 O-B stars over the whole range of galactic longitudes. It was discovered that these stars are grouped in specific directions. The authors are not convinced that this effect is not caused by the selection of the observational material. According to (Ref. 15), a comparison of the distribution of O-B stars with that of neutral hydrogen shows that the voids in the distribution pattern for these stars correspond qualitatively to hydrogen arms.

Baade (Ref. 9) showed that in the M31 spiral arms, the relative number of hot stars increases with the distance from the nucleus, whereas the relative number of dust clouds decreases.

Roessiger (Ref. 18) notes that, if one assumes that the hydrogen distribution pattern given in (Ref. 15) is reliable, then the star arms are displaced toward the center of the Galaxy by 300-500 parsecs with respect to the hydrogen arms. This is especially noticeable with the external spirals. The star and hydrogen arms could not have been separated by such a distance during the existence of the hot stars -- 10^6 years. Consequently, they could not have been combined when these stars were formed. Such a conclusion contradicts the hypothesis of star formation from hydrogen, if one assumes that hydrogen was completely used up at the locations where they were formed.

From these examples, the cosmogonic importance of a further accumulation

of data on the relative distribution of hot star groups and masses of interstellar matter is clearly apparent. The data on the distribution of the O-B2 stars, obtained in the present work, agree with the results of the articles cited.

The B5 - B7 stars are found between 400 to 1500 parsecs. In this interval, our attention is drawn to a portion with an increased star density at the distance of about 1000 parsecs. Data on the distribution of early-type stars are given in Table 3. To facilitate a comparison with the data of other investigators, the spatial densities are expressed in terms of the number of stars per 1000 parsec^3.

TABLE 3

O—B2			B5					
r, pc	n	$\delta \cdot 10^4$	r, pc	n	$\delta \cdot 10^3$	r, pc	n	$\delta \cdot 10^3$
0—1200	0	0.0	400— 500	1	0.4	1000—1100	8	8.0
1200—1500	5	10.3	500— 600	1	0.4	1100—1200	4	3.3
1500—2000	14	10.5	600— 700	1	0.3	1200—1300	2	1.4
2000—2500	19	8.4	700— 800	1	0.2	1300—1400	1	0.6
2500—3000	16	5.1	800— 900	4	6.1			
3000—4000	4	0.8	900—1000	10	12.1			

The B8 - G5 stars and Late Giants. In the article (Ref. 3) the region being investigated is divided into six portions with homogeneous absorption. In order to clarify the dependence between the distribution of the B8 - G5, gF8 - K5 stars, and that of absorbing matter, the star distribution was studied separately in each of the indicated six portions. There are no gaps between the regions in which the O - B2, B3 - B7, B8 - A0, etc., stars which may be readily observed are located. /161

The spatial densities were calculated by counting the stars in portions of space every 100 parsecs. Dispersion σ of the absolute magnitudes was taken according to (Ref. 14). To calculate it, a correction was introduced in the absolute magnitude obtained as the average for a given spectral interval (Ref. 11):

$$M_0 = \bar{M} - \frac{\sigma^2}{A(m)} \cdot \frac{dA(m)}{dm}. \qquad (1)$$

The distance of star groups and the spatial densities must be calculated by using the adjusted absolute magnitude M_0.

Table 4 gives the number of stars in the corresponding distance intervals, the densities of absorbing matter in stellar magnitudes per 1 kpc, and the spatial star densities per 1000 pc^3, as well as the total number of stars and the average densities for the whole region. The B8 - A5 stars are distributed along the line of sight in a very nonuniform manner. Figure 1 presents a diagram showing the distribution of absorbing clouds and the maxima of the spatial

TABLE 4

/162

r, pc	I			II			III			IV			V			VI			Entire Region	
	n	A_{pg}	δ	n	A_{pg}	δ	n	A_{pg}	δ	n	A_{pg}	δ	n	A_{pg}	δ	n	A_{pg}	δ	n	δ
B8—A0																				
0—100	—	0.0	—	—	0.0	—	—	0.0	—	—	0.0	—	—	0.0	—	—	0.0	—	—	—
100—200	—	3.8	—	—	0.0	—	1	4.0	0.24	—	6.8	—	—	5.8	—	—	5.0	—	1	0.05
200—300	2	3.8	0.19	1	3.8	0.23	3	4.0	0.23	4	6.8	0.53	5	5.8	0.24	—	5.5	—	15	0.30
300—400	6	16.0	0.24	4	3.6	0.48	1	0.8	0.04	3	0.4	0.20	3	0.3	0.07	1	1.0	0.18	18	0.16
400—500	—	0.5	—	3	3.6	0.36	5	0.8	0.14	4	0.4	0.16	10	0.3	0.10	2	14.4	0.22	24	0.13
500—600	1	0.5	0.02	4	3.6	0.20	12	11.9	0.22	1	0.4	0.03	12	0.3	0.12	2	0.8	0.16	32	0.12
600—700	1	0.5	0.02	3	0.8	0.11	6	0.0	0.08	15	25.4	0.30	17	6.7	0.12	4	0.8	0.21	46	0.12
700—800	8	12.6	0.07	5	0.8	0.13	5	0.0	0.05	2	25.4	0.03	42	6.7	0.23	7	4.5	0.28	69	0.13
800—900	2	12.6	0.03	2	2.6	0.04	13	8.4	0.10	—	0.8	—	41	6.7	0.17	3	4.5	0.09	59	0.09
900—1000	—	0.0	—	8	5.0	0.13	13	8.4	0.08	—	0.8	0.01	2	0.8	0.01	—	4.5	—	23	0.03
1000—1100	—	0.0	—	2	2.9	0.03	—	0.2	—	—	0.8	—	—	0.8	—	—	4.5	—	2	0.02
A2—A5																				
0—100	—	0.0	—	—	0 0	—	—	0.0	—	2	0.0	0.94	—	0.0	—	—	0.0	0.25	2	0.66
100—200	1	3.8	0.25	—	0.0	—	—	4.0	—	1	6.8	0.94	2	5.8	0.26	1	5.0	0.25	5	0.23
200—300	4	3.8	0.37	—	3.8	—	5	4.0	0.38	3	6.8	0.40	11	5.8	0.53	—	5.5	0.25	23	0.46
300—400	6	16.0	0.28	7	3.6	0.84	4	0.8	0 18	1	0.4	0.07	6	0.3	0.15	2	1.0	0.36	26	0.23
400—500	1	0.5	0.03	4	3.6	0.29	6	0.8	0.16	2	0.4	0.08	11	0.3	0.16	4	14.4	0.44	28	0.15
500—600	2	0.5	0.04	7	3.6	0.34	12	11.9	0.22	4	0.4	0.11	9	0.3	0.09	1	0.8	0.07	35	0.13
600—700	1	0.5	0.01	6	0.8	0.21	3	0.0	0.04	2	25.4	0.04	11	6.7	0.08	—	0.8	—	23	0.06
700—800	4	12.6	0.04	2	0.8	0.05	1	0.0	0.01	—	25.4	—	5	6.7	0.03	—	4.5	—	12	0.02
800—900	1	12.6	0.01	—	2.6	—	2	8.4	0.01	—	0.8	—	—	6.7	—	—	4.5	—	2	0.01

/163

F0 — F5																				
0—100	1	0.0	1.75	3	0.0	13.34	—	0.0	—	1	0.0	2.52	3	0.0	2.74	1	0.0	6.68	9	2.96
100—200	5	3.8	1.25	2	0.0	1.27	10	4.0	2.37	5	6.8	1.80	16	5.8	2.09	2	5.0	1.91	40	1.88
200—300	8	3.8	0.74	7	3.8	1.64	13	4.0	0.98	13	6.8	1.72	28	5.8	1.35	—	5.5	—	69	1.31
300—400	11	16.0	0.52	4	3.6	0.48	4	0.8	0.18	—	0.4	—	5	0.3	0.12	—	1.0	—	24	0.21
400—500	3	0.5	0.09	4	3.6	0.29	7	0.8	0.19	1	0.4	0.04	5	0.3	0 07	3	14.4	0.33	23	0.12
500—600	1	0.5	0.02	1	3.6	0.05	—	11.9	—	—	0.4	—	1	0.3	0.01	—	0.8	—	3	0.01
dF8—G2																				
0—100	9	0.0	15.75	5	0.0	22.23	1	0.0	1.66	5	0.0	12.58	9	0.0	8.22	3	0.0	20.05	32	10.53
100—200	32	3.8	8.00	14	0.0	8.89	26	4.0	6.17	25	6.8	8.99	81	5.8	10.57	14	5.0	13.37	192	9.02
200—300	48	3.8	4.42	25	3.8	5.85	57	4.0	4.31	40	6.8	5.30	81	5.8	3.89	8	5.5	2.81	259	5.23
dG5																				
0—100	6	0.0	10.50	2	0.0	8.89	—	0.0	—	1	0.0	2.52	4	0.0	3.65	—	0.0	—	13	4.28
100—200	29	3.8	7.25	16	0.0	10.16	10	4.0	2.37	9	6.8	3.24	17	5.8	2.22	3	5.0	2.86	84	3.95
200—300	1	3.8	0.92	1	3.8	0.23	5	4.0	0.38	3	6.8	0.40	3	5.8	0.14	—	5.5	—	13	0.26

(Continuation of TABLE 4)

gF8—K5

0—100	—	0.0	—	—	0.0	—	—	0.0	—	—	0.0	—	—	0.0	—	—	0.0	—	—	—
100—200	—	3.8	—	—	0.0	—	—	4.0	—	—	6.8	—	—	5.8	—	—	5.0	—	—	—
200—300	1	3.8	0.09	—	3.8	—	1	4.0	0.08	—	6.8	—	1	5.8	0.05	—	5.5	—	3	0.06
300—400	8	16.0	0.38	1	3.6	0.12	—	0.8	—	—	0.4	—	9	0.3	0.22	—	1.0	—	18	0.16
400—500	—	0.5	—	5	3.6	0.36	5	0.8	0.14	2	0.4	0.08	7	0.3	0.10	6	14.4	0.66	25	0.13
500—600	5	0.5	0.10	5	3.6	0.24	16	11.9	0.29	—	0.4	—	14	0.3	0.14	2	0.8	0.15	42	0.15
600—700	5	0.5	0.07	5	0.8	0.18	5	0.0	0.07	4	25.4	0.08	19	6.7	0.14	—	0.8	—	38	0.10
700—800	5	12.6	0.05	9	0.8	0.23	6	0.0	0.06	—	25.4	—	—	6.7	—	1	4.5	0.04	21	0.04
800—900	—	12.6	—	2	2.6	0.04	2	8.4	0.02	—	0.8	—	1	6.7	0.01	1	4.5	—	5	0.01
900—1000	—	12.6	—	2	5.0	0.03	1	8.4	0.01	—	0.8	—	—	0.8	—	—	4.5	—	3	0.01

star densities for each of the six portions. The clouds are represented by bands; the density maxima of the B8 - A0 stars -- by open circles; density maxima of the A2 - A5 stars -- by solid circles; and density maxima of the gF8 - K5 stars -- by triangles. Out of 24 density maxima of B8 - A5 stars and 8 density maxima of the gF8 - K5 stars, 20 and 6, respectively, are located in the dust clouds. The fact that the B8 - A5 and gF8 - K5 star groupings are predominantly located in dust clouds apparently cannot be considered accidental, since the latter occupy only 58% of the region being investigated. Schaefer (Ref. 20), when studying the regions $\ell = +24°$, $b = -10°$, $0°$, $+10°$, also discovered a tendency of the A0 - A44 stars and late giants to group in the dust clouds. Ramberg (Ref. 16) detected "clouds composed of dust and stars" in the region of Lacerta. According to the results of his investigation, the star density increases in dust clouds.

/164

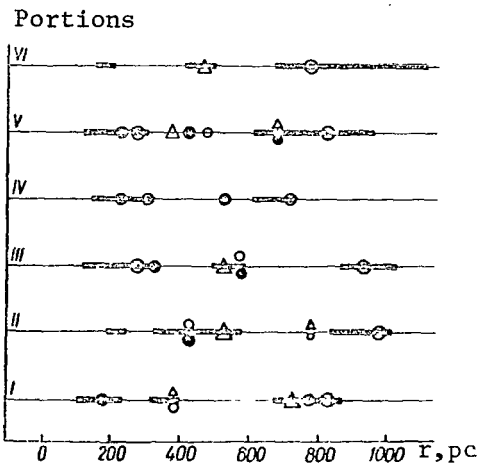

Figure 1

The tendency to group is less apparent with the F0 - G5 dwarfs (see Table 4). The dG8 - K dwarfs can be calculated completely only up to a distance not greater than 50 - 100 parsecs; therefore, one may not draw any conclusions with respect to these stars.

In the derivation and utilization of formula (1) for the computation of dispersion, it is assumed that the luminosity function is of a definite exponential form, and is applicable to the entire region under investigation. However, the fact that the tendency to group in dust clouds is manifested to a different degree with stars of different classes may lead to a difference between the luminosity functions for a space occupied by clouds, and for a space free from absorbing matter. It is impossible to determine such a difference on the basis of the present work, since not all the star classes are accessible to observation at sufficiently large distances.

Distribution of Stars According to Their Distances From the Plane of the Galactic Equator

In studies on the distribution of stars according to their distances from the symmetry plane of the Galaxy, the stars have been calculated over definite areas in space every 5 parsecs of the distance from this plane. The distance of the Sun from it, z_0, was taken as 13.5 pc. Dispersion of the absolute magnitude was taken into account according to (Ref. 14). Calculation of dispersion is equivalent to a certain change in the distance of a star group from the equatorial plane. The corrected distance z is related to the distance not corrected, z' by the formula

$$\lg(z-z_0)=\lg(z'-z_0)+\frac{\sigma^2}{10.86}\cdot\frac{z'-z_0}{A(z')}\cdot\frac{dA(z')}{dz'}. \qquad (2)$$ /165

Figures 2 - 4 show the results derived from calculating density as a function of the z-coordinate for stars of various spectral classes (in Figure 3: •—• -- B8 - A0, o—o -- A2 - A5, ×—× -- gF8 - K5)

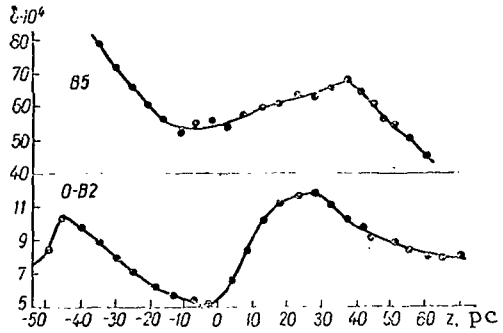

Figure 2

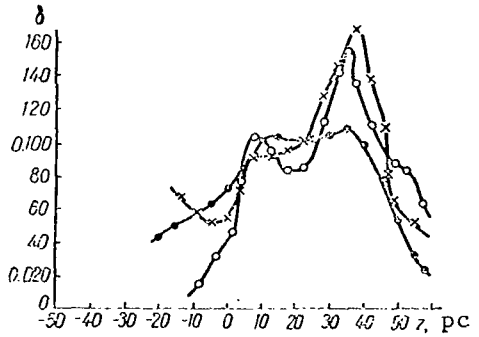

Figure 3

The quantitiy z is plotted along the abscissa in parsecs; along the ordinate -- the densities, in the number of stars per 1000 pc^3. For the O - B5 stars, there are two density maxima: at the distance 40 - 50 pc south, and 30 - 40 pc north, of the equatorial plane. At z = 0 there is a density minimum. This may be a consequence of both a real grouping of these stars, and the fact that in the region of the equator there is a concentration of the densest absorbing /166 clouds. In the latter case, one may assume that at low galactic latitudes, the O - B5 stars were not taken completely into account. In the case of observations with more powerful instruments, this minimum may be filled by fainter stars.

For the B8 - A5 stars and late giants, there are density maxima at the distance of 35 - 40 pc north from the galactic plane. In both directions away from this point, the density increases. We could not determine whether there is a density maximum south of the equatorial plane for these stars, since the B8 - A5 stars with z = -35 pc and more do not occur in the region being investigated.

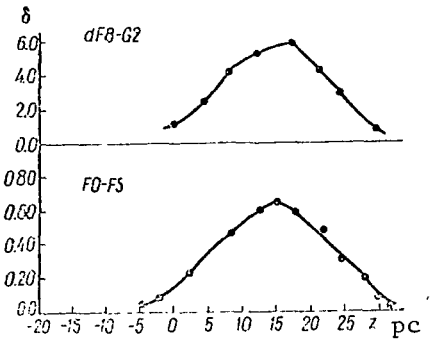

Figure 4

For the dwarfs of the F and G classes, the density maximum is at the distance z = +15 pc. Obviously, the distribution of stars of these classes differs from the distribution of earlier type stars of the main sequence and that of the late giants.

* * *

The study of the spatial distribution of stars in the region $\alpha = 18^h50^m$, $\delta = +5°$ makes it possible to draw the following conclusions:

1. The early-type O - B2 stars are found at distances of 1200 - 3000 pc. The spiral arm of Satittarius passes at that distance. Absorbing matter at these distances is practically absent.

2. B8 - A5 stars and late giants are traced to a distance of 800 - 900 pc. They exhibit a tendency to group in dust clouds. Apparently, the latter are directly connected with the portions of a stellar field having an increased density.

3. For F and G dwarfs, the tendence to group is only slightly manifested.

4. The regions of the maximum star density do not coincide with the plane of the galactic equator. For O - B5 stars the density maxima are located at the distances z = +35 pc and z = -45 pc. For B8 - A5 stars and late giants, the density maximum is at the distance z = + 35 pc. We did not succeed in /167
discovering a second maximum for these stars, since stars of these classes with z = -30 pc and more do not occur in the region under investigation.

There is a density maximum for FO - G2 dwarfs at the distance z = +15 pc. Apparently, the spatial distribution of these stars differs from the distribution of earlier type stars of the main sequence and late giants.

5. The results obtained give a preliminary idea of the structure of the Sagittarius spiral arm, and a portion of the neighboring section in the region under investigation. In order to obtain a more complete picture, additional observations of 15 - 16^m stars in the region of the galactic equator and negative galactic latitudes are necessary.

REFERENCES

1. Voroshilov, V. I. et al. Katalog fotograficheskikh, fotovizual'nykh i fotokrasnykh velichin 22 000 zvezd (Catalog of Photographic, Photovisual, and Photored Magnitudes of 22,000 Stars). Izdatel'stvo AN USSR, Kiev, 1962.

2. Voroshilov, V. I. Izvestiya Glavnoy Astronomicheskoy Observatorii (GAO), AN USSR, 4, 2, 1962.
3. Voroshilov, V. I. Izvestiya GAO, AN USSR, 5, 1, 1963.
4. Zonn, V. Astronomicheskiy Zhurnal (A Zh), 33, 855, 1956.
5. Pronik, I. I. Izvestiya Krimskoy Astrofizicheskoy Observatorii (KAO), 23, 1960.
6. Pronik, I. I. Izvestiya KAO, 25, 1961.
7. Pronik, I. I. A Zh, 39, 362, 1962.
8. Uranova, T. A. A Zh, 36, 740, 1959.
9. Baade, W. Mitt. der Astron. Ges., 1955, 51, 1956.
10. Van der Berg, S. P.A.S.P., 70, 109, 1956.
11. Bok, B. J. The Distribution of the Stars in Space. Chicago, 1937.
12. Eklöf, O. Arkiv für Astronomi, 2, 3, 213, 1959.
13. Mc Cuskey, S. W., Seyfert, C. K. Aph. J., 106, 1, 1947.
14. Mc Cuskey, S. W. Aph. J., 123, 458, 1956.
15. Oort, J. H., Kerr, F. T., Westerhout, G. Monthly Not. Roy. Astr. Soc., 118, 4, 379, 1958.
16. Ramberg, J. Stockholm Observ. Ann., 20, 1, 1957.
17. Reddish, V. C. The Observ., 82, 926, 14, 1962.
18. Rössiger, S. Die Sterne, 9-10, 174, 1962.
19. Rubin, V. C. et al. A. J., 67, 8, 1962.
20. Schäfer, H. Veröff der Univ. Sternw. zu Bonn, 58, 1960.

THE MILKY WAY IN THE CONSTELLATION AQUILA

G. L. Fedorchenko

In the article the results are given of a study of the Milky Way in the Rift. The study was performed on the basis of magnitudes and spectra of stars up to $12^m.0$-$12^m.5$. The results of other investigations are used. The author discusses the special features of dust and stellar components, their connection with one another and with neutral hydrogen.

The link, consisting of early-type stars and dust clouds between the Carina-Cygnus and Sagittarius arms, is absent in longitudes -- 340°-20°, which is the main feature of the investigated galactic region.

Some considerations are given as to the position of the Sagittarius arm in the Northern sky.

This article summarizes the work performed by the author, which investigates the galactic structure on the basis of the photometric data and spectra of stars up to 12.0-$12^m.5$. The investigation by the author of the dust and stellar components in the "fork" of the Milky Way made it possible to form a concept of the structural characteristics of the region of the Galaxy, corresponding to longitudes 12-22°. Moreover, on the basis of the data obtained and the results of other investigations of a similar character in the neighboring regions, we may study the structure of a more extensive region in the internal section of the Galaxy. /169

The principal features of the galactic region being studied are the following:

1. The directions 12-22° at short distances (up to 1500-2000 pc) intersect the space between the spiral arms in Carina-Cygnus and Sagittarius.

2. At longer distances (up to 8000 pc) these directions pass through the interior of the hydrogen arm in Sagittarius.

3. The region being investigated is located in the "fork" in the Milky Way, which is formed by dust clouds situated at short distances from each other.

4. The longitudinal region 12-22° is a region "which is avoided by" the objects of stellar Population I (O and B stars, galactic star clusters, and stellar associations). This fact is used in determining the northern boundary of the Sagittarius arm.

Until very recently, the galactic structure in the directions indicated

has hardly been investigated. Our aim was to investigate in detail the distribution of dust matter and the stellar components. This would allow us to determine the structure of the Galaxy between the arms in Carina-Cygnus and Sagittarius, to explain the apparent pattern of star distribution, and to obtain additional data on the structure of the Sagittarius arm. /170

Dust Component

The pattern of the distribution of dust was obtained on the basis of interstellar absorption in the four regions -- A, B, C, and D -- whose arrangement is shown in Figure 1.

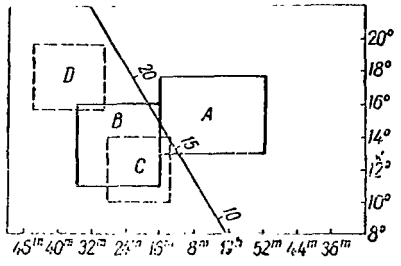

Figure 1

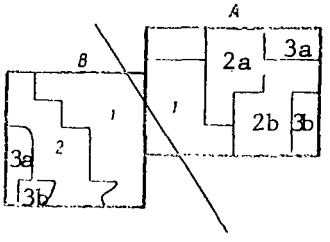

Figure 2

Absorption in Regions A and B. The factual information, procedure and results of the study of the interstellar absorption in regions A and B, are contained in (Ref. 2, 7-10). We have made use of the average pattern of absorption in these regions. The corresponding portions with the same absorption are shown in Figure 2; the absorption curves for them are shown in Figure 3.

Absorption in Regions C and D. The regions C and D have been investigated by the Polish astronomers (the observatory in Toruń) G. Iwaniszewski (Ref. 16) and C. Iwaniszewska (Ref. 15). At first, we planned to take advantage of these authors' results when studying the structure of the "fork" in the Milky Way, because their regions are adjacent to our A and B regions, and they partially overlap. However, a comparison of our absorption curves with those from Toruń revealed that they differ considerably. This was discovered, for instance, in comparing the color excess curves in the regions II and III of G. Iwaniszewski with the curve especially calculated from our data for the overlapping portions (Figure 4). The differences in the excesses amounted to $0^m.25$, which amounts to $1^m.0$ in absorption. The curves for portion ξ of C. Iwaniszewska's region and portion 1 of our B region also differ considerably. /171

We attempted to find the reason for the discrepancies described, and discovered that there were systematic errors in the photometric series of C. Iwaniszewska and G. Iwaniszewski. Nevertheless, in order to obtain reliable data on the absorption in the regions indicated, we investigated the absorption in them, making use of the initial data only -- magnitudes and spectra -- from (Ref. 15) and (Ref. 16).

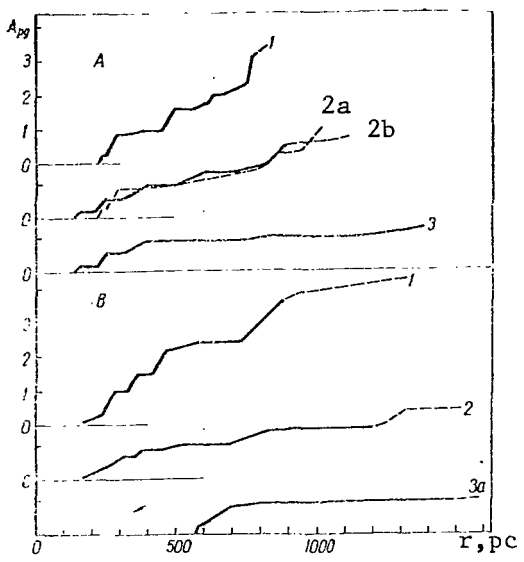

Figure 3

First of all, we compared the spectra and magnitudes in the regions C and D with other determinations. It follows from the comparison of the spectral estimates with the estimates of the HD catalog that in the Toruń spectral classification there are no noticeable systematic errors. The best agreement between the classifications may be noted for the B8 - A2 stars. /172

The situation is different in the case of stellar magnitudes. Thus, the comparison of G. Iwaniszewski and G. Iwaniszewska's photographic magnitudes with ours in the B region (Figure 5, a, dots) reveals substantial discrepancies. In all likelihood, the reason for this is the fact that in the magnitudes, obtained by relating the stars to the KSA 87 Region, C. Iwaniszewska and G. Iwaniszewski introduced incorrect corrections for the reduction to the system of the Northern polar series. This is confirmed by the good agreement between the initial, uncorrected photographic magnitudes from the catalogs in question (Ref. 13), and our determinations (Figure 5, a, crosses).

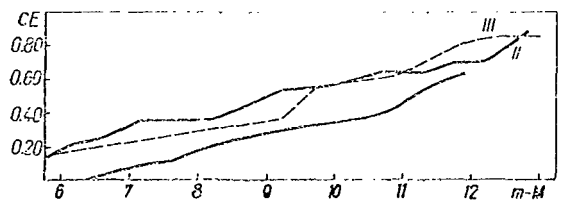

Figure 4

When comparing the photovisual magnitudes from the Toruń catalog with our determinations in the B regions, discrepancies were also found, although they were somewhat smaller than those for the photographic magnitudes (Figure 5b).

To make the corrections to the stellar magnitudes in the C and D regions more precise, we studied the dependence of the color indices on the brightness for the non-reddened stars of a definite subclass. As a result, for the C region (of G. Iwaniszewski) we did not discover any noticeable error in the color index scale in the photographic magnitude interval from 10 to 13^m. The error in the null points of the indices was $0^m.20$. In the photographic magnitudes of G. Iwaniszewski (see Figure 5), however, one should introduce a correction for the null point, equal to $0^m.50$. For the D region (of /173

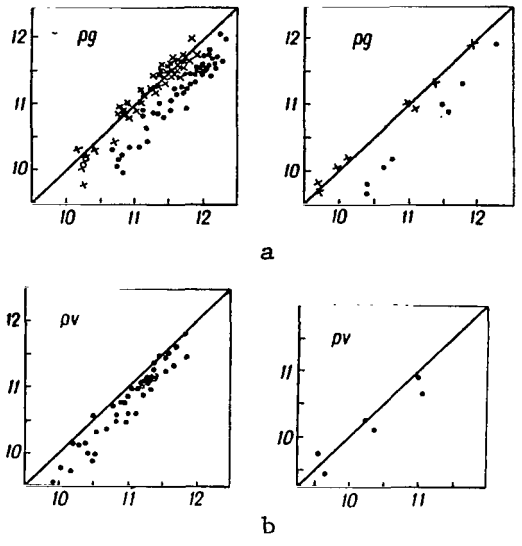

Figure 5

C. Iwaniszewska) it has been established that, in the case of the photographic magnitudes which were not corrected by C. Iwaniszewska for the null point and the scale (Ref. 13), an error in the color exponent scale was found only for the stars with $m_{pg} < 9^m.5$, and the error in the null point was equal to $-0^m.14$.

After introducing the corrections indicated, we employed the normal Allen index. For greater reliability, the absorption was calculated from the B8-A2 stars, whose spectra are the most precise.

The division (division into portions with identical absorption) of the C and D regions was based on the form of the color excess curves versus distance modulus curves. The division proved to be entirely different from the one obtained by the Toruń astronomers. Figure 6 shows both versions of the division (heavy line denotes our version). This difference may serve as still another proof that the division based on the form of the Milky Way is unacceptable.

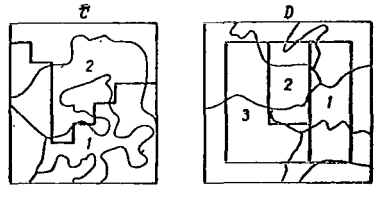

Figure 6

The results derived from studying the behavior of CE with m - M, in separate portions of the C and D regions, are presented in Figure 7. The total absorption curves, calculated for $\gamma = 4$, are given in Figure 8.

We then compared the absorption curves in the adjacent and overlapping portions of the A, B, C, and D regions. In Figure 9a, we compare the color

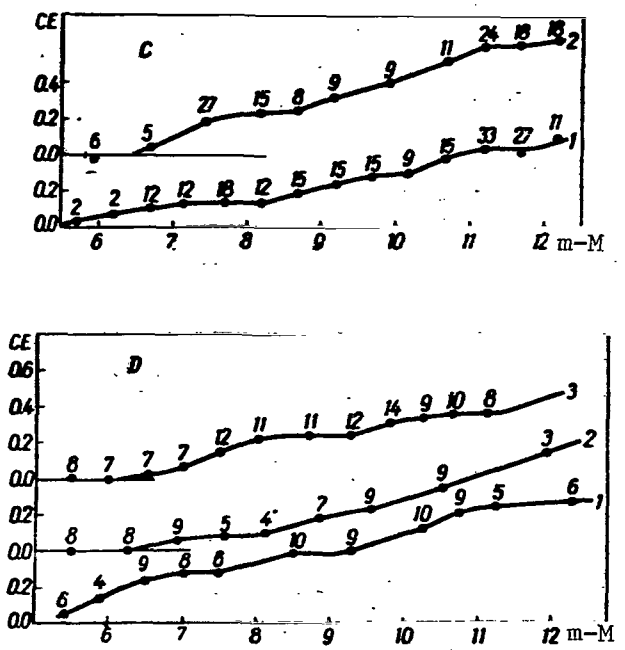

Figure 7

excess curves for portion 1 of Region A and portion 1 of region B. The magnitudes of the absorption in these portions, which are contiguous to the galactic equator, are almost identical. In Figure 9b, we compare the absorption curves for portion 2 of region C and portion 1 of region B. The curves in these overlapping portions coincide very well. In Figure 9c, portion 3 of region D and portion 2 of region B are compared. The difference in the nature of the absorption is somewhat more noticeable than in Figure 9b. /174

Therefore, one may assume that the results derived from analyzing the regions under investigation agree quite well.

Discussion of the results obtained by studying absorption in the Milky Way "fork". The following items were employed in the analysis of absorption in the Milky Way "fork": the author's studies of the A, B, C, and D regions, the investigation by S. McCuskey in the LF regions (Refs. 17, 18), data on the interstellar absorption, obtained by H. Weaver (Ref. 20) for the direction $l = 10^{\circ}$, the results of the study by I. I. Pronik (Ref. 5) for the direction $l = 343^{\circ}$, V.I. Voroshilov's investigation (Ref. 3) for the direction $l = 5^{\circ}$, and the study by S. Apriamashvili in two regions for the directions $l = 356$ and $4^{\circ}.5$ (Ref. 1).

As a result of the investigation of the A, B, C, D regions, we established /175 the fact that absorption is anomalously high at longitudes 12-22°. In these directions, we discovered absorption with a coefficient of $2.5\text{-}4^{m}.0$ per kpc within the nearest kiloparsec. It is interesting to note that nowhere in the

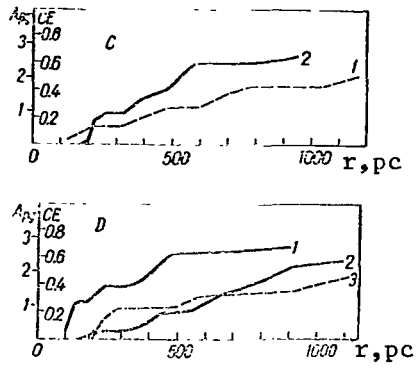

Figure 8

northern portion of the Milky Way is there such strong absorption at short distances as at longitudes 340-25°. Thus, according to the data by S. McCuskey (Ref. 18), the maximum absorption in the longitudinal range 33-182° amounts to $2^m.3$ (regions LF 6), and the average absorption over all LF regions is about 1^m.

Since the regions which we have investigated cover a large range of galactic latitudes (from +6 to -6°), we may examine the question of dust distribution with respect to the galactic plane. The absorption curves for the regions, situated symmetrically with respect to the galactic equator, differ considerably. Thus, below the equator, region 1 (B), corresponding to the darker portion of the "fork", is characterized by a more intensive increase in absorption up to 400 pc, than region 1 (A) above the equator. The behavior of absorption is also somewhat different in the regions with average latitudes +3.5 and -3°.5. At the same time, the distribution of the average absorption coefficients with latitude is almost symmetrical (Ref. 10).

Examining the absorption curves for the regions in question and comparing them with the curves for the region of H. Weaver (l = 10°), and that of V. I. Voroshilov (l = 5°), one can notice almost identical absorption behavior in these directions (Figure 10), in spite of the fact that the directions considerably differ from each other in longitude. The same absorption increase behavior is exhibited by the curves for regions C (portion 2) and D (intermediate curve for the entire region), and region A (portion 1). Such a phenomenon can only be explained by the fact that there is an extended cluster of dust nebulae, which is intersected by the directions indicated and which is characterized by almost identical absorption in these directions. The cluster can be positively traced from 0 to 22° longitude with a small gap around 13-14°. Absorption in the region of I. I. Pronik (l = 343°), however, is very "mottled" and, apparently, cannot be attributed to the cluster indicated. /176

As may be seen from Figure 10, the absorption begins in the cluster at a distance of 100 pc, and increases approximately up to 800-1000 pc. After this

point, the increase either comes to an end or becomes insignificant. The average characteristics of the cluster portion which are investigated are the following: longitudinal extension -- from approximately 0 to 22°; latitudinal extension -- from +2 to -3°. The cluster extends in depth up to 900 pc, and 3-4 clouds may be observed along the line of sight. The average absorption along the entire length amounts to 4^m; the absorption coefficient is 5^m per kpc.

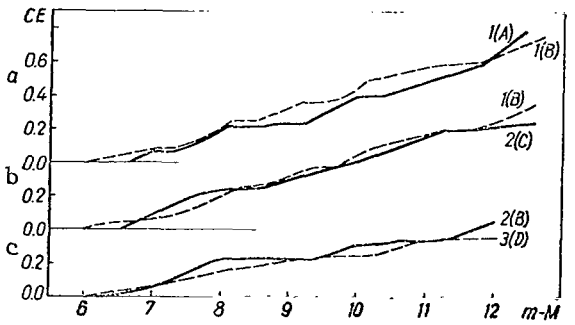

Figure 9

In his article, which investigated the luminosity function (Ref. 18), S. McCuskey made an attempt to obtain the general pattern of the absorption distribution in the galactic plane. However, S. McCuskey's regions are /177 situated at different galactic latitudes; therefore, the pattern obtained by him is not reliable. This especially pertains to region LF 1 (l = 12°, b = -7°), which is of interest to us. The material which we had at our disposal allowed us to investigate the distribution of dust over the portions whose centers lay at the same galactic latitude +3°. Moreover, this choice of latitudes made it possible to make use of S. McCuskey's data for his regions LF2 and LF3. In addition, we utilized the data obtained for our region A (portions 4, 5, 6), for the region of V. I. Voroshilov (portion 2), and I. I. Pronik's region (portions 33, 34, 39, 41, 42). The result obtained (Figure 11, dotted line denotes the distribution obtained by McCuskey) differs from S. McCuskey's result in that the absorption increase in the direction being studied is 4-5 times more intensive than in the region LF1. This is perfectly natural. Region LF1 is situated at latitude -7°, so that the line of sight corresponding to the center of the region leaves the dust layer at short distances from the Sun.

In order to obtain a more complete picture of the distribution of separate clouds in the cluster discovered, we studied the cloud distribution projected onto the galactic plane. The results are presented in Figure 12a (the cross section was compiled for the latitude interval from -1 to -1°.5). A different degree of blackness corresponds to different values of the absorption coefficient per kpc in the interior of the cloud. One can notice the existence of separate cloud groups at the average distances of 270, 520, and 800 pc. This is confirmed by Figure 12b, which represents a cross section along the meridian l = 16°, obtained from the absorption curves for only regions A and B, -- i.e., from the most homogeneous material.

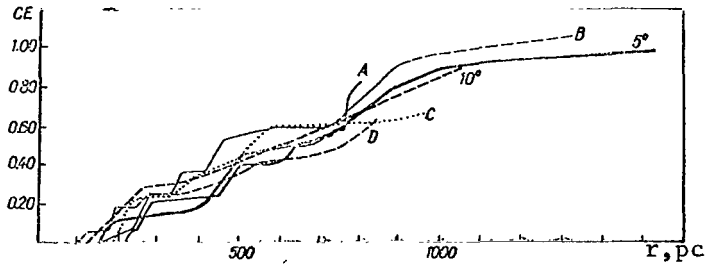

Figure 10

A detailed study of absorption in regions A and B makes it possible to estimate the dimensions of the dust clouds, and also to make certain statements /178 concerning the structure of the absorbing matter.

Some difficulties are entailed in estimating the average dimensions of the clouds; these difficulties are caused by the color excess method. As a rule, in these portions of the absorption curves which correspond to short distances,

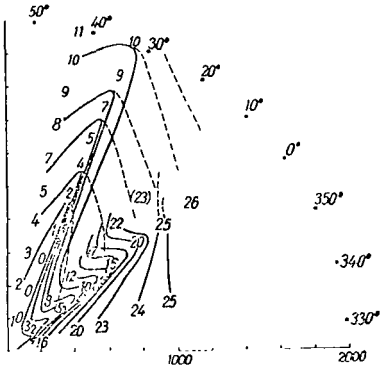

Figure 11

the clouds are comparatively small, with the horizontal portions being sharply separated. The dimensions of the clouds increase with the distance, and the sharpness of the curve details decreases. The curves often exhibit a general increase, in which it is possible to separate the individual clouds.

The phenomenon described is caused by two factors. First, the usual /179 number of stars on the basis of which a curve is plotted decreases with the distance. This fact influences the accuracy of the curve. Secondly, as a rule, the division into portions with the same absorption is performed on the basis of the Milky Way pattern (or from star counts), and the pattern of the Milky Way is in turn determined by the influence of the closest clouds (located no farther than 400 pc). In this case the division, which correctly expresses the distribution of only the closest clouds, is extrapolated to

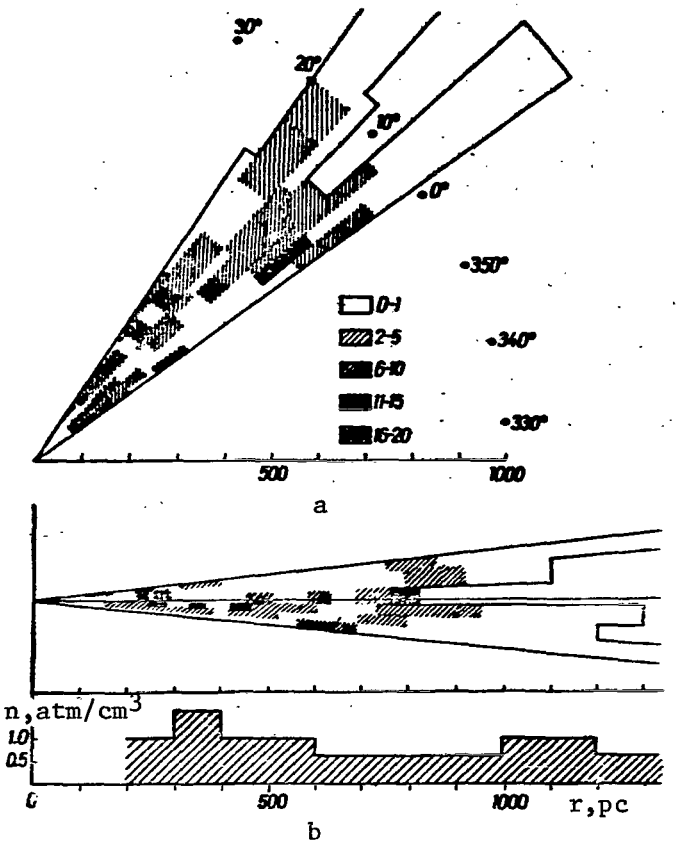

Figure 12

larger distances. Therefore, starting with a definite distance, the curves give a highly averaged, distorted absorption pattern. Under these conditions, the concept of the size of dust clouds becomes uncertain, and this clearly causes the great differences in estimates of size.

The difficulties indicated could have been overcome: First, by having at our disposal the magnitudes and spectra of weaker stars of small luminosity; secondly, by changing the division method. The former is so far unattainable, and the latter requires a special elaboration. Division into two or more stages is one of the variants we have proposed, and also applied in calculating absorption. The region under investigation was divided into equal portions (1 x 1° squares), and for each one of them the CE curve was plotted. The squares with the same CE behavior were united, and the average CE curves were plotted for the portions obtained. Starting at a distance of 300-400 pc, the process was repeated. In this way we have obtained a reliable division up to a distance of 700-800 pc, and, consequently, more reliable values of the dimensions of the dust clouds.

After analyzing the absorption curves for region A from this point of view, we have obtained the following results: the dependence of the cloud dimensions on the distance, up to 700-800 pc, is insignificant. The average diameter of a cloud, calculated from the absorption curves, is 40 pc with the average absorption coefficient 20-25^m per kiloparsec. Practically all the absorption in this distance range occurs in the clouds. This means that the structure of the dust can be more readily represented as "nebulae and voids", rather than as rarefied dust with nebulae floating in it.

As already noted, regions A and B are "prominent" in the sense that thus far, no objects of spiral population, except dust, have been observed in them. W. Becker (Ref. 11), H. Weaver (Ref. 21) and other investigators explain this phenomenon by a real absence of the objects indicated in the direction in question. On this basis, they assume that a longitude of about 350-0° represents the limit of the Sagittarius arm in the northern sky. /180

Let us assume that a high dust concentration in the Milky Way "fork" is the principal cause of "avoidance" in the 12-22° longitudinal direction. The quantitative absorption characteristics of the regions being studied allow us to verify this assumption. We shall proceed from the fact that the absorption increases up to the distance of 1000 pc, where it is equal to 4^m. Beginning at that distance, it remains unchanged or increases very slowly. Let us assume that it is unchanged. For the limiting photographic magnitude, equal to 12^m, the stars with M = -3.2 (B0-B2) should be observed in the absence of absorption up to distances corresponding to the modulus 15.2. When the absorption is taken into account, the modulus will be 11.2 (or 1700 pc). If the absorption increases after 1000 pc, this distance will be somewhat shorter.

Thus, the absence of the B0-B2 stars in the catalogs with the limiting photographic stellar magnitude up to 12^m in the "fork" of the Milky Way corresponds to their real absence up to a distance of 1700 pc. The above reasoning is even more valid for objects of lesser luminosity. Basing our considerations, for the moment, on data regarding interstellar absorption, we can explain the "avoidance" for the stars of Population I at longitudes 12-22° by a strong interstellar absorption at a comparatively large (above 1700 pc) distance from the Sagittarius arm. In order to penetrate the Sagittarius arm under these conditions, and to study it successfully, it is necessary to know the spectra and magnitudes of early type stars up to 14-15^m.

One important task is to investigate the relative distribution of dust and gas in the Galaxy. Figure 12b shows the density behavior of neutral hydrogen according to radioastronomical data for $l \approx 16°$, and the distribution of clouds of absorbing matter according to our data for regions A and B. By comparing these graphs, one cannot discover any correlation in the distribution of both components for a given direction. On the basis of this comparison, the conclusion may only be reached that, in the part of the Milky Way which is under investigation, the cluster of dust nebulae is located in a region with a high density of neutral hydrogen (0.6 -1.6 atm/cm^3).

Method of calculating stellar densities. The spectra and true moduli of stellar distances were employed as the initial data in this portion of the work. The true moduli were computed on the basis of data regarding absorption in the regions A and B. The spatial densities (D) were calculated by employing the so-called "individual" method (terminology employed by V. Zonn). This method employs a direct calculation of the volumetric cones and of the stars included within them in the corresponding distance limits. This makes it possible to calculate the stellar densities. We selected this method, because it does not necessitate any assumptions regarding the form of the luminosity function in the corresponding volume of space. The determination of the luminosity function represents one of the aims of our research.

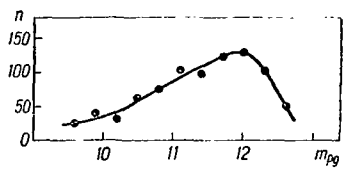

Figure 13

Difficulties complicating the calculation arise during the course of this investigation. These difficulties consist of the fact that the limiting distances, up to which we may calculate the stellar densities, are different for different groups of sub-classes, and also for sections with a different absorption. In order to provide a reliable calculation of densities, it is very important to make a correct determination of the limiting stellar magnitude which would completely encompass stars of different spectral types. The limiting m_{pg}, for which the spectral class is known, was first calculated. For this purpose, the number of stars (which were accurately classified within an accuracy of the sub-class) was calculated for different values of m_{pg} in region A. The results derived from the calculation (Figure 13) show that $11^m.9$ may be assumed to be the largest limiting stellar magnitude. In order to completely encompass all the bright stars, our data were supplemented with the catalog AGK_2. Stars of the G, K and M classes represented an exception; the AGK_2 catalog did not divide these stars into giants and dwarfs. The smallest limiting magnitude of $9^m.5$ was assumed for these stars.

The stellar densities were calculated for the following spectral groups: B5-B7, B8-A0, A1-A3, A5-A8, gG5-K, dF8-G2, dG5-G8. The distance moduli were combined, so that a distance of approximately 100 pc was encompassed.

Table 1 presents the limits within which all the stars of different spectral groups are encompassed in sections with a different absorption; these values were calculated on the basis of the absorption curves. Table 2 presents the volumes corresponding to the assumed limits of the distance moduli, within which the stellar densities were calculated (the volumes were calculated per one square degree in the plane of a figure). /182

The densities were calculated without dividing the regions into sections at comparatively close distances (up to m-M=8), where the maximum values of

TABLE 1

Region and Section	B5—B7	B8—A0	A1—A3	A5—A8	F0—F5	dE8—G2	gG5—K
A							
1	0— 9.3	0— 9.4	0—8.9	0—8.3	0—7.5	4.5 -6.7	7.3—8.8
2	0— 9.8	0— 9.8	0—9.5	0—8.4	0—7.5	4.5—6.7	7.5—9.2
3	0—10.7	0—10.6	0—9.9	0—8.7	0—7.6	4.5—6.8	7.5—9.6
B							
1	0— 9.8	0— 9.3	0—8.5	0—7.8	—	—	—
2	0—11.0	0—10.4	0—9.4	0—8.3	—	—	—
3	0—11.3	0—10.8	0—9.9	0—8.9	—	—	—

TABLE 2

$m-M$	$V \cdot 10^{-3}$, pc^3	$m-M$	$V \cdot 10^{-3}$, pc^3
4.5—5.9	0.32	9.7— 9.9	31.88
5.0—5.9	0.28	10.0—10.1	29.91
6.0—7.0	1.31	10.2—10.3	39.45
7.1—7.7	2.68	10.4—10.5	52.10
7.8 -8.2	4.50	10.6—10.7	68.63
8.3—8.6	6.65	10.8—10.9	91.18
8.7—9.0	11.47	11.0—11.1	119.68
9.1—9.3	13.85	11.2—11.3	157.31
9.4—9.6	21.14	11.4	96.46

the z-coordinate of the region centers did not exceed 40 pc. At larger distances the sections presented in Table 1 were investigated individually. Tables 3 and 4 present the results derived from determining the stars for separate spectral groups in different sections, within the corresponding distance limits, as well as the calculated stellar densities.

Characteristics of the distribution of stellar spatial densities. We shall discuss the results derived from calculating the stellar densities. /184

Stars of class A (Figure 14). The distribution of B8-A0 stars may be reliably studied up to the largest distances (850 pc) close to the galactic equator. The mean density of these stars within 160-250 pc is 0.16* in both regions. The stars were not distributed uniformally: in section 1 of region A, the density changed within 0.17-0.35, and in section 1 of region B it changed from 0.09 to 0.20. The stellar density was greater above the equator than it was under the equator, by approximately a factor of 1.6. In sections adjacent to

* The density pertaining to 10^3 pc^3 is given at this point and in the following.

TABLE 3

/183

Sp / m_0—M	Region A												Region B					
	B8—A0		A1—A3		A5—A8		gG5—K		F0—F5		dF8—G2		B8—A0		A1—A3		A5—A8	
	n	D	n	D	n	D	n	D	n	D	n	D	n	D	n	D	n	D
6.0—7.0	7	0.19	2	0.06	5	0.14	—	—	—	—	—	—	4	0.12	7	0.11	8	0.24
7.1—7.7	13	0.18	8	0.11	22	0.30	—	—	—	—	—	—	11	0.16	19	0.28	36	0.54
7.8—8.2	32	0.26	14	0.11	21	0.17	17	0.14	—	—	—	—	18	0.16	20	0.18	—	—
6.0—6.7	—	—	—	—	—	—	—	—	—	—	79	3.87	—	—	—	—	—	—
6·0—7.5	—	—	—	—	—	—	—	—	156	1.89	—	—	—	—	—	—	—	—
D_{av}	0.22		0.10		0.20		0.14		1.89		3.87		0.15		0.22		0.44	

the galactic equator, there was no decrease in density with distance. This phenomenon was quite clearly expressed in sections located at large galactic latitudes; this may be explained by the decrease in stellar densities in a direction perpendicular to the galactic density.

The density distribution of A1-A3 stars may be traced close to the galactic density up to a distance of 530-650 pc. Just like B8-A0 stars, they are not uniformly distributed in space (see Figure 14). Their mean density within 160-520 pc equals 0.18. In contrast to B8-A0 stars, the density of A1-A3 stars is smaller above the galactic plane than it is below it (by a factor of 1.5).

The densities for A5-A8 stars were calculated up to a distance of 350-450 pc (see Figure 14). The mean density of stars of this type is comparatively large (0.26), and its value is approximately twice as great below the galactic plane as it is above it.

If the tables and graphs showing the density distribution are examined, three condensations of A-stars may be observed at the mean distances of 300, 490, and 750 pc. It is our opinion that these data may serve as a basis for discovering new galactic star clusters in the Milky Way region being studied.

The densities of stars F and G were only calculated for region A, for which we employed data pertaining to stars of the F0-F5, dF8-G2 and gG5-K types. However, it is impossible to trace the behavior of stellar densities for the first two spectral groups, since the F0-F5 stars may only be studied between 0-300 pc, and the dF8-G2 stars may only be studied between 80-220 pc. Therefore, for these spectral types, we confined ourselves to calculating only the mean densities having the values 1.98 and 4.25, respectively. The densities of the giants G5-K do not depend on distance and latitude to as great an extent as densities of the B8-A stars (see Table 4), and they have a mean value of 0.14.

/186

Characteristics of the distribution of stars in class B. It was difficult

TABLE 4

Sp / m_0-M	B8—A0		A1—A3		gG5—K		B8—A0		A1—A3		gG5—K		B8—A0		A1—A3		gG5—K	
	n	*D*	*n*	*D*	*n*	*D*	*n*	*D*	*n*	*D*	*n*	*D*	*n*	*D*	*n*	*D*	*n*	*D*
Region *A*	1						2						3					
8,3— 8,6	15	0,23	13	0,20	10	0,16	6	0,07	12	0,14	13	0,15	4	0,12	2	0,06	3	0,09
8,7— 9,0	19	0,17	9	0,08	9	0,08	17	0,11	24	0,16	19	0,12	3	0,05	3	0,05	5	0,09
9,1— 9,2	15	0,18																
9,1— 9,3	25	0,19					19	0,10	7	0,04	23	0,13	1	0,02	6	0,09	3	0,05
9,3— 9,4	38	0,35					46	0,17										
9,4— 9,6							22	0,05	22	0,08			3	0,03	5	0,05	5	0,05
9,7— 9,9													1	0,00	3	0,02		
10,0—10,1													4	0,03				
10,2—10,3													1	0,00				
10,4—10,5													5	0,02				
Region *B*	1						2						3					
8,3— 8,6	15	0,20	16	0,22			5	0,08	16	0,24			2	0,06	3	0,11		
8,7— 9,0	12	0,09					6	0,05	4	0,04			6	0,13	6	0,13		
9,1— 9,3	13	0,08					11	0,08	17	0,12			2	0,04	11	0,20		
9,4— 9,6							16	0,08					6	0,07	5	0,06		
9,7— 9,9							9	0,03					6	0,05	3	0,02		
10,0—10,1							5	0,02					7	0,06				
10,2—10,3							2	0,01					5	0,03				
10,4—10,5													3	0,01				
10,6—10,7													3	0,01				

to calculate the densities of stars of this type due to the small number of them. The entire region A+B was divided into three sections (Figure 15, dotted line), and the following limits were chosen based on the distance moduli: 6.0-9.3; 9.4-9.9; 10.0-10.9. The results of the calculations (Table 5) only indicate that the density of these stars is approximately two times smaller in sections located at the galactic latitude 3.5-4°.0 than it is in the equatorial region, where it comprises 0.0036. The mean density within 160-1500 pc equals 0.0026 -- i.e., it is two orders of magnitude lower than for B8-A0 stars.

The number of B0-B7 stars is considerably smaller in region A (13) than it is in region B (36), although the first region is larger than the second in terms of area. Comparing the number of stars in the different sections of regions A and B with the nature of the absorption increase at large distances, we were able to explain this phenomenon by a different absorption.

Let us study the list of B0-B3 stars (Table 6). There are almost no B0-B3 stars in both regions up to a distance of 1700 pc (m-M = 11.2). The B0-B3 stars which we observed at larger distances apparently belong to the spiral arm of Sagittarius. The mean distance of the majority of B0-B3 stars

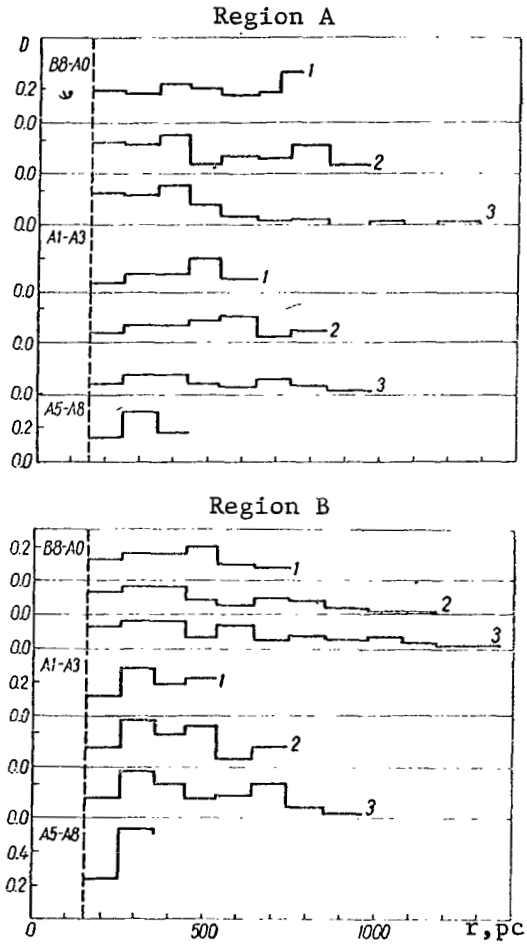

Figure 14

in the list is 1740 pc. We may assume that it determines the position of the /187 leading edge of the arm of Sagittarius, which is intercepted by the line of

TABLE 5

Limits m_0-M	a			b			c		
	n	$V\cdot10^{-5}$, pc^3	$D\cdot10^5$, pc^3	n	$V\cdot10^{-5}$, pc^3	$D\cdot10^5$, pc^3	n	$V\cdot10^{-5}$, pc^3	$D\cdot10^5$, pc^3
6.0— 9.3	3	8.34	0.36	2	7.29	0.27	1	5.67	0.18
9.4— 9.9	—	—	—	1	9.54	0.10	1	7.42	0.13
10.9—10.9	—	—	—	—	—	—	12	39.34	0.30

TABLE 6

Region, Number of Map	Sp	m_{pg}	m_0-M
A, LVI	B3	12.64	11.2
B, 11—1	B:	12.02	11.0
11—3	B:	12.09	11.4:
15—1	B3	11.91	12.0
15—1	B2	12.00	12.7
15—4	B0	9.85	11.4
15—5	B0	11.87	11.1

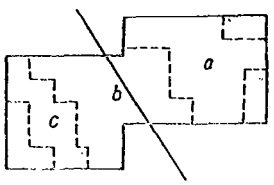

Figure 15

sight in the direction 12-22°. These conclusions concur with the calculations presented in the section on absorption.

Distribution of Stellar Densities Along the z-Coordinate

The length of the regions which we studied along the galactic latitude from -6 to +6° made it possible to follow the behavior of density with the z-coordinate for stars of certain spectral groups -- B8-A0, A1-A3 and gG5-K. In regions A and B, two sections (a and b), were distinguished, which were distributed symmetrically with respect to the galactic equator (Figure 16, dotted line) and which encompassed latitudes up to $\pm$ 5°.2. Taking into account the limits between which there are no selection errors (see Table 1), we were able to distinguish layers, which were parallel to the galactic plane and which were 10 pc thick, in the spatial cones corresponding to sections a and b. Figure 17 shows an approximate cross section of one of these cones. The mean stellar density was calculated for each layer. Table 7 presents the intervals of the z-coordinate, the true distance moduli (corresponding to the limits defining the layers in terms of depth), the number of stars in the layers, and the stellar densities. The following conclusions were reached on the basis of the graphs which were compiled showing the behavior of density:

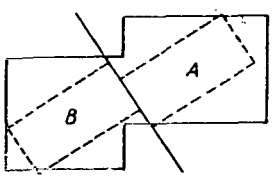

Figure 16

1. For B8-A3 stars, the density changed unevenly with the z-coordinate, /188 and gave no indication of strict symmetry with respect to the galactic density. The maximum densities of B8-A0 stars were observed above the equatorial plane, and the maximum densities of A1-A3 stars almost coincided with them.

2. The density gradient of A1-A3 stars was smaller than the density

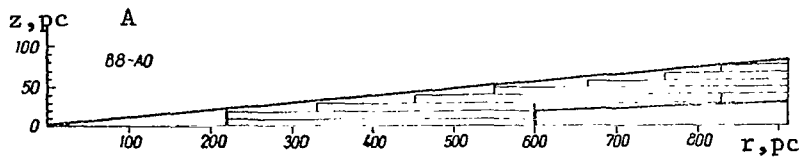

Figure 17

gradient of B8-A0 stars.

The mean curves showing the behavior of D with $|z|$ (Figure 18, dots) were compiled on the basis of the combined computational results for B8-A0 and A1-A3 stars. It is known that the exponential law may be assumed on the average for the change in the stellar density with the z-coordinate

$$D = D_0 e^{-\frac{|z|}{\beta}},$$

where D_0 is the density in the galactic plane; β -- a constant. According to the studies by B. V. Kukarkin and P. P. Parenyy, the sub-systems of the plane component may be characterized by the values of β between 44-100 pc. The behavior of the densities, which is shown in Figure 18, is closely approximated for a value of β which equals 45 pc for B8-A0 stars, and which equals 50 pc for A1-A3 stars.

Luminosity function for 14-18° longitudes. If we determine the luminosity function as the number of stars in a cubic parsec with the absolute magnitudes within the limits of M-1/2, M+1/2, then this function may be written as follows at this distance

$$\Phi(M) = \sum \frac{e^{-\frac{(M-M_s)^2}{2\sigma_s^2}}}{\sqrt{2\pi}\sigma_s} D(r) = \sum a_s(M) D(r),$$

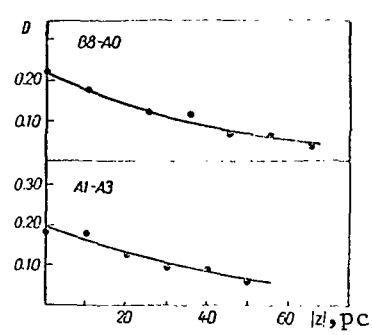

Figure 18

where M_s and σ_s are the mean values of the absolute magnitude and its dispersion in the given spectral interval; D(r) -- density of stars of this interval. /189

If we know the density of stars belonging to different spectral groups for different distances, we may calculate the luminosity function for the direction 14-18° corresponding to regions A and B. The values of D, M_s and σ_s given in Table 8 were used for the calculations. Beginning

TABLE 7

|z|, nc \ Sp	B8—A0			A1—A3			gG5—K		
	m_0-M	n	D	m_0-M	n	D	m_0-M	n	D
Region A									
0— 10	6.7— 9.4	27	0.26	6.7—8.9	14	0.20	7.5—8.8	11	0.22
10— 20	6.7— 9.4	12	0.12	6.7—8.9	3	0.04	7.5—8.8	6	0.12
20— 30	7.6— 9.3	17	0.19	7.6—8.9	10	0.18	7.6—8.9	5	0.09
30— 40	8.3— 9.6	20	0.19	8.3—9.5	11	0.12	8.3—9.2	16	0.27
40— 50	8.7— 9.8	10	0.09	8.7—9.5	5	0.07	8.7—9.3	8	0.21
50— 60	9.1— 9.8	4	0.05	9.1—9.5	2	0.05	9.1—9.2	1	0.11
60— 70	9.4— 9.8	1	0.02	9.4—9.5	0	0.00			
70— 80	9.7— 9.8	0	0.00						
Region B									
0— 10	6.7— 9.4	19	0.18	6.7—8.5	5	0.11			
10— 20	6.7— 9.4	11	0.11	6.7—8.5	10	0.23			
20 — 30	7.6— 9.3	5	0.06	7.6—8.5	5	0.16			
30 — 40	8.3— 9.3	3	0.04	8.3—8.8	3	0.11			
40 — 50	8.7— 9.4	3	0.05	8.7—9.3	3	0.06			
50 — 60	9.1— 9.8	6	0.07						
60 - 70	9.4 10.3	8	0.05						
70 - 80	9.7—10.4	4	0.03						
80 — 90	10.0—10.4	3	0.03						
90—100	10.3—10.4	1	0.03						

with F stars, the stellar densities were only taken for region A, since these stars were not studied in region B. The general distance interval, for which the densities were taken during the calculations, range from 160-520 pc. For B5-B7 stars, the density of which was low, the limit increased to 1000 pc. For F8-G2 dwarfs, the densities were only known at distances of 80-220 pc.

Figure 19 gives the luminosity function obtained -- 1, as well as the functions (which are average for circumsolar space) which were calculated by /190
P. van Rhijn -- 2 (Ref. 19), and the functions calculated by S. McCuskey -- 3 (Ref. 18).

TABLE 8

Sp	Distance, pc	Number of Stars	$D\cdot10^3$, pc^3	M_s	σ_s
B5 -B7	0—1000	15	0.0039	—1.0	±0.7
B8 -A0	160 -- 520	107	0.161	+0.1	0.8
A1 -A3	160— 520	119	0.179	1.1	0.8
A5 -A8	160— 440	78	0.264	2.4	0.8
F0—F5	100— 320	173	1.98	3.7	0.8
dF8—G2	80— 200	124	4.25	5.0	0.8
dG5—G8	50— 160	53	5.029	6.2	0.8
gG5—K	290— 520	43	0.142	1.4	0.8

Function 2 was obtained by studying the proper motion of stars, and function 3 was found on the basis of direct data regarding stellar densities. In the calculations, we did not take into account stars earlier than B5. However, this did not influence the results, since the density of these stars in the region of space being studied was practically negligible. For this reason, it is not possible to consider giants of the class M. The fact that all the dwarfs K and M were not included signifies that the portion of the curve we compiled, beginning with M = 5, is inaccurate.

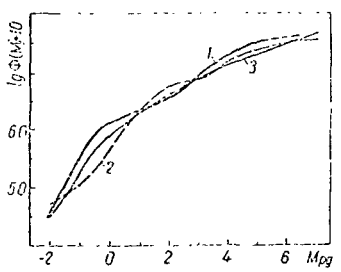

Figure 19

A comparison of the luminosity function which we calculated with the functions of P. van Rhijn and S. McCuskey shows that the general form of the function in the direction being studied is approximately identical, with the exception of a certain rise in our curve in the region of absolute magnitudes from -1.5 to +0.5. This points to an increased density of B5-A0 stars, which represents a distinguishing feature of the galactic region being studied.

Comparison of the distribution of stars, dust, and gas. The distribution of stars is not related to neutral hydrogen. The situation is somewhat different when dust and stars are compared, whose distribution evinces a specific relationship. Attention should first of all be called to the arrangement of condensations of class A stars at approximately the same distances at which groups of dust clouds are located. In order to make a quantitative evaluation of the phenomenon, the mean number of stars in the clouds and outside of the clouds was calculated for region A. The calculations were performed for different spectral groups on the basis of absorption curves. In addition, we calculated the areas occupied by dust clouds in different sections of region A. This provided us with the mean ratio of stellar densities in the clouds to the mean densities in the intervals between them. All of these data are presented in Table 9. As may be seen from the table, the majority of B8-A0 stars is located in clouds which occupy about one third of the area. A large concentration in the clouds is also characteristic for the G5-K giants. The A1-A8 stars are not as closely related with the clouds. The ratios of the densities in the clouds to the densities in the intervals change between 2.6-5.1 for class A stars and comprise 3.5 for G5-K giants. The maximum concentration of stars in the clouds occurs for the spectral group B8-A0. /191

It is interesting to note that the density ratios which we obtained depend on the absolute magnitude (see Table 9).

Table 9 also presents results derived from similar calculations for F0-F5 and dF8-G2 stars. They are not as accurate, since they were obtained for a smaller area in space.

TABLE 9

Sp	r, pc	n	n_{cl}/n	V_{cl}/V	D_{cl}/D_{inter}	$M_{av.}$
B8—A0	0—800	205	0.71	0.32	5.1	+0.1
A1—A3	0—600	72	0.57	0.32	2.8	+1.1
gG5—K	0—600	77	0.61	0.32	3.3	+1.4
A5—A8	0—450	43	0.70	0.47	2.6	+2.4
F0—F5	0—320	163	0.41	0.26	2.0	+3.7
dF8—G2	80—230	103	0.19	0.18	1.0	+5.0

* Cl - denotes cloud

We evaluated the results of these calculations as representing reliable substantiation of the relationship between dust and stars, particularly stars of the B8-A3 and gG5-K type.

Structure of the Milky Way at the 0-22° Longitudes

It is known that the spiral structure of the galaxy not only consists of the main arms, but also consists of branches, which contribute to a very complex picture, in general. The nature of the branches is the same as the nature of the arms -- i.e., they are formed by stars of the O and B type, by gas, and by dust. The region of the galaxy, which is located between the Sun /192
and the Sagittarius arm in directions with a mean longitude of 10°, up to a distance of 1500-2000 pc, is filled with clouds of neutral hydrogen, having a density which is characteristic for hydrogen arms (0.6-1.0 atm/cm^3). This cloud combines the Sagittarius arms and the Carina - Cygnus arms. The question of the distribution of the spiral population representatives in the region of this hydrogen link then arises: the O and B stars, their associations, and the dust.

Dust component. As has been noted, interstellar absorption at 0-20° longitudes up to a distance of 900-1000 pc is caused by a cloud cluster, and increases rapidly. At larger distances, there is an insignificant increase in the absorption. In actuality, in section 1 of region B at distances of 1000-1500 pc it is characterized by the mean coefficient -- 1^m per kiloparsec. This value is obtained for section 2 within the same distance limits.

It follows from the study of V. I. Voroshilov (Ref. 3) that, beginning with 1000 pc, for a mean longitude of 5° the mean absorption coefficient in all (with the exception of one) sections of the regions studied did not exceed 1^m, and comprised $0^m.7$ on the average. This same phenomenon was observed in the region studied by I. I. Pronik (Ref. 5) (ℓ = 343°, b = 0°), where the absorption was only great up to a distance of 1000 pc. We employed the data of I. I. Pronik to calculate the absorption, which was average for the entire region, beginning at a distance of 1000 pc. At a distance of 2000 pc (from 1000 to 3000 pc) the absorption increased by less than a factor of 1^m. Thus, the absorption was also insignificant at distances exceeding 1000 pc in the direction of 343°. Absorption at distances of 2000-3000 pc in the LF2 region of S. McCuskey was also the same (Ref. 18).

The above statements foster the conclusion that at the 343-22° longitudes

(and possibly up to 33°) powerful dust clouds, which form the "fork" of the Milky Way, are distributed approximately up to the distance 1000 pc, and do not continuously fill the space between the Carina-Cygnus and Sagittarius arms. It also follows from the studies mentioned above that this "dust gap" (with a mean absorption coefficient of no more than 1^m per kiloparsec) extends up to a distance of 2500-3000 pc. This fact, as well as the presence of powerful dust clouds in the directions studied, closely coincides with the predominant distribution of dust observed in the galaxy in the form of an inner border of the spiral arms. Figure 20 presents a diagram showing the structure of the Milky Way region which we studied.

Early-type stars. In the directions studied, the line of sight intersects /193 the interval between the Carina-Cygnus and Sagittarius arms, and then the Sagittarius arm. We shall summarize the data making it possible to determine the position of this spiral in the northern sky.

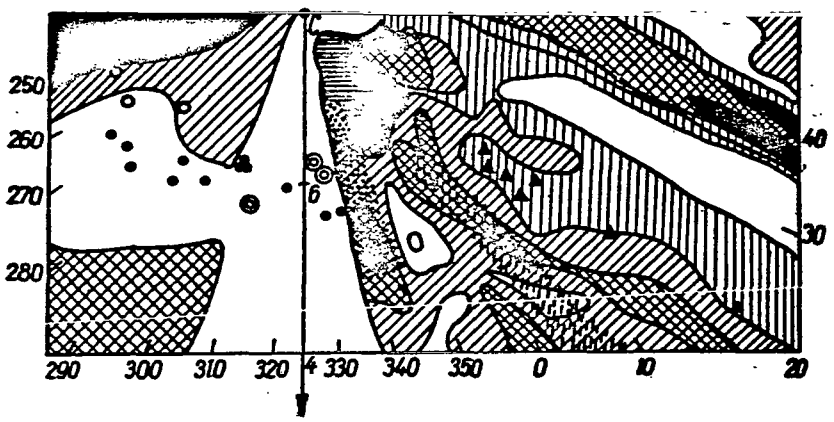

o Galactic star clusters — Bright giants O-B

O-associations — BO-B2 (data of V. Voroshilov)

▲ BO-B3 (regions A and B) — Cluster of Nebulae

BO-B3 (data of I. Pronik) — Neutral Hydrogen

Figure 20

According to H. Weaver (Ref. 21), bright stars of the Sagittarius arm are distributed as is shown in Figure 20. It follows from the catalog of W. Hiltner (Ref. 12) (the catalog contains only the exact distances of early-type stars, determined photoelectrically) that all of these stars are located beyond 1000 pc.

Individual studies of fainter stars ($m_{pg} \geqslant 12$) substantiate these data. I. I. Pronik (Ref. 6) determined the beginning of the arm in the direction

343° at a distance of 600-1000 pc. V. I. Vorishilov (Ref. 4) indicated that there were absolutely no O-B2 stars in the direction 5° up to a distance of 1200 pc. We found a value of 1700 pc for the distance to the leading edge of the Sagittarius arm, based on the BO-B3 stars. Consequently, it may be concluded that at the 0-20° longitudes the optical arms of Carina-Cygnus and Sagittarius are not combined, but they are combined in the hydrogen spiral structure. Once again this substantiates the lack of agreement between the hydrogen and optical pictures of the galactic spiral structure.

We noted above that the limiting longitude, up to which the Sagittarius /194
arm extends in the northern portion of the Milky Way, cannot be determined precisely. We also pointed out that several authors (W. Becker, H. Weaver) give 350° as this limit, justifying this by the absence of early-type stars in this direction. The significant absorption (which they discovered as a result of their investigations) in the direction 12-22°, and also a certain number of BO-B3 stars around 12^m provide a basis for assuming that the optical arm of Sagittarius may extend at least to a longitude of 20° in the northern section of the Milky Way. Data on the magnitudes and spectra of stars fainter than 12^m are requisite in order to perform this study successfully.

REFERENCES

1. Apriamashvili, S.P. Abastum. Byulleten 30, 49, 1964.
2. Voroshilov, V.I., et al. Katalog velichin 22 000 zvezd (catalogue of 22,000 Stars). Izdatel'stvo AN USSR, Kiev, 1962.
3. Voroshilov, V.I. Izvestiya Glavnoy Astronomicheskoy Observatorii (GAO), AN USSR, 5, 1, 117, 1963.
4. Voroshilov, V.I. Present Collection, page 129.
5. Pronik, I.I. Izvestiya Krymskoy Astrofizicheskoy Observatorii (KrAO), 22, 152, 1960.
6. Pronik, I.I. Izvestiya GAO AN USSR, 23, 46, 1960.
7. Fedorchenko, G.L. Izvestiya GAO AN USSR, 4, 2, 113, 1963.
8. Fedorchenko, G.L. Izvestiya GAO AN USSR, 4, 2, 134, 1963.
9. Fedorchenko, G.L. Izvestiya GAO AN USSR, 5, 1, 128, 1963.
10. Fedorchenko, G.L. V kn: Issledovaniya po fizike zvezd i diffuznoy materii (In the book: Research on Stellar Physics and Diffuse Matter). Izdatel'stvo AN USSR, Kiev, 1964.
11. Becker, W. Vistas in Astronomy, 2, 1515, 1956.
12. Hiltner, W.A. Contr. from the McDonald Obs., 269, 389, 1956.
13. Iwaniszewska, C. Bull. of the Astr. Obs. in Toruń, 14, 41, 1956.
14. Iwaniszewski, H. Bull. of the Astr. Obs. in Toruń, 14, 15, 1956.
15. Iwaniszewska, C. Bull. Obs. Astr. Univ. in Toruń, 24, 1, 1960.
16. Iwaniszewski, H. Bull. Obs. Astr. Univ. in Toruń, 30, 1, 1962.
17. McCuskey, S.W., Seyfert, C.K. Aph. J., 106, 1, 1, 1947.
18. McCuskey S.W. Aph. J., 123, 3, 458, 1956.
19. Rhijn, P.J.van Groningen Pub., 47, 1936.
20. Weaver, H. Aph. J., 110, 2, 190, 1949.
21. Weaver, H. A. J., 58, 7, 177, 1953.

EFFECT OF THE EARTH'S ATMOSPHERIC TURBULENCE ON THE LIGHT COLLECTION OF TELESCOPES

I. G. Kolchinskiy

The article deals with the influence of the optical instability of the atmosphere on the quality of star focal images, made with telescopes having various diameters. Estimations of the part of reduction to transatmospheric star brightness due to atmospheric turbulence are given.

L. A. Chernov (Ref. 11), and also N. G. Denisov and V. I. Tatarskiy (Ref. 3), have shown that intensity distribution in the focal image of a precise object (a star) differs from the distribution in the case of a uniform medium for a nonaberrational objective. This is due to fluctuations in phase and amplitude at the front of a light wave, which is propagated in a nonuniform medium, with fluctuations in density. When there are fluctuations, the intensity is smaller at the focal point than would follow from the theory of diffraction. The effective radius of the image increases, since the curve showing the intensity distribution in the focal image has large "wings". Due to this fact, the exposure time for obtaining photographic images of stars having a definite stellar magnitude increases considerably, and light collection of the telescope decreases. /196

The relative intensity decrease at the focal point, as compared with the theory of diffraction, depends upon the amount by which the mean square value of vibration ("incoming angle" of light rays) exceeds the angle of diffraction, which is determined by the ratio λ/D, where λ is the wavelength, and D is the objective diameter. This same ratio determines the radius of the diffraction disc of the stellar image, which may be calculated according to the following formula in angular dimensions

$$\alpha_r = \frac{1{,}22\lambda}{D}, \tag{1}$$

and in linear dimensions, according to the following formula /197

$$\rho = \frac{1{,}22\lambda F}{D}, \tag{2}$$

where F is the focal distance of the objective.

The ratio between the mean intensity at the focal point, in the presence of fluctuations I, and the intensity without fluctuations I_0 may be determined by the function G(a) (3):

$$G(a) = \frac{16}{\pi}\int_0^1 e^{-ax^{5/3}}\{\arccos x - x\sqrt{1-x^2}\}\,x\,dx, \tag{3}$$

where x = r/D is the relative distance from the center of a circular diaphragm having the diameter D;

$$2a = 2{,}91 \frac{4\pi^2}{\lambda^2} LC_n^2 D^{5/3};$$

$L = L_0 \sec z$ - "air mass", traversed by a ray at the zenith distance z;
C_n^2 - parameter characterizing the pulsation intensity of the refractive index included in the law of "two-thirds" power:

$$D_n(r) = C_n^2 r^{2/3} \quad (L_0 \gg r \gg l_0); \tag{4}$$

where $D_n(r)$ is the structural pulsation function; l_0 and L_0 - inner and outer turbulence scales.

In the case of a layer in which C_n^2 does not change with altitude, the mean square of fluctuations of incident angles $\overline{\vartheta^2}$ is determined by the following expression

$$\overline{\vartheta^2} = 2{,}91 D^{-\frac{1}{3}} L_0 \sec z C_n^2. \tag{5}$$

Taking the value α_r into account (1), we obtain

$$2a = 4\pi^2 \cdot 1.49 \frac{\overline{\vartheta^2}}{\alpha_r^2} = 59.1 \frac{\overline{\vartheta^2}}{\alpha_r^2}. \tag{6}$$

Thus, a is proportional to the ratio of the mean square of vibration to the square of the angular radius of the diffraction disc $\left(a = \frac{2\pi^2 \vartheta^2}{(\lambda/D)^2}\right)$.

Figure 1 presents a curve showing the values of the function G(a) (Ref. 3). The weaker the intensity at the focal point, as compared with the theoretical intensity, the greater the objective diameter in the case of the same vibration -- i.e., the smaller the angular radius of the diffraction disc of the image. With an increase in the mean quadratic vibration amplitude -- i.e., generally speaking, when there is an increase in the zenith distance -- the ratio $\frac{I}{I_0}$ will also decrease. /198

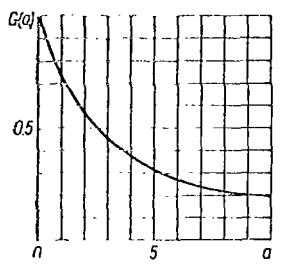

Figure 1

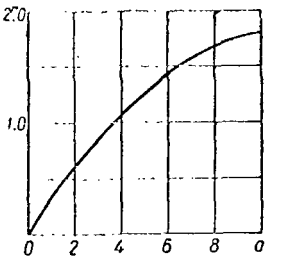

Figure 2

Figure 2 presents the intensity loss as a result of turbulence, expressed in stellar magnitudes. Intensity attenuation is quite large at the focal

point. Even in the case of a = 1, it is about $0^m.3$.

We shall try to determine the limits within which the value of a may change in astronomical practice. In order to determine these limits, we shall start with the empirical data provided by Danzhon and Kuder, regarding the relationship between the angle of turbulence and the radius of the diffraction disc when the quality of the image varies (Ref. 2). This relationship may be characterized by a well known table (Table 1). We shall identify the turbulence angle with the angle ϑ -- more precisely, with $\sqrt{\overline{\vartheta^2}}$. It may be seen from Table 1 that the ratio ϑ^2/α_r^2 may change from a value of about $\frac{1}{16}$, for very good images, up to values of 2-4 for very poor images. In this connection, á changes from 3.7 to 100-200. Thus, the intensity loss comprises no less than $1^m.0$ in stellar magnitudes. We must keep the fact in mind that this condition of Danzhon and Kuder is an arbitrary condition, and pertains to visual observations employing instruments with an average dimension, whose objectives do not exceed several tens of centimeters.

TABLE 1 /199

$\frac{\sqrt{\vartheta^2}}{\alpha_r}$	IMAGE QUALITY	$\frac{\overline{\vartheta^2}}{\alpha_r^2}$
$< \frac{1}{4}$	Perfect diffraction image without perceptible deformation, possibly slightly disturbed.	$< \frac{1}{16}$
$\frac{1}{4}$	Unbroken diffraction rings with bunches of light passing through them.	$\frac{1}{16}$
$\frac{1}{2}$	Image slightly disturbed, rings broken in places; edges of diffraction disc disturbed.	$\frac{1}{4}$
1	Great disturbence of the image; diffraction rings disappear, bundle of rays removed from spot, immediately disappearing.	1
>1.5	Image in the form of a turbulent diffusion spot of comparatively stable form, scattered with small, agitated shafts of light. If there were no turbulence, the image of a star would resemble a planetary image.	> 2.5

In every case, it may be seen from these data that a has values which are close to unity, and greater than unity, during astronomical observations. This is due to the fact that very good images of stars, for which the diffraction picture is clearly apparent, are very rarely observed.

In the region of values a >> 1, the function G(a) changes approximately as $a^{-6/5}$. If only D changes for one and the same vibration we then have

$$G(a) \sim (D^{5/3})^{-6/5} = D^{-2},$$

i.e., G(a) decreases as D^{-2}.

A strange result is thus obtained. When the diameter of the objective increases, due to fluctuations the intensity in the focal image of the star decreases to such a great extent that it balances out the expected advantage to be gained from an increase in the diameter. But one fact must be kept in mind. It is known that the illumination of the stellar image in the focus of the telescope is not, generally speaking, proportional to D^2, but to D^4/F^2 (Ref. 6, 9). This may be explained by the fact that the angular diameter of the diffraction disc changes in inverse proportion to D, and the light flux changes in proportion to D^2. The linear diameter of the diffraction disc is /200
proportional to F. We may apply the dependence D^4/F^2, if the diameter of the diffraction disc of the stellar image is greater than the mean dimensions of the grain of the photographic image, which corresponds to a sufficiently large F/D. Table 2 presents the radius of the stellar image for different values of $\frac{F}{D}$ ($\lambda \sim 550$ millimicron). For F/D ∿ 15 the stellar image diameter is approximately 20 microns, which exceeds the diameter of the photographic emulsion grain by at least several factors.

TABLE 2

$\frac{F}{D}$	micron	$\frac{F}{D}$	micron
1	0.67	9	6.63
2	1.34	10	6.70
3	2.02	11	7.37
4	2.68	12	8.05
5	3.35	13	8.72
6	.02	14	9.40
7	4.69	15	10.07
8	5.35		

It has been indicated in courses on astrophysics [for example, (Ref. 1)] that the theoretical light collection of telescopes must be proportional to one-fourth power of the opening diameter. S. K. Kostinskiy (Ref. 1) has written: "However, due to the structure of the retina during visual observations or the structure of the sensitive layer of a photographic plate during photography, it must be assumed that the light collection of telescopes is only proportional to the square of the diameter" (for stars). It is possible that this is the case for small F/D. However, for large F/D and for large diameters of the image, in my opinion, it seems more logical to assume that the reason for the reduction in illumination in the stellar image does not lie in the nature of the light-sensitive layer, but in the influence of fluctuations. Since G(a) ∿ D^{-2} usually during astronomical observations, in actuality the illumination of the stellar image at the focus will not be proportional to D^4/F^2, but only to D^2/F^2, as is characteristic in general for extended objects. When there is no turbulence, for example, in the case of astronomical observations on the Moon, it is possible that the formula D^4/F^2 will be closer to reality for stars than it is for D^2/F^2, particularly in the case of fine-grain emulsions.

It also follows from the theory of L. A. Chernov (Ref. 11) that the ratio I/I_0 is proportional to $\frac{a^2}{h^2}$ for fairly large fluctuations -- i.e., where a is the correlation scale in the Gauss law which describes the correlation relationship between pulsations of the refractive index; h - dimension of the diaphragm, assumed to be square. Thus, the conclusions reached by L. A. Chernov for the case of large fluctuations coincide with the conclusions of N. G. Denisov and V. I. Tatarskiy for the case of large a. /201

Let us examine certain examples.

In his time, G. A. Tikhov (Ref. 8) compared the photographic conditions for the variable star RT Persei whose brightness changed from 9.5 to $10^m.5$, by means of specific light filters on two instruments: a Bredikhina astrograph (D = 17 cm, F = 20 cm) and a Pulkova 30-inch refractor (D = 72.6, cm, F = 1412 cm). An exposure of no less than 15 minutes was necessary for photographing this star on a Bredikhina astrograph by means of a light filter with a pass band of 495-615 millimicrons and a mean band of 555 millimicrons. In order to obtain the image of RT Persei in the focus of a 30-inch refractor, an exposure of no less than 50 minutes was necessary. Based on theory, in view of the fact that the area of the refractor objective was 20 times greater than the area of the objective of the Bredikhina astrograph, G. A. Tikhov expected that the exposure on the refractor would be less than 1 minute. G. A. Tikhov reached the conclusion that the lack of agreement which he obtained in the exposures could be explained by the large linear dimensions of the images and by the great influence of vibration when the focal distance of the 30-inch refractor equalled 14 m.

In actuality, one could not hope to gain any advantage with the exposure on a 30-inch refractor, as compared with the Bredikhina astrograph. The relative aperture of the first was 1/19.5, and the relative aperture of the second was 1/4.7. The ratio of the light collection of both instruments was 1/17.3 -- i.e., the ratio of the squares of these numbers. Thus, illumination of the image in a 30-inch refractor is 17.3 times less than in a Bredikhina astrograph. Correspondingly, the exposure for RT Persei must be increased by at least a factor of 17, i.e., several hours. It is no wonder that the image was underexposed with an exposure of 50 minutes. Naturally, this is a very rough estimate, since the difference in achromatization of both instruments would have to have had an influence, in spite of the fact that the same filter was employed. In addition, it is very likely that the photography on the astrograph and the refractor was performed at different times, and the meteorological conditions would have to have been different.

According to S. Cheiner (Ref. 13), losses of the limiting stellar magnitude due to the fact that the atmosphere is not quiet during photographic observations may comprise about $0^m.75$. It may be seen from Figure 2 that such an intensity loss may occur at the focus -- for example, when the parameter a changes from 3 to $\sqrt{8}$, which corresponds to an increase in the angle of turbulence by a factor of $\sqrt{8/3} = 1.6$. Unfortunately, we do not know what atmospheric agitation or what instrument formed the basis of Cheiner's /202

estimate.

There are also indications that, for the 100-inch telescope of Mount Wilson Observatory, the limiting stellar magnitude changes by 3^m for a poor quality image (Ref. 12). This brightness decrease fully agrees with the curve shown in Figure 2, and may correspond to an increase in turbulence by several factors, as compared with its mean value in a quiet atmosphere.

Let us investigate the manner in which the illumination of the stellar image must change at the focal point when the zenith distance changes. Let us employ the following notation: I - the light intensity in the focal image, and I_0 - the same intensity in the absence of an atmosphere. In this case, I must be the function of atmospheric absorption and must depend on fluctuations. In general form, we may write

$$\frac{I(z, a)}{I_0} = k(z)\,G(a), \tag{7}$$

where k(z) characterizes customary (Bouguer) light attenuation; G(a) - the function, and a depends on sec z (or on L). At the zenith, we have

$$\frac{I(0, a_0)}{I_0} = k(0)\,G(a_0), \tag{8}$$

where a_0 is the value of a for z = 0°. Thus, reduction to the zenith may be calculated according to the following relationship

$$\frac{I(z, a)}{I(0, a_0)} = \frac{k(z)}{k(0)} \cdot \frac{G(a)}{G(a_0)} \tag{9}$$

The quantity $\frac{k(z)}{k(0)}$ is none other than $\frac{k(z)}{k(0)} = p^{(\sec z - 1)}$, where p is the transmission coefficient of the atmosphere. The ratio $G(a)/G(a_0)$ must be determined according to a curve. In the case of $a \sim 1$, it is impossible to employ asymptotic relationships. Such values of a are characteristic for astronomical observations. For different stellar magnitudes at the zenith distance z and at the zenith, we obtain /203

$$m_z - m_0 = 2.5\,(\sec z - 1)\lg p - 2.5\lg\frac{G(a)}{G(a_0)} \tag{10}$$

or

$$m_z - m_0 = 2.5\lg[pG(a_0)] - 2.5\sec z\lg p - 2.5\lg G(a)$$

In the case of G(a) = 1, this formula coincides with the customary formula

$$m_z - m_0 = 2.5\lg p - 2.5\sec z\lg p.$$

We shall assume that a = 3 at the zenith under certain meteorological conditions. In the case of z = 60° a = 6, since sec 60° = 2. The corresponding correction to the Bouguer law in stellar magnitudes may be determined according to the curve shown in Figure 2, as the difference of the ordinates in the case of a = 6 and a = 3 -- i.e., $1^m.42 - 0^m.84 = 0^m.58$. For a = 4 and

$a = 8\ 1^m.64-1^m.02 = 0^m.62$. Thus, the deviation from the Bouguer law is characterized by the term 2.5 lg G(a) = 2.5 lg $G(a_0 \sec z)$, if we set $a = a_0 \sec z$.

The Bouguer straight lines may actually curve at sufficiently large zenith distances, but the reason for this has not been adequately explained. Thus, N. N. Sytinskaya (Ref. 7) assumes that these curves are due to a change in the transmission coefficient, particularly in the case when the so-called long method of determining the transmission is employed. V. G. Fesenkov (Ref. 10) has also pointed out the curvature of the Bouguer lines, beginning with z = 60 - 70°. V. B. Nikonov (Ref. 5) assumes that the curvature of the Bouguer lines is caused by the Forbes effect and smooth changes in transmission. It is fully possible that the phenomenon we have investigated also contributes to the curvature of the Bouguer lines.

Let us now investigate what the reduction must be to stellar brightness outside of the atmosphere. It is apparent that it depends on the angle of turbulence and the greater the diameter of the telescope objective, the larger it is. It may be seen from Table 3 that the intensity loss of the focal image due to fluctuations, when the star is located at the zenith, is quite large for large telescopes. However, it is small for telescopes with a small aperture. The estimates we obtained pertain primarily to limiting stellar magnitudes, which essentially depend on the plate sensitivity threshold or the radiation receiver. For stellar images which differ from the limiting images, the data presented in Table 3 are probably too high. The limiting penetration capacity during observations outside of the atmosphere also depends on the background brightness of the sky, which is appreciable under these conditions. /204

TABLE 3

	Angle of Turbulence 0".30			Angle of Turbulence 0".20		
D, см	a	G(a)	Δm	a	G(a)	Δm
10	2.30	0.52	0.68	0.57	0.83	0.23
20	8.89	0.20	1.75	2.22	0.50	0.75
30	19.8	0.090	2.60	4.95	0.32	1.24
40	36.6	0.019	3.28	9.15	0.20	1.75
50	55.2	0.032	3.73	13.8	0.132	2.20
60	79.2	0 022	4.10	19.8	0.092	2.65
70	10 .0	0.017	4.40	26.2	0.070	2.78
80	146.9	0.012	4.77	36.6	0.050	3.26
90	178.1	0.010	5.00	44.5	0.041	3.48
100	218.2	0.008	6.21	54.5	0.034	3.70
200	1112	0.0016	6.97	276	0.0066	4.45
300	1980	0.0009	7.60	495	0.0037	6.10
400	2700	0.00066	7.90	675	0.0027	6.43

The quantities shown in Table 3 all make it possible to represent the efficiency of a telescope when there is no atmosphere. We should point out that the standards of photographic stellar magnitudes are based on the so-called Göttingen Werke actinometers. When the first study was carried out, an instrument with D = 45 mm and F = 460 mm was employed, while the second

study employed an instrument with D = 145 mm, F = 814 mm (Ref. 4). As may be seen from Table 2, with such instruments, a portion of the reduction for changing to extra-atmospheric magnitudes, which depends on fluctuations, does not exceed several tenths of a stellar magnitude.

Since α depends on λ, G(a) also depends on λ. It thus follows that G(a) is not the same for stars having different colors. Let us employ the following notation: $\lambda_{1\ eff}$ and $\lambda_{2\ eff}$ -- photographically effective wavelengths for two stars of different spectral classes. If $\lambda_{1\ eff} > \lambda_{2\ eff}$, then -- since $a \sim \frac{c}{\lambda^2}$, where c are now assumed to be constant -- $a_1 < a_2$ and, consequently, $G(a_1) > G(a_2)$ -- i.e., the "bluish" and "blue" stellar images are attenuated to a greater extent than the "red" images. The attenuation difference depends on the difference λ_{eff}. If we assume: spectral class - λ_{eff}; B_0 - 412 millimicrons; M - 443 millimicrons $(\lambda_{eff})_{B_0}/(\lambda_{eff})_M = 0.93$. The square of this quantity yields the following relationship /205

$$\frac{a_{B_0}}{a_M} = 1.15.$$

If it is assumed that $a_M = 3$, then $a_{B_0} = 3.45$. According to Figure 2, the difference between the corresponding attenuations is about $0^m.1$; thus, the influence of this phenomenon on the difference between the color indices is comparatively small.

REFERENCES

1. Ambartsumyan, V.A., et al. Kurs astrofiziki i zvezdnoy astronomii (Course on Astrophysics and Stellar Astronomy). Vol. 1. Gosudarstvennoye Teoreticheskoye i Tekhnicheskoye Izdatel'stvo Moscow-Leningrad, 1934.
2. Danzhon, A., Kuder, A. A.Zh. No. 1, 17, 1940.
3. Denisov, N.G., Tatarskiy, V.I. Izvestiya Vuzov. Radiofizika 6, 3, 488, 1963.
4. Martynov, D.Ya. Kurs prakticheskoy astrofiziki (Course on Practical Astrophysics). Fizmatgiz, Moscow, 1960.
5. Nikonov, V.B. Byulleten Abastum. Observatorii, 14, 1953.
6. Orlov, S.V. A.Zh. 22, 1, 3, 1945.
7. Sytinskaya, N.N. A.Zh. 21, 230, 1944.
8. Tikhov, G.A. Izvestiya Rosskogo Astronomicheskogo Obshchestva, 16, 5, 1910.
9. Tudorovskiy, A.I. Teoriya opticheskikh priborov (Theory of Optical Devices). Vol. 2. Izdatel'stvo AN SSSR, Moscow, 1952.
10. Fesenkov, V.G. A.Zh. 22, 4, 219, 1945.
11. Chernov, L.A. Rasprostraneniye voln v srede so sluchaynymi

neodnorodnostyami (Propagation of Waves in a Medium with Random Inhomogeneities). Izdatel'stvo AN SSSR, Moscow, 1958.
12. Sidgwick, I. B. Amateurs Astronomers Handbook. London, 1954.
13. Scheiner, I. Photographie der Gestirne (Photography of Stars). Leipzig, 1897.

Scientific Translation Service
4849 Tocaloma Lane
La Canada, California

NASA-Langley, 1967 —— 30 F-455

"The aeronautical and space activities of the United States shall be conducted so as to contribute . . . to the expansion of human knowledge of phenomena in the atmosphere and space. The Administration shall provide for the widest practicable and appropriate dissemination of information concerning its activities and the results thereof."

—NATIONAL AERONAUTICS AND SPACE ACT OF 1958

NASA SCIENTIFIC AND TECHNICAL PUBLICATIONS

TECHNICAL REPORTS: Scientific and technical information considered important, complete, and a lasting contribution to existing knowledge.

TECHNICAL NOTES: Information less broad in scope but nevertheless of importance as a contribution to existing knowledge.

TECHNICAL MEMORANDUMS: Information receiving limited distribution because of preliminary data, security classification, or other reasons.

CONTRACTOR REPORTS: Scientific and technical information generated under a NASA contract or grant and considered an important contribution to existing knowledge.

TECHNICAL TRANSLATIONS: Information published in a foreign language considered to merit NASA distribution in English.

SPECIAL PUBLICATIONS: Information derived from or of value to NASA activities. Publications include conference proceedings, monographs, data compilations, handbooks, sourcebooks, and special bibliographies.

TECHNOLOGY UTILIZATION PUBLICATIONS: Information on technology used by NASA that may be of particular interest in commercial and other non-aerospace applications. Publications include Tech Briefs, Technology Utilization Reports and Notes, and Technology Surveys.

Details on the availability of these publications may be obtained from:

SCIENTIFIC AND TECHNICAL INFORMATION DIVISION

NATIONAL AERONAUTICS AND SPACE ADMINISTRATION

Washington, D.C. 20546